Approximations and exact properties of density functionals from the strong-interaction limit of DFT

Giarrusso, S.

2020

document version
Publisher's PDF, also known as Version of record

A Clara

This thesis has been reviewed by:

prof.dr. P.W. Ayers
prof.dr. E.J. Baerends
dr. P.F. Loos
dr. A. Pribram-Jones
dr. J. Toulouse
prof.dr. L. Visscher

VRIJE UNIVERSITEIT

Approximations and exact properties of density functionals from the strong-interaction limit of DFT

ACADEMISCH PROEFSCHRIFT

ter verkrijging van de graad Doctor of Philosophy
aan de Vrije Universiteit Amsterdam,
op gezag van de rector magnificus
prof.dr. V. Subramaniam,
in het openbaar te verdedigen
ten overstaan van de promotiecommissie
van de Faculteit der Bètawetenschappen
op maandag 2 maart 2020 om 13.45 uur
in de aula van de universiteit,
De Boelelaan 1105

door

Sara Giarrusso

geboren te Rome, Italië

promotor: prof.dr. P. Gori Giorgi
copromotor: dr. K.J.H. Giesbertz

Contents

Introduction

The full mathematical description of a many-body quantum system is encrypted in the renowned Schrödinger equation (SE).

Such equation, however, features both a many-body interaction operator, which brings in the unsolved classical many-body problem, and the quantum kinetic energy operator, which increases the complexity of the equation. Its closed-form solution is therefore practically unreachable.

Since roughly a century, the goal of the electronic structure theory community has been that of finding more accurate and more compact ways to approximate the solution to the SE, i.e. the wave function, or the electronic properties which depend on it, in order to achieve a deeper understanding of matter at the electronic scale.

Notwithstanding their communal goal, electronic structure methods have been traditionally characterised by a sort of dichotomy, namely that between the so-called Wave Function-based methods and Density Functional Theory (DFT).

Simplistically, while the formers construct different *ansatz* for the N-electron wave function which can be optimised variationally, DFT rephrases the problem posed by the SE in terms of a physical observable: the electron density.

Both approaches have their own strengths and drawbacks and, in some sense, they complement each other. In recent years, the number of works where these approaches conflate has been increasing (references [1–3] are just a few examples).

This work is mainly focused on Density Functional Theory.

Overview of the thesis and Main contributions

The first three chapters of this thesis form its theoretical backbone. In particular, chapter 1 reviews fundamentals of Density Functional Theory, chapter 2 gives a detailed presentation of the conditional amplitude formalism and of its relevance in the context of DFT and chapter 3 illustrates the theory of strictly correlated electrons from a physical perspective, still mentioning some more mathematical aspects, and reviews its most important applications to physical and chemical problems.

In chapter 4, we assess a particular class of density functional approximations, based on the idea of interpolating between the weak- and the strong-interaction limit of DFT, on the quite challenging case of gold and silver clusters of small to medium size. This class of functionals had been previously extensively tested only on main-group chemistry [4]. Our results show that although not spectacularly accurate, this class of functionals performs quite well for atomization energies calling for a self-consistent implementation in the future. In fact, a renovated in-

terest for such functionals has been demonstrated by very recent works [5, 6]. The results of the assessment conducted in our work, as well as in similar studies on different test sets [4, 7], indicate that their performances are optimal when used as a correlation correction to the Hartree-Fock (HF) method (see table 4.2). Such unexpected outcome prompted us into exploring the possibility of adopting adiabatic connection interpolations also in the context of HF theory. We began by investigating its strong-interaction limit providing first formal results in chapter 5. We show, for example, that the minimizer of the asymptotic Hamiltonian of eq 5.8 is a functional of the HF density alone (eq 5.9) and find exact relations between the strong-interaction limit of the HF and of the DFT adiabatic connection integrands (eq 5.17).

In chapters 6 and 7, we focus on the response part of the KS potential. This component is typically heavily misrepresented by standard functionals. Our contributions in this topic comprise a relation (eq 6.29) between two different definitions of response potentials (eq 2.54 and 6.18) and the derivation of the response potential in the strong-interaction limit of DFT (eq 6.38), satisfying an interesting sum rule in the N-electron 1D (eq 7.16) and spherical two-electron (eq 7.20) cases.

Furthermore, the study of a simple 1D model for a stretched heteronuclear molecule highlights several similarities between the KS and the SCE potentials in the dissociation limit. For instance, we find that the location of the maxima of both potentials coincides (see fig 6.10) and corresponds to the distance at which the density integrates to one (eq 6.51) clarifying how the Hartree-XC potential can correctly dissociate a bond into fragments with integer number of electrons. We also show how the shape of the co-motion function (see sec 3.3) becomes independent of the internuclear distance, R, for large R (saturation phenomenon) and retains information on the relation between the asymptotic decays of the fragment densities (see fig 6.12 and eq 6.53) which is reminiscent of the behaviour of the exact Hartree-XC potential. Finally, we signal the presence of a secondary peak in the kinetic potential, v_{kin} (eq 2.19), located far away on the side of the more electronegative fragment (fig 6.13).

In the last chapter, we investigate the feasibility of introducing a position-dependent mass carefully devised such that a non-interacting auxiliary system endowed with this mass can deliver the same kinetic energy density as the interacting one. It turns out that there is plenty of freedom to realise such matching, in addition to several fundamental questions. We discuss different possible settings and illustrate them for simple cases to show advantages and disadvantages of each one.

Atomic units are adopted throughout this thesis.

1

The density as basic variable

In the time-independent framework, an exhaustive description of a many-body quantum system can be accomplished by solving the time-independent Schrödinger equation (SE)

$$\hat{H}|\Psi\rangle = E|\Psi\rangle \tag{1.1}$$

where $\hat{H}$ is the operator for the total energy of the system.
In the Born-Oppenheimer and non-relativistic approximations and considering isolated atomic matter, $\hat{H}$ can be written as

$$\hat{H} = \underbrace{-\sum_{i}^{N} \frac{\nabla^2_{\mathbf{r}_i}}{2}}_{\hat{T}} + \underbrace{\sum_{i,j>i}^{N} \frac{1}{|\mathbf{r}_i - \mathbf{r}_j|}}_{\hat{V}_{ee}} \underbrace{-\sum_{i}^{N}\sum_{A}^{M} \frac{Z_A}{|\mathbf{r}_i - \mathbf{R}_A|}}_{\hat{V}_{ext}} \tag{1.2}$$

where N is the number of electrons, M that of the nuclei, and Z_A are the nuclear charges.

It is quite self-evident that, even after simplifying the physical interacting Hamiltonian as in eq 1.2, the solution to eq 1.1 is still a highly complicated mathematical object, living in a highly multidimensional space, $\left(\mathbb{R}^3 \otimes \mathbb{Z}_2\right)^N$, where the "extra" degree of freedom, possessed by each electron on top of its spatial freedom, is a fundamental characteristic of quantum particles: their so-called "spin".
Anyhow, as scientists or merely as observers, we are used to measure and interact with matter in three dimensions or four if we include passing of time. In a way, the fact that we can reproduce results and that we rely on previous measurements or previously observed effects to shape matter into technology is somehow an indication that, for all the purposes we are concerned with, $\left(\mathbb{R}^3 \otimes \mathbb{Z}_2\right)^N$ is a way redundant control space.

In some way, a smaller, 3(or 4)-dimensional mathematical object has to be a sufficient tool in our hands to understand what we see and make predictions on what we have not yet explored experimentally.
This naif idea was formulated in mathematical terms by P. Hohenberg and W. Kohn in 1964 [8] (HK) and since then, the electron probability density has been recognized as the most natural minimally-dimensional mathematical object that would serve this scope.

The electron probability density, or just (electron) density, is defined as

$$n(\boldsymbol{r}) := \langle\Psi|\hat{n}|\Psi\rangle = N\int |\Psi(\boldsymbol{r}\sigma,\mathbf{x}_2,\cdots,\mathbf{x}_N)|^2 \mathrm{d}\sigma\mathrm{d}\mathbf{x}_2\cdots\mathrm{d}\mathbf{x}_N \tag{1.3}$$

with $\hat{n} = \sum_i^N \delta(\boldsymbol{r}_i - \boldsymbol{r})$, $|\Psi\rangle = \Psi(\boldsymbol{r}\sigma,\mathbf{x}_2,\cdots,\mathbf{x}_N)$, $\mathbf{x}_i = \boldsymbol{r}_i\sigma$, the spatial and spin coordinates of the electrons, where we have taken electron 1 as the reference electron dropping the subscript, i.e. $\boldsymbol{x}_1 = \boldsymbol{x}$, and it measures the probability of finding any of the N electrons in a specific point in space with arbitrary spin[1] while the other electrons have arbitrary position and spin.[2]

Early attempts to use the density as a basic variable were present in the electronic structure theory community long before HK was published [10–12] and in this sense HK was also presented as an exactification of these intuition-based works. However, quite elegant arguments for the use of the density as a basic variable were already put forward and attributed to spectroscopist E. Bright Wilson[3] and hold for the particular, yet of major importance, case of an external potential of Coulomb type, in other words for a Hamiltonian of the likes of eq 1.2.
What E. Bright Wilson pointed out is that, since the density

i. integrates to the total number of electrons;

ii. has cusps located at the position of the nuclei;

iii. satisfies the cusp condition:

$$\lim_{|\boldsymbol{r}-\mathbf{R}_A|\to 0}\left(\frac{\partial}{\partial r} + 2\,Z_A\right) n(\boldsymbol{r}) = 0; \tag{1.4}$$

[1] Whereas $n(\mathbf{x}) = N\int|\Psi(\mathbf{x},\mathbf{x}_2,\cdots,\mathbf{x}_N)|^2\mathrm{d}\mathbf{x}_2\cdots\mathrm{d}\mathbf{x}_N$ measures the probability of finding an electron in a specific point in space and with a certain spin.

[2] Note that here we stick to the following normalization of the N-electron wavefunction: $\int|\Psi|^2\mathrm{d}\mathbf{x}_1\cdots\mathrm{d}\mathbf{x}_N = 1$, which is the most commonly encountered; however a different normalization might be more consistent with the probability interpretation of the (square modulus of the) N-electron wavefunction [9] and would change the normalisation constant in the definition of the density from N to $\frac{1}{(N-1)!}$.

[3] There is no "formal" attribution to E. Bright Wilson: rather, the theoretical chemist N. C. Handy bothered noting down in the literature (see refs [13, 14]) a personal communication from his colleague R. B. Parr narrating that the spectroscopist commented on W. Kohn presentation in 1965 bringing up the arguments mentioned.

it encodes all the ingredients (N, R_A and M, and Z_A) that specifies the Hamiltonian in eq 1.2. In this sense HK was, more than an exactification of references [10–12], an extension of Bright Wilson's arguments allowing for a unique mapping between an electron probability density and an external potential of any kind, paving the way for much further developments.

1.1. Hohenberg-Kohn theorem(s)

Traditionally, the fundamental results proven and published in reference [8] are referred to as the "Hohenberg-Kohn theorem(s)"(HK).[4]

Let us start by considering the Hamiltonian in eq 1.2 and define the one-body external potential v as $v(\boldsymbol{r}) = \sum_A^M \frac{Z_A}{|\mathbf{r}-\mathbf{R}_A|}$ so that $\hat{V}_{ext} = \sum_i^N v(\boldsymbol{r}_i)$.

For a fixed number of electrons, fixing a particular one-body external potential[5] up to an additive constant, c, determines the ground state (GS) wavefunction, Ψ, satisfying eq 1.1 and generating the corresponding density, via eq 1.3.

In formulas, the mapping

$$v + c \underset{N}{\longrightarrow} \Psi \longrightarrow n \tag{1.5}$$

is the trivial one.

The invertibility of 1.5 is proven in sec. I of [8].

The inversion of the left half of 1.5, i.e. $\Psi \longrightarrow v + c$, is quite immediate (and not dealt with explicitly in the paper), since two different wavenfunctions, Ψ and Ψ', are necessarily solutions to two different SE unless $v - v' = E - E'$. To show that explicitly, let us write

$$\left(\hat{T} + \hat{V}_{ee} + \sum_i^N v(\boldsymbol{r}_i)\right)\Psi = E\Psi \tag{1.6}$$

$$\left(\hat{T} + \hat{V}_{ee} + \sum_i^N v'(\boldsymbol{r}_i)\right)\Psi' = E'\Psi' \tag{1.7}$$

Assuming that v and v' differ by more than an additive constant and deliver the same GS wavefunction, $\Psi = \Psi'$, leads to contradiction by subtraction of eqs 1.6 and 1.7.

[4] Such "theorem" is typically presented in textbooks as having a first and a second part of the proof, although this is not an original distinction of the authors. Quite hilariously, which part of the total proof is what and sometimes even if there are two theorems rather than one or which part among the results published in HK is the theorem, varies from textbook to textbook! Without giving a specific numbering, we will mainly stick to the original paper [8] and to the widely appreciated reference book on density functional theory referenced in [15].

[5] Let us reiterate that, according to eq 1.2, fixing the external potential translates into fixing the number, M, the position, $\mathbf{R}_A$, and the charges, Z_A, of the nuclei – which is a representative external potential for an isolated molecular/metallic system –, however the external potential can be kept completely general as long as it is a one-body local potential, $\hat{V}_{ext} = \sum_i^N v(\boldsymbol{r}_i)$.

The inversion of the right half of 1.5, i.e. $n \longrightarrow \Psi$,[6] is less direct but the proof is astonishingly simple and it's again by *reductio ad absurdum*.
Defining $\Psi_0 = \underset{\Psi \text{ a.s.} \to N}{\operatorname{argmin}} \langle \Psi | \hat{H} | \Psi \rangle$ and $\Psi_0' = \underset{\Psi \text{ a.s.} \to N}{\operatorname{argmin}} \langle \Psi | \hat{H}' | \Psi \rangle$ – where "Ψ a.s." stands for a 'search over all antisymmetric wavefunctions' – by the minimal property of the GS ("variational principle")

$$\begin{aligned} E_0 &= \langle \Psi_0 | \hat{H} | \Psi_0 \rangle < \langle \Psi_0' | \hat{H} | \Psi_0' \rangle \\ &= \langle \Psi_0 | \hat{H} | \Psi_0 \rangle < \langle \Psi_0' | \hat{H}' + \hat{V} - \hat{V}' | \Psi_0' \rangle \\ &= \langle \Psi_0 | \hat{T} + \hat{V}_{ee} | \Psi_0 \rangle + \int n(\boldsymbol{r}) v(\boldsymbol{r}) \mathrm{d}\boldsymbol{r} < E_0' + \int n'(\boldsymbol{r}) \big(v(\boldsymbol{r}) - v'(\boldsymbol{r}) \big) \mathrm{d}\boldsymbol{r} \end{aligned} \tag{1.8}$$

and, by interchanging the roles of primed and unprimed quantities,

$$E_0' < E_0 + \int n(\boldsymbol{r}) \big(v'(\boldsymbol{r}) - v(\boldsymbol{r}) \big) \mathrm{d}\boldsymbol{r}. \tag{1.9}$$

If we now assume that two different wavefunctions, Ψ' and Ψ, both lead to the same density, $n' = n$, then we can add up eqs 1.8 and 1.9 and conclude

$$E_0 + E_0' < E_0 + E_0' \tag{1.10}$$

which is a contradiction therefore proving the invertibility of the mapping.

The invertibility of the mapping means that the expectation value of an operator $\hat{A}$ in the GS wavefunction is also a functional of the GS density

$$A[n_0] = \langle \Psi_0[n_0] | \hat{A} | \Psi_0[n_0] \rangle.^{7} \tag{1.11}$$

In sec. II of HK, the universal functional, $F[n]$, is defined

$$F[n] \coloneqq \langle \Psi[n] | \hat{T} + \hat{V}_{ee} | \Psi[n] \rangle. \tag{1.12}$$

The universal functional is defined only for v-representable densities, $n : \exists\, v \to n$, by which we mean densities that are GS of an (interacting) Hamiltonian with

[6] This part of the proof is the only one that requires modification if we are dealing with degenerate ground states, see next footnote

[7] In the case of degenerate ground states, it may happen that, although $\Psi \neq \Psi'$, the inequality become an equality ($E_0 = E_0'$) and therefore the unique mapping $n \longrightarrow \Psi$ is no longer established as there is no contradiction (relation 1.10). However since this circumstance can only be met if $E_0 = E_0'$, which means only if the different Ψ and Ψ' come from the same potential, v, the mapping $n \longrightarrow v$ can still be established and, via the potential, we can access the GS energy as well as the set of all degenerate GS wavefunctions coming from that potential, $\{\Psi_0^i[v]\}$, but we cannot use the density as basic variable to get to all observables that depend specifically on the wavefunction (for example the spin) as this latter no longer maps to one specific GS wavefunction among the set of possible ones. See [15–18] for further reference.

external potential v.
The total GS energy of a system is rewritten as the following functional of the density

$$E_v[n] = F[n] + \underbrace{\int n(\boldsymbol{r})\, v(\boldsymbol{r}) \mathrm{d}\boldsymbol{r}}_{V_v[n]} \tag{1.13}$$

where the subscript v highlights that the expression of the density functional for the energy of a system on the l.h.s. of the equation depends on the external potential in the way shown on the r.h.s.
The variational principle is then introduced in the context of density functionals, i.e.

$$E_v[n_0] = \langle \Psi_0[n_0] | \hat{H}_v | \Psi_0[n_0] \rangle \leq \langle \Psi[n] | \hat{H}_v | \Psi[n] \rangle = E_v[n] \tag{1.14}$$

where the equal sign only holds for $n = n_0$, with n_0 the ground state density of the Hamiltonian with external potential v.
Equation 1.14 tells us that the density functional for the energy of a system delivers the lowest possible value if and only if the input density is the ground state one.
Of course, this variational principle is of lesser use than the one in terms of the wavefunction as we actually do not know the exact functional form of $E_v[n]$.
Knowing it, one could in principle obtain the the GS energy of the Hamiltonian with external potential v by minimising eq 1.14 under the constraint that the density stays properly normalised

$$\frac{\delta}{\delta\, n(\boldsymbol{r})} \left\{ E_v[n] - \mu \left(\int n(\boldsymbol{r}) \mathrm{d}\boldsymbol{r} - N \right) \right\} = 0 \tag{1.15}$$

Introducing eq 1.13 into eq 1.15

$$\frac{\delta\, E_v[n]}{\delta\, n(\boldsymbol{r})} = \mu = \frac{\delta\, F[n]}{\delta\, n(\boldsymbol{r})} + v(\boldsymbol{r}), \tag{1.16}$$

we also derive

$$v[n_0](\boldsymbol{r}) = -\frac{\delta\, F[n]}{\delta\, n}\Big|_{n=n_0}(\boldsymbol{r}) + \mu \tag{1.17}$$

which tells us that the external potential is the functional derivative of the HK functional evaluated at the GS density associated with that potential minus a constant shift.

1.2. The Levy-Lieb and Levy Functionals

The variational principle of eq 1.14 suggests that – for a given external potential– we can find the minimum GS density and energy by performing a search over all suitable densities

$$E_{v_0}[n_0] = \min_{\substack{n: \\ \exists\, v \to n}} \left(F[n] + \int n(\boldsymbol{r})\, v_0(\boldsymbol{r}) \mathrm{d}\boldsymbol{r} \right). \tag{1.18}$$

where n_0 is the minimizer. The formal simplicity of this search is hampered by the fact that the constraints guaranteeing that the search only hit (interacting) v-representable densitiesare mathematically involved and not known in general.
To achieve a much easier characterization of the densities entering the constrained search for the GS energy, the domain of the universal functional, F,[8] was extended by Levy [19, 20] by introducing the Levy-Lieb functional, F_{LL}, later shown by Lieb to have a minimum [21]. The Levy-Lieb functional is defined as

$$F_{\mathrm{LL}}[n] := \min_{\Psi \to n} \langle \Psi | \hat{T} + \hat{V}_{ee} | \Psi \rangle \tag{1.19}$$

and defines a corresponding energy functional

$$E_v[n] = F_{\mathrm{LL}}[n] + \int n(\boldsymbol{r}) v(\boldsymbol{r}) \mathrm{d}\boldsymbol{r} \tag{1.20}$$

Via F_{LL} the constrained search for the GS energy is now split in two steps

$$E_{v_0}[n_0] = \inf_n \left(\min_{\Psi \to n} \langle \Psi | \hat{T} + \hat{V}_{ee} | \Psi \rangle + \int n(\boldsymbol{r}) v_0(\boldsymbol{r}) \mathrm{d}\boldsymbol{r} \right) \tag{1.21}$$

where we are searching over N-representable densities, i.e. densities that can be generated by some wavefunction. The advantage over eq 1.18 is that the set of N-representable densities is characterized explicitly [22]: any density which is non-negative ($n \geq 0$), normalisable and with a finite Weiszäcker kinetic energy functional ($n(\boldsymbol{r})^{\frac{1}{2}} \in H^1$) belongs to the set. Note that the space of v-representable densities is a subset of that of N-representable ones. Moreover the functional F_{LL} is not convex thus its minimum could be a local one. To avoid this inconvenient property, Lieb defined a different but related functional, F_{L} [21].
In order to introduce F_{L}, let us first discuss how the HK functional, F_{HK}, has to be modified in order to account for degenerate ground states.
For a q-fold degenerate GS multiplet $\{|\Psi_i\rangle, i = 1, \cdots q\}$ each of the possible states forming the multiplet may deliver a different density n_i.
Let us define the density matrix operator, $\hat{D}$

$$\hat{D} = \sum_{i=1}^{q} \lambda_i |\Psi_i\rangle\langle\Psi_i| \quad \sum_{i=1}^{q} \lambda_i = 1 \quad 0 \leq \lambda_i \leq 1 \tag{1.22}$$

and the GS expectation value of any operator, $\hat{O}$

$$\langle \hat{O} \rangle = \mathrm{Tr} \hat{D} \hat{O} \tag{1.23}$$

[8] It is common to label the functional "F" of eq 1.12 as "F_{HK}", where the subscript stands for "Hohenberg-Kohn", to distinguish it from other similar functionals that were introduced afterwards (see later discussion).

where the trace operation for any operator is defined as

$$\mathrm{Tr}\hat{O} = \sum_{i=1}^{\infty} \langle \Phi_i | \hat{O} | \Phi_i \rangle \tag{1.24}$$

and $\{|\Phi_i\rangle\}$ is any complete set of states.

If we choose the complete set to be the degenerate GS multiplet $\{|\Psi_i\rangle, i = 1, \cdots q\}$ then

$$\langle \hat{O} \rangle = \sum_{i=1}^{\infty} \langle \Phi_i | \hat{D}\hat{O} | \Phi_i \rangle = \sum_{i=1}^{q} \lambda_i \langle \Psi_i | \hat{O} | \Psi_i \rangle \tag{1.25}$$

from which it is immediate to see that the non-degenerate case is included as the special case where $\lambda_1 = 1$.
If, furthermore, $\hat{O} = \hat{n}$ we can extend the definition of the density in 1.3 to ensembles

$$n(\boldsymbol{r}) = \sum_{i=1}^{q} \lambda_i \langle \Psi_i | \hat{n} | \Psi_i \rangle = \sum_{i=1}^{q} \lambda_i \, n_i(\boldsymbol{r}). \tag{1.26}$$

As mentioned in footnote 7, it can be shown that each multiplet of degenerate ground states is associated to only one potential and thus the set of corresponding GS densities is said to be ensemble-v-representable (Ev), therefore we can unambiguously define the ensemble-HK-functional, F_{EHK}

$$F_{\mathrm{EHK}}[n] = \mathrm{Tr}\hat{D}[n]\left(\hat{T} + \hat{V}_{ee}\right) \tag{1.27}$$

on the set of Ev-densities and extend the energy functional to degenerate ground states

$$E_v[n] = F_{\mathrm{EHK}}[n] + \int n(\boldsymbol{r})\, v(\boldsymbol{r}) \mathrm{d}\boldsymbol{r} = \mathrm{Tr}\hat{D}[n]\hat{H}_v. \tag{1.28}$$

Again, the set of Ev-representable densities, the sole kind of densities that should enter in a minimisation of $E_v[n]$, is difficult to characterise.
In other words, we run into a similar problem as that encountered for the non-degenerate case and a similar way around is found by extending the domain of F_{EHK} to all EN-representable densities, meaning all the ensemble densities that can be generated by some density matrix,

$$F_{\mathrm{L}}[n] := \min_{\hat{D} \to n} \mathrm{Tr}\hat{D}\left(\hat{T} + \hat{V}_{ee}\right), \tag{1.29}$$

where eq 1.29 defines the Lieb functional F_{L}. We are now also able to write a proper variational principle, i.e.

$$E_{v_0}[n_0] = \inf_n \left(F_{\mathrm{L}}[n] + \int n(\boldsymbol{r})\, v_0(\boldsymbol{r}) \mathrm{d}\boldsymbol{r} \right). \tag{1.30}$$

1.3. Kohn-Sham scheme: bypassing the hardest problem

The basic idea of Kohn and Sham [23] (1965) essentially builds up on the success of Hartree Fock theory and resides in adopting an auxiliary "non-interacting" quantum system (the KS system), endowed with a fermionic wavefunction treating the electrons as described by single-particle functions (KS orbitals).

Compared to Hartree Fock theory, Kohn-Sham-DFT (KS-DFT) has the most noticeable merit of being still an *exact* Density Functional Theory, since all interaction effects of the original quantum system are enclosed in the auxiliary one by means of an effective local potential, called the KS potential, v_s.

Its enormous success stems from bypassing the hardest technical problem in the field, namely that of finding a reasonably accurate representation of the kinetic energy explicitly in terms of the electron density.

Instead of tackling such problem, KS-DFT approach is that of simply sticking to the non-intuitive purely quantum mechanical expression of the kinetic energy operator for which a wave function is needed, and treat the remainder problem as a pure density functional. The kinetic energy expression proposed is still necessarily a density functional by virtue of the HK theorem(s) but in an implicit, highly non trivial way.

Formally, KS-DFT relies on an essential condition, namely, the composition of two bijective mappings between two local potentials and a unique GS density

$$v \longleftrightarrow n \longleftrightarrow v_s. \tag{1.31}$$

A density allowing for 1.31 is said to be both interacting and non-interacting v-representable.
Only for such densities, we can establish the connection between the KS picture and the interacting one, via eqs 1.43 and 1.49.

Whether the two domains coincide is still an open issue. It has been shown (see reference [21] and references therein) that it is always possible to find a non-interacting Ev-representable density, n_k, that approximates any interacting Ev-representable density, n_0, *arbitrarily* closely, i.e. for every $\epsilon > 0$, the p-norm of their difference is lesser or equal than ϵ

$$||n_k - n_0||_p \leq \epsilon \tag{1.32}$$

with $p = 1$ and $p = 3$.

The above property is enough to provide a sound theoretical basis for numerical implementations of the Kohn-Sham scheme, see refs [15, 17, 18, 21, 24] for more extended discussions.

1.3.1. Kinetic energy functional minimisation[9]

The kinetic energy of a "non-interacting" system (by which we mean a system without two-body or higher many-body operators) can be calculated from the expression

$$\begin{aligned}\tilde{T}_s[\{\tilde{\psi}_i,\tilde{\psi}_i^*\}] = -\frac{1}{2}\sum_{i=1}^{N}\langle\tilde{\Psi}_s|\nabla^2_{\mathbf{r}_i}|\tilde{\Psi}_s\rangle &= -\frac{1}{2}\int \mathrm{d}\mathbf{x}\left[\nabla^2_{\mathbf{r}}\tilde{\gamma}_s(\mathbf{r},\mathbf{r}')\right]_{\mathbf{r}'=\mathbf{r}} \\ &= -\frac{1}{2}\sum_{i=1}^{N}\langle\tilde{\psi}_i|\nabla^2|\tilde{\psi}_i\rangle, \end{aligned} \tag{1.33}$$

where the $\tilde{\psi}_i$ are generic single particle wavefunctions (orbitals) from which the N-electron Slater determinant, $\tilde{\Psi}_s$, is constructed and $\tilde{\gamma}_s$ is the corresponding one-body-reduced density matrix (1RDM). Note that the last equality only follows if we choose an orthogonal set of orbitals (which we do for convenience) and that the ground state wavefunction of a non-interacting system can typically, but not always,[10] be expressed as a single Slater determinant.

Let us now optimize the set of orbitals in order to attain the minimum kinetic energy possible under the constraints of its orthormality and that of a prescribed density, delivered from the set according to eq 1.3.
To perform an independent minimization, we write the Lagrangian

$$\begin{aligned}L_n[\{\tilde{\psi},\tilde{\psi}^*\},v_s,\tilde{\boldsymbol{\epsilon}}] := \tilde{T}_s[\{\tilde{\psi},\tilde{\psi}^*\}] &- \sum_{i,j}^{N}\tilde{\epsilon}_{ij}\left(\langle\tilde{\psi}_i|\tilde{\psi}_j\rangle - \delta_{ij}\right) \\ &+ \int \tilde{v}_s(\mathbf{r})\left(\sum_{i,\sigma}|\tilde{\psi}_i|^2 - n\right)(\boldsymbol{r})\,\mathrm{d}\boldsymbol{r}, \end{aligned} \tag{1.34}$$

with $\sum_{i,j}^{N}\tilde{\epsilon}_{ij}$ the Lagrange multipliers enforcing orthonormality (integral condition) and $\tilde{v}_s$ the Lagrange multiplier enforcing the prescribed density at each point in space (local condition).

Setting the Lagrangian first-order variation, δL_n, to zero

$$0 = \delta L_n = \sum_{i}^{N}\int\left(\delta\tilde{\psi}_i^*\frac{\delta L_n}{\delta\tilde{\psi}_i^*} + \frac{\delta L_n}{\delta\tilde{\psi}_i}\delta\tilde{\psi}_i + \delta\tilde{v}_s\frac{\delta L_n}{\delta\tilde{v}_s} + \sum_{j}^{N}\delta\tilde{\epsilon}_{ij}\frac{\delta L_n}{\delta\tilde{\epsilon}_{ij}}\right)(\mathbf{x})\,\mathrm{d}\mathbf{x}, \tag{1.35}$$

and considering that we want eq 1.35 satisfied for any arbitrary variation $\delta\tilde{\psi}_i^*, \delta\tilde{\psi}_i, \delta\tilde{v}_s$ and $\delta\tilde{\epsilon}_{ij}$, we have four equations for the four functional derivatives

[9] This derivation is closely inspired to the lecture notes authored by Dr. K.J.H. Giesbertz

[10] For cases where the single Slater determinant description cannot deliver the prescribed density see references [17, 25, 26]

$$0 = \begin{cases} \dfrac{\delta L_n}{\delta \tilde{\psi}_i^*}(\boldsymbol{x}) \longrightarrow \left(-\dfrac{1}{2}\nabla^2 + \tilde{v}_s(\mathbf{r})\right)\tilde{\psi}_i(\mathbf{x}) = \displaystyle\sum_j^N \tilde{\epsilon}_{ij}\tilde{\psi}_j(\mathbf{x}) & (1.36) \\ \dfrac{\delta L_n}{\delta \tilde{\psi}_i}(\boldsymbol{x}) \longrightarrow \left(-\dfrac{1}{2}\nabla^2 + \tilde{v}_s(\mathbf{r})\right)\tilde{\psi}_i^*(\mathbf{x}) = \displaystyle\sum_j^N \tilde{\epsilon}_{ji}\tilde{\psi}_j^*(\mathbf{x}) & (1.37) \\ \left(\displaystyle\sum_\sigma \dfrac{\delta L_n}{\delta \tilde{v}_s}\right)(\boldsymbol{r}) \longrightarrow \left(\displaystyle\sum_{i,\sigma} |\tilde{\psi}_i|^2\right)(\boldsymbol{r}) = n(\boldsymbol{r}) & (1.38) \\ \dfrac{\delta L_n}{\delta \tilde{\epsilon}_{ij}} \longrightarrow \langle\tilde{\psi}_i|\tilde{\psi}_j\rangle = \delta_{ij} & (1.39) \end{cases}$$

that need to be simultaneously satisfied.

The matrix of the coefficients, $\tilde{\boldsymbol{\epsilon}}$, can be symmetric (both Hermitian and real-valued) since the Lagrangian must be real-valued and the inner product used is Hermitian. Therefore, we can diagonalise it. Moreover, given that all the Lagrange multipliers are real-valued, and the order of conjugation and differentiation can be interchanged, eq 1.36 already contains eq 1.37 which can therefore be discarded.

In the end, we obtain the canonical KS equations

$$\left(-\frac{1}{2}\nabla^2 + v_s(\mathbf{r})\right)\psi_i(\mathbf{x}) \equiv \epsilon_i\psi_i(\mathbf{x}), \tag{1.40}$$

where eq 1.40 is expressed as converged to the fixed point at which $\{\tilde{\psi}_i\} \longrightarrow \{\psi_i[n]\}$, $\tilde{\boldsymbol{\epsilon}} \longrightarrow \{\epsilon_i[n]\}$, and $\tilde{v}_s \longrightarrow v_s[n]$.
The total GS energy of the non-interacting system is simply the sum of the N-lowest eigenvalues

$$E_s[n] = \langle\Phi[n]|\hat{H}_s|\Phi[n]\rangle = \sum_i^N \epsilon_i[n] \tag{1.41}$$

with $\hat{H}_s[n] = \hat{T} + \sum_i^N v_s[n](\boldsymbol{r}_i)$.

1.3.2. Connection to the interacting system

The usefulness as well as the derivation itself of eqs 1.40 hinge on the assumption that a v_s exists that enforce the equivalence between the density of the non-interacting system and a desired one, eq 1.38, typically the one of the interacting problem. If it does not exist then the Lagrangian of eq 1.34 does not have a minimum. If it does exist, however, we can ask ourselves what are the connections between the non-interacting system and the interacting one.

Let us define the equivalent of the Levy-Lieb functional for a system without interaction

$$T_s[n] \coloneqq \min_{\Psi\to n} \langle\Psi|\hat{T}|\Psi\rangle = T_s[\{\psi_i[n], \psi_i^*[n]\}] \tag{1.42}$$

and let us rewrite the total GS energy of a system, eq 1.13, as

$$E_v[n] = T_s[n] + \underbrace{F[n] - T_s[n]}_{=:E_{Hxc}[n]} + V[n] \tag{1.43}$$

where we have introduced the energy term, E_{Hxc} called the "Hartree-exchange-correlation", which can be further decomposed

$$E_{Hxc}[n] = (T + V_{ee} - T_s)[n] = (T_c + U + U_{xc})[n] = (U + E_{xc})[n] \tag{1.44}$$

where $T_c = T - T_s$, $U_{xc} = V_{ee} - U$ and $U[n] = \frac{1}{2}\int \frac{n(\boldsymbol{r})n(\boldsymbol{r}')}{|\boldsymbol{r}-\boldsymbol{r}'|}\mathrm{d}\boldsymbol{r}\mathrm{d}\boldsymbol{r}'$.
Using eqs 1.15 and 1.43, we write

$$\mu = \frac{\delta E_v[n]}{\delta n}(\boldsymbol{r}) = \left(\frac{\delta T_s[n]}{\delta n} + \frac{\delta E_{Hxc}[n]}{\delta n} + v\right)(\boldsymbol{r}) \tag{1.45}$$

Now we rewrite $\frac{\delta E_{Hxc}[n]}{\delta n}$, using $\frac{\delta U[n]}{\delta n} = v_{\mathrm{H}}$ and defining

$$v_{xc} \coloneqq \frac{\delta E_{xc}[n]}{\delta n} \tag{1.46}$$

as $\frac{\delta E_{Hxc}[n]}{\delta n} = v_{\mathrm{H}} + v_{xc}$ and evaluate $\frac{\delta T_s[n]}{\delta n}$ using that, at the optimal orbitals and multipliers,

$$T_s[n] \equiv L_n[\{\psi_i[n], \psi_i^*[n]\}, v_s[n], \boldsymbol{\epsilon}[n]]. \tag{1.47}$$

The derivative $\left.\frac{\delta L_n}{\delta n}\right|_n$ is then simply

$$\left.\frac{\delta L_n[\{\psi_i[n], \psi_i^*[n]\}, v_s[n], \boldsymbol{\epsilon}[n]]}{\delta n}\right|_n = -v_s \tag{1.48}$$

by virtue of the stationarity conditions which makes all derivatives vanish but the term $\left.\frac{\partial L_n}{\partial n}\right|_n = -\int v_s[n](\boldsymbol{r}')\frac{\delta n(\boldsymbol{r}')}{\delta n(\boldsymbol{r})}\mathrm{d}\boldsymbol{r}'$ which depends explicitly on the density.

Combining eqs 1.45, 1.46 and 1.48 we find

$$v_s = v_{\mathrm{H}} + v_{xc} + v - \mu \tag{1.49}$$

where a convenient way to fix the gauge freedom in the constant shift is to set all potentials as vanishing asymptotically, $\{v_{\mathrm{H}}, v_{xc}, v\}(|\boldsymbol{r}| \to \infty) \sim 0$.

By virtue of eq 1.49, we are now able to solve eq 1.40 self-consistently without knowing the target density in advance: information on the target density in any standard KS self-consistent code is introduced via input of an external potential, v.

$$v_s^{(i)} = v_{\mathrm{H}}[n^{(i)}] + v_{xc}[n^{(i)}] + v \tag{1.50}$$

$$n^{(i+1)} = \underset{n}{\mathrm{argmin}}\left(T_s[n] + \int v_s^{(i)}(\boldsymbol{r})n(\boldsymbol{r})\mathrm{d}\boldsymbol{r}\right) \tag{1.51}$$

At convergence this iterative procedure delivers the same density as the one from which the fictitious external potential, v_s, was constructed (a fixed point). Moreover, supposing that we know the exact form of the functional E_{xc} and of its functional derivative v_{xc}, the converged density and the total energy calculated either from eq 1.43 or from

$$E_v[n] = \sum_i^N \epsilon_i[n] + E_{Hxc}[n] - \int v_{Hxc}(\boldsymbol{r}) n(\boldsymbol{r}) \mathrm{d}\boldsymbol{r} \tag{1.52}$$

with $v_{Hxc} = v_{\mathrm{H}} + v_{xc}$, would be exactly (numerical errors excepted) that of the interacting system. In practice, however, one needs to build approximations for these related unknown functionals: E_{xc} and v_{xc}.

1.4. The density-fixed adiabatic connection formalism

The density-fixed adiabatic connection formalism is a very powerful and long-established tool to construct approximation for the exchange-correlation energy [27–30]. Consider the λ-dependent Levy-Lieb functional[11] where the interaction is scaled by a real and positive coupling parameter λ, namely

$$F_\lambda[n] \coloneqq \min_{\Psi \to n} \langle \Psi | \hat{T} + \lambda \hat{V}_{ee} | \Psi \rangle, \tag{1.53}$$

assuming that n is v-representable for all λ, one can write a series of λ-dependent Hamiltonian with fixed density

$$\hat{H}_\lambda = \hat{T} + \lambda \hat{V}_{ee} + \hat{V}^\lambda, \tag{1.54}$$

where $\hat{V}^\lambda = \sum_i^N v^\lambda(\boldsymbol{r}_i)$ and

$$v^\lambda[n_0](\boldsymbol{r}) = -\frac{\delta F_\lambda[n]}{\delta n}\Big|_{n=n_0}(\boldsymbol{r}) \tag{1.55}$$

is the local external potential that delivers the prescribed density as the ground-state density of Hamiltonian 1.54 at each λ, i.e. $n_\lambda(\boldsymbol{r}) = n_1(\boldsymbol{r}) \equiv n(\boldsymbol{r})$, and $\Psi_\lambda(\boldsymbol{x}_1, \cdots, \boldsymbol{x}_N)$ is the ground state wavefunction of Hamiltonian 1.54 at each λ.
Equation 1.55 is derived in analogy with eq 1.17 in the usual assumption of v-representability of n at all λ.
By applying the following basic theorem of calculus

$$F_1 - F_0 = \int_0^1 \frac{\partial F_\lambda}{\partial \lambda} \mathrm{d}\lambda \tag{1.56}$$

[11] From now on we shall always use the Levy-Lieb functional unless otherwise specified, thus, for notational simplicity, we shall only write "F" implying "F_{LL}".

and considering that

$$\frac{\partial F_\lambda}{\partial \lambda} = \langle \Psi_\lambda | \frac{\partial \hat{H}_\lambda}{\partial \lambda} | \Psi_\lambda \rangle, \tag{1.57}$$

by virtue of the stationarity of Ψ_λ w.r.t. $\langle \hat{H}_\lambda \rangle$, we find

$$T + V_{ee} - T_s{}^{12} = \int_0^1 \langle \Psi_\lambda | \hat{V}_{ee} | \Psi_\lambda \rangle \, \mathrm{d}\lambda \tag{1.58}$$

which by comparison with eq 1.44 gives a compact and exact formula for the exchange-correlation (XC) energy

$$E_{xc}[n] = \int_0^1 W_\lambda[n] \, \mathrm{d}\lambda \tag{1.59}$$

where the density functional W_λ is defined as

$$W_\lambda[n] \coloneqq \langle \Psi_\lambda[n] | \hat{V}_{ee} | \Psi_\lambda[n] \rangle - U[n]. \tag{1.60}$$

W_λ is referred to as the adiabatic connection integrand.

A number of exact properties of the adiabatic connection integrand are known. Following the derivation in [31], we start by writing

$$\langle \hat{H}_\lambda \rangle_{\lambda'} \geq \langle \hat{H}_\lambda \rangle_\lambda \tag{1.61}$$

$$\langle \hat{H}_{\lambda'} \rangle_\lambda \geq \langle \hat{H}_{\lambda'} \rangle_{\lambda'} \tag{1.62}$$

where $\langle \hat{H}_\alpha \rangle_{\alpha'} = \langle \Psi_{\alpha'} | \hat{H}_\alpha | \Psi_{\alpha'} \rangle$ by variational arguments.
Then we substitute $\hat{H}_\lambda = \hat{H}_{\lambda'} + (\lambda - \lambda')\hat{V}_{ee} + (\hat{V}_\lambda - \hat{V}_{\lambda'})$ into the l.h.s. of 1.61, finding

$$\langle \hat{H}_{\lambda'} \rangle_{\lambda'} + (\lambda - \lambda')\langle \hat{V}_{ee} \rangle_{\lambda'} + \int (v_\lambda - v_{\lambda'}) \, n \geq \langle \hat{H}_\lambda \rangle_\lambda \tag{1.63}$$

Finally, summing eq 1.63 and eq 1.62, we find

$$(\lambda - \lambda') \left(\langle \hat{V}_{ee} \rangle_{\lambda'} - \langle \hat{V}_{ee} \rangle_\lambda \right) \geq 0 \tag{1.64}$$

eq 1.64 tells us that

$$\langle \hat{V}_{ee} \rangle_{\lambda'} \geq \langle \hat{V}_{ee} \rangle_\lambda \quad \text{if} \quad \lambda \geq \lambda' \tag{1.65}$$

and considering definition 1.60, it shows that $W_{\lambda'} \geq W_\lambda$ if $\lambda \geq \lambda'$ or in other words that W_λ is a monotonically decreasing function of λ which can be written as

$$\frac{\mathrm{d} W_\lambda}{\mathrm{d} \lambda} \leq 0 \tag{1.66}$$

[12] Since when the coupling parameter goes to zero, $\lambda = 0$, we recover all the KS quantities introduced so far, the subscripts "s" and "0" will be used interchangebly hereafter unless otherwise specified.

assuming differentiability of the adiabatic connection integrand at any λ.

Its small λ expansion reads [32]

$$W_{\lambda\to 0}[n] = E_x[n] + \sum_{n=2}^{\infty} n\, E_c^{GLn}\, \lambda^{n-1}, \tag{1.67}$$

where the first term is simply the exchange energy expression as defined in Hartree-Fock theory applied to the KS orbitals (therefore becoming a density functional)

$$E_x = -\sum_{i=1,j>i}^{N} \int \frac{\psi_i^*(\boldsymbol{x})\psi_j^*(\boldsymbol{x})\psi_i(\boldsymbol{x}')\psi_j(\boldsymbol{x}')}{|\boldsymbol{r}-\boldsymbol{r}'|} \mathrm{d}\boldsymbol{x}\mathrm{d}\boldsymbol{x}'. \tag{1.68}$$

Because E_x is order constant in λ, it is also the value of W_λ when $\lambda = 0$, i.e. $E_x = W_0$.

The next terms, E_c^{GLn}, are the coefficients of the Görling-Levy perturbation series [32], which are very similar to the Möller-Plesset coefficients but contain extra corrections coming from the constraint that the density be the target one at all orders in λ.

The first one of them is order linear in λ and it corresponds to half the slope of W_λ in zero, $E_c^{GL2} = \frac{W_0'}{2}$, and is calculated from

$$E_c^{GL2}[n] = -\frac{1}{4}\sum_{abij} \frac{|\langle\psi_i\psi_j||\psi_a\psi_b\rangle|^2}{\epsilon_a+\epsilon_b-\epsilon_i-\epsilon_j} - \sum_{ia} \frac{|\langle\psi_i|\hat{v}_x^{\mathrm{KS}} - \hat{v}_x^{\mathrm{HF}}|\psi_a\rangle|^2}{\epsilon_a-\epsilon_i} \tag{1.69}$$

where $i, j, \cdots$ and $a, b, \cdots$ are occupied and virtual KS orbitals, respectively, and where $\hat{v}_x^{\mathrm{KS}} = v_x(\boldsymbol{r})$ is the functional derivative of the exchange energy, $v_x(\boldsymbol{r}) = \frac{\delta E_x}{\delta n}(\boldsymbol{r})$, while $\hat{v}_x^{\mathrm{HF}}$ is an integral kernel, namely $\left(\hat{v}_x^{\mathrm{HF}}\psi_i\right)(\mathbf{x}) := \int v_x^{\mathrm{HF}}(\mathbf{x},\mathbf{x}')\psi_i(\mathbf{x}')\mathrm{d}\mathbf{x}'$ with $v_x^{\mathrm{HF}}(\mathbf{x},\mathbf{x}') = -\sum_{j=1}^{N} \frac{\psi_j^*(\mathbf{x}')\psi_j(\mathbf{x})}{|\boldsymbol{r}-\boldsymbol{r}'|}$. As for the exchange energy, every term is evaluated on the KS orbitals.[13]

Subsequent terms grow in complexity and their computation is absent from the literature.

The large λ expansion of W_λ reads [34]

$$W_{\lambda\to\infty}[n] = W_\infty[n] + \frac{1}{\sqrt{\lambda}} W_\infty'[n] + \cdots \tag{1.70}$$

[13] Rigourously, to evaluate e.g. W_0', KS orbitals that are correct only up to first order, i.e. orbitals coming from an EXX OEP procedure [33], are sufficient; and at every order it is sufficient to have the orbitals coming from a localised potential exact up to the former order; of course the exact KS orbitals (correct at all orders) would be perfectly fine.

However, a clear distinction has to be made among KS and HF orbitals: these latters come from a non-local potential and do not enter in any of the expressions pertaining the DFT adiabatic connection integrand.

where the density functionals W_∞ and W'_∞ will be introduced and discussed in chapter 3.

Let us only remark here that, because in the large λ expansion there is no linear term in λ, despite its notation (now established in the literature), the coefficient of the next leading order term does *not* correspond to the value of the slope of W_λ, i.e. $W'_\infty \neq \left.\frac{\mathrm{d}W_\lambda}{\mathrm{d}\lambda}\right|_{\lambda\to\infty}$.

Finally, W_λ satisfies the so-called Lieb-Oxford (LO) bound [35]

$$W_\lambda[n] \geq -C_{\mathrm{LO}} \int n(\boldsymbol{r})^{\frac{4}{3}}\,\mathrm{d}\boldsymbol{r} \tag{1.71}$$

At the state of the art, the LO constant, C_{LO}, is known to be rigourously 1.4442 [36]$\leq C_{\mathrm{LO}} \leq 1.6358$ [37].

For a given density profile, the smallest value of W_λ (the largest one in magnitude) is the quantity $\lim_{\lambda\to\infty} \lambda\, E_{xc}[n_{\frac{1}{\lambda}}]$ [38] where $n_\gamma(\boldsymbol{r})$ is the uniformly scaled density, defined as

$$n_\gamma(\boldsymbol{r}) \coloneqq \gamma^3 n(\gamma\boldsymbol{r}). \tag{1.72}$$

It also coincides with W_∞ to be discussed in chapter 3.

For densities coming from different numbers of electrons, N, it can be proven that the LO constant, C_{LO}^N, increases with N, $C_{\mathrm{LO}}^N \leq C_{\mathrm{LO}}^{N+1}$, meaning that any value found for finite N is a lower bound on the optimal constant.

2

Conditional probability and exact decomposition of the λ–dependent external potential

The theory of conditional probability amplitudes first developed by Hunter [39, 40] offers an excellent tool for deriving an exact differential equation for the square root of the density.
We will start by deriving an exact decomposition of the effective potential for the square root of the density (introduced in eq 2.11) in terms of correlated density matrices, then, we will present the same decomposition in terms of KS density matrices and, lastly, we will generalise it to density matrices at any value of the coupling parameter and hereupon derive scaling relations.

2.1. An effective equation for the square root of the density

Let us recall eq 1.1 and let us relabel $\hat{H}$ as $\hat{H}^N(\boldsymbol{r},\boldsymbol{r}_2,\cdots,\boldsymbol{r}_N)$ and write $|\Psi\rangle$ as $\Psi^N(\boldsymbol{r}\sigma,\mathbf{x}_2,\cdots,\mathbf{x}_N)$ where we have taken electron 1 as the reference electron, as in eq 1.3. Note furthermore that we shall only be concerned with the GS wavefunction and energy, sometimes called Ψ_0 and E_0. We shall omit the "0" subscript for simplification of the notation. To be more precise, as we are going to generalise the treatment of this section to any Hamiltonian of the likes of eq 1.54 in section 2.3, a subscript is rather being used to identify the coupling strength.

Following references [41, 42], we partition the Hamiltonian for N electrons in three parts: the Hamiltonian for $N-1$ electrons (with $i=2,...,N$), the one-body terms acting on electron 1, and the remaining interaction between electron 1 and all the others

$$\hat{H}^N(\boldsymbol{r},\boldsymbol{r}_2,\cdots,\boldsymbol{r}_N)=\hat{H}^{N-1}(\boldsymbol{r}_2,\cdots,\boldsymbol{r}_N)-\frac{\nabla_{\boldsymbol{r}}^2}{2}+v(\boldsymbol{r})+\sum_{i=2}^{N}\frac{1}{|\boldsymbol{r}-\boldsymbol{r}_i|}. \tag{2.1}$$

In the same spirit, we factorize the N-particle wavefunction

$$\Psi^N(\boldsymbol{r}\sigma,\mathbf{x}_2,\cdots,\mathbf{x}_N)=\sqrt{\frac{n(\boldsymbol{r})}{N}}\,\Phi(\sigma,\mathbf{x}_2,\cdots,\mathbf{x}_N;\boldsymbol{r}) \tag{2.2}$$

into the so-called *marginal* and *conditional (probability) amplitudes*, represented respectively by the square root of the density as a function of coordinates of electron 1 divided by the number of electrons N and a function of the other $N-1$ electronic positions, $\Phi(\sigma,\mathbf{x}_2,\cdots,\mathbf{x}_N;\boldsymbol{r})$, which depends on electron 1 in a parametric way.
Physically speaking, $\Phi(\sigma,\mathbf{x}_2,\cdots,\mathbf{x}_N;\boldsymbol{r})$ is a sort of $(N-1)$-particle wavefunction that describes how the electronic cloud of $N-1$ electrons readjusts as a function of the position of electron 1. Indeed, its modulus square integrates to one for any value of the position vector of the reference electron

$$\int|\Phi(\sigma,\mathbf{x}_2,\cdots,\mathbf{x}_N;\boldsymbol{r})|^2\,\mathrm{d}\sigma\mathrm{d}\mathbf{x}_2\cdots\mathrm{d}\mathbf{x}_N=1\quad\forall\,\boldsymbol{r}, \tag{2.3}$$

as it is easily verified by using the modulus squared of eq 2.2 and the definition of the electronic density $n(\boldsymbol{r})$, eq 1.3.
We now apply eq 2.1 to eq 2.2,

$$\left(\hat{H}^{N-1}(\boldsymbol{r}_2,\cdots,\boldsymbol{r}_N)-\frac{\nabla_{\boldsymbol{r}}^2}{2}+v(\boldsymbol{r})+\sum_{i=2}^{N}\frac{1}{|\boldsymbol{r}-\boldsymbol{r}_i|}\right)\quad\sqrt{\tfrac{n(\boldsymbol{r})}{N}}\,\Phi(\sigma,\mathbf{x}_2,\cdots,\mathbf{x}_N;\boldsymbol{r})\quad=$$
$$=E^N\quad\sqrt{\tfrac{n(\boldsymbol{r})}{N}}\,\Phi(\sigma,\mathbf{x}_2,\cdots,\mathbf{x}_N;\boldsymbol{r}) \tag{2.4}$$

and then multiply to the left both members by $\Phi(\sigma,\mathbf{x}_2,\cdots,\mathbf{x}_N;\boldsymbol{r})$ and integrate over the spin variable of the reference electron[1] and the spatial and spin variables of

[1] Of course, it is also possible to make the exact same treatment spin-resolved: rewriting the conditional amplitude as a parametric function of both position vector and spin variable, $\Phi(\mathbf{x}_2,\cdots,\mathbf{x}_N;\boldsymbol{r}\sigma)$, dropping the summation over σ and defining all the one-body potentials appearing in eq 2.7, as functions of the combined spin and spatial coordinates $\boldsymbol{x}$.

electrons $2,\cdots,N$,

$$\begin{aligned}\sqrt{\frac{n(\boldsymbol{r})}{N}}\int \Phi^*(\sigma,\mathbf{x}_2,\cdots,\mathbf{x}_N;\boldsymbol{r})\hat{H}^{N-1}(\boldsymbol{r}_2,\cdots,\boldsymbol{r}_N)\Phi(\sigma,\mathbf{x}_2,\cdots,\mathbf{x}_N;\boldsymbol{r})\,\mathrm{d}\sigma\mathrm{d}\mathbf{x}_2\cdots\mathrm{d}\mathbf{x}_N+\\ -\int \Phi^*(\sigma,\mathbf{x}_2,\cdots,\mathbf{x}_N;\boldsymbol{r})\frac{\nabla^2_{\boldsymbol{r}}}{2}\sqrt{\frac{n(\boldsymbol{r})}{N}}\Phi(\sigma,\mathbf{x}_2,\cdots,\mathbf{x}_N;\boldsymbol{r})\,\mathrm{d}\sigma\mathrm{d}\mathbf{x}_2\cdots\mathrm{d}\mathbf{x}_N+\\ +v(\boldsymbol{r})\sqrt{\frac{n(\boldsymbol{r})}{N}}\int |\Phi(\sigma,\mathbf{x}_2,\cdots,\mathbf{x}_N;\boldsymbol{r})|^2\,\mathrm{d}\sigma\mathrm{d}\mathbf{x}_2\cdots\mathrm{d}\mathbf{x}_N+\\ +\sqrt{\frac{n(\boldsymbol{r})}{N}}\int \Phi^*(\sigma,\mathbf{x}_2,\cdots,\mathbf{x}_N;\boldsymbol{r})\left(\sum_{i=2}^{N}\frac{1}{|\boldsymbol{r}-\boldsymbol{r}_i|}\right)\Phi(\sigma,\mathbf{x}_2,\cdots,\mathbf{x}_N;\boldsymbol{r})\,\mathrm{d}\sigma\mathrm{d}\mathbf{x}_2\cdots\mathrm{d}\mathbf{x}_N=\\ =E^N\sqrt{\frac{n(\boldsymbol{r})}{N}}\int |\Phi(\sigma,\mathbf{x}_2,\cdots,\mathbf{x}_N;\boldsymbol{r})|^2\,\mathrm{d}\sigma\mathrm{d}\mathbf{x}_2\cdots\mathrm{d}\mathbf{x}_N.\end{aligned}$$

Now we use eq. 2.3, which tells us that the gradient $\nabla_{\boldsymbol{r}}$ and the Laplacian $\nabla^2_{\boldsymbol{r}}$ applied to its left-hand-side is zero. This, in turn, implies for real wavefunctions, i.e. for conditional amplitudes of the kind $\Phi(\sigma,\mathbf{x}_2,\cdots,\mathbf{x}_N;\boldsymbol{r})=e^{i\theta}R(\sigma,\{\boldsymbol{x}_i\};\boldsymbol{r})$ where the imaginary part is just a trivial phase factor onto which the gradient has no action, that the mixed terms are zero, i.e.

$$\begin{aligned}\int \Phi^*(\sigma,\mathbf{x}_2,\cdots,\mathbf{x}_N;\boldsymbol{r})\frac{\nabla^2_{\boldsymbol{r}}}{2}\sqrt{\frac{n(\boldsymbol{r})}{N}}\Phi(\sigma,\mathbf{x}_2,\cdots,\mathbf{x}_N;\boldsymbol{r})\,\mathrm{d}\sigma\mathrm{d}\mathbf{x}_2\cdots\mathrm{d}\mathbf{x}_N=\\ \sqrt{\frac{n(\boldsymbol{r})}{N}}\int \Phi^*(\sigma,\mathbf{x}_2,\cdots,\mathbf{x}_N;\boldsymbol{r})\frac{\nabla^2_{\boldsymbol{r}}}{2}\Phi(\sigma,\mathbf{x}_2,\cdots,\mathbf{x}_N;\boldsymbol{r})\,\mathrm{d}\sigma\mathrm{d}\mathbf{x}_2\cdots\mathrm{d}\mathbf{x}_N+\frac{\nabla^2_{\boldsymbol{r}}}{2}\sqrt{\frac{n(\boldsymbol{r})}{N}}\end{aligned}\tag{2.5}$$

and moreover that

$$\begin{aligned}\int \Phi(\sigma,\mathbf{x}_2,\cdots,\mathbf{x}_N;\boldsymbol{r})\nabla^2_{\boldsymbol{r}}\Phi(\sigma,\mathbf{x}_2,\cdots,\mathbf{x}_N;\boldsymbol{r})\,\mathrm{d}\sigma\mathrm{d}\mathbf{x}_2\cdots\mathrm{d}\mathbf{x}_N=\\ -\int |\nabla_{\boldsymbol{r}}\Phi(\sigma,\mathbf{x}_2,\cdots,\mathbf{x}_N;\boldsymbol{r})|^2\,\mathrm{d}\sigma\mathrm{d}\mathbf{x}_2\cdots\mathrm{d}\mathbf{x}_N.\end{aligned}\tag{2.6}$$

Therefore considering the properties of $\Phi(\sigma,\mathbf{x}_2,\cdots,\mathbf{x}_N;\boldsymbol{r})$ expressed in eqs 2.3, and 2.6, and simplifying out the normalization factor from both sides, we see that eq 2.4

becomes

$$\left(\int \Phi^*(\sigma,\mathbf{x}_2,\cdots,\mathbf{x}_N;\boldsymbol{r})\hat{H}^{N-1}(\boldsymbol{r}_2,\cdots,\boldsymbol{r}_N)\Phi(\sigma,\mathbf{x}_2,\cdots,\mathbf{x}_N;\boldsymbol{r})\,\mathrm{d}\sigma\mathrm{d}\mathbf{x}_2\cdots\mathrm{d}\mathbf{x}_N\right.$$
$$-\frac{\nabla_{\boldsymbol{r}}^2}{2}+v(\boldsymbol{r})+\frac{1}{2}\int|\nabla_{\boldsymbol{r}}\Phi(\sigma,\mathbf{x}_2,\cdots,\mathbf{x}_N;\boldsymbol{r})|^2\,\mathrm{d}\sigma\mathrm{d}\mathbf{x}_2\cdots\mathrm{d}\mathbf{x}_N+$$
$$\left.+\int\left(\sum_{i=2}^{N}\frac{|\Phi(\sigma,\mathbf{x}_2,\cdots,\mathbf{x}_N;\boldsymbol{r})|^2}{|\boldsymbol{r}-\boldsymbol{r}_i|}\right)\mathrm{d}\sigma\mathrm{d}\mathbf{x}_2\cdots\mathrm{d}\mathbf{x}_N\right)\sqrt{n(\boldsymbol{r})}=$$
$$=E^N\sqrt{n(\boldsymbol{r})},$$

which is a Schrödinger-like equation for the square root of the density, as we have a kinetic term plus other terms that are multiplicative potentials, being pure functions of the position vector.
Collecting all local potentials in one,

$$\begin{aligned}\tilde{v}_{\mathrm{eff}}(\boldsymbol{r}) \quad = \quad & \int\Phi^*(\sigma,\mathbf{x}_2,\cdots,\mathbf{x}_N;\boldsymbol{r})\hat{H}^{N-1}(\boldsymbol{r}_2,\cdots,\boldsymbol{r}_N)\Phi(\sigma,\mathbf{x}_2,\cdots,\mathbf{x}_N;\boldsymbol{r})\,\mathrm{d}\sigma\mathrm{d}\mathbf{x}_2\cdots\mathrm{d}\mathbf{x}_N+\\
&+\frac{1}{2}\int|\nabla_{\boldsymbol{r}}\Phi(\sigma,\mathbf{x}_2,\cdots,\mathbf{x}_N;\boldsymbol{r})|^2\,\mathrm{d}\sigma\mathrm{d}\mathbf{x}_2\cdots\mathrm{d}\mathbf{x}_N+v(\boldsymbol{r})+\\
&+\int\Phi^*(\sigma,\mathbf{x}_2,\cdots,\mathbf{x}_N;\boldsymbol{r})\left(\sum_{i=2}^{N}\frac{1}{|\boldsymbol{r}-\boldsymbol{r}_i|}\right)\Phi(\sigma,\mathbf{x}_2,\cdots,\mathbf{x}_N;\boldsymbol{r})\,\mathrm{d}\sigma\mathrm{d}\mathbf{x}_2\cdots\mathrm{d}\mathbf{x}_N,\end{aligned}\tag{2.7}$$

it follows

$$-\frac{\nabla^2}{2}\sqrt{n(\boldsymbol{r})}+\tilde{v}_{\mathrm{eff}}(\boldsymbol{r})\sqrt{n(\boldsymbol{r})}=E^N\sqrt{n(\boldsymbol{r})}.\tag{2.8}$$

2.1.1. The Density Decay

Equation 2.8 proves itself useful, for example, for deriving the decaying behaviour of the density in finite systems (atoms and molecules) when $|\boldsymbol{r}|$ is very far from the barycenter of all nuclear charges.
For a general single-particle Schrödinger equation,

$$-\frac{\nabla^2}{2}\phi(\boldsymbol{r})+v(\boldsymbol{r})\phi(\boldsymbol{r})=\epsilon\phi(\boldsymbol{r}),\tag{2.9}$$

we have that $\phi(\boldsymbol{r})\sim e^{-\sqrt{-2\epsilon}|\boldsymbol{r}|}$ when $|\boldsymbol{r}|\to\infty$ only if $v(|\boldsymbol{r}|\to\infty)=0$. If, instead, $v(|\boldsymbol{r}|\to\infty)=C$ then, for $|\boldsymbol{r}|\to\infty$, $\phi(\boldsymbol{r})\sim e^{-\sqrt{2(-\epsilon+C)}|\boldsymbol{r}|}$. This means that, if we want to obtain the asymptotic decay of $n(\boldsymbol{r})$ from eq 2.8, we have to find that constant C that shifts the effective potential $\tilde{v}_{\mathrm{eff}}(\boldsymbol{r})$ so that it vanishes at large distances (or equivalently the constant that appears in the exponential together with $-\epsilon$).

Looking at the different pieces appearing in eq 2.7, we see that the external potential

$$v(\boldsymbol{r}) = -\sum_{A}^{N} \frac{Z_A}{|\boldsymbol{r} - \mathbf{R}_A|}$$

and the last contributing potential

$$\int \Phi^*(\sigma, \mathbf{x}_2, \cdots, \mathbf{x}_N; \boldsymbol{r}) \left(\sum_{i=2}^{N} \frac{1}{|\boldsymbol{r} - \boldsymbol{r}_i|} \right) \Phi(\sigma, \mathbf{x}_2, \cdots, \mathbf{x}_N; \boldsymbol{r}) \, \mathrm{d}\sigma \mathrm{d}\mathbf{x}_2 \cdots \mathrm{d}\mathbf{x}_N,$$

clearly vanish when $\boldsymbol{r}$ is far away from all nuclear charges (i.e. in that region of space where the density is negligeable).
Concerning the other terms, we can use physical arguments to support the following statements, leaving room for more rigorous derivations.
For the term $\int \Phi^*(\sigma, \mathbf{x}_2, \cdots, \mathbf{x}_N; \boldsymbol{r}) \hat{H}^{N-1}(\boldsymbol{r}_2, \cdots, \boldsymbol{r}_N) \Phi(\sigma, \mathbf{x}_2, \cdots, \mathbf{x}_N; \boldsymbol{r}) \, \mathrm{d}\sigma \mathrm{d}2 ... \mathrm{d}N$, we expect that the conditional amplitude when electron 1 is very far from the nuclei will collapse to the ground-state wavefunction of the cation, $\Psi^{N-1}(\mathbf{x}_2, \cdots, \mathbf{x}_N)$ [43], if this is accessible,[2] and that, consequently, the expectation value accounted for in that term will collapse to the ground-state energy of the cation, E^{N-1}.
If this is the case we may also expect the term $\int |\nabla_{\boldsymbol{r}} \Phi(\sigma, \mathbf{x}_2, \cdots, \mathbf{x}_N; \boldsymbol{r})|^2 \, \mathrm{d}\sigma \mathrm{d}\mathbf{x}_2 \cdots \mathrm{d}\mathbf{x}_N$ to vanish since the conditional amplitude essentially becomes insensitive for a change in the position of electron 1 very far away from the nuclei. A case in which this assumption does not hold is the less usual case of nodal planes extending to infinity [44, 45].
Therefore we can define $v_{\mathrm{eff}}(\boldsymbol{r}) = \tilde{v}_{\mathrm{eff}}(\boldsymbol{r}) - E_0^{N-1}$, in which the first term now becomes

$$\int \Phi^*(\sigma, \mathbf{x}_2, \cdots, \mathbf{x}_N; \boldsymbol{r}) \left(\hat{H}^{N-1}(\boldsymbol{r}_2, \cdots, \boldsymbol{r}_N) - E^{N-1} \right) \Phi(\sigma, \mathbf{x}_2, \cdots, \mathbf{x}_N; \boldsymbol{r}) \, \mathrm{d}\sigma \mathrm{d}\mathbf{x}_2 \cdots \mathrm{d}\mathbf{x}_N, \tag{2.10}$$

so that the corresponding equation for $\sqrt{n(\boldsymbol{r})}$ reads

$$-\frac{\nabla^2}{2} \sqrt{n(\boldsymbol{r})} + v_{\mathrm{eff}}(\boldsymbol{r}) \sqrt{n(\boldsymbol{r})} = \left(E^N - E^{N-1} \right) \sqrt{n(\boldsymbol{r})}. \tag{2.11}$$

Considering that $\left(E_0^N - E_0^{N-1} \right) = -I_p$ (the first ionization potential), this derivation gives a clear physical grasp of where the exponential decay of the density with the square root of the first ionization potential comes from

$$\sqrt{n(\boldsymbol{r})} \sim e^{-\sqrt{2I_p}|\boldsymbol{r}|}. \tag{2.12}$$

[2] Meaning that, for example, the spin ground state of the cation does not require spin flips with respect to the one of the neutral system, otherwise the relaxation to the ground state cannot occur.

2.1.2. Effective one-body potentials

We now take a closer look at the three terms found for the effective potential $v_{\text{eff}}(\boldsymbol{r})$ in the previous section.

The term with the easiest physical interpretation is the so-called conditional potential

$$v_{cond}(\boldsymbol{r}) \coloneqq \int \Phi^*(\sigma, \mathbf{x}_2, \cdots, \mathbf{x}_N; \boldsymbol{r}) \left(\sum_{i=2}^{N} \frac{1}{|\boldsymbol{r} - \boldsymbol{r}_i|} \right) \Phi(\sigma, \mathbf{x}_2, \cdots, \mathbf{x}_N; \boldsymbol{r}) \, \mathrm{d}\sigma \mathrm{d}\mathbf{x}_2 \cdots \mathrm{d}\mathbf{x}_N. \tag{2.13}$$

Using the definition of the pair density, $P_2(\boldsymbol{r}, \boldsymbol{r}')$

$$P_2(\boldsymbol{r}, \boldsymbol{r}') \coloneqq N(N-1) \int |\Psi(\boldsymbol{r}\sigma, \boldsymbol{r}'\sigma', \cdots, \boldsymbol{x}_N)|^2 \mathrm{d}\sigma \mathrm{d}\sigma' \mathrm{d}\boldsymbol{x}_3 \cdots \mathrm{d}\boldsymbol{x}_N, \tag{2.14}$$

where we have relabeled $\boldsymbol{x}_2 = \boldsymbol{r}'\sigma'$, we can equivalently write

$$v_{cond}(\boldsymbol{r}) = \int \frac{P_2(\boldsymbol{r}, \boldsymbol{r}')}{|\boldsymbol{r} - \boldsymbol{r}'|} \mathrm{d}\boldsymbol{r}' \tag{2.15}$$

This potential is traditionally considered as made up of two different contributions, i.e. $v_{cond}(\boldsymbol{r}) = v_{\text{H}}(\boldsymbol{r}) + v_{xc\text{-}hole}(\boldsymbol{r})$, where v_{H} has been defined in sec 1.3.2, while to define $v_{xc\text{-}hole}$ we use the definition of the exchange-correlation pair-correlation function, $g_{xc}(\boldsymbol{r}, \boldsymbol{r}')$,

$$g_{xc}(\boldsymbol{r}, \boldsymbol{r}') \coloneqq \frac{P_2(\boldsymbol{r}, \boldsymbol{r}')}{n(\boldsymbol{r}) n(\boldsymbol{r}')} - 1. \tag{2.16}$$

Then

$$v_{xc,hole}(\mathbf{r}) = \int n(\mathbf{r}') \frac{g_{xc}(\mathbf{r}, \mathbf{r}')}{|\boldsymbol{r} - \boldsymbol{r}'|} \mathrm{d}\boldsymbol{r}'. \tag{2.17}$$

The numerator in eq 2.17 is often called the exchange correlation hole

$$h_{xc}(\boldsymbol{r}, \boldsymbol{r}') \coloneqq n(\mathbf{r}') \, g_{xc}(\mathbf{r}, \mathbf{r}').^{3} \tag{2.18}$$

Thus, $v_{cond}(\boldsymbol{r})$ is the electrostatic potential of the density depleted of its exchange correlation hole.

The term that comes from the kinetic energy operator acting on the conditional amplitude

$$v_{kin}(\boldsymbol{r}) \coloneqq \frac{1}{2} \int |\nabla_{\boldsymbol{r}} \Phi(\sigma, \mathbf{x}_2, \cdots, \mathbf{x}_N; \boldsymbol{r})|^2 \, \mathrm{d}\sigma \mathrm{d}\mathbf{x}_2 \cdots \mathrm{d}\mathbf{x}_N \tag{2.19}$$

is called kinetic potential.

[3] Note that, as the pair density is symmetric, i.e. $P_2(\boldsymbol{r}, \boldsymbol{r}') = P_2(\boldsymbol{r}', \boldsymbol{r})$, also $g_{xc}(\mathbf{r}, \mathbf{r}')$ is so, while $h_{xc}(\boldsymbol{r}, \boldsymbol{r}')$, being the product of a symmetric function of $(\boldsymbol{r}, \boldsymbol{r}')$ and the density in one point $(\boldsymbol{r}')$ is no longer symmetric.

Using the definition of the one-body reduced density matrix (1RDM)

$$\gamma(\boldsymbol{r},\boldsymbol{r}') := N\int \Psi^*(\boldsymbol{r}\sigma,\boldsymbol{x}_2,\cdots,\boldsymbol{x}_N)\Psi(\boldsymbol{r}'\sigma,\boldsymbol{x}_2,\cdots,\boldsymbol{x}_N)\mathrm{d}\sigma\mathrm{d}\mathbf{x}_2\cdots\mathrm{d}\mathbf{x}_N \tag{2.20}$$

it can be also expressed as

$$v_{kin}(\boldsymbol{r}) = \frac{\nabla_{\boldsymbol{r}}\cdot\nabla_{\boldsymbol{r}'}\gamma(\boldsymbol{r},\boldsymbol{r}')|_{\boldsymbol{r}'=\boldsymbol{r}}}{2\,n(\boldsymbol{r})} - \frac{|\nabla n(\boldsymbol{r})|^2}{8n(\boldsymbol{r})^2}. \tag{2.21}$$

Finally, the term coming from the $N-1$ Hamiltonian is equal to

$$\begin{aligned} v_{N-1}(\boldsymbol{r}) \quad = \quad & \int \Phi^*(\sigma,\mathbf{x}_2,\cdots,\mathbf{x}_N;\boldsymbol{r})\,\hat{H}^{N-1}(\boldsymbol{r}_2,\cdots,\boldsymbol{r}_N)\,\Phi(\sigma,\mathbf{x}_2,\cdots,\mathbf{x}_N;\boldsymbol{r})\mathrm{d}\sigma\mathrm{d}\mathbf{x}_2\cdots\mathrm{d}\mathbf{x}_N \\ & -E^{N-1} \end{aligned} \tag{2.22}$$

It is evident that these three potentials are always positive, as in eqs 2.13 and 2.19 the integrands are squared quantities, and the integrand in eq 2.22 must be positive by virtue of the variational principle.
In a pure Hohenberg-Kohn-DFT approach (also called orbital-free DFT, because it does not use orbitals, but only the density itself), these three terms give the effective potential for the square root of the density. Unfortunately, orbital-free DFT suffers from the lack of an accurate kinetic energy functional as already discussed (see sec 1.3).
To obtain an expression for the exchange-correlation potential in the KS scheme we need to use the KS reference state and energy, as explained in the next section.

2.2. Effective potential for the square root of the density in terms of KS density matrices

Suppose that, for the same physical density n, we have found the exact KS potential, v_s. The KS Hamiltonian is then given by

$$\hat{H}_s^N = -\sum_i^N \frac{\nabla^2_{\boldsymbol{r}_i}}{2} + \sum_{i=1}^N v_s(\boldsymbol{r}_i) \tag{2.23}$$

which has Ψ_s^N as its ground state.

If we repeat the same manipulations of section 2.1 starting by a partitioned KS Hamiltonian and a KS conditional amplitude that mirror eqs 2.1 and 2.2, i.e.

$$\hat{H}_s^N(\boldsymbol{r}_1,\cdots,\boldsymbol{r}_n) = \hat{H}_{s*}^{N-1}(\boldsymbol{r}_2,\cdots,\boldsymbol{r}_N) - \frac{\nabla^2_{\boldsymbol{r}}}{2} + v_s(\boldsymbol{r}), \tag{2.24}$$

$$\Psi_s^N(\boldsymbol{x}_1,\cdots,\boldsymbol{x}_N) = \sqrt{\frac{n(\boldsymbol{r})}{N}}\,\Phi_s(\sigma,\boldsymbol{x}_2,\cdots,\boldsymbol{x}_N;\boldsymbol{r}), \tag{2.25}$$

we get:

$$v_{s,kin}(\boldsymbol{r}) = \frac{1}{2}\int |\nabla_{\boldsymbol{r}}\Phi_s(\sigma,\boldsymbol{x}_2,\cdots,\boldsymbol{x}_N;\boldsymbol{r})|^2\,\mathrm{d}\sigma\mathrm{d}\boldsymbol{x}_2\cdots\mathrm{d}\boldsymbol{x}_N, \tag{2.26}$$

which can be written in terms of the H occupied KS orbitals,

$$v_{s,kin}(\boldsymbol{r}) = \frac{1}{2}\sum_{i=1}^{H}|\nabla\frac{\psi_i(\boldsymbol{r})}{\sqrt{n(\boldsymbol{r})}}|^2 = \frac{1}{2n(\boldsymbol{r})}\sum_{i=1}^{H}|\nabla\psi_i(\boldsymbol{r})|^2 - \frac{|\nabla n(\boldsymbol{r})|^2}{8n(\boldsymbol{r})^2}, \tag{2.27}$$

and

$$\begin{aligned} v_{s,N-1}(\boldsymbol{r}) \quad = \quad & \int \Phi_s^*(\sigma,\boldsymbol{x}_2,\cdots,\boldsymbol{x}_N;\boldsymbol{r})\,\hat{H}_{s*}^{N-1}(\boldsymbol{r}_2,\cdots,\boldsymbol{r}_N)\,\Phi_s(\sigma,\boldsymbol{x}_2,\cdots,\boldsymbol{x}_N;\boldsymbol{r})\,\mathrm{d}\sigma\mathrm{d}\boldsymbol{x}_2\cdots\mathrm{d}\boldsymbol{x}_N \\ & -E_{s*}^{N-1} \end{aligned} \tag{2.28}$$

Again, this term can be written using the KS orbitals and orbital energies,

$$v_{s,N-1}(\boldsymbol{r}) = \sum_{i=1}^{H}(\epsilon_H - \epsilon_i)\frac{|\psi_i(\boldsymbol{r})|^2}{n(\boldsymbol{r})}, \tag{2.29}$$

where ϵ_H is the energy of the KS highest occupied molecular orbital (HOMO).

A critical remark is due here: contrary to the fully interacting case, $\hat{H}_{s*}^{N-1}$ is *not* the KS Hamiltonian for the $N-1$-particle system, since the KS potential is the one obtained for the N-particles problem, which is not the one that would be obtained for the ground state density of the cation.[4] Analogously, the energy term E_{s*}^{N-1} is *not* the KS energy of the $N-1$-particle system but rather the sum of all the $H-1$ orbital energies ϵ_i of the N-particles problem.

The effective KS potential for the square root of the density is nothing but the sum of the foreshown potentials plus the KS potential itself (the conditional potential being absent as there is no Coulomb repulsion between the particles),

$$v_{\mathrm{eff}}(\boldsymbol{r}) = v_s(\boldsymbol{r}) + v_{s,kin}(\boldsymbol{r}) + v_{s,N-1}(\boldsymbol{r}). \tag{2.30}$$

2.2.1. Exact decomposition of the XC potential into physically transparent terms

We compare now the resulting effective equations obtained in the previous sections [42, 46–48].

[4] Think about the simple example of the He atom ($N=2$): the exact KS potential must yield a single orbital, doubly occupied, equal to $\sqrt{\frac{n(\boldsymbol{r})}{2}}$, where $n(\boldsymbol{r})$ is the density of the He atom. When we remove one electron from this $N=2$ KS system, we have the same orbital as before, now singly occupied. This orbital is different than the square root of the density of He^+, which is a single exponential. In fact, the exact KS potential of He^+ is simply $-2/r$, which is definitely different from the KS potential of He.

From sec 2.1 we have

$$-\frac{\nabla^2}{2}\sqrt{n(\boldsymbol{r})}+\big(\,v(\boldsymbol{r})+v_{kin}(\boldsymbol{r})+v_{N-1}(\boldsymbol{r})+v_{cond}(\boldsymbol{r})\big)\sqrt{n(\boldsymbol{r})}=-I_P\sqrt{n(\boldsymbol{r})}, \tag{2.31}$$

while from sec 2.2 we have

$$-\frac{\nabla^2}{2}\sqrt{n(\boldsymbol{r})}+\big(v_s(\boldsymbol{r})+v_{s,kin}(\boldsymbol{r})+v_{s,N-1}(\boldsymbol{r})\big)\sqrt{n(\boldsymbol{r})}=\epsilon_H\sqrt{n(\boldsymbol{r})}. \tag{2.32}$$

The density can be written in terms of the KS orbitals as $n(\boldsymbol{r})=\sum_{i=1}^{H}|\psi_i(\boldsymbol{r})|^2$, and the decay of the KS orbitals is governed by their respective eigenvalues. The most diffuse orbital, i.e. the one with the smallest occupied orbital energy in absolute value, is the one of the HOMO. Thus, for large $|\boldsymbol{r}|$, the density decay will be dominated by the uppermost orbital, $\psi_N(\boldsymbol{r})$, which leads to the identification $\epsilon_H=-I_p$ [49, 50].
Then, the r.h.s of eqs 2.31 and 2.32 are the same and we can compare the two clusters of local potentials in brackets and derive thereby an exact expression for the KS potential,

$$\begin{aligned} v_s(\boldsymbol{r}) &= v(\boldsymbol{r})+v_{\mathrm{H}}(\boldsymbol{r})+v_{xc}(\boldsymbol{r})= \\ &= v(\boldsymbol{r})+v_{kin}(\boldsymbol{r})+v_{N-1}(\boldsymbol{r})+v_{cond}(\boldsymbol{r})-v_{s,kin}(\boldsymbol{r})-v_{s,N-1}(\boldsymbol{r}) \end{aligned} \tag{2.33}$$

Simplifying out the external potential from both sides and solving w.r.t. v_{xc}, we have

$$v_{xc}(\boldsymbol{r})=v_{kin}(\boldsymbol{r})-v_{s,kin}(\boldsymbol{r})+v_{N-1}(\boldsymbol{r})-v_{s,N-1}(\boldsymbol{r})+v_{xc\text{-}hole}(\boldsymbol{r}), \tag{2.34}$$

Equation 2.34 gives an exact expression for the XC potential in terms of wave-function quantities (one-body-reduced density matrix and pair density) and KS quantities (orbitals and orbital energies). Some of these components embody non-intuitive, though typical, features of the exact KS potential.
As an example, in fig 2.1 we have sketched how the exact KS potential for a stretched heteronuclear molecule (the simple case of LiH) looks like. The two separated atoms have highest occupied atomic orbitals with different energies, the 2s orbital of Li being higher in energy than the 1s orbital of H. Another way to see this is that the more electronegative atom, the hydrogen, can attract some charge from the less electronegative one. To bring the chemical potential of the two atoms at the same level, the exact KS potential builds an appropriate step in the midbond and another one far away from the molecule on the other side of the hydrogen atom in order to bring the potential to zero again. The step height is exactly the difference between the ionization potentials of the two atoms. This way, the HOMO energies of the two atoms forming the molecule are equalized, as it should be for a doubly occupied bonding orbital in the spin-restricted framework (i.e., without

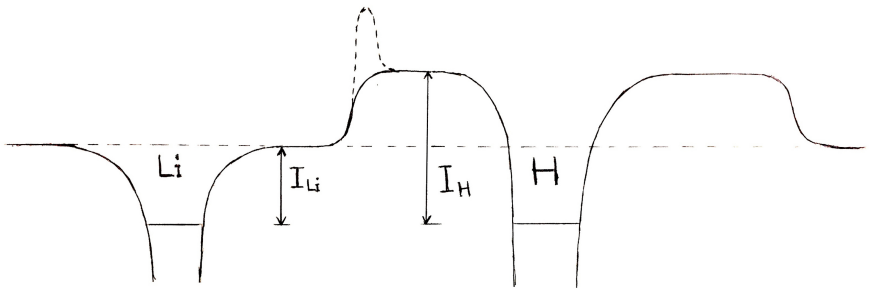

Figure 2.1: Sketch of the exact KS potential at the dissociation limit of the LiH molecule

associating different spatial orbitals to different spins). In the neighborhood of the H atom, the KS potential looks like the one of an isolated H atom. Only by looking far away from the H nucleus, we see that the ionization potential of the stretched LiH molecule is essentially equal to the one of the Li atom. It has been shown [46, 48, 51, 52] that this step structure is built by the difference $v_{N-1}(\boldsymbol{r}) - v_{s,N-1}(\boldsymbol{r})$ appearing in eq 2.34, which has been grouped in one potential called $v_{resp}(\boldsymbol{r})$, as it can also be seen as the response part of the XC potential (see end of sec 2.2.2).

Another feature that is very important for the proper description of challenging electronic structures is highlighted in fig 2.2, where the KS potential for the hydrogen molecule at large internuclear distance is sketched. Here the chemical potentials are the same, so there is no step. However, in the midbond region there is a peak that increases for increasing bond lengths but saturates for large enough distances between the two atoms. That peak essentially decreases the probability that electron around nucleus A tunnels to nucleus B, and, in the limit of infinitely stretched molecule, its height becomes equal to the ionization potential of the hydrogen atom [42, 53–55]. In other words, this is how the KS potential manages to localize non-interacting fermions that would otherwise accumulate some charge also in the midbond region, contrarily to the real interacting electrons.

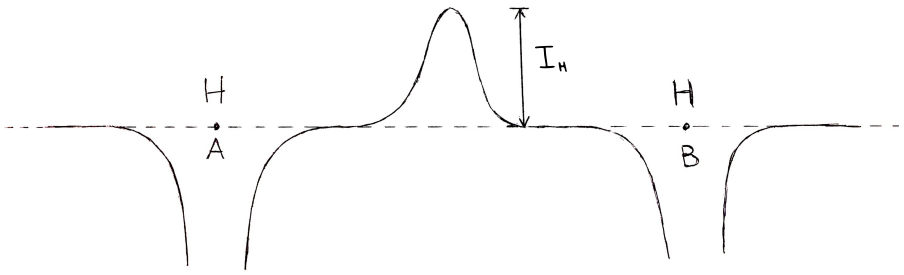

Figure 2.2: Sketch of the exact KS potential at the dissociation limit of the H_2 molecule.

This peak comes from the difference $v_{kin}(\boldsymbol{r}) - v_{s,kin}(\boldsymbol{r})$ [42, 54–57], which for the special case $N = 2$ considered here is just equal to $v_{kin}(\boldsymbol{r})$ of eq 2.19 and can be understood in simple terms: if we imagine electron 1 being, say, around nucleus A, then the gradient of the conditional amplitude in eq 2.19 will undergo a steeper increase the closer electron 1 gets to the midbond, reaching its maximum when electron 1 crosses the bond midpoint. In fact, at this point electron 2 has to hop on the other nucleus in order to have one and only one electron around each nucleus. The peak is actually also present in the heterolytic dissociation and is shown in fig 2.1 as a dashed line. Most available functionals approximate in a satisfying way the electrostatic hole potential of eq 2.17, which is typically the dominant part for the description of the total energy and other properties, but fail severely in the description of the peak and of the step structure. For example the upshift of orbital energies in LDA is due to a too high response potential [58, 59].
In the everlasting quest for better XC functionals, approximating directly the XC potential has always been of interest (although there are other problems appearing when the potential is not the functional derivative of a density functional [60]) and the exact decomposition of the KS potential foreshown provides very helpful guidelines in the design of approximate XC potentials.

In this spirit, Staroverov and coworkers have developed an algorithm to construct sensible XC potentials from correlated wavefunctions in finite basis sets [52, 61–63]. While in ref [64] a simple approximation (called 'GLLB') to the response potential $v_{N-1}(\boldsymbol{r}) - v_{a,N-1}(\boldsymbol{r})$ has been proposed. More recently, the GLLB response potential has been used to correct the band gap of solids obtained from semilocal functionals [65], and the vertical ionization potentials of molecules [59].

2.2.2. XC potential in terms of kinetic and interaction components and their response parts

It is possible to connect the analysis of the effective one-body potentials depicted so far with other expressions for the exchange-correlation energy. Rewriting the total energy by making use of the von Weizsäcker kinetic energy functional, $T_W[n]$, which is N times the kinetic energy of the normalized "density orbital", i.e.

$$T_W[n] \coloneqq -\frac{1}{2}\int \sqrt{n(\boldsymbol{r})}\,\nabla^2\sqrt{n(\boldsymbol{r})}\,\mathrm{d}\boldsymbol{r}, \tag{2.35}$$

we can obtain other expressions for the KS potential involving integrals of the response part of known functions [60], as shown in the next paragraphs.

Let us start by considering the following decomposition of the total energy

$$E[n] = T_W[n] + (T[n] - T_W[n]) + V[n] + V_{ee}[n]. \tag{2.36}$$

Using the expression for $v_{kin}(\boldsymbol{r})$ of eq 2.21, it is immediate to show that

$$\begin{aligned} T[n] - T_W[n] &= \int n(\boldsymbol{r})\, v_{kin}(\boldsymbol{r})\,\mathrm{d}\boldsymbol{r} = \\ &= \underbrace{\frac{1}{2}\int \nabla_{\boldsymbol{r}}\cdot\nabla_{\boldsymbol{r}'}\gamma(\boldsymbol{r},\boldsymbol{r}')|_{\boldsymbol{r}'=\boldsymbol{r}}\,\mathrm{d}\boldsymbol{r}}_{=T[n]} - \underbrace{\frac{1}{8}\int \frac{|\nabla n(\boldsymbol{r})|^2}{n(\boldsymbol{r})}\mathrm{d}\boldsymbol{r}}_{=T_W[n]}. \end{aligned} \tag{2.37}$$

Using eqs 2.15,6.13 it is also easy to see that

$$V_{ee}[n] = \frac{1}{2}\int n(\boldsymbol{r})\, v_{cond}(\boldsymbol{r}) = \frac{1}{2}\int n(\boldsymbol{r})\, n(\boldsymbol{r}')\frac{g_{xc}(\boldsymbol{r},\boldsymbol{r}')+1}{|\boldsymbol{r}-\boldsymbol{r}'|}\mathrm{d}\boldsymbol{r}\mathrm{d}\boldsymbol{r}'. \tag{2.38}$$

Thus, eq 2.36 reads

$$\begin{aligned} E[n] = -\frac{1}{2}\int \sqrt{n(\boldsymbol{r})}\,\nabla^2\sqrt{n(\boldsymbol{r})}\,\mathrm{d}\boldsymbol{r} + \int n(\boldsymbol{r})\, v_{kin}(\boldsymbol{r})\,\mathrm{d}\boldsymbol{r} + \frac{1}{2}\int n(\boldsymbol{r})\, v_{cond}(\boldsymbol{r})\,\mathrm{d}\boldsymbol{r} \\ + \int n(\boldsymbol{r})\, v(\boldsymbol{r})\mathrm{d}\boldsymbol{r}. \end{aligned} \tag{2.39}$$

The effective potential of sec 2.1.1 is exactly the functional derivative of the Von Weizsäcker kinetic energy with opposite sign and up to a constant shift

$$v_{eff}(\boldsymbol{r}) = -\frac{\delta T_W[n]}{\delta n(\boldsymbol{r})} = \frac{\nabla^2\sqrt{n(\boldsymbol{r})}}{2\sqrt{n(\boldsymbol{r})}} - I_p \tag{2.40}$$

This result is easily derived by comparing definition 2.35 and eq 2.11 inverted so as to provide a definition of the effective potential.
Upon differentiation with respect to the density of eq 2.39 and considering that the energy is stationary w.r.t. change in the density, we find

$$\begin{aligned} v_{eff}(\boldsymbol{r}) &= \frac{\delta(E[n] - T_W[n])}{\delta n(\boldsymbol{r})} \\ &= v_{kin}(\boldsymbol{r}) + v(\boldsymbol{r}) + v_H(\boldsymbol{r}) + v_{xc\text{-}hole}(\boldsymbol{r}) + v^{resp}_{kin}(\boldsymbol{r}) + v^{resp}_{xc\text{-}hole}(\boldsymbol{r}), \end{aligned} \tag{2.41}$$

where the response potentials involve the density response of v_{kin}

$$v^{resp}_{kin}(\boldsymbol{r}) = \int n(\boldsymbol{r}')\frac{\delta v_{kin}(\boldsymbol{r}')}{\delta n(\boldsymbol{r})}\mathrm{d}\boldsymbol{r}' \tag{2.42}$$

and g_{xc}

$$v^{resp}_{xc\text{-}hole}(\boldsymbol{r}) = \frac{1}{2}\int \frac{n(\boldsymbol{r}')n(\boldsymbol{r}'')}{|\boldsymbol{r}' - \boldsymbol{r}''|}\frac{\delta g_{xc}(\boldsymbol{r}', \boldsymbol{r}'')}{\delta n(\boldsymbol{r})}\mathrm{d}\boldsymbol{r}'\mathrm{d}\boldsymbol{r}''. \tag{2.43}$$

The comparison between eq. 2.41 and eq. 2.31 shows that

$$v_{N-1}(\boldsymbol{r}) = v^{resp}_{kin}(\boldsymbol{r}) + v^{resp}_{xc\text{-}hole}(\boldsymbol{r}), \tag{2.44}$$

which motivates why the terms of the effective potential associated to the $N-1$ Hamiltonian are also called "response" parts of the potential.

We now repeat the same analysis for the KS system. Consider eq. 2.32 and divide both sides by $\sqrt{n(\boldsymbol{r})}$:

$$-\frac{\nabla^2\sqrt{n(\boldsymbol{r})}}{2\sqrt{n(\boldsymbol{r})}} + v_s(\boldsymbol{r}) + v_{s,kin}(\boldsymbol{r}) + v_{s,N-1}(\boldsymbol{r}) = \epsilon_H \tag{2.45}$$

On the other hand we also know that

$$\frac{\delta T_s[n]}{\delta n(\boldsymbol{r})} = -v_s(\boldsymbol{r}) + \epsilon_H, \tag{2.46}$$

which we can rewrite as

$$\frac{\delta\left(T_W[n] + (T_s - T_W)[n]\right)}{\delta n(\boldsymbol{r})} = -v_s(\boldsymbol{r}) + \epsilon_H \tag{2.47}$$

Working out the l.h.s. gives

$$-\frac{\nabla^2\sqrt{n(\boldsymbol{r})}}{2\sqrt{n(\boldsymbol{r})}}+v_{s,kin}(\boldsymbol{r})+v^{resp}_{s,kin}(\boldsymbol{r})=-v_s(\boldsymbol{r})+\epsilon_H, \tag{2.48}$$

where we have used the relation

$$T_s[n]-T_W[n]=\int v_{s,kin}(\boldsymbol{r})n(\boldsymbol{r})\mathrm{d}\boldsymbol{r}, \tag{2.49}$$

which mirrors eq 2.37 for the KS kinetic energy rather then the interacting one.

Comparing eq. 2.45 and eq. 2.48 gives

$$v_{s,N-1}(\boldsymbol{r})=v^{resp}_{s,kin}(\boldsymbol{r})=\int n(\boldsymbol{r}')\frac{\delta v_{s,kin}(\boldsymbol{r}')}{\delta n(\boldsymbol{r})}\mathrm{d}\boldsymbol{r}'. \tag{2.50}$$

Therefore

$$v_{N-1}(\boldsymbol{r})-v_{s,N-1}(\boldsymbol{r})=v^{resp}_{c,kin}(\boldsymbol{r})+v^{resp}_{xc\text{-}hole}(\boldsymbol{r}), \tag{2.51}$$

where

$$v^{resp}_{c,kin}(\boldsymbol{r})=\int n(\boldsymbol{r}')\frac{\delta v_{c,kin}(\boldsymbol{r}')}{\delta n(\boldsymbol{r})}\mathrm{d}\boldsymbol{r}' \tag{2.52}$$

with

$$v_{c,kin}(\boldsymbol{r})=v_{kin}(\boldsymbol{r})-v_{s,kin}(\boldsymbol{r}). \tag{2.53}$$

Finally, the terms appearing in the r.h.s. of eq 2.51 are often collected in one called v_{resp}

$$v_{resp}(\boldsymbol{r})\coloneqq v^{resp}_{c,kin}(\boldsymbol{r})+v^{resp}_{xc\text{-}hole}(\boldsymbol{r}). \tag{2.54}$$

2.3. λ-dependent effective one-body potentials[5]

Assuming that a single GS wavefunction, Ψ^N_λ, for the λ-dependent Hamiltonian introduced in eq 1.54, $\hat{H}^N_\lambda$,[6] exists at any λ, it is possible to extend the decomposition of the effective potential for the square root of the density in terms of infinitely many systems depending on the coupling strength.
Let us start by writing

$$\hat{H}^N_\lambda(\boldsymbol{r},\cdots,\boldsymbol{r}_N)=\hat{H}^{N-1}_{\lambda^*}(\boldsymbol{r}_2,\cdots,\boldsymbol{r}_N)-\frac{\nabla^2_{\boldsymbol{r}}}{2}+\lambda\sum_{i=2}^{N}\frac{1}{|\boldsymbol{r}-\boldsymbol{r}_i|}+v^\lambda(\boldsymbol{r}), \tag{2.55}$$

[5] The idea of generalizing to any value of the coupling parameter λ the concept of conditional amplitude as well as that of the local potentials that can be written in terms of this latter has appeared originally in the work of reference [66] presented in chapter 6.

[6] Ψ^N_λ and $\hat{H}^N_\lambda$ are exactly the same objects introduced in sec 1.4 and used in the previous section (sec 2.3). Nonetheless throughout this section they are labeled with a superscript for the number of electrons, N, as this latter plays a key role hereinafter. For the same reason, the GS energy associated to Ψ^N_λ and $\hat{H}^N_\lambda$ will be indicated as E^N_λ.

and

$$\Psi_\lambda^N(\boldsymbol{r}\sigma,\boldsymbol{x}_2,\cdots,\boldsymbol{x}_N)=\sqrt{\frac{n(\boldsymbol{r})}{N}}\Phi_\lambda(\sigma,\boldsymbol{x}_2,\cdots,\boldsymbol{x}_N;\boldsymbol{r}), \tag{2.56}$$

respectively.
By applying the r.h.s. of eq 2.55 to the r.h.s. of eq 2.56, multiplying by $\Phi_\lambda^*(\sigma,\boldsymbol{x}_2,\cdots,\boldsymbol{x}_N;\boldsymbol{r})$ to the left and integrating over all variables except $\boldsymbol{r}$ as worked out in sec 2.2.1, we again obtain few distinct one-body potentials, viz.

$$v_{\lambda,N-1}(\boldsymbol{r}) \coloneqq \int \Phi_\lambda^*(\sigma,\boldsymbol{x}_2,\cdots,\boldsymbol{x}_N;\boldsymbol{r})\hat{H}_{\lambda*}^{N-1}\Phi_\lambda(\sigma,\boldsymbol{x}_2,\cdots,\boldsymbol{x}_N;\boldsymbol{r})\mathrm{d}\sigma\mathrm{d}\mathbf{x}_2\cdots\mathrm{d}\mathbf{x}_N - E_{\lambda*}^{N-1}, \tag{2.57}$$

where the subtraction of the quantity $E_{\lambda*}^{N-1}$ makes this potential go to zero when $|\boldsymbol{r}|\to\infty$ if, as expected in most cases, $\Phi_\lambda(\sigma,\boldsymbol{x}_2,\cdots,\boldsymbol{x}_N;\boldsymbol{r})$ asymptotically collapses to $\Psi_\lambda^{N-1}(\boldsymbol{x}_2,\cdots,\boldsymbol{x}_N)$;

$$v_{\lambda,kin}(\boldsymbol{r}) \coloneqq \frac{1}{2}\int |\nabla_{\boldsymbol{r}}\Phi_\lambda(\sigma,\boldsymbol{x}_2,\cdots,\boldsymbol{x}_N;\boldsymbol{r})|^2\mathrm{d}\sigma\mathrm{d}\mathbf{x}_2\cdots\mathrm{d}\mathbf{x}_N, \tag{2.58}$$

which also goes usually to zero when $|\boldsymbol{r}|\to\infty$ as $v_{\lambda,N-1}(\boldsymbol{r})$ does. Exceptions for both potentials are encountered in the case of nodal planes extending to infinity, as already discussed in sec 2.1.1.
Lastly,

$$v_{\lambda,cond}(\boldsymbol{r}) = \int \sum_{i=2}^{N}\frac{1}{|\boldsymbol{r}-\boldsymbol{r}_i|}|\Phi_\lambda(\sigma,\boldsymbol{x}_2,\cdots,\boldsymbol{x}_N;\boldsymbol{r})|^2\mathrm{d}\sigma\mathrm{d}\mathbf{x}_2\cdots\mathrm{d}\mathbf{x}_N, \tag{2.59}$$

which tends manifestly to zero when $|\boldsymbol{r}|\to\infty$ and can be decomposed into a λ-independent, v_{H}, and a λ-dependent part, $v_{\lambda,xc\text{-}hole}$,

$$v_{\lambda,xc\text{-}hole}(\boldsymbol{r}) = v_{\lambda,cond}(\boldsymbol{r}) - v_{\mathrm{H}}(\boldsymbol{r}). \tag{2.60}$$

As well as a Schrödinger equation for the square root of the density

$$\left(-\frac{\nabla^2}{2} + v_{\lambda,eff}(\boldsymbol{r}) + v^\lambda(\boldsymbol{r})\right)\sqrt{n(\boldsymbol{r})} = (E_\lambda^N - E_{\lambda*}^{N-1})\sqrt{n(\boldsymbol{r})}, \tag{2.61}$$

where

$$v_{\lambda,eff}(\boldsymbol{r}) \coloneqq v_{\lambda,N-1}(\boldsymbol{r}) + v_{\lambda,kin}(\boldsymbol{r}) + \lambda\, v_{\lambda,cond}(\boldsymbol{r}), \tag{2.62}$$

and $E_{\lambda*}^{N-1}$ is the ground-state energy of the $N-1$ system in the same effective potential as the N-particle one, i.e. of $\hat{H}_{\lambda*}^{N-1}$ of eq 2.55 (thus $E_{\lambda*}^{N-1} = E_\lambda^{N-1}$ only for $\lambda = 1$).

Comparison with eq 2.11 shows that,

- for any finite λ, the difference $E_\lambda^N - E_{\lambda*}^{N-1}$ in eq 2.61 equals minus the exact ionization potential, I_p, of the physical system, which dictates the asymptotic decay of the density as already discussed in secs 2.1.1 and 2.2.1

$$E_\lambda^N - E_{\lambda*}^{N-1} = -I_p; \tag{2.63}$$

- the sum $\left(v_{\lambda,eff} + v^\lambda\right)$ has to be λ-independent and equal to the effective potential, v_{eff}.

Thus, we can explicitly write the λ-dependent external potential as a difference between a λ-independent and a λ-dependent term

$$v^\lambda(\boldsymbol{r}) = v_{eff}(\boldsymbol{r}) - v_{\lambda,eff}(\boldsymbol{r}). \tag{2.64}$$

Note that, when $\lambda = 0$, the potential $v_{\lambda,eff}$ becomes exactly the so-called "Pauli" potential, $v_P = v_{eff} - v_s$ [67, 68].

2.4. Scaling properties

Coordinates scaling and scaling of the coupling parameter in eq 1.54 can be related to one another [69]. In order to show their relation, let us start by writing the λ-dependent Schrödinger equation

$$\left(-\sum_{i=1}^{N}\frac{\nabla_{\boldsymbol{r}_i}^2}{2} + \sum_{i=1,j>i}^{N}\frac{\lambda}{|\boldsymbol{r}_i - \boldsymbol{r}_j|} + \sum_{i=1}^{N} v^\lambda(\boldsymbol{r}_i)\right)\Psi_\lambda(\boldsymbol{r}_1,\cdots,\boldsymbol{r}_N) = E_\lambda\,\Psi_\lambda(\boldsymbol{r}_1,\cdots,\boldsymbol{r}_N) \tag{2.65}$$

where we have left the spin indexes out for notational convenience as they will remain untouched along the whole treatment. We remind that Ψ_λ delivers the density n at each λ.
Upon substitution

$$\boldsymbol{r} = \alpha\,\boldsymbol{r}' \tag{2.66}$$

we find

$$\left(-\sum_{i=1}^{N}\frac{1}{\alpha^2}\frac{\nabla_{\boldsymbol{r}'_i}^2}{2} + \sum_{i=1,j>i}^{N}\frac{\lambda}{\alpha|\boldsymbol{r}'_i - \boldsymbol{r}'_j|} + \sum_{i=1}^{N} v^\lambda(\alpha\,\boldsymbol{r}'_i)\right)\Psi_\lambda(\alpha\,\boldsymbol{r}'_1,\cdots,\alpha\,\boldsymbol{r}'_N) = \tag{2.67}$$

$$E_\lambda\,\Psi_\lambda(\alpha\,\boldsymbol{r}'_1,\cdots,\alpha\,\boldsymbol{r}'_N)$$

Multiplying both sides of eq 2.67 by α^2, then taking $\alpha = \frac{1}{\lambda}$ and defining a wavefunction ξ such that

$$\Psi_\lambda(\boldsymbol{r}_1,\cdots,\boldsymbol{r}_N) = \lambda^{\frac{3N}{2}}\,\xi(\lambda\,\boldsymbol{r}_1,\cdots,\lambda\,\boldsymbol{r}_N), \tag{2.68}$$

we find

$$\left(-\sum_{i=1}^{N}\frac{\nabla^2_{\boldsymbol{r}'_i}}{2}+\sum_{i=1,j>i}^{N}\frac{1}{|\boldsymbol{r}'_i-\boldsymbol{r}'_j|}+\frac{1}{\lambda^2}\sum_{i=1}^{N}v^{\lambda}\left(\frac{\boldsymbol{r}'_i}{\lambda}\right)\right)\xi(\boldsymbol{r}'_1,\cdots,\boldsymbol{r}'_N)= \tag{2.69}$$
$$\frac{1}{\lambda^2}E_{\lambda}\,\xi(\boldsymbol{r}'_1,\cdots,\boldsymbol{r}'_N).$$

Applying definition 1.3 to calculate the density associated to $\xi(\boldsymbol{r}'_1,\cdots,\boldsymbol{r}'_N)$ and eq 2.68 we find

$$\begin{aligned}N\int|\xi(\boldsymbol{r}'_1,\cdots,\boldsymbol{r}'_N)|^2\mathrm{d}\boldsymbol{r}'_2\cdots\mathrm{d}\boldsymbol{r}'_N=\\ \frac{N}{\lambda^3}\int|\Psi_{\lambda}\left(\frac{\boldsymbol{r}_1}{\lambda},\cdots,\frac{\boldsymbol{r}_N}{\lambda}\right)|^2\mathrm{d}\left(\frac{\boldsymbol{r}_2}{\lambda}\right)\cdots\mathrm{d}\left(\frac{\boldsymbol{r}_N}{\lambda}\right)\\ =\frac{1}{\lambda^3}\,n\left(\frac{\boldsymbol{r}_1}{\lambda}\right)=n_{\frac{1}{\lambda}}(\boldsymbol{r}_1),\end{aligned} \tag{2.70}$$

where the last equality results from definition 1.72.
Thus, eq 2.69 tells us that $\xi(\boldsymbol{r}'_1,\cdots,\boldsymbol{r}'_N)$ is the ground state of a Hamiltonian at full coupling strength ($\lambda=1$) delivering a density $n_{\frac{1}{\lambda}}\left(\frac{\boldsymbol{r}'_1}{\lambda}\right)$, i.e. $\xi(\boldsymbol{r}'_1,\cdots,\boldsymbol{r}'_N)=\Psi_1[n_{\frac{1}{\lambda}}](\boldsymbol{r}'_1,\cdots,\boldsymbol{r}'_N)$ and we have found that

$$\Psi_{\lambda}[n](\boldsymbol{r}_1,\cdots,\boldsymbol{r}_N)=\lambda^{\frac{3N}{2}}\Psi_1[n_{\frac{1}{\lambda}}](\lambda\boldsymbol{r}_1,\cdots,\lambda\boldsymbol{r}_N). \tag{2.71}$$

From eq 2.69 one also deduces the behaviour of the external potential as well as that of the ground state energy w.r.t. uniform scaling of the density, namely

$$\frac{1}{\lambda^2}v^{\lambda}[n](\boldsymbol{r})=v^1[n_{\frac{1}{\lambda}}](\lambda\boldsymbol{r}) \tag{2.72}$$

$$\frac{1}{\lambda^2}E_{\lambda}[n]=E_1[n_{\frac{1}{\lambda}}] \tag{2.73}$$

Insertion into the definitions of the λ-dependent local one-body potentials (eqs 2.57, 2.58, 2.59, and 2.60) of eqs 2.71, 2.56 and, just for $v_{\lambda,N-1}$, also 2.72 leads to the following local scaling relations

$$v_{\lambda,N-1}[n](\boldsymbol{r}) = \lambda^2 v_{1,N-1}[n_{\frac{1}{\lambda}}](\lambda\boldsymbol{r}) \tag{2.74}$$

$$v_{\lambda,kin}[n](\boldsymbol{r}) = \lambda^2 v_{1,kin}[n_{\frac{1}{\lambda}}](\lambda\boldsymbol{r}) \tag{2.75}$$

$$v_{\lambda,cond}[n](\boldsymbol{r}) = \lambda\, v_{1,cond}[n_{\frac{1}{\lambda}}](\lambda\boldsymbol{r}) \tag{2.76}$$

and subsequently

$$v_{\lambda,xc\text{-}hole}[n](\boldsymbol{r}) = \lambda\, v_{1,xc\text{-}hole}[n_{\frac{1}{\lambda}}](\lambda\boldsymbol{r}). \tag{2.77}$$

Combination of eqs 2.74, 2.75 and 2.76 together with definition 2.62 gives

$$v_{\lambda,eff}[n](\boldsymbol{r}) = \lambda^2 v_{1,eff}[n_{\frac{1}{\lambda}}](\lambda\boldsymbol{r}), \tag{2.78}$$

Note that the scaling of the effective potential introduced in eq 2.11 can be independently calculated to be

$$v_{eff}[n](\boldsymbol{r}) \quad = \quad \lambda^2 v_{eff}[n_{\frac{1}{\lambda}}](\lambda\boldsymbol{r}) \tag{2.79}$$

and is consistent with eqs 2.72, 2.78 and 2.61.

Moving onto global quantities, the definition of the Von Weizsäcker energy functional (eq 2.35) immediately gives that

$$T_{VW}[n] \quad = \quad \lambda^2 T_{VW}[n_{\frac{1}{\lambda}}]. \tag{2.80}$$

Defining

$$T_\lambda[n] := \langle\Psi^N_\lambda[n]|\hat{T}|\Psi^N_\lambda[n]\rangle, \tag{2.81}$$

$$V_{ee,\lambda}[n] := \langle\Psi^N_\lambda[n]|\hat{V}_{ee}|\Psi^N_\lambda[n]\rangle, \tag{2.82}$$

and

$$W_\lambda[n] := V_{ee,\lambda}[n] - U[n] \tag{2.83}$$

use of eqs 2.75 together with 2.80 for the kinetic and 2.76 and 2.77 for the electron-electron interaction terms gives

$$T_\lambda[n] \quad = \quad \lambda^2 T_1[n_{\frac{1}{\lambda}}] \tag{2.84}$$

$$V_{ee,\lambda}[n] \quad = \quad \lambda V_{ee,1}[n_{\frac{1}{\lambda}}] \tag{2.85}$$

and

$$W_\lambda[n] \quad = \quad \lambda W_1[n_{\frac{1}{\lambda}}] \tag{2.86}$$

Finally, combination of eqs 2.84 and 2.85 together with definition 1.53 gives

$$F_\lambda[n] = \lambda^2 F_1[n_{\frac{1}{\lambda}}]. \tag{2.87}$$

Moreover, from a GS wavefunction at any λ which delivers a density n

$$\Psi_\lambda(\boldsymbol{r}_1,\cdots,\boldsymbol{r}_N) \to n(\boldsymbol{r}_1) \tag{2.88}$$

one can obtain a uniformly scaled density n_γ (eq 1.72) by scaling it as

$$\gamma^{\frac{3N}{2}}\Psi_\lambda(\gamma\boldsymbol{r}_1,\cdots,\gamma\boldsymbol{r}_N) \to \gamma^3 n(\gamma\boldsymbol{r}_1). \tag{2.89}$$

Inserting the scaled Ψ_0 into the functional defined in eq 1.42, immediately shows that [70]

$$T_s[n] = \lambda^2 T_s[n_{\frac{1}{\lambda}}] \tag{2.90}$$

with $\gamma = \frac{1}{\lambda}$.
Thus, also for the correlation contribution alone it holds that

$$T_{c,\lambda}[n] = \lambda^2 T_{c,1}[n_{\frac{1}{\lambda}}] \tag{2.91}$$

having defined

$$T_{c,\lambda}[n] := (T_\lambda - T_s)[n]. \tag{2.92}$$

3
Strictly Correlated Electrons

At the end of sec 1.4, we have introduced some density functionals called W_∞ and W'_∞ appearing in the large λ expansion of the adiabatic connection integrand, W_λ. Since it was posed [71–73], the question as to what happens to all key players of the density-fixed adiabatic connection formalism (sec 1.4) as $\lambda \to \infty$ (the so-called strongly-interacting limit) has offered a complementary scenario to the KS picture with a rather unique structure.
Both weakly-interacting and strongly-interacting limits are simplified descriptions of the realistic situation where kinetic and electron-electron interaction effects need to compromise in the minimization of the total energy, however, while the mathematical simplicity is embodied, in the former, in single-particle orbitals, these are replaced, in the latter, by completely different and distinctive objects, called *co-motion functions*.
Compared to the KS orbitals, the co-motion functions are also non-trivial density functionals, however their explicit dependence on the density is known in some cases [73].
In the electronic structure theory community the strongly-interacting limit (SIL) of DFT is equivalently known under the acronym SCE which stands for "strictly correlated electrons".

The physical picture in the case of extreme electron-electron interaction overlaps to some extent with a branch of mathematics named Optimal Transport, which will be briefly introduced in sec 3.2.
Nevertheless, in the mathematical community, the two acronyms "SIL" and "SCE" are being used with different meanings.
V_{ee}^{SIL} represents the exact limit of the Levy-Lieb λ-dependent functional up to first

order [74, 75]

$$\lim_{\lambda\to\infty}\frac{F_\lambda[n]}{\lambda}=V_{ee}^{\mathrm{SIL}}[n]+o(\lambda), \tag{3.1}$$

while the SCE functional, V_{ee}^{SCE}, is a specific form in which the problem posed by V_{ee}^{SIL} may be solved.
In particular, $V_{ee}^{\mathrm{SIL}}\equiv V_{ee}^{\mathrm{SCE}}$ when the functional V_{ee}^{SIL} can be expressed in terms of optimal transport maps (as briefly discussed in sec 3.2).
Nevertheless, in references [76, 77] it is argued that, casting the deterministic expression of the interaction energy operator (see eq 3.13) *variationally*, into a search over all possible transport maps $\{\mathbf{f}_i\}$ giving the density, n, i.e.

$$V_{ee,opt}^{\mathrm{SCE}}=\frac{1}{2}\inf_{\{\mathbf{f}_i\}:n}\left(\int n(\boldsymbol{r})\sum_{i=1}^{N-1}\frac{1}{|\boldsymbol{r}-\mathbf{f}_i(\boldsymbol{r})|}\mathrm{d}\boldsymbol{r}\right) \tag{3.2}$$

the two objects are arbitrarily close.
Therefore, $V_{ee}^{\mathrm{SIL}}=V_{ee,opt}^{\mathrm{SCE}}$.
The question remains whether the inf in eq 3.2 can always be sharpen to a min for the Coulomb cost or, if not, in which cases it can. Throughout this chapter, we shall simply assume $V_{ee}^{\mathrm{SIL}}=V_{ee}^{\mathrm{SCE}}$ without discriminating between optimal and non-optimal maps.

3.1. General Structure of the (DFT) $\lambda\to\infty$ Limit

When $\lambda\to\infty$, the λ-dependent Hamiltonian of eq 1.54 reduces to [34, 73–75]

$$\hat{H}_{\lambda\to\infty}\sim\lambda(\hat{V}_{ee}+\hat{V}^{\mathrm{SCE}}), \tag{3.3}$$

where $\hat{V}^{\mathrm{SCE}}=\sum_{i=1}^{N}v^{\mathrm{SCE}}(\boldsymbol{r}_i)$ is the one body potential that makes the classical potential energy operator[1]

$$E_{\mathrm{pot}}^{\mathrm{SCE}}(\boldsymbol{r}_1,\cdots,\boldsymbol{r}_N)=\hat{V}_{ee}(\boldsymbol{r}_1,\cdots,\boldsymbol{r}_N)+\hat{V}^{\mathrm{SCE}}(\boldsymbol{r}_1,\cdots,\boldsymbol{r}_N) \tag{3.4}$$

deliver the prescribed ground-state density $n(\boldsymbol{r})$ such that both $\hat{V}^{\mathrm{SCE}}$ and E_{pot} are functional of the density [34, 73, 79].
The ground state energy of eq 3.3 is given by

$$E_{\lambda\to\infty}[n]=\lambda\inf_{|\Psi|^2\to n}\int E_{\mathrm{pot}}^{\mathrm{SCE}}[n](\boldsymbol{r}_1,\cdots,\boldsymbol{r}_N)|\Psi(\boldsymbol{x}_1,\cdots,\boldsymbol{x}_N)|^2\mathrm{d}\boldsymbol{x}_1\cdots\mathrm{d}\boldsymbol{x}_N \tag{3.5}$$

and it is achieved by a $|\Psi|^2$ which is zero everywhere except where the potential energy surface $E_{\mathrm{pot}}[n](\boldsymbol{r}_1,\cdots,\boldsymbol{r}_N)$ attains its global minimum (in other words the

[1] Sometimes v^{SCE} is also denoted as "v_∞" [6, 78] as it is the external potential appearing in the asymptotic Hamiltonian of eq 3.3.

minimum of the potential energy defines the support of $|\Psi|^2$).
The reason why the kinetic energy operator disappears from the λ-dependent Hamiltonian as $\lambda \to \infty$ (eq 3.3) is that its expectation value, $T_\lambda[n]$ (eq 2.81), is subleading w.r.t. $V_{ee,\lambda}[n]$ (eq 2.82) in this limit.
In particular, assuming that $T_{\lambda\to\infty}$ is due, to first order, to zero point oscillations around the equilibrium positions (a conjecture first proposed in reference [72] and for which gradually further arguments have been produced [34, 74, 80] although no rigorous proof is available yet), it can be shown that $T_{\lambda\to\infty} \sim O(\sqrt{\lambda})$.
As a consequence, the λ-dependent Levy-Lieb functional of eq 1.53 tends asymptotically to $\lambda\, V_{ee}^{SCE}[n]$ with [71, 73]

$$V_{ee}^{\mathrm{SCE}}[n] \coloneqq \inf_{\Psi\to n} \langle\Psi|\hat{V}_{ee}|\Psi\rangle. \tag{3.6}$$

Eq 3.6 presents the SCE functional, $V_{ee}^{SCE}[n]$, as the natural counterpart of the KS functional, $T_s[n]$ (eq 1.42).
Moreover, just as for T_s, by inserting the wavefunction for the scaled density (see eq 2.89), we immediately see that

$$V_{ee}^{\mathrm{SCE}}[n] = \lambda\, V_{ee}^{\mathrm{SCE}}[n_{\frac{1}{\lambda}}]. \tag{3.7}$$

Note that, because $\hat{H}_{\lambda\to\infty}$ contains only classical operators, there are two important and related *caveat*s in this limit.
The first one is that, the object that attains the lowest value of $\langle\hat{V}_{ee}\rangle$ lives in the space of distributions,[2]thus it is not technically in the space of allowed wavefunctions, i.e. $\Psi_{\lambda\to\infty} \notin L^2$, and the kinetic energy as expected diverges (we are in fact violating Heisenberg principle), but its leading diverging term is only $o(\lambda)$ as already discussed.
The second one is that, in order for the external potential to be able to enforce a *smooth* density in this limit, the set $M[n]$ of all configurations where $E_{\mathrm{pot}}[n](\boldsymbol{r}_1,\cdots,\boldsymbol{r}_N)$ is minimum

$$M[n] \coloneqq \{(\boldsymbol{r}_1,\cdots,\boldsymbol{r}_N)\colon E_{\mathrm{pot}}[n](\boldsymbol{r}_1,\cdots,\boldsymbol{r}_N) = \min\} \tag{3.8}$$

cannot be made up of just a sum of discrete points, but it needs to feature a *continuum* of a minimum dimensionality, D, equal to that of the domain of the density ($n\colon \mathbb{R}^D \to \mathbb{R}_+$).
Consequently, the modulus squared of the minimizing wavefunction collapses into a distribution that lives in a D-dimensional subspace of the full $\left(\mathbb{R}^D \otimes \mathbb{Z}_2\right)^N$ configuration space.

[2]The constraint of the density can make things more complicated, in particular the support of $|\Psi|^2$ is singular only if the inf of eq 3.2 is a min, something which we are assuming in the next lines.

We can write it as

$$\left|\Psi_{\text{SCE}}[n](\boldsymbol{r}_1,\cdots,\boldsymbol{r}_N)\right|^2 = \frac{1}{N!}\sum_{\wp=1}^{N!}\int d\mathbf{s}\,\frac{n(\mathbf{s})}{N}\prod_{i=1}^{N}\delta(\mathbf{r}_i-\mathbf{f}_{\wp(i)}[n](\mathbf{s})), \tag{3.9}$$

such that its integral recovers the density according to eq 1.3 and where the co-motion functions $\mathbf{f}_i[n](\boldsymbol{r})$ exactly parametrize the set $M[n]\subset\mathbb{R}^D$, i.e.

$$M[n] = \{\big(\mathbf{f}_1[n](\boldsymbol{r}),\cdots,\mathbf{f}_N[n](\boldsymbol{r})\big)\colon \boldsymbol{r}\in\mathbb{R}^D\}. \tag{3.10}$$

The co-motion functions then determine the position of each of the $(N-1)$ electrons as a function of that of a reference one realizing the perfect correlation among the electrons (their "correlated dance").
Note that, within the SCE limit, no information is retained about the statistics of the particles [80], therefore the particles spin variables are considered as always integrated out.
Note, furthermore, that there are several possible ways in which the N perfectly correlated electrons can be arranged given their indistinguishability. Such consideration is accounted for in expression 3.9 by a sum over all possible permutations, $\wp$, of a given configuration (see appendix A for further discussions).
By virtue of electrons indistinguishability, the co-motion functions also need to possess the highly non-local property that

$$n(\mathbf{f}_i(\boldsymbol{r}))\mathrm{d}\mathbf{f}_i(\boldsymbol{r}) = n(\boldsymbol{r})\mathrm{d}\boldsymbol{r} \qquad (i=1,\ldots,N) \tag{3.11}$$

which ensures that the probability of finding one electron at position $\boldsymbol{r}$ in the volume element $\mathrm{d}\boldsymbol{r}$ be the same of finding electron i at position $\mathbf{f}_i(\boldsymbol{r})$ in the volume element $\mathrm{d}\mathbf{f}_i(\boldsymbol{r})$.
There are $(N-1)$ non trivial co-motion functions meaning that the N-th co-motion function is just the identity and they also satisfy cyclic group properties[3]

$$\begin{aligned}
\mathbf{f}_1(\mathbf{r}) &\equiv \mathbf{f}(\mathbf{r}),\\
\mathbf{f}_2(\mathbf{r}) &\equiv \mathbf{f}\big(\mathbf{f}(\mathbf{r})\big),\\
&\cdots\\
\mathbf{f}_{N-1}(\mathbf{r}) &\equiv \underbrace{\mathbf{f}\big(\mathbf{f}(\ldots\mathbf{f}(\mathbf{r})\ldots)\big)}_{N-1\text{ times}},\\
\mathbf{f}_N(\mathbf{r}) &\equiv \underbrace{\mathbf{f}\big(\mathbf{f}(\ldots\mathbf{f}(\mathbf{r})\ldots)\big)}_{N\text{ times}} = \mathbf{r};
\end{aligned} \tag{3.12}$$

[3] Although, in the literature, it is more frequent to enumerate the co-motion functions such that $\mathbf{f}_1(\boldsymbol{r})\equiv\boldsymbol{r}$ and such that the function whose N-th action generates all the other co-motion functions in the group be $\mathbf{f}_2(\boldsymbol{r})\equiv\mathbf{f}(\boldsymbol{r})$, throughout this work we prefer the other choice documented in ref [81].

for a recent review on the mathematical properties of the co-motion functions see reference [77]. The corresponding SCE functional of eq 3.6 can then be written explicitly as [73, 82]

$$V_{ee}^{SCE}[n] = \frac{1}{2}\int n(\boldsymbol{r}) \sum_{i=1}^{N-1} \frac{1}{|\boldsymbol{r} - \mathbf{f}_i(\boldsymbol{r})|} \mathrm{d}\boldsymbol{r}, \tag{3.13}$$

and it yields the strong-coupling (or low-density) asymptotic value of the exact Hartree-exchange-correlation functional [74, 75].
Despite its extreme non-locality, its functional derivative

$$v_{Hxc}^{\mathrm{SCE}}(\boldsymbol{r}) \coloneqq \frac{\delta V_{ee}^{\mathrm{SCE}}[n]}{\delta n(\boldsymbol{r})} \tag{3.14}$$

can be computed from the exact force equation [73, 83]

$$\nabla v_{Hxc}^{SCE}(\boldsymbol{r}) = -\sum_{i=1}^{N-1} \frac{\boldsymbol{r} - \mathbf{f}_i(\boldsymbol{r})}{|\boldsymbol{r} - \mathbf{f}_i(\boldsymbol{r})|^3}. \tag{3.15}$$

According to eq 1.55, the one-body potential $v^{\mathrm{SCE}}(\boldsymbol{r})$ of eq 3.3 is exactly equal to minus $v_{Hxc}^{\mathrm{SCE}}(\boldsymbol{r})$: in fact, the gradient of $v_{Hxc}^{\mathrm{SCE}}(\boldsymbol{r})$ represents the net repulsion felt by an electron in $\boldsymbol{r}$ due to the other $N-1$ electrons at positions $\mathbf{f}_i(\boldsymbol{r})$, while $v^{\mathrm{SCE}}(\boldsymbol{r})$ exactly compensates this net force, in such a way that, we reiterate, the classical potential energy operator $E_{\mathrm{pot}}^{\mathrm{SCE}}$ is stationary (and minimum) on the manifold parametrized by the co-motion functions.
Moreover, the SCE potential has a simple scaling following from eqs 3.7 and 3.14

$$\begin{aligned}
v_{Hxc}^{SCE}[n](\boldsymbol{r}) = \lambda \frac{\delta V_{ee}^{\mathrm{SCE}}\left[n_{\frac{1}{\lambda}}\right]}{\delta n(\boldsymbol{r})} &= \lambda \int \frac{\delta V_{ee}^{\mathrm{SCE}}\left[n_{\frac{1}{\lambda}}\right]}{\delta n_{\frac{1}{\lambda}}(\boldsymbol{r}')} \frac{\delta n_{\frac{1}{\lambda}}(\boldsymbol{r}')}{\delta n(\boldsymbol{r})} \mathrm{d}\boldsymbol{r}' \\
&= \lambda \int v_{Hxc}^{SCE}\left[n_{\frac{1}{\lambda}}\right](\boldsymbol{r}')\, \lambda^{-3} \delta\left(\boldsymbol{r} - \frac{\boldsymbol{r}'}{\lambda}\right) \mathrm{d}\boldsymbol{r}' \\
&= \lambda^{-2} \int v_{Hxc}^{SCE}\left[n_{\frac{1}{\lambda}}\right](\boldsymbol{r}')\, \delta\left(\frac{1}{\lambda}\left(\lambda\boldsymbol{r} - \boldsymbol{r}'\right)\right) \mathrm{d}\boldsymbol{r}' \\
&= \lambda^{-2} \int v_{Hxc}^{SCE}\left[n_{\frac{1}{\lambda}}\right](\boldsymbol{r}')\, \lambda^{3} \delta\left(\lambda\boldsymbol{r} - \boldsymbol{r}'\right) \mathrm{d}\boldsymbol{r}' \\
&= \lambda\, v_{Hxc}^{SCE}\left[n_{\frac{1}{\lambda}}\right](\lambda\boldsymbol{r})
\end{aligned} \tag{3.16}$$

where we have used the property of Delta functions that $\delta(\alpha\boldsymbol{x}) = |\alpha|^{-n}\delta(\boldsymbol{x})$ and $\frac{\delta n_\gamma(\boldsymbol{r}')}{\delta n(\boldsymbol{r})} = \gamma^3 \delta(\boldsymbol{r} - \gamma\boldsymbol{r}')$ which is a result of the same property.[4]

[4] This is actually a general result of the definition of scaled density (1.72): namely that if a scaling relation holds for global quantities then the functional derivatives of these latters w.r.t. the density keep the same scaling, as seen for many examples in sec 2.4.

As a last remark, we note that eq 3.15 defines $v_{Hxc}^{\mathrm{SCE}}(\boldsymbol{r})$ up to a constant, which is fixed by imposing that $v^{\mathrm{SCE}}(\boldsymbol{r}) = -v_{Hxc}^{\mathrm{SCE}}(\boldsymbol{r})$ go to zero when $|\boldsymbol{r}| \to \infty$.

3.2. The strong-interaction limit of DFT in the context of Optimal Transport

The strong-interaction limit of DFT can be recast in the context of Optimal Transport theory, as pointed out, independently, by Buttazzo *et al.* [84] and by Cotar *et al.* [85].
Optimal Transport is a branch of mathematics founded by French mathematician Gaspard Monge [86] which poses the problem of finding the optimal way of transporting a given mass (e.g. of soil) having a certain distribution μ into another desired distribution ν subject to a cost function, $c(x, y)$ (e.g. the Euclidean distance). The distributions μ and ν are called the *marginals*.
The Monge solution is an optimal map which assigns $\mu(x)$ at every point x to a unique final destination $y = T(x)$ in the target distribution $\nu(y)$.
A relaxed formulation of the Monge problem, introduced in 1942 by Soviet mathematician and economist Leonid Kantorovich, brought major advances to the field [87]. In particular, the Kantorovich formulation allows for some mass piled on a point x of the original distribution $\mu(x)$ to be spread over different points in the target distribution ν with different probabilities. Therefore the Kantorovich solution is a transport plan that gives rather the *probability* that, at optimality, a given $\mu(x)$ be transported to y in ν. Thanks to this formulation, it has been possible to solve many Monge problems that had remained open for a couple of centuries and in the last twenty years optimal transport has developed into one of the most active fields in mathematics [88].

In density functional theory both the starting and the target distributions are represented by the electron density and the number of total distributions equals N, where N is the number of electrons. Therefore, we are dealing with a multimarginal problem with identical marginals.
For the $N = 2$ case, the co-motion function, $f(x)$ with $x \in \mathbb{R}^D$, for any dimension and any distribution, $\forall\{D, \mu\}$, turns out to be exactly the solution to the Monge problem subject to the Coulomb repulsion cost [84, 85].
Another case in which the co-motion functions are proven to be exactly the optimal maps is the 1D case for general N and μ and convex cost function [89].
However, to prove the existence of a set of optimal maps in the multimarginal case and for Coulomb cost, in any dimension other than $1D$, is still an open issue [90].

A very convenient formulation of the Kantorovich problem is its dual formulation, referred to as dual-(Monge-)Kantorovich problem, which in the case of Coulomb

cost is usually written as

$$V_{ee}^{\mathrm{SCE}}[n_0] = \sup_u \left(\int n_0(\boldsymbol{r}) u(\boldsymbol{r}) : \sum_{i=1}^{N} u(\boldsymbol{r}_i) \leq \sum_{i,j>i}^{N} \frac{1}{r_{ij}} \right) \tag{3.17}$$

and corresponds to a maximisation w.r.t. potential under linear constraints.
The optimal u is called the Kantorovich potential and has the same profile of the SCE potential with opposite sign and shifted by a positive constant which fixes the total energy to zero, i.e. $u(\boldsymbol{r}) = -v^{\mathrm{SCE}} + C$.
We shall see how eq 3.17 is analogous to expressing the asymptotic value of the λ-dependent Levy-Lieb functional, $\lim_{\lambda\to\infty} \frac{F_\lambda[n_0]}{\lambda}$ via the Lieb variational principle [21]. We thus need to make a small digression to introduce this latter.

3.2.1. Lieb maximisation along the adiabatic connection

In eq 1.21 we have illustrated the Hohenberg-Kohn variational principle, introduced in sec 1.1, in terms of the Levy-Lieb functional. Let us now simply extend it to the λ-dependent Levy-Lieb functional, $F_\lambda[n]$.[5]
From variational arguments we can write

$$\langle \Psi_n | \hat{T} + \lambda \hat{V}_{ee} | \Psi_n \rangle + \int n(\boldsymbol{r}) v_0(\boldsymbol{r}) \mathrm{d}\boldsymbol{r} \quad \geq \quad \underbrace{\langle \Psi_{v_0} | \hat{T} + \lambda \hat{V}_{ee} + \hat{V}_0 | \Psi_{v_0} \rangle}_{E_{\lambda,n_0}[v_0]} \tag{3.18}$$

with the definitions

$$\langle \Psi_n | \hat{T} + \lambda \hat{V}_{ee} | \Psi_n \rangle \quad := \quad \min_{\Psi \to n} \langle \Psi | \hat{T} + \lambda \hat{V}_{ee} | \Psi \rangle \tag{3.19}$$

$$\langle \Psi_v | \hat{T} + \lambda \hat{V}_{ee} + \hat{V} | \Psi_v \rangle \quad := \quad \min_{\Psi} \langle \Psi | \hat{T} + \lambda \hat{V}_{ee} + \hat{V} | \Psi \rangle \tag{3.20}$$

and $\hat{V}_0 = \sum_i^N v_0(\boldsymbol{r}_i)$.
Eq 3.18 tells us that, since the sum of the Levy-Lieb functional evaluated on any density, n, and the inner product between this density and a given potential, v_0, is always greater than or equal to the energy of the system whose ground state density is precisely that associated to v_0, in order to find such minimizing energy and density we need to perform a minimisation over all N-representable densities, i.e.

$$E_{\lambda,n_0}[v_0] = \inf_n \left(F_\lambda[n] + \int n(\boldsymbol{r}) v_0(\boldsymbol{r}) \mathrm{d}\boldsymbol{r} \right) \tag{3.21}$$

where the last equation is identical to eq 1.21 extended to any λ-dependent system.

[5] In rigourous terms, we should rather be working with the Lieb functional (eq 1.29), extended to λ-dependent Hamiltonians [91], as the Levy-Lieb functional is not convex.

Switching the role of density and potential we can also write (with $\hat{V} = \sum_i^N v(\boldsymbol{r}_i)$ as usual)

$$\begin{aligned}
&\langle\Psi_v|\hat{T}+\lambda\hat{V}_{ee}+\hat{V}|\Psi_v\rangle \leq \langle\Psi_{n_0}|\hat{T}+\lambda\hat{V}_{ee}|\Psi_{n_0}\rangle + \int v(\boldsymbol{r})n_0(\boldsymbol{r}) \\
&\langle\Psi_v|\hat{T}+\lambda\hat{V}_{ee}+\hat{V}|\Psi_v\rangle - \int v(\boldsymbol{r})n_0(\boldsymbol{r}) \leq \underbrace{\langle\Psi_{n_0}|\hat{T}+\lambda\hat{V}_{ee}|\Psi_{n_0}\rangle}_{F_\lambda[n_0]}
\end{aligned} \tag{3.22}$$

which tells us that, since the energy corresponding to any external potential, v, minus the inner product between this potential and a given density, n_0, is always smaller than or equal to the Levy-Lieb functional evaluated on n_0, we need to perform a maximisation over all suitable potentials[6] in order to find the optimal potential (i.e. the one associated to the given density) and calculate $F_\lambda[n_0]$ from the energy expression

$$F_\lambda[n_0] = \sup_v \left(E_{\lambda,n}[v] - \int v(\boldsymbol{r})n_0(\boldsymbol{r})\mathrm{d}\boldsymbol{r} \right).^7 \tag{3.23}$$

To connect to sec 1.3 we can evaluate eq 3.23 for $\lambda = 0$

$$\begin{aligned}
F_0[n_0] &= \sup_v \left(E_{0,n_0}[v] - \int v(\boldsymbol{r})n_0(\boldsymbol{r})\mathrm{d}\boldsymbol{r} \right) \\
&= \sup_v \left(\min_\Psi \langle\Psi|\hat{T}+\hat{V}|\Psi\rangle - \int v(\boldsymbol{r})n_0(\boldsymbol{r})\mathrm{d}\boldsymbol{r} \right) \\
&= \sup_v \left(\min_\Psi \left\{ \langle\Psi|\hat{T}|\Psi\rangle + \int v(\boldsymbol{r})\left(n_\Psi - n_0\right)(\boldsymbol{r})\mathrm{d}\boldsymbol{r} \right\} \right) \\
&= \sup_v \left(\langle\Psi_{\mathrm{SD}}|\hat{T}|\Psi_{\mathrm{SD}}\rangle + \int v(\boldsymbol{r})\left(n_{\Psi_{\mathrm{SD}}} - n_0\right)(\boldsymbol{r})\mathrm{d}\boldsymbol{r} \right)
\end{aligned} \tag{3.25}$$

where, in the last line, we have used that the minimum kinetic energy of a non-interacting quantum system is the one coming from a (normalised) Slater determinant.[8]

[6] What are these suitable potentials is a very delicate subject as, even in a strictly convex treatment, there is no explicit way to characterise the dual space of the N-representable density matrices. Implicitly, if we call the latter $\mathscr{I}$ we can then label the former as $\mathscr{I}^*$.

[7] Similarly to what we have seen in section 1.2

$$\sup_v \left(E_{\lambda,n_0}[v] - \int v(\boldsymbol{r})n_0(\boldsymbol{r})\mathrm{d}\boldsymbol{r} \right) = E_{\lambda,n_0}[v_0] - \int v_0(\boldsymbol{r})n_0(\boldsymbol{r})\mathrm{d}\boldsymbol{r} \tag{3.24}$$

with v_0 the maximizer. And we might be tempted to write $E_{\lambda,n_0}[v_0] - \int v_0(\boldsymbol{r})n_0(\boldsymbol{r})\mathrm{d}\boldsymbol{r} = F_{\lambda,v_0}[n_0]$. However, by virtue of the Hohenberg Kohn theorem, F is not a functional of both the external potential *and* the density contrary to the total energy, and the dependence on the maximizer cancels out, i.e. $E_{\lambda,n_0}[v_0] - \int v_0(\boldsymbol{r})n_0(\boldsymbol{r})\mathrm{d}\boldsymbol{r} = F_\lambda[n_0]$.

[8] This is a reasonable conjecture, however, in footnote 10 chapter 1, we have referenced some exceptions concerning the case when the external potential is the exact KS one, i.e. the optimal one for eq 3.25.

We thus see that the last expression in parenthesis, if we add the extra condition that the orbitals forming the Slater determinant are orthogonal to each other (something which we require for sheer computational convenience), is precisely our Lagrangian expression of eq 1.34.

3.2.2. Dual-Kantorovich formulation

We now define the strictly correlated electrons energy, E_{SCE}, as

$$E_{\mathrm{SCE}} = \lim_{\lambda\to\infty} \frac{E_\lambda}{\lambda} \tag{3.26}$$

Combining eqs 3.3, 3.23 and 3.26, we can obtain the strong-interaction limit of the Levy-Lieb functional from

$$\lim_{\lambda\to\infty} \frac{F_\lambda[n_0]}{\lambda} = \sup_v \left(\inf_\Psi \langle\Psi|\hat{V}_{ee} + \hat{V}_v|\Psi\rangle - \int v(\boldsymbol{r}) n_0(\boldsymbol{r}) \mathrm{d}\boldsymbol{r} \right). \tag{3.27}$$

Just as in the former example of T_s, the equation above coincides with V_{ee}^{SCE} of eq 3.6 by construction, in fact it is analogous to writing a minimization over the electron-electron interaction operator subject to a density constraint

$$V_{ee}^{\mathrm{SCE}}[n_0] = \sup_v \left(\inf_\Psi \left\{ \langle\Psi|\hat{V}_{ee}|\Psi\rangle + \int v(\boldsymbol{r}) \left(n_\Psi - n_0\right) \mathrm{d}\boldsymbol{r} \right\} \right). \tag{3.28}$$

We have already discussed at length that, being left with only multiplicative operators determining a potential energy surface, $\hat{V}_{ee}(\boldsymbol{r}_1,\cdots,\boldsymbol{r}_N) + \hat{V}_v(\boldsymbol{r}_1,\cdots,\boldsymbol{r}_N) = E_{\mathrm{pot}}[v](\boldsymbol{r}_1,\cdots,\boldsymbol{r}_N)$, the modulus squared of the optimal Ψ will – if the problem allows for a Monge solution – look as a distribution of the likes of eq 3.9 although a different one for each external potential, v. The expectation value of the potential energy on its GS wavefunction will then coincide with the minimum value of the potential energy surface, i.e.

$$\inf_\Psi \int E_{\mathrm{pot}}[v](\boldsymbol{r}_1,\cdots,\boldsymbol{r}_N) |\Psi_v(\boldsymbol{x}_1,\cdots,\boldsymbol{x}_N)|^2 \mathrm{d}\boldsymbol{x}_1\cdots\mathrm{d}\boldsymbol{x}_N = E_{\mathrm{pot}}[v]\Big|_{\min} \tag{3.29}$$

thus we can discard $|\Psi_v|^2$ to find the optimal classical positions for any external potential v determining E_{pot} and its minimum

$$\begin{aligned}
V_{ee}^{\mathrm{SCE}}[n_0] &= \sup_v \left(\inf_\Psi \int E_{\mathrm{pot}}[v](\boldsymbol{r}_1,\cdots,\boldsymbol{r}_N) |\Psi(\boldsymbol{x}_1,\cdots,\boldsymbol{x}_N)|^2 \mathrm{d}\boldsymbol{x}_1\cdots\mathrm{d}\boldsymbol{x}_N - \int v(\boldsymbol{r}) n_0(\boldsymbol{r}) \mathrm{d}\boldsymbol{r} \right) \\
&= \sup_v \left(E_{\mathrm{pot}}[v]\Big|_{\min} : - \int v(\boldsymbol{r}) n_0(\boldsymbol{r}) \mathrm{d}\boldsymbol{r} = 0 \right) \\
&= \sup_v \left(- \int v(\boldsymbol{r}) n_0(\boldsymbol{r}) \mathrm{d}\boldsymbol{r} : E_{\mathrm{pot}}[v]\Big|_{\min} = 0 \right) \\
&= \sup_v \left(- \int v(\boldsymbol{r}) n_0(\boldsymbol{r}) \mathrm{d}\boldsymbol{r} : E_{\mathrm{pot}}[v] \geq 0 \right)
\end{aligned} \tag{3.30}$$

where in the second line we use eq 3.29 and rewrite the constraint in an equivalent form and in the third line we exploit the intrinsic symmetry of the Lagrangian construction to exchange the role of the quantity to maximise and of its constraint. Lastly, we use that, by definition, $E_{\text{pot}}[v]\Big|_{\min} = 0 \Rightarrow E_{\text{pot}}(\boldsymbol{r}, \cdots, \boldsymbol{r}_N) \geq 0$ and calling $v = -u$ we get back precisely eq 3.17.

3.3. The co-motion functions

For the evaluation of eqs 3.13 and 3.15 the co-motion functions are needed.
To determine them, one needs to solve the intricate differential equation 3.11.
So far, it has been possible to (semianalytically) solve it only for $1D$ densities [72] and for the spherically symmetric ones [73].
For the former case, as mentioned, the proposed solution was later proven to be the optimal one (therefore the Kantorovich solution is of Monge-type) [89].
For the latter case, the proposed expression, also renowned as the SGS conjectured solution to the Kantorovich problem, has later been shown to be the optimal one, for $N = 2$, in references [84, 85].
For $N \geq 3$, counterexamples have been put forward for which the optimal solution is either a map with different structure or rather a plan [77, 92].
In reference [77], however, numerical findings illustrate that the value of the true minimum is very close to the one obtained via eq 3.13. Moreover, the systems studied seem to indicate that for a spherical density of interest in quantum chemistry, endowed with a typical shell structure, the SGS conjecture is the optimal solution, while more exotic cases out of the realm of Coulomb systems might have a non-Monge solution.
Most remarkably, it is further shown that, even when the SGS co-motion functions are not the optimal transport plan, the functional derivative w.r.t. the density of the interaction energy functional built from eq 3.13 still coincides with the potential found via integration of eq 3.15, as conjectured.

The key quantity for the construction of the co-motion functions is a monotone function denoted with N_e, $N_e : \mathbb{R}^D \to \mathbb{R}_+$, which measures the amount of electron density enclosed in a volume determined by the position vector. In particular, N_e asymptotically yields the number of electrons. For this reason, it is referred to as the "cumulant function". The co-motion functions are given in terms of the cumulant function and its inverse $N_e^{-1}(y)$, defined for $y \in (0, N)$.

One-dimensional systems Let us define the cumulant function for a 1D density

$$N_e(x) = \int_{-\infty}^{x} \mathrm{d}y\, n(y). \tag{3.31}$$

We also define the distances, a_i, such that the cumulant evaluated in these points gives an integer number of electron, $N_e(a_i) = i$.

By requiring that the co-motion functions fulfill (3.11) for a 1D density, one finds [72, 89]

$$f_i(x) = \begin{cases} N_e^{-1}\big(N_e(x) + i\big) & \text{for } x < \bar{a}_i \\ N_e^{-1}\big(N_e(x) + i - N\big) & \text{for } x > \bar{a}_i \ , \end{cases} \tag{3.32}$$

where $\bar{a}_i = a_{N-i} = N_e^{-1}(N - i)$.

From this explicit form of the co-motion functions, it is clear that

$$\int_x^{f_i(x)} n(y)\,\mathrm{d}y = i \tag{3.33}$$

which means that the strictly correlated electron located at $f_i(x)$ is separated from the reference electron located in x, for any x, by a chunk of density that always integrates to an integer number equal to i. This picture even holds if one regards the system to be periodic, so that particles disappearing at $+\infty$ reappear at $-\infty$. Put in different form

$$\int_{f_i(x)}^{f_{i+1}(x)} n(y)\,\mathrm{d}y = 1 \tag{3.34}$$

which tells us that two adjacent strictly correlated electrons are always separated by a chunk of density that integrates to one.

Spherically symmetric systems Since, in the spherically symmetric cases, the external potential does not depend on the relative angles, it is possible to decouple the angular from the radial component of the co-motion functions.
Then, the radial component is built in analogy with the $1D$ case. In particular, defining the following cumulant function

$$N_e(r) = \int_0^r 4\pi x^2\, n(x)\,\mathrm{d}x, \tag{3.35}$$

the radial co-motion functions $f_i(r)$ with $i = 1, \cdots, N$ of ref [73] are given

$$\begin{aligned} f_{2k-1}(r) &= \begin{cases} N_e^{-1}[2k - N_e(r)] & r \le a_{2k} \\ N_e^{-1}[N_e(r) - 2k] & r > a_{2k} \end{cases} \\ f_{2k}(r) &= \begin{cases} N_e^{-1}[2k + N_e(r)] & r \le a_{N-2k} \\ N_e^{-1}[2N - 2k - N_e(r)] & r > a_{N-2k} \end{cases} \end{aligned} \tag{3.36}$$

where N is the number of electrons, the integer index k runs from 1 to $\frac{N-1}{2}$ for N odd and from 1 to $\frac{N}{2}$ for N even and a_i are the (radial) distances for which – as in the 1D case – $N_e(a_i) = i$, with i integer. The relative angles between the electrons are found by minimizing the total repulsion energy between the N electrons in the radial configuration dictated, for each given distance from the

origin r of the reference electron, by the strictly correlated radial positions of the other $N-1$ [73, 93].
Analogously to the $1D$ case, the co-motion functions satisfy the following important and interesting property that

$$\begin{aligned} \int_r^{f_i(r)} y^2 n(y)\,\mathrm{d}y &= \frac{i}{4\pi} \\ \int_{f_i(r)}^{f_{i+1}(r)} y^2 n(y)\,\mathrm{d}y &= \frac{1}{4\pi} \end{aligned} \tag{3.37}$$

where we have taken into account the volume element $4\pi y^2$.

3.4. Applicability of the SCE formalism to physical and chemical problems

Although being an exact limit of the density-fixed adiabatic connection framework of DFT, the applicability of the SCE/SIL formalism encounters still two major kinds of limitations.
The first one is that it appears often too remote from the regime of interest in most physical and particularly chemical challenges.
The second one is that the computation of the strong interaction energy functional and potential, V_{ee}^{SCE} and $v^{\mathrm{SCE}}(\boldsymbol{r})$, for a general $3D$ density and general number of electrons, is a very hard task for which several different algorithms are currently appearing but are still far from routinary.
We can say that there are mainly three flavours of calculating the strong interaction ingredients

- Construct the co-motion functions (sec 3.3) and apply eqs 3.13 and 3.15.
  Although subject to the limitations just discussed, this approach is the one that allows to treat the largest number of electrons (see e.g. fig 7.2 of reference [94] where $N = 100$ for a relatively simple density profile) and is the one pursued throughout this work.

- Use the dual-Kantorovich formulation which is a linear programming problem scaling exponentially with N [95, 96].
  Very recently, an approach based on novel theoretical results [97] to solve the dual-Kantorovich problem within a relaxed but still well defined formulation (providing upper and lower bounds to the exact solution) has appeared [98] which seems rather promising in terms of numerical efficiency and theoretical insight.

- Use an approach called the *Entropic regularization* of Optimal Transport [99, 100] and the Sinkhorn algorithm [101].

This approach also scales exponentially with N. It extends the original Kantorovich problem allowing for some regularizing parameter τ to introduce an entropic energy term which competes with the interaction one in the optimisation. When $\tau \to 0$, you recover exactly the strong interaction limit of DFT. This approach has many desirable mathematical properties and might bring new theoretical insight.

3.4.1. The KS-SCE method

Equation 3.6 provides a well defined functional, in terms of which one can exactly partition the total energy as

$$E_v[n] = T_s[n] + T_c[n] + V_{ee}^{\mathrm{SCE}}[n] + V_{ee}^{\mathrm{d}}[n] + V[n] \tag{3.38}$$

where

$$V_{ee}^{\mathrm{d}}[n] = V_{ee}[n] - V_{ee}^{\mathrm{SCE}}[n] \geq 0. \tag{3.39}$$

This idea of expressing the energy in terms of the two functionals T_s and V_{ee}^{SCE} that are located at the two extremes of the adiabatic connection of sec 1.4 is labeled KS-SCE method, for obvious reasons.
As a zeroth-order approximation, one can neglect the two corrections T_c and V_{ee}^{d} and set $E_{Hxc} \approx V_{ee}^{\mathrm{SCE}}$ as originally proposed in reference [83].
Such simple approximation possesses the very neat property of being a rigourous lower bound to the energy as it models the minimum of a sum into a sum of minima

$$\min_{\Psi \to n} \langle \Psi | \hat{T} + \hat{V}_{ee} | \Psi \rangle \approx \min_{\Psi \to n} \langle \Psi | \hat{T} | \Psi \rangle + \min_{\Psi \to n} \langle \Psi | \hat{V}_{ee} | \Psi \rangle. \tag{3.40}$$

Consequently, such simple approximation turns out to be accurate in the two extremes of very low and very high densities [102]. In particular, it has proven capable of capturing the strong-correlation physics, delivering rather accurate densities for systems in which electrons are confined in quasi-1D and quasi-2D geometries [79, 83, 93, 103]. The accurate description of strongly correlated systems is out of reach for most (if not all) other density functional approximations (DFAs).
However, the accuracy of this method in the intermediate-correlation regime seems limited. Its limitation needs to be extensively assessed by solving the KS equations (eq 1.40) with $v_{Hxc} \approx v_{Hxc}^{\mathrm{SCE}}$ for different chemical and physical problems.

As briefly sketched in the beginning of this section, this is not an easy task since the computation of the SCE functional can be obtained only for quite specific cases and the assessment has been only carried over model or simple chemical systems [95, 104–106]. Nonetheless in reference [105], allowing to explore the trend of the resulting energy w.r.t. fractional number of electrons has provided a unique result and an independent "numerical proof" that the exact spin-restricted KS formalism should feature the discontinuity in the HOMO eigenvalue for open shell systems, illustrating the incredible capabilities of the SCE structure to be immune to certain

weaknesses almost ubiquitous in DFAs and to resolve long-standing DFT problems without imposing any *ad hoc* condition on or giving extra flexibility to its functional expression (like is done, e.g., in a spin-unrestricted treatment).

In the following we list some other exact and very desirable properties of the SCE potential as a model for the Hartree-exchange-correlation potential

1. As said, the definite integral over the density between any two co-motion functions must give exactly one (compare eq 3.37). Therefore, bringing the reference electron to infinity implies that the distance among any of the electrons in the bulk of the density and the reference electron needs to be infinite

$$|\boldsymbol{r} - \mathbf{f}_i(\boldsymbol{r})| \sim |\boldsymbol{r}| \qquad |\boldsymbol{r}| \to \infty, \tag{3.41}$$

Combining it with eq 3.15 we get

$$\nabla v_{Hxc}^{\mathrm{SCE}}(\boldsymbol{r}) \sim -\frac{N-1}{r^2} \qquad |\boldsymbol{r}| \to \infty, \tag{3.42}$$

which, by integration, leads to

$$v_{Hxc}^{\mathrm{SCE}}(\boldsymbol{r}) \sim \frac{N-1}{r} + c \qquad |\boldsymbol{r}| \to \infty, \tag{3.43}$$

showing that the SCE potential has the correct asymptotic behaviour.

2. From eq 3.15, it is also apparent that the associated effective charge is correctly $N-1$ meaning that it is not affected by the self-interaction error. Equivalently, since the pair density $P_{2,\mathrm{SCE}}(\boldsymbol{r},\boldsymbol{r}')$ coming from the SCE wavefunction (eq 3.9) via eq 6.12 is properly normalised, the following two sum-rules [107]

$$\int h_{xc}(\boldsymbol{r},\boldsymbol{r}')\mathrm{d}\boldsymbol{r} = -1 \tag{3.44}$$

$$\int h_{xc}(\boldsymbol{r},\boldsymbol{r}')\, n(\boldsymbol{r})\mathrm{d}\boldsymbol{r} = -n(\boldsymbol{r}') \tag{3.45}$$

are still satisfied if we substitute the exact XC hole $h_{xc}(\boldsymbol{r},\boldsymbol{r}')$ with the one coming from the SCE description $\left(\frac{P_{2,\mathrm{SCE}}(\boldsymbol{r},\boldsymbol{r}')}{n(\boldsymbol{r})} - n(\boldsymbol{r}')\right)$.

3. The corresponding interaction energy functional automatically satisfies the Lieb-Oxford bound and actually is the one that challenges it the most, for a given density profile [108], as sketched in sec 1.4.

To conclude, it seems reasonable to design DFAs which amend the extreme correlation and the lack of the kinetic contribution of the SCE description but are otherwise inspired to its mathematical structure [109–111].

3.4.2. Interaction-Strength Interpolations along the adiabatic connection

One of the most fruitful application of the information enclosed in the strong-interaction limit of DFT is in the construction of DFAs as interpolations along the adiabatic connection.
The idea of constructing models for the adiabatic connection integrand, W_λ (eq 1.60) to get an expression for the exchange-correlation energy via eq 1.59, was explored relatively lately compared to the appearance in the literature of the adiabatic connection formalism (see e.g. [27]).
One of the first uses was suggested by Becke in his "half-and-half" theory [112, 113] with a simple linear interpolation in the range $0 \leq \lambda \leq 1$ used as ansatz for W_λ.
In reference [114], two models for approximating W_λ, also in the range $0 \leq \lambda \leq 1$, are proposed, which are inspired to the theory of Padé approximants [115] and satisfy certain constraints on atomization energies. In particular the [2|2]-Padé ansatz introduces the idea of constraining the approximate function to recover the weak-interaction expansion linear coefficient (see eq 1.67).
Since 1999, Seidl *et al* pioneered the route of constructing interpolations in the more balanced range $0 \leq \lambda < \infty$ [71, 116, 117] and other interpolation formulas, in the same spirit, have been developed since [34, 118]. The underlying idea is that by using a function of λ able to link the result from perturbation theory with the $\lambda \to \infty$ expansion of $W_\lambda[n]$, an approximate resummation of the perturbative series is obtained [117].
Recently, this approach has gained renovated interest and studies aiming at a more extended assessment and implementation of such density functional approximations are emerging, concerning both their global [7, 119, 120] and their different local forms [6, 121, 122].

Recalling eq 1.70 and, combining eqs 1.60 and 3.13, we can now obtain the explicit form of the constant term W_∞

$$W_\infty[n] = \frac{1}{2}\int n(\boldsymbol{r}) \sum_{i=1}^{N-1} \frac{1}{|\boldsymbol{r} - \mathbf{f}_i[n](\boldsymbol{r})|} \mathrm{d}\boldsymbol{r} - U[n]. \tag{3.46}$$

Combining eqs 1.66 and 3.1, we understand also the role of the W_∞ as an exact lower bound for the adiabatic connection integrand, and, consequently, as the value that, for a given density profile, challenges the LO bound the most (eq 1.71).

Picturing the electrons as performing zero point (harmonic) oscillations about their $\lambda \to \infty$ positions[9], at finite but large λ, allows to write the following formula

[9] See reference [72] for an extended introduction to the problem and the special case of spherical two electron densities and reference [34] for a much more detailed treatment and the general result.

for the next coefficient in the expansion 1.70, $W'_\infty[n]$

$$W'_\infty[n] = \frac{1}{4}\sum_{\mu=4}^{3N}\int \frac{n(\boldsymbol{r})}{N}\omega_\mu[n](\boldsymbol{s}) \tag{3.47}$$

where the ω_μ are the eigenvalues of the Hessian matrix $M_{\mu\nu}(\boldsymbol{s})$ which measures the (multivariable) curvature of the potential energy surface $E_{\text{pot}}^{\text{SCE}}$ on the manifold parametrized by the co-motion functions (thus $\boldsymbol{s}$ is typically a vector in $\mathbb{R}^D$ in a curvilinear coordinate system).

Since it hinges upon the computation of the co-motion functions, the explicit computation of W_∞, via eq 3.46, is as much limited as that of the co-motion functions itself, see sec 3.3. That of W'_∞ (eq 3.47) is even more limited due to the presence of the Hessian matrix eigenvalues.

For this reason, these two terms are mostly approximated using a semi-local model labeled "Point-charge-plus-Continuum" (PC) [117].

Without going into any of the details of the model, we list the corresponding gradient expansion formulas, i.e.

$$W_\infty^{\text{PC}} = \int \left(A\, n^{4/3} + B\,\frac{|\nabla n|^2}{n^{4/3}}\right)(\mathbf{r})\, d\mathbf{r}, \tag{3.48}$$

$$W'^{\text{ PC}}_\infty = \int \left(C\, n^{3/2} + D\,\frac{|\nabla n|^2}{n^{7/6}}\right)(\mathbf{r})\, d\mathbf{r} \tag{3.49}$$

where $A = -9(4\pi/3)^{1/3}/10$, $B = 3[3/(4\pi)]^{1/3}/350$, $C = \sqrt{3\pi}/2$, $D = -0.028957$.

Note that the above value of the D coefficient was established by requiring that, for the He atom case, the PC model match the exact SCE functional, while the original value of this parameter, $\tilde{D} = 0.02558$, was fixed, before the exact SCE value was available, by the condition that it match the MGGA functional of reference [123]. Other choices are also possible (e.g. the use of the Hydrogen atom as a reference). Regardless of the choice made for the D parameter, the accuracy of the PC model as an approximation for the zero-point oscillations term, $W'^{\text{ PC}}_\infty \approx W'_\infty$, has proven to be much more system dependent than that of the functional for the lower bound, $W_\infty^{\text{PC}} \approx W_\infty$, as shown in reference [34].

Combining such ingredients from the strong-interaction expansion with the ones from the weak-interaction counterpart (eq 1.67), a series of XC functionals can be derived depending on the chosen interpolating function and on whether the $\lambda \to \infty$ expansion includes or not the order $1/\sqrt{\lambda}$.

Interaction Strength Interpolation (ISI) formula [116, 117, 124]

$$W_\lambda^{\text{ISI}} = W_\infty + \frac{X}{\sqrt{1+\lambda Y} + Z}\ , \tag{3.50}$$

with

$$X = \frac{xy^2}{z^2}\ ,\ Y = \frac{x^2y^2}{z^4}\ ,\ Z = \frac{xy^2}{z^3} - 1\ ; \tag{3.51}$$

$$x = -2W_0',\ y = W_\infty'\ ,\ z = W_0 - W_\infty\ . \tag{3.52}$$

Via eq 1.59, the corresponding XC energy functional reads

$$E_{xc}^{\mathrm{ISI}} = W_\infty + \frac{2X}{Y}\left[\sqrt{1+Y} - 1 - Z\ln\left(\frac{\sqrt{1+Y}+Z}{1+Z}\right)\right]\ . \tag{3.53}$$

Revised ISI (revISI) formula [34]

$$W_\lambda^{\mathrm{revISI}} = W_\infty + \frac{b\left(2 + c\lambda + 2d\sqrt{1+c\lambda}\right)}{2\sqrt{1+c\lambda}\left(d + \sqrt{1+c\lambda}\right)^2}, \tag{3.54}$$

where

$$\begin{aligned} b &= -\frac{4W_0'(W_\infty')^2}{(W_0 - W_\infty)^2}\ ,\ c = \frac{4(W_0'W_\infty')^2}{(W_0 - W_\infty)^4}\cdot, \\ d &= -1 - \frac{4W_0'(W_\infty')^2}{(W_0 - W_\infty)^3}\ . \end{aligned} \tag{3.55}$$

$$E_{xc}^{\mathrm{revISI}} = W_\infty + \frac{b}{\sqrt{1+c} + d}\ . \tag{3.56}$$

Seidl-Perdew-Levy (SPL) formula [71]

$$W_\lambda^{\mathrm{SPL}} = W_\infty + \frac{W_0 - W_\infty}{\sqrt{1+2\lambda\chi}}\ , \tag{3.57}$$

where

$$\chi = \frac{W_0'}{W_\infty - W_0}\ . \tag{3.58}$$

$$E_{xc}^{\mathrm{SPL}} = (W_0 - W_\infty)\left[\frac{\sqrt{1+2\chi} - 1 - \chi}{\chi}\right] + W_0\ . \tag{3.59}$$

Liu-Burke (LB) formula [118]

$$W_\lambda^{\mathrm{LB}} = W_\infty + \beta(y + y^4)\ , \tag{3.60}$$

where

$$y = \frac{1}{\sqrt{1+\gamma\lambda}}\ ,\ \beta = \frac{W_0 - W_\infty}{2}\ ,\ \gamma = \frac{4W_0'}{5(W_\infty - W_0)}\ . \tag{3.61}$$

$$E_{xc}^{\mathrm{LB}} = 2\beta\left[\frac{1}{\gamma}\left(\sqrt{1+\gamma} - \frac{1+\gamma/2}{1+\gamma}\right) - 1\right] + W_0. \tag{3.62}$$

As a last remark, we note that ISI and revISI use all four known ingredients in the expansions 1.67 and 1.70, while SPL and LB formulas do not use W'_∞.

These functionals, which are all based on an adiabatic connection integrand interpolation (ACII), will be generally referred to as ACII functionals. They are non-empirical in the sense that they are approximate perturbation-theory resummations, include full exact exchange, and describe correctly correlation in the weak-interaction limit. Therefore, they are well-suited to try to overcome the limitations of semilocal and hybrid DFT approaches. Their most severe problem could be the lack of size consistency[10] for species made of different atoms, an error that is absent in the case of homogeneous clusters. However, it has been recently shown that size consistency in the ACII functionals can be restored in a very simple way at no extra computational cost [127].

[10] Note that the size consistency issue is actually quite subtle [125, 126].

4

Assessment of interaction-strength interpolation formulas for gold and silver clusters

The performance of functionals based on the idea of interpolating between the weak and the strong-interaction limits the global adiabatic-connection integrand is carefully studied for the challenging case of noble-metal clusters. Different interpolation formulas are considered and various features of this approach are analyzed. It is found that these functionals, when used as a correlation correction to Hartree-Fock, are quite robust for the description of atomization energies, while performing less well for ionization potentials. Future directions that can be envisaged from this study and a previous one on main group chemistry are discussed.

4.1. Introduction and framework

Noble metal clusters, in particular those made of silver and gold, are of high interest for different areas of materials science and chemistry as well as for technological applications [128–148]. Noble metals clusters display, in fact, peculiar properties that differ from those of the bulk materials, due to the higher reactivity of the surface atoms. Moreover, these properties can be often tuned by varying the size and shape of the clusters [129, 136, 139, 141, 149–154]. For these reasons, the study of the electronic properties of metal clusters is currently a very active

research field [155–165], with many available experimental techniques [166–173]. Nonetheless, in most cases information from theoretical calculations is fundamental to provide a better understanding of the results and to aid the correct interpretation of the experimental data [155, 156, 165, 174–178].

Computational studies of noble metal clusters are, however, not straightforward [179] because of the small single-particle energy gap, implying a possible multi-reference character of the electronic states, and due to the complex correlation effects characterizing such systems. For these reasons, in principle an accurate description of the electronic structure can only be achieved by high-level correlated multi-reference approaches [180, 181]. However, these methods are hardly applicable for the study of clusters, due to the very high computational cost.

On the other hand, "conventional" single-reference wave-function methods (e.g. Møller-Plesset perturbation theory [182, 183], configuration interaction [184, 185], or coupled cluster [186, 187]) often display important basis set and/or truncation errors, even for relatively small cluster sizes, which prevent the achievement of accurate, reliable, results. Thus, one of the most used computational tools to study noble metal clusters is Kohn-Sham density-functional theory (DFT) [188–190].

DFT calculations on noble metal clusters are often performed using a semilocal approximation for the exchange-correlation (XC) functional, e.g. the generalized gradient approximation (GGA) [191] or the meta-GGA's [192] . This is an efficient approach [151, 152, 159, 161, 163, 164, 174, 175, 193–195], but in various cases it has also shown limited accuracy, especially in the not so rare case when it is necessary to discriminate between isomers with rather similar energies (for example in the prediction of the two- to three-dimensional crossover in gold and silver clusters [164, 176]). However, unlike in the case of main group molecular calculations, the use of hybrid functionals, which include a fraction of exact exchange, is not able to provide a systematic improvement. Instead, it often leads to a worsening of the results [164, 195]. The origin of this problem possibly traces back on the too simplistic idea of mixing a fixed fraction of exact exchange with a semilocal approximation.

In the hybrid wavefunction-DFT formalism a certain fraction a of the electron-electron interaction is treated within a wave function method, while the remaining energy is captured with a semilocal functional. In a compact notation [1] this can be written as

$$E_0 = \min_{\Psi \in \mathrm{SD}} \left\{ \langle \Psi | \hat{T} + a\,\hat{V}_{ee} + \hat{V} | \Psi \rangle + \bar{E}^{a}_{\mathrm{Hxc}}[n_\Psi] \right\}, \tag{4.1}$$

where the complementary Hartree-exchange-correlation functional $\bar{E}^{a}_{\mathrm{Hxc}}$ depends on Ψ only through its density n_Ψ. When the minimization over Ψ in eq 4.1 is restricted to single Slater determinants Ψ_{SD}, we obtain the usual hybrid functional approximation, which mixes a fraction a of Hartree-Fock exchange with a semilocal functional, while using second-order perturbation theory to improve the wavefunction Ψ leads to single-parameter double-hybrid functionals [1]. The XC part $E_{xc}[n]$

of $\bar{E}^{a}_{\mathrm{Hxc}}$ that needs to be approximated in the standard hybrid functionals formalism is usually modeled starting from the adiabatic connection formula [114, 196–198], eq 1.59. Most hybrid functionals then employ a simple ansatz for the density-fixed linear adiabatic connection integrand, for example [197, 198]

$$W_\lambda[n] = W_\lambda^{\mathrm{DFA}}[n] + \left(E_x - E_x^{\mathrm{DFA}}\right)(1-\lambda)^{p-1} \ , \tag{4.2}$$

where DFA denotes a density functional approximation (i.e. a semilocal functional), E_x denotes the Hartree-Fock exchange functional (eq 1.68), and p is a parameter. Substituting eq 4.2 into eq 1.59, yields the usual linear mixing between the exact exchange and the density functional approximation with $a = 1/p$. However, eq 4.2 is a quite arbitrary expression for W_λ. It only satisfies the constraint that $W_0 = E_x$ but for $\lambda \neq 0$ it incorporates no exact information and it is not even recovering the correct weak-interaction limit behavior. Thus, most of the accuracy of hybrids relies on the empiricism included into the parameter p and the DFA. This seems to work well for main-group molecular systems but not for other systems such as metal clusters considered here. The ACII functionals have been rarely tested on systems of interest for practical applications, with the exception of a recent assessment of the ISI functional for main-group chemistry [199]. This investigation has revealed interesting features of this functional and suggested possibilities for future applications.

In this work we move away from main group chemistry to assess different ACII functionals for the description of the electronic properties of noble metal clusters, made up of gold and silver. As we have mentioned above, these are very important systems for materials science and chemical applications but their proper computational description is still a challenge. Thus, the testing of high-level DFT methods for this class of systems has a great practical interest. Moreover, the application of non-empirical XC functionals, constructed on a well defined theoretical framework, to the challenging problem of the simulation of electronic properties of noble metal clusters can help to highlight new properties and limitations of such approaches.

4.2. Computational details

In this work we have tested four ACII XC functionals, which are based on an interpolation of the density-fixed linear adiabatic connection integrand, namely ISI [116, 117, 124, 199], revISI [34], SPL [71], and LB [118] (see sec 3.4.2 for details). Additionally, for comparison, we have included results from the Perdew-Burke-Ernzerhof (PBE) [200] and the PBE0 [197, 201] functionals, which are among the most used semilocal and hybrid functionals, respectively, as well as from the B2PLYP double hybrid functional [202], which also includes a fraction of second-order Møller-Plesset correlation energy (MP2). We have also considered a comparison with the second- third- and fourth-order Møller-Plesset perturbation theory (MP2, MP3, MP4) [182] results. This is because, as explained in sec 3.4.2, the

ACII functionals can be seen as an approximate resummation of perturbation theory, so that it is interesting to compare them with the first few lower orders. The reference results used in the assessment are specified below for each test set considered:

Small gold clusters. This set consists of the Au_2, Au_2^-, Au_3, Au_3^+, Au_3^-, and Au_4 clusters. For all these systems we have calculated the atomization energies; for the anions as well as for Au_3 we have computed the ionization potential (IP) energies. The geometries of all clusters have been taken from ref [159]; they are shown in fig 4.1. Reference energies have been calculated at the CCSD(T) level of theory [203–206].

Small silver clusters. This set includes Ag_2, Ag_2^+, Ag_2^-, Ag_3, Ag_3^+, Ag_3^-, Ag_4. As for the small gold clusters case, we have computed the atomization energies of all the silver clusters and the IP of the anions as well as of Ag_3. The geometries of all systems have been taken from Ref. [164]; they are shown in fig 4.1. Reference values for the energies have been obtained from CCSD(T) [203–206] calculations.

Binary gold-silver clusters. This set considers the AuAg, $AuAg^-$, Au_2Ag, Au_2Ag^-, $AuAg_2$, and $AuAg_2^-$ clusters. Atomization energies have been calculated for all system, while IPs have been computed for the anions. Note that for the anions we considered as atomization energy the average with respect to the two possible dissociation channels, that is $AuAg^- \rightarrow Au + Ag^-$ and $AuAg^- \rightarrow Au^- + Ag$; $Au_2Ag^- \rightarrow Au_2 + Ag^-$ and $Au_2Ag^- \rightarrow Au_2^- + Ag$; $AuAg_2^- \rightarrow Au + Ag_2^-$ and $AuAg_2^- \rightarrow Au^- + Ag_2$. The geometries of the binary clusters have been obtained considering the structures reported in ref [195] (see fig 4.1) and optimizing them at the revTPPS/def2-QZVP level of theory [207, 208]. Reference energies have been calculated at the CCSD(T) level of theory [203–206].

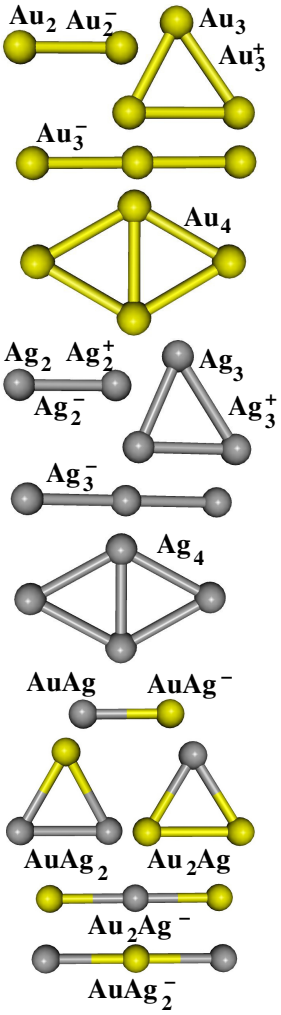

Figure 4.1: Structures of the small gold, silver and binary gold-silver clusters.

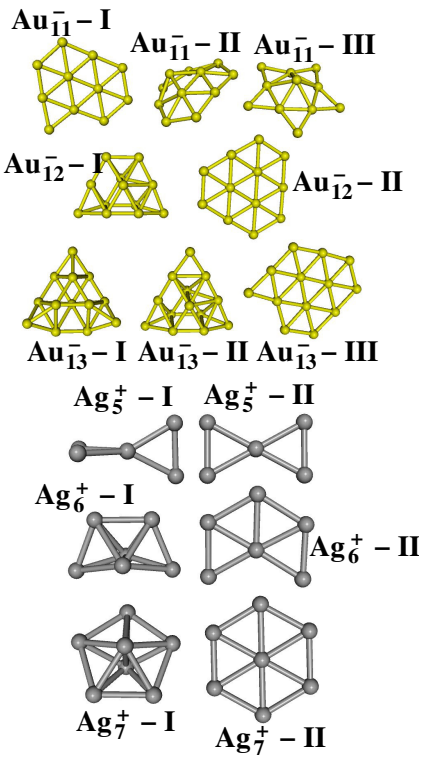

Figure 4.2: Structures of the gold and silver clusters considered for the 2D-3D dimensional crossover problem.

Gold 2D-3D crossover. This set includes the Au_{11}^-, Au_{12}^-, and Au_{13}^- clusters, that are involved in the two- to three-dimensional crossover of gold clusters. The geometries of all systems have been taken from ref [176] and are shown in fig 4.2.

Silver 2D-3D crossover. This set consists of the Ag_5^+, Ag_6^+, and Ag_7^+ clusters, which are relevant to study the two- to three-dimensional crossover of silver clusters. Geometries have been obtained optimizing at the revTPPS/def2-QZVP level of theory [207, 208], the lowest lying structures reported in ref [164]. The structures are reported in fig 4.2.

All the required calculations have been performed with the TURBOMOLE program package [209, 210], employing, unless otherwise stated, the aug-cc-pwCVQZ-PP basis set [211] and a Stuttgart-Koeln MCDHF 60-electron effective core potential [212]. The calculations concerning the ISI, revISI, SPL, and LB functionals have been performed in a post-self-consistent-field (post-SCF) fashion, using Hartree-Fock orbitals. This choice is consistent with the results of ref [199], where it has been found that the ISI functional yields much better results when used as a correlation correction for the HF energy. The PBE and PBE0 calculations have been performed using a full SCF procedure; B2PLYP calculations have been carried out as described in ref [202], considering a SCF treatment of the exchange and semilocal correlation part and adding the second-order MP2 correlation fraction as a post-SCF correction.

4.3. Results

In this section we analyze the performance of the ACII XC functionals for the description of the electronic properties of gold, silver and mixed Au/Ag clusters. The results are compared to those obtained from other approaches, such as semilocal and hybrid DFT as well as wave-function perturbation theory.

4.3.1. Total Energies

To start our investigation we consider, in table 4.1, the errors on total energies computed with different methods with respect to the CCSD(T) reference values. Although this quantity is usually not of much interest in practical applications (where energy differences are usually considered), the analysis of the errors on total energies will be useful to understand the performances of the different functionals for more practical properties such as atomization or ionization energies.

Inspection of the data shows that the ACII functionals do not perform very well for the total energy. In fact, they yield the highest mean absolute errors (MAEs), being even slightly worse than the semilocal PBE approach and giving definitely larger errors with respect to perturbation theory (MP2, MP3, and MP4) and to the double hybrid B2PLYP functional. Among the ACII functionals, the SPL and especially the LB approach perform systematically better than ISI and revISI. Thus LB yields errors which are often 30% smaller than ISI, even though they are still usually larger than those of the other non-ACII methods. On the other hand, considering the standard deviation of the errors (last line of table 4.1) we note that the ACII results display a quite small dispersion around the average (with LB and SPL again slightly better than ISI and revISI). This is related to the fact that the ACII functionals all give a quite systematic underestimation (in magnitude) of the energy of all systems. In contrast, PBE, PBE0, and partly B2PLYP give larger values of the standard deviation. This depends on the fact that these methods describe quite accurately some systems (e.g. Ag clusters), which are the ones that effectively contribute to produce a quite low MAE, but they give significantly larger errors for other systems. This behavior is a signature of the too simplistic nature of these functionals, which cannot capture equally well the physics of all systems.

The observed standard deviations suggest that, when energy differences are considered, the ACII functionals can benefit from a cancellation of the systematic error, such that rather accurate energy differences can be obtained. We must remark also that the standard deviation values reported in table 4.1 allow only a partial understanding of the problem because they are obtained from all the data but, depending on the property of interest, some energy differences may be more relevant than others, e.g. for atomization energies the difference between a cluster energy and the energy of the composing atoms is the most relevant. Thus, for example MP methods all yield quite low standard deviations, but a closer look at the results shows that the errors for atoms are quite different than those for the clusters (much more different than for ACII methods); hence, we can expect that, despite a quite good MAE and a small standard deviation, MP2, MP3, and MP4 atomization energies can display a limited accuracy. A more detailed analysis of the relationship between the data reported in table 4.1 and some relevant energy difference properties will be given in section 4.4.

Table 4.1: Errors on total energies (eV/atom) of small gold, silver, and binary clusters. For each set of clusters the mean absolute error (MAE) is reported. In the bottom part of the table we report also the statistics for the overall set (mean error (ME), MAE, and standard deviation).

	PBE	PBE0	B2PLYP	ISI	revISI	SPL	LB	MP2	MP3	MP4
Au	-4.93	-3.75	-1.73	2.84	2.93	2.65	1.97	-0.33	0.98	-0.27
Au+	-4.58	-3.73	-1.64	2.63	2.70	2.50	1.89	-0.10	0.68	-0.15
Au-	-4.94	-3.47	-1.65	3.26	3.38	3.02	2.25	-0.35	1.44	-0.41
Au2	-4.96	-3.66	-1.69	2.89	2.99	2.67	1.94	-0.53	1.22	-0.43
Au2-	-4.97	-3.58	-1.66	3.06	3.17	2.83	2.08	-0.46	1.40	-0.44
Au3	-4.97	-3.65	-1.67	2.89	3.00	2.67	1.94	-0.54	1.29	-0.48
Au3+	-4.90	-3.68	-1.66	2.80	2.90	2.59	1.88	-0.50	1.15	-0.43
Au3-	-4.94	-3.54	-1.66	2.98	3.10	2.73	1.96	-0.65	1.40	-0.55
Au4	-4.96	-3.62	-1.67	2.86	2.97	2.63	1.87	-0.66	1.33	-0.54
ME	-4.91	-3.63	-1.67	2.91	3.01	2.70	1.97	-0.46	1.21	-0.41
MAE	4.91	3.63	1.67	2.91	3.01	2.70	1.97	0.46	1.21	0.41
Ag	-0.89	-0.36	0.21	3.24	3.39	2.91	2.18	-0.26	1.04	-0.27
Ag+	-0.44	-0.25	0.38	2.99	3.13	2.71	2.04	-0.19	0.76	-0.20
Ag-	-0.99	-0.21	0.24	3.68	3.85	3.31	2.53	-0.08	1.39	-0.32
Ag2	-0.96	-0.30	0.22	3.32	3.49	2.97	2.19	-0.37	1.18	-0.38
Ag2+	-0.79	-0.34	0.28	3.14	3.28	2.82	2.11	-0.26	0.95	-0.27
Ag2-	-1.00	-0.27	0.24	3.50	3.67	3.14	2.37	-0.22	1.34	-0.33
Ag3	-0.95	-0.30	0.25	3.32	3.49	2.96	2.19	-0.39	1.23	-0.40
Ag3+	-0.85	-0.30	0.27	3.21	3.37	2.86	2.11	-0.41	1.10	-0.38
Ag3-	-0.97	-0.23	0.25	3.45	3.63	3.07	2.27	-0.38	1.32	-0.43
Ag4	-0.95	-0.27	0.24	3.29	3.47	2.91	2.12	-0.51	1.24	-0.45
ME	-0.88	-0.28	0.26	3.31	3.48	2.97	2.21	-0.31	1.15	-0.34
MAE	0.88	0.28	0.26	3.31	3.48	2.97	2.21	0.31	1.15	0.34
AuAg	-2.93	-1.95	-0.72	3.10	3.24	2.81	2.06	-0.47	1.20	-0.41
AuAg-	-2.97	-1.91	-0.70	3.27	3.41	2.97	2.20	-0.37	1.36	-0.39
AuAgAu	-3.58	-2.49	-1.00	3.03	3.16	2.76	2.01	-0.51	1.28	-0.46
AuAgAu-	-3.57	-2.40	-1.00	3.14	3.28	2.84	2.06	-0.57	1.36	-0.50
AgAuAg	-2.26	-1.38	-0.37	3.18	3.33	2.86	2.10	-0.46	1.26	-0.43
AgAuAg-	-2.32	-1.34	-0.40	3.30	3.46	2.96	2.18	-0.46	1.36	-0.47
ME	-2.94	-1.91	-0.70	3.17	3.31	2.87	2.10	-0.47	1.30	-0.44
MAE	2.94	1.91	0.70	3.17	3.31	2.87	2.10	0.47	1.30	0.44
				Overall statistics						
ME	-2.82	-1.88	-0.66	3.13	3.27	2.85	2.10	-0.40	1.21	-0.39
MAE	2.82	1.88	0.87	3.13	3.27	2.85	2.10	0.40	1.21	0.39
Std.Dev.	1.81	1.51	0.87	0.24	0.27	0.18	0.16	0.15	0.20	0.10

4.3.2. Atomization and Ionization energies

A first example of an important energy difference is the atomization energy. The atomization energy values calculated for the sets of gold, silver, and binary clusters with all the methods are reported in table 4.2. Observing the data it appears that, as anticipated, for atomization energies the ACII functionals work fairly well. In particular, SPL and LB, yield mean absolute relative errors (MAREs) of about 2-3% for all kinds of clusters, being competitive with the B2PLYP functional. The ISI and revISI functionals perform slightly worse, displaying a systematic underbinding and giving overall MAREs of 4% and 6%, respectively. Moreover, unlike for SPL and LB, non-negligible differences exist in the description of the different materials with gold clusters described better than silver ones. Overall the ISI and revISI functionals show a comparable performance as PBE and better than PBE0. Finally, the MP results show a quite poor performance, exhibiting MAREs ranging form 10% to 20%. In addition, we can note that MP2 results are closer to MP4 results than MP3 ones not only from a quantitative point of view but also qualitatively (MP2 and MP4 always overbind while MP3 always consistently underbinds). This is a clear indication of the difficult convergence of the perturbative series for the metal clusters electronic properties.

In table 4.3, we report the computed ionization potential energies, which are other important energy differences to consider for metal clusters. In this case the ACII functionals perform rather poorly, being the worst methods, if we exclude MP3. As in the case of atomization energies, SPL and LB (especially the latter) show a slightly better performance than ISI and revISI. Nevertheless, the results are definitely worst than for B2PLYP, PBE and even PBE0. A rationalization of this failure will be given in section 4.4.

4.3.3. 2D-3D crossover

To conclude this section, we consider the problem of the two- to three-dimensional (2D-3D) crossover of anionic gold clusters and cationic silver clusters.

Different studies have indicated that for anionic gold clusters the dimensional crossover occurs between Au_{11}^- (2D) and Au_{13}^- (3D), with the 2D and 3D Au_{12}^- structures being almost isoenergetic.[175, 176] On the other hand, for cationic silver clusters it has been suggested that the dimensional transition occurs already for Ag_5^+, which has a 2D structure with a slightly lower energy than the 3D one, while Ag_6^+ and Ag_7^+ display lowest energy 3D structures.[165, 213] Anyway, this is a quite difficult problem because experimentally it is not trivial to distinguish clusters of the same size but different dimensionality. A computational support is thus required [165, 174–176, 213, 214]. However, to describe correctly the energy ordering of several noble metal clusters with very similar energies is a hard task for any computational method [159, 176, 215, 216]. For this reason, this is a very interesting problem from the computational point of view and a hard

Table 4.2: Atomization energies (eV) of small gold, silver, and binary clusters. Note that for anionic binary clusters the average between the two possible dissociation paths has been considered (see section 4.2). For each set of clusters the mean error (ME), the mean absolute error (MAE), the mean absolute relative error (MARE), and the standard deviation are reported. In the bottom part of the table we report also the statistics for the overall set.

	PBE	PBE0	B2PLYP	ISI	revISI	SPL	LB	MP2	MP3	MP4	CCSD(T)
Au_2	2.33	2.08	2.20	2.17	2.14	2.24	2.33	2.67	1.79	2.60	2.27
Au_2^-	1.97	1.83	1.83	1.86	1.84	1.90	1.95	2.14	1.51	2.09	1.89
Au_3	3.57	3.14	3.26	3.28	3.23	3.39	3.54	4.08	2.51	4.07	3.45
Au_3^+	6.06	5.60	5.67	5.71	5.66	5.82	5.97	6.54	4.98	6.38	5.79
Au_3^-	4.90	4.52	4.73	4.87	4.81	5.00	5.17	5.80	4.05	5.57	4.87
Au_4	6.18	5.51	5.81	5.95	5.85	6.14	6.40	7.37	4.60	7.10	6.03
ME	0.12	-0.27	-0.14	-0.08	-0.13	0.03	0.18	0.71	-0.81	0.58	
MAE	0.12	0.27	0.14	0.08	0.13	0.06	0.18	0.71	0.81	0.58	
MARE	3%	7%	3%	2%	4%	1%	4%	17%	21%	14%	
Std.Dev.	0.08	0.16	0.06	0.06	0.07	0.08	0.13	0.39	0.37	0.30	
Ag_2	1.82	1.59	1.69	1.53	1.50	1.59	1.66	1.93	1.41	1.91	1.70
Ag_2^+	1.85	1.69	1.64	1.58	1.57	1.59	1.61	1.70	1.51	1.67	1.62
Ag_2^-	1.53	1.39	1.37	1.32	1.31	1.35	1.38	1.51	1.15	1.48	1.41
Ag_3	2.73	2.37	2.45	2.31	2.27	2.41	2.52	2.94	2.00	2.94	2.56
Ag_3^+	4.84	4.45	4.50	4.36	4.32	4.47	4.59	5.03	4.05	4.90	4.52
Ag_3^-	3.70	3.32	3.49	3.38	3.32	3.50	3.63	4.12	3.06	4.01	3.57
Ag_4	4.80	4.24	4.47	4.39	4.30	4.58	4.80	5.59	3.78	5.28	4.59
ME	0.19	-0.13	-0.05	-0.16	-0.20	-0.07	0.03	0.41	-0.43	0.32	
MAE	0.19	0.15	0.06	0.16	0.20	0.07	0.06	0.41	0.43	0.32	
MARE	7%	5%	2%	6%	7%	3%	2%	13%	15%	10%	
Std.Dev.	0.07	0.14	0.06	0.07	0.09	0.05	0.09	0.32	0.23	0.22	
AuAg	2.22	1.97	2.11	2.05	2.02	2.13	2.21	2.53	1.80	2.46	2.18
$AuAg^-$	1.83	1.69	1.71	1.74	1.72	1.78	1.83	2.00	1.47	1.92	1.77
Au_2Ag	3.65	3.26	3.42	3.47	3.41	3.59	3.73	4.28	2.80	4.22	3.65
Au_2Ag^-	4.96	4.58	4.84	4.97	4.91	5.12	5.28	5.90	4.36	5.63	5.04
$AuAg_2$	3.33	2.94	3.08	3.06	3.00	3.17	3.30	3.80	2.56	3.75	3.28
$AuAg_2^-$	3.83	3.40	3.58	3.48	3.42	3.60	3.74	4.25	3.00	4.14	3.63
ME	0.04	-0.29	-0.14	-0.13	-0.18	-0.03	0.09	0.53	-0.60	0.43	
MAE	0.07	0.29	0.14	0.13	0.18	0.06	0.09	0.53	0.60	0.43	
MARE	2%	9%	4%	4%	6%	2%	3%	16%	19%	13%	
Std.Dev.	0.09	0.14	0.08	0.07	0.08	0.06	0.08	0.23	0.21	0.18	
					Overall statistics						
ME	0.12	-0.22	-0.11	-0.12	-0.17	-0.02	0.10	0.54	-0.60	0.44	
MAE	0.13	0.23	0.11	0.12	0.17	0.06	0.11	0.54	0.60	0.44	
MARE	4%	7%	3%	4%	6%	2%	3%	15%	18%	12%	
Std.Dev.	0.10	0.16	0.08	0.07	0.08	0.07	0.11	0.33	0.31	0.25	

Table 4.3: Ionization potentials (eV) of small gold, silver, and binary clusters. For each set of clusters the mean error (ME), the mean absolute error (MAE), the mean absolute relative error (MARE), and the standard deviation are reported. In the bottom part of the table we report also the statistics for the overall set.

	PBE	PBE0	B2PLYP	ISI	revISI	SPL	LB	MP2	MP3	MP4	CCSD(T)
Au	9.54	9.22	9.29	9.00	8.97	9.05	9.13	9.42	8.91	9.32	9.20
Au^-	2.30	2.00	2.21	1.86	1.84	1.92	2.01	2.31	1.82	2.42	2.29
Au_2^-	1.94	1.75	1.84	1.56	1.55	1.58	1.62	1.78	1.53	1.91	1.91
Au_3	7.05	6.76	6.89	6.57	6.55	6.62	6.69	6.97	6.44	7.01	6.86
Au_3^-	3.63	3.38	3.67	3.45	3.41	3.53	3.63	4.03	3.36	3.92	3.70
ME	0.10	-0.17	-0.01	-0.30	-0.33	-0.25	-0.17	0.11	-0.38	0.12	
MAE	0.13	0.18	0.06	0.30	0.33	0.25	0.17	0.16	0.38	0.12	
MARE	2%	6%	2%	10%	11%	9%	6%	4%	12%	3%	
Std.Dev.	0.17	0.14	0.07	0.08	0.08	0.09	0.11	0.18	0.07	0.08	
Ag	8.04	7.70	7.76	7.35	7.33	7.40	7.45	7.67	7.31	7.66	7.59
Ag^-	1.40	1.15	1.28	0.86	0.85	0.90	0.95	1.13	0.95	1.35	1.31
Ag_2	8.02	7.60	7.80	7.30	7.26	7.40	7.50	7.90	7.21	7.90	7.68
Ag_2^-	1.11	0.96	0.97	0.66	0.65	0.66	0.67	0.72	0.69	0.92	1.01
Ag_3	5.93	5.63	5.71	5.30	5.28	5.34	5.39	5.58	5.26	5.70	5.64
Ag_3^-	2.38	2.10	2.32	1.93	1.90	1.99	2.06	2.31	2.02	2.42	2.31
ME	0.22	-0.06	0.05	-0.36	-0.38	-0.31	-0.25	-0.04	-0.35	0.07	
MAE	0.22	0.10	0.07	0.36	0.38	0.31	0.25	0.14	0.35	0.10	
MARE	6%	5%	2%	17%	17%	15%	13%	8%	15%	4%	
Std.Dev.	0.16	0.11	0.08	0.07	0.07	0.07	0.09	0.18	0.07	0.10	
$AuAg^-$	1.46	1.30	1.35	1.05	1.04	1.07	1.09	1.19	1.07	1.34	1.39
Au_2Ag^-	3.16	2.90	3.17	2.87	2.84	2.94	3.03	3.34	2.95	3.30	3.18
$AuAg_2^-$	2.35	2.04	2.24	1.79	1.76	1.84	1.91	2.17	1.83	2.28	2.15
ME	0.09	-0.16	0.01	-0.34	-0.36	-0.29	-0.23	-0.01	-0.29	0.07	
MAE	0.10	0.16	0.05	0.34	0.36	0.29	0.23	0.13	0.29	0.10	
MARE	5%	7%	3%	17%	18%	15%	12%	7%	15%	4%	
Std.Dev.	0.11	0.11	0.07	0.03	0.03	0.04	0.07	0.18	0.05	0.10	
					Overall statistics						
ME	0.15	-0.12	0.02	-0.33	-0.36	-0.28	-0.22	0.02	-0.35	0.09	
MAE	0.16	0.14	0.06	0.33	0.36	0.28	0.22	0.15	0.35	0.11	
MARE	4%	6%	2%	14%	15%	13%	11%	6%	14%	4%	
Std.Dev.	0.16	0.12	0.08	0.07	0.07	0.07	0.09	0.18	0.07	0.09	

Table 4.4: Relative energies (eV) with respect to conformer I (see Computational details) of 2D and 3D anionic gold clusters and cationic silver clusters. For the gold clusters the data include the correction terms reported in table IV of Ref. [176].

		PBE	PBE0	BLOC	B2PLYP	ISI	revISI	SPL	LB	MP2
Au_{11}^--I	2D	0.000	0.000	0.000	0.000	0.000	0.000	0.000	0.000	0.000
Au_{11}^--II	3D	0.217	0.224	0.206	0.147	0.083	0.090	0.070	0.054	-0.006
Au_{11}^--III	3D	0.270	0.179	0.354	0.254	0.265	0.251	0.302	0.344	0.499
Au_{12}^--I	3D	0.000	0.000	0.000	0.000	0.000	0.000	0.000	0.000	0.000
Au_{12}^--II	2D	-0.450	-0.340	0.008	-0.144	0.710	0.669	0.789	0.882	1.228
Au_{13}^--I	3D	0.000	0.000	0.000	0.000	0.000	0.000	0.000	0.000	0.000
Au_{13}^--II	3D	-0.027	-0.032	0.037	-0.024	0.497	0.495	0.499	0.527	0.618
Au_{13}^--III	2D	-0.111	0.056	0.386	0.248	0.802	0.894	0.917	0.824	1.069
Ag_5^+-I	3D	0.000	0.000	0.000	0.000	0.000	0.000	0.000	0.000	0.000
Ag_5^+-II	2D	0.021	0.025	0.024	0.020	0.021	0.020	0.018	0.017	0.013
Ag_6^+-I	3D	0.000	0.000	0.000	0.000	0.000	0.000	0.000	0.000	0.000
Ag_6^+-II	2D	-0.005	0.055	0.280	0.007	0.220	0.211	0.241	0.265	0.348
Ag_7^+-I	3D	0.000	0.000	0.000	0.000	0.000	0.000	0.000	0.000	0.000
Ag_7^+-II	2D	-0.099	0.000	0.303	-0.059	0.286	0.270	0.318	0.352	0.474

test for any electronic structure approach. In table 4.4, we report the energies calculated for the anionic gold clusters and cationic silver clusters relevant for the 2D-3D transition. The table shows, for comparison, also the results obtained with the BLOC meta-GGA functional [216–218], which is expected to be one of the most accurate approaches for this kind of problems. Observing the data, one can immediately note that the PBE, PBE0 and even B2PLYP methods are not reliable for the dimensional crossover of noble metal clusters. In fact, PBE always favors 2D structures, whereas PBE0 predicts the 2D-3D transition at a too large cluster dimension for gold, Au_{13}^- (although the 3D geometry with lowest energy is not the same as the one we find with BLOC and all ACII functionals), and for silver the energies of the 2D and 3D clusters differ slightly for both $n = 6$ and $n = 7$, not evidencing a clear transition at the expected cluster size. A similar behaviour is found for the B2PLYP functional, which was instead one of the best for the atomization energies and IPs of small clusters. The ACII functionals overall perform all quite similarly, predicting for all clusters the expected ordering and agreeing well with BLOC results for the cationic Ag clusters but tending to favor 3D structures in the anionic Au clusters. We note that this behavior is somehow inherited from the MP2 method, which however performs much worse than any of the ACII functionals considered here.

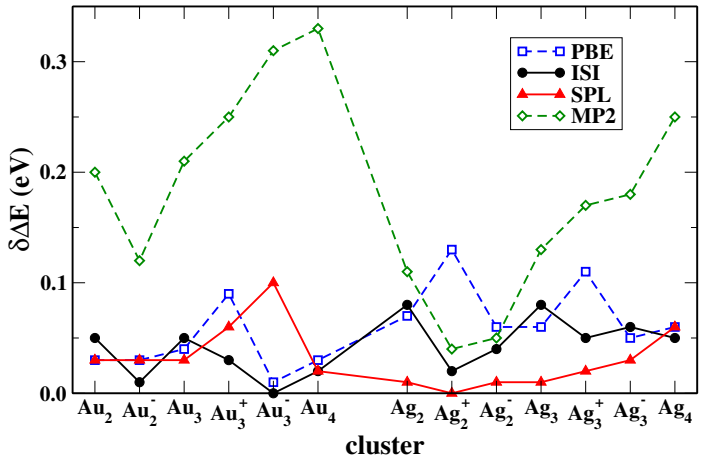

Figure 4.3: Difference in the total energy error between a cluster and its constituent atoms (see eq 4.3).

4.4. Discussion and Analysis of the results

In the previous section we saw that the ACII functionals perform rather well for the calculation of atomization energies of noble metal clusters. As mentioned above, a good rationalization of the observed results can be obtained in terms of the energy errors that the different methods display for the total energies of atoms and of the clusters. These have been reported in table 4.1.

4.4.1. Energy differences

For a better visualization here we additionally plot, in fig 4.3, the quantity

$$\begin{aligned} \delta\Delta E &= \Delta E(M_n M_m^- M_l^+) - \\ &- \sum_n \Delta E(M_n) - \sum_m \Delta E(M_n^-) - \sum_l \Delta E(M_n^+) \ , \end{aligned} \tag{4.3}$$

where ΔE are the total energy errors (the ΔE per atom are reported in table 4.1), M=Au or Ag, and n, m, l are integers such that $M_n M_m^- M_l^+$ corresponds to a given cluster (e.g. for Au_3^+ we have M=Au, $n=2$, $m=0$, and $l=1$). This quantity provides a measure of how different the energy error is for a given cluster compared to that of its constituent atoms. Inspection of the plots shows that the smaller $\delta\Delta E$ values are yielded by the ISI and SPL (revISI and LB, not reported, give similar results). These functionals are also among the best performers for the atomization energies. On the other hand, for PBE we observe that the $\delta\Delta E$ is small for gold clusters, with the exception of Au_3^+, while for silver clusters is larger. Indeed, looking to table 4.2 we can find that PBE performs well for gold clusters, with the exception of Au_3^+ that

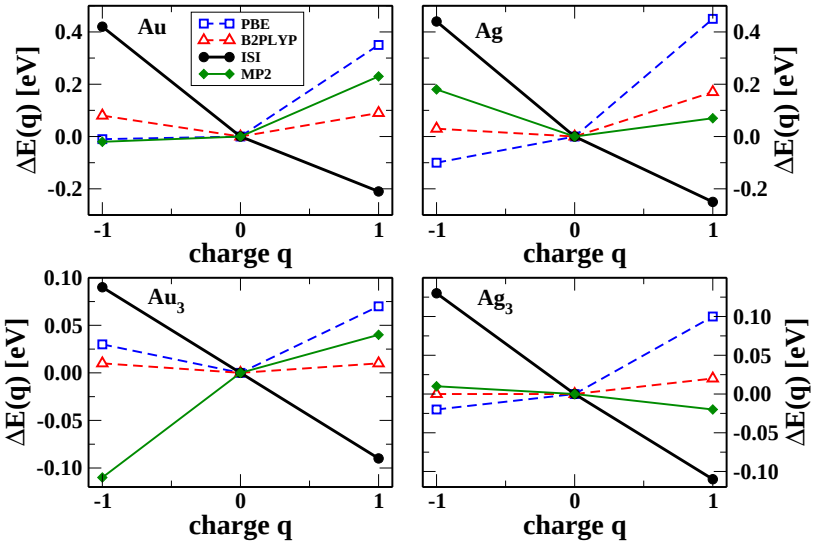

Figure 4.4: Variation of the energy error with the total charge of the system (Au top left, Au_3 bottom left, Ag top right, Ag_3 bottom right). The values are scaled to the neutral system value (see eq 4.4).

yields an error of 0.27 eV (more than twice larger than the MAE), while it performs less well for silver clusters. Finally, for MP2 the values of $\delta\Delta E$ are generally very large. Thus, despite MP2 is on average quite accurate in the description of the total energies (see table 4.1) it fails to produce accurate atomization energies because of accumulation of the errors.

A similar analysis, can be made on the results of the ionization potential calculations (reported in table 4.3). However, in this case the difference to consider is between the neutral and the charged species. Then, a different behavior is observed. In fact, while for most of the considered methods the total energy error is not much different between a neutral and a charged species of the same cluster, for the ACII functionals we always observe an increase of the error with the charge. This situation is schematized in fig 4.4, where we plot, for several examples, the quantity

$$\Delta(q) = \Delta E(A^q) - \Delta E(A^0) \ , \tag{4.4}$$

with A being any of the systems under investigation and $q = -1, 0, 1$. As a consequence, the ACII functionals are generally the worst performers for the calculation

of ionization potentials, while PBE and especially B2PLYP perform well thanks to the more homogeneous description of the differently charged species.

This analysis shows that, although the quality of the total energies produced by a functional is a key element to understand the performance of the functional, the basic property to observe is not the quality of the absolute energies, but rather the variance of the errors. Furthermore, the contrasting behaviors we have observed for the description of the atomization energies and of the ionization potentials highlights the subtleties inherent to such calculations. In particular, the accuracy of the ACII functionals has been shown to be not much dependent on the investigated material (Au or Ag) nor on the system's size but to be quite sensitive to the charge state of the computed system. The first feature is a positive one. This is related, as we saw, to the computation of atomization energies, but even more importantly it indicates that the idea beyond the construction of the ACII functionals is in general quite robust such that the functionals, although not very accurate in absolute terms (see table 4.1) are well transferable to systems of different size and composition. This is not a trivial result since, as we documented, other methods (e.g. PBE and PBE0, but even MP4) do not share this property. On the contrary, the dependence of the ACII functionals on the charge state of the system indicates a clear limitation of such approaches. They are in fact unable to describe with similar accuracy systems with qualitatively different charge distributions. As a consequence, the ionization potential calculations are problematic for ACII functionals.
Note however that, because accurate experimental data are not available for all the systems, our assessment of the performances of the ACII functionals on small clusters, see fig 4.1, and Tables 4.1, 4.2, and 4.3, is carried out w.r.t. CCSD(T) values. This allows a more direct and sensible comparison of the results, whereas the comparison with experimental data would require the consideration of further effects such as thermal/vibronic ones as well as spin-orbit coupling.[159, 176] Of course CCSD(T) results cannot be considered "exact" for metal clusters. Nevertheless, an accurate comparison with available experimental data from literature shows that, for atoms (regarding ionization energies) [219, 220] and neutral dimers and trimers (regarding both ionization and atomization energies) [221–223], CCSD(T) yields results within 0.04 eV from the experimental ones. While for the charged dimers and trimers (regarding both ionization and atomization energies), CCSD(T) results are within 0.2 eV [220, 224, 225] from the experimental ones but this is only partly ascribable to the diminished accuracy of the CCSD(T) calculation *per se* and possibly due to the large error bars associated to these measures on the experimental side and on the increased importance of correcting terms on the computational side.

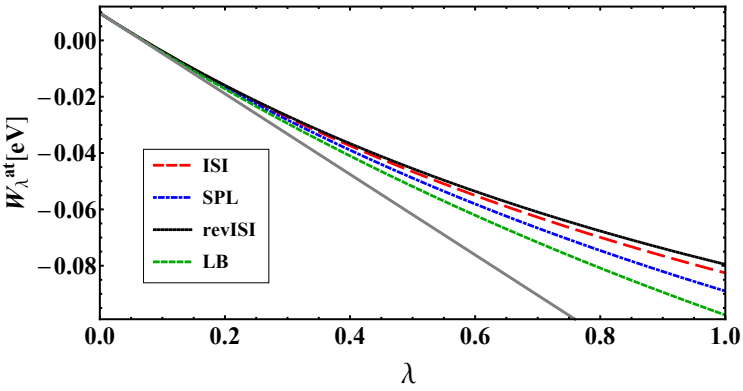

Figure 4.5: Atomization adiabatic connection integrands (see eq 4.5) corresponding to ISI, revISI, SPL, and LB for the Au_2 case; the thick curve in gray corresponds to the linear expansion for the atomization adiabatic connection integrand (eq 4.6)

4.4.2. AC curves: gold dimer showcase

To rationalize the origin of the limitations of the ACII functionals as well as to understand in depth the differences and the similarities between the different interpolation formulas it would be necessary to inspect in some detail the shape of the density-fixed linear adiabatic connection integrand defining ISI, revISI, SPL, and LB. However, contrary to small atoms and molecules (see, e.g., refs [91, 226, 227]), for noble metal clusters there exists no reference adiabatic connection integrands to compare to. Thus, such a detailed analysis is not really possible. Nevertheless, some useful hints can be obtained by a semi-qualitative comparison of the various adiabatic connection curves. As an example, in fig 4.5 we report, for the Au_2 case (the other systems studied here have very similar features), the atomization adiabatic connection integrand, defined as

$$W_\lambda^{at}(Au_2) = W_\lambda(Au_2) - 2W_\lambda(Au) \ , \tag{4.5}$$

for ISI, revISI, SPL, and LB. The integrated value (between 0 and 1) of this quantity corresponds to the XC atomization energy calculated with a given ACII functional. For discussion we have plotted also the weak interacting limit expansion truncated at linear order in λ for the atomization adiabatic connection integrand, which is defined as

$$W_{\lambda,LE}^{at}(Au_2) = W_{\lambda,LE}(Au_2) - 2W_{\lambda,LE}(Au), \tag{4.6}$$

where the linear expansion (LE) of the AC integrand for a species X is $W_{\lambda,LE}(X) = E_x(X) + 2\lambda E_c^{GL2}(X)$ in agreement with eq 1.67 and in the case of HF orbitals $E_c^{GL2}(X) = E_c^{MP2}(X)$. Because of the weak-interacting limit constraint, all the curves plotted in the figure share the same $\lambda = 0$ value, which corresponds to the Hartree-Fock exchange atomization energy, as well as the same slope at this point. The

curves remain very similar up to $\lambda \approx 0.2$, which is not strictly dictated by the weak-interacting limit constraint but rather by a possible lack of flexibility in the interpolation formulas. For values of $\lambda \gtrsim 0.2$, the curves associated to the various functionals start to differ, due to the different ways they approach the W_∞ value for $\lambda = \infty$. Note that in this case ISI and revISI are further constrained to recover the W'_∞ slope, whereas SPL and LB do not have this constraint. The interpolation towards the strong-interaction limit is therefore the main feature differentiating the various ACII functionals, even in the range $0 \leq \lambda \leq 1$. In general, revISI is the slowest to approach the asymptotic W_∞ value, whereas LB is the fastest. So the former will usually yield the smaller XC energies, whereas the latter will produce the larger XC energies (in magnitude). In fact, turning to the Au_2 example reported in fig 4.5, the inspection of the plot shows that revISI is indeed the slowest to move towards the asymptotic W_∞^{at} value (for Au_2 $W_\infty^{at} = -0.239$). Consequently, in table 4.2 it yields the smallest atomization energy (it underestimates the Au_2 atomization energy by 0.13 eV). On the opposite, LB is the fastest to move towards the asymptotic W_∞^{at} value, thus it gives the larger atomization energy (overestimating it by 0.06 eV). In this specific case, the SPL functional, which behaves almost intermediately between revISI and LB, yields a very accurate value of the atomization energy, underestimating it by only 0.03 eV. Thus, we have seen that there are two main features that can determine the performance of an ACII functional. The first one is surely the behavior towards the strong-coupling limit, which is able to influence the shape of the adiabatic connection integrand curve for $\lambda \gtrapprox 0.2/0.3$. This behavior is indeed modeled differently by the various functionals examined in this work, but it appears that none of them can really capture the correct behavior in the range of interest $0.3 \leq \lambda \leq 1$. This is possibly due to the fact that information on the $\lambda = \infty$ point is not sufficient to guide correctly the interpolation at the quite small λ values of interest for the calculation of XC energies. A second factor that is relevant for the functionals' performance is the small λ behavior. At very small λ values this is determined by eq 1.67, but for larger values of the coupling constant (at least for $0.1 \leq \lambda \leq 0.2$) the shape of the curve should depart from the slope given by E_c^{GL2} in order to correctly describe the higher-order correlation effect. Instead, we have observed that all the ACII functionals provide the same behavior up to $\lambda \approx 0.2$. This indicates that the interpolation formulas have not enough flexibility to differentiate from the asymptotic behavior imposed at $\lambda = 0$.

4.4.3. Role of the reference orbitals

The ACII functionals are orbital-dependent nonlinear functionals, thus they are usually employed to compute the XC energy in a post-SCF fashion (as we did in this work). Then, the results depend on the choice of the orbitals used for the calculation. Recent work [199] has evidenced that ISI results for main-group chemistry are much improved when Hartree-Fock orbitals are used. This has been

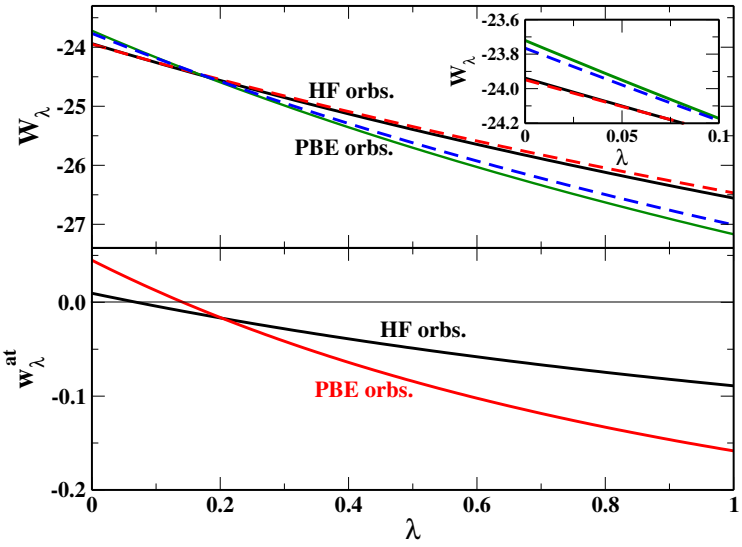

Figure 4.6: Top: Adiabatic connection integrands computed with the SPL formula (eq 3.57) for Au_2 (solid line) and Au (dashed line) using Hartree-Fock and PBE orbitals; the Au curve is multiplied by a factor of 2; the inset shows the weak-interaction part of the curves. Bottom: Atomization adiabatic connection integrands (see eq 4.5) computed with the SPL formula for the Au_2 case.

basically traced back to the characteristics of the Hartree-Fock single-particle energy gap (which determines the magnitude of E_c^{GL2} and thus the weak-interaction behavior of the curves).

For gold and silver clusters, after some test calculations, we found a similar result for all the ACII formulas considered. For this reason, all the results reported in section 4.3 are based on Hartree-Fock orbitals. To clarify this aspect, we have reported in fig 4.6 both the bare and the atomization adiabatic connection integrands computed with the SPL formula (similar results are obtained for the other formulas) for Au_2 and Au using either Hartree-Fock and PBE orbitals. It can be seen that the adiabatic connection curve of Au_2, obtained from Hartree-Fock orbitals, is very similar to twice the Au curve. Hence, the atomization adiabatic connection integrand is rather flat, yielding (correctly) a moderate atomization XC energy. This behavior depends partly on the fact that in Hartree-Fock calculations Au_2 has almost twice the exchange energy of Au but, primarily, it traces back to the fact that the Au_2 MP2 correlation energy is almost perfectly two times larger than the Au one (which in turn depends on the fact that the two systems have very close single-particle energy gaps – 7.604 eV and 7.707 eV, respectively – and on the size-extensivity of the MP2 method). Thus, the adiabatic connection integrands for

Au_2 and twice the Au have almost identical slopes at $\lambda = 0$ and similar behaviors for $\lambda \leq 1$. Instead, when PBE orbitals are used, larger differences between the Au_2 and twice the Au curves can be noted. These originate only partially from the fact that, in the case of PBE orbitals, the exact exchange contributions of Au_2 and twice Au are not much similar (they differ by 0.045 eV). Mostly they depend on the rather different GL2 correlation energies for the systems ($E_c^{\mathrm{GL2}}(\mathrm{Au_2}) - 2E_c^{GL2}(\mathrm{Au}) = -0.173eV$), which in turn trace back to the fact that the single particle energy gaps computed for Au_2 and Au are very different: 2.014 eV and 0.718 eV, respectively. Consequently, the atomization adiabatic connection integrand curve calculated with PBE orbitals is steeper than the Hartree-Fock-based one and therefore it yields significantly larger atomization XC energies. This results in a strong tendency of PBE-based ACII functionals to overbind the noble metal clusters.

4

4.4.4. Further analysis of the ACII's formulas

We have seen in Sec. 4.3 that SPL and LB formulas show overall better performances than ISI and revISI. As mentioned, the main difference between the two groups is that the former use a three-parameters interpolation formula while the latter make use of a fourth ingredient from the $\lambda \to \infty$ limit, i.e. the zero-point oscillation term $W'_\infty[\rho]$. The revISI formula also recovers the exact expansion at large λ to higher orders [34]. However, we have to keep in mind that the ingredients coming from the strong interaction limit are not computed exactly, but approximated with the semilocal PC model. Comparison with the exact $W_\infty[\rho]$ and $W'_\infty[\rho]$ for light atoms [34, 73] suggests that the PC approximation of the $W_\infty[\rho]$ term is more accurate than the one for $W'_\infty[\rho]$. Moreover, the parameters appearing in the PC model for $W_\infty[\rho]$ are all determined by the electrostatics of the PC cell, while in the case of $W'_\infty[\rho]$ the gradient expansion does not give a physical result, and one of the parameters has to be fixed in other ways, for example by making the model exact for the He atom [34]. Keeping in mind that the information from $W'_\infty[\rho]$ is less accurate (and maybe less relevant in the HF context), it can be interesting to consider a variant of ISI and revISI, in which we replace $W'^{\mathrm{PC}}_\infty[\rho]$ with the curvature at $\lambda = 0$ (obtained from MP3) as input ingredient.
The ISI and revISI formulas have four parameters that need to be fixed by four equations. In the standard forms (see sec 3.4.2) the four equations are obtained by imposing that W_λ^{ISI} recovers the first two terms of the weak-interacting limit expansion, eq 1.67, and the first two terms in the strongly-interacting limit expansion, eq 1.70for large λ. For the first time we have explored an alternative choice that is to constrain ISI and revISI to recover the first three terms of eq 1.67 for small λ, and only the first term of eq 1.70 for large λ. The structure of the interpolation

formula is thus formally the same, but the parameters are given by

$$\begin{aligned} X = &\quad -2(W_0 - W_\infty) + \frac{W_0''}{(W_0')^2}(W_0 - W_\infty)^2, \\ Y = &\quad -2\frac{W_0''}{W_0'} + \frac{4W_0'}{(W_0 - W_\infty)}, \\ Z = &\quad -3 + \frac{W_0''}{(W_0')^2}(W_0 - W_\infty); \end{aligned} \tag{4.7}$$

for ISI, and

$$\begin{aligned} b = &\quad -2(W_0 - W_\infty) + \frac{4W_0''(W_0 - W_\infty)^2}{3(W_0')^2}, \\ c = &\quad -\frac{4W_0''}{3W_0'} + \frac{2W_0'}{(W_0 - W_\infty)}, \\ d = &\quad -3 + \frac{4W_0''(W_0 - W_\infty)}{3(W_0')^2}; \end{aligned} \tag{4.8}$$

for revISI.

However, while in the standard ISI and revISI interpolation formulas the parameters, $Y[\rho]$ and $c[\rho]$, which appear under square root, are given by the sum of squared quantities (see eqs 3.51, and 3.55), in these modified versions this is not true and they can become negative. In the cases studied here both parameters turn out to be always negative and smaller than one, meaning that there is, for each species, a critical lambda, λ_c, always larger than one, after which the function takes imaginary values. In particular we found an average $\bar{\lambda}_c^{ISI} \approx 4$ with values spanning from 2.5 to 5.7, and an average $\bar{\lambda}_c^{revISI} \approx 180$ with values spanning from 6 to over 3×10^3. As a general trend we thus see that the modified revISI appears to be more robust than the modified ISI in the sense that it becomes imaginary at significantly larger λ values.

Another important point to consider is that, as explained in Sec. 4.4.3, we are using the ACII functionals with Hartree-Fock orbitals, which means that they are used as a correlation functional for the Hartree-Fock energy. In other words, the ACII correlation functionals are used here as an approximate resummation of the Møller-Plesset perturbation series: they recover the exact MP2 at weak coupling, and perform much better than MP3 and MP4 for atomization energies (see table 4.2). Thus, a first question that needs to be addressed is whether the PC model used here to compute the infinite coupling strength functional is accurate also for the Hartree-Fock adiabatic connection, in which the λ-dependent Hamiltonian reads

$$\hat{H}^\lambda = \hat{T} + \hat{V}_{\text{HF}} + \hat{V}_{\text{ext}} + \lambda(\hat{V}_{ee} - \hat{V}_{\text{HF}}), \tag{4.9}$$

with $\hat{V}_{\text{HF}}$ the Hartree-Fock non local potential operator. When $\lambda \to \infty$, the problem defined by $\hat{H}^\lambda$ of eq 4.9 is not the same as the one of the density-fixed adiabatic connection arising in DFT. The results of this study may suggest that the PC model

can provide a decent approximation of the leading $\lambda \to \infty$ term in the HF adiabatic connection integrand, at least when dealing with isoelectronic energy differences. A careful study of the problem is the object of on-going work and first important results are going to be illustrated in the next chapter.

4.5. Conclusions and perspectives

We have assessed the performance of functionals based on the idea of interpolating between the weak and the strong-interaction limits the global adiabatic-connection integrand (ACII functionals) for noble-metal clusters, analyzing and rationalizing different features of this approach. The study presented here extends a previous preliminary assessment on main group chemistry [199], and explores different interpolation formulas.

We have found that the ACII functionals, although not spectacularly accurate, are quite robust for the description of atomization energies, as their performance tends to be the same for different species and different cluster sizes, which is a positive feature. We should also stress that this good performance is achieved by using 100% of Hartree-Fock exchange, and thus avoiding to rely on error cancellation between exchange and correlation. Rather, as clearly shown in fig. 4.3, this is achieved by performing in a very similar way for the description of a cluster and its constituent atoms. On the other hand, the ACII functionals are found to be inaccurate for ionization energies, as they are not capable to describe different charged states of the same system with the same accuracy, as shown in fig. 4.4.

As in the case of main-group chemistry [199], we have found that the ACII functionals perform much better when used with Hartree-Fock orbitals, which means that they are used as a correlation functional for the Hartree-Fock energy. In other words, the ACII correlation functionals are used here as an approximate resummation of the Møller-Plesset perturbation series: they recover the exact MP2 at weak coupling, and perform much better than MP3 and MP4 for atomization energies (see table 4.2). Thus, a first question that needs to be addressed is whether the PC model used here to compute the infinite coupling strength functionals is accurate also for the Hartree-Fock adiabatic connection of Eq. (4.9), which is the object of a current investigation. The results of this study and of reference [199] suggest that the PC model can provide a decent approximation of the $\lambda \to \infty$ HF adiabatic connection integrand, at least when dealing with isoelectronic energy differences.

Another promising future direction is the development of ACII functionals in which the interpolation is done in each point of space, on energy densities [121, 228, 229]. These local interpolations are more amenable to construct size-consistent approximations, but need energy densities all defined in the same gauge (the one of the electrostatic potential of the exchange-correlation hole seems so far to be the most suitable for this purpose [230]). In this framework, the simple PC model, which performs globally quite well, does not provide accurate approximations pointwise

[229], and needs to be replaced with models based on integrals of the spherically averaged density [231, 232], which, in turn, needs a careful implementation, which is the focus of on-going efforts [232]. Finally, recent models for $\lambda = 1$ could be also used in this framework [109], both locally and globally.

5

Strong-interaction limit of an adiabatic connection in Hartree-Fock theory

We show that the leading term in the strong-interaction limit of the adiabatic connection that has as weak-interaction expansion the Møller-Plesset perturbation theory can be fully determined from a functional of the Hartree-Fock orbitals. We analyze this functional and highlight similarities and differences with the strong-interaction limit of the density-fixed adiabatic connection case of Kohn-Sham density functional theory.

5.1. Introduction to the Hartree-Fock adiabatic connection

Mixing KS DFT with Hartree-Fock (HF) ingredients is an approximation strategy that has a long history in chemistry, already starting with hybrids [112, 113, 233–237] and double hybrids [1, 238–240], but also by simply inserting the HF density into a given approximate XC density functional [241–246].
Recently, as the previous chapter has given an example, it has also been observed that rather accurate interaction energies can be obtained from models for $W_\lambda^{\mathrm{DFT}}[n]$ that interpolate between the two limits of eq 1.67 – retaining only the first term, GL2, in the GL series – and of eq 1.70, using HF densities and orbitals as input, i.e., by constructing *de facto* an approximate resummation of the Møller-Plesset (MP) series, a procedure that lacks so far a theoretical justification.

Motivated in particular by these last findings, we analyze in this work the Hartree-Fock adiabatic connection [eq 5.1 below] whose Taylor expansion around

$\lambda = 0$ is the MP series (eq 5.4 below) and show that the leading term in the $\lambda \to \infty$ expansion of its GS wavefunction is determined by a functional of the HF density, see eq 5.9 below. We also highlight similarities and differences with the DFT case, showing that the large λ expansion in HF theory has a structure similar to the one of eq 1.70.

We keep the notation general, as only few key properties of the HF operators are important here. We consider the adiabatic connection (see, e.g., ref [247])

$$\hat{H}_\lambda^{\rm HF} = \hat{T} + \hat{V}_{\rm ext} + \hat{J} + \hat{K} + \lambda(\hat{V}_{ee} - \hat{J} - \hat{K}), \tag{5.1}$$

with $\hat{V}_{\rm ext}$ the (nuclear) external potential and $\hat{J} = \hat{J}[n^{\rm HF}]$ and $\hat{K} = \hat{K}[\{\phi_i^{\rm HF}\}]$ the standard HF Coulomb and exchange operators, which are fixed once for all in the initial HF calculation, and do not depend on λ, but only on the HF density $n^{\rm HF}$ and occupied HF orbitals $\{\phi_i^{\rm HF}\}$ (eq 5.1 coincides with eq 4.9 introduced in the previous chapter with $\hat{V}_{\rm HF} = \hat{J} + \hat{K}$).
In the ground state $\Psi_\lambda^{\rm HF}$ of $\hat{H}_\lambda^{\rm HF}$, the density $n_\lambda(\mathbf{r})$ changes with λ: $n_{\lambda=0}(\mathbf{r})$ is the HF density $n^{\rm HF}(\mathbf{r})$, and $n_{\lambda=1}(\mathbf{r})$ is the exact physical density $n(\mathbf{r})$. Note that Teale *et al.* [227] have analyzed a related adiabatic connection, in which the external potential is kept fixed; in that framework in the limit $\lambda \to \infty$ all the electrons but one escape to infinity. From eq 5.1, the Hellmann-Feynman theorem yields the exact formula

$$E_{xc}^{\rm HF} = \int_0^1 W_\lambda^{\rm HF}\, d\lambda \tag{5.2}$$

for the XC energy in the HF framework, with

$$W_\lambda^{\rm HF} \equiv \langle \Psi_\lambda^{\rm HF} | \hat{V}_{ee} - \hat{J} - \hat{K} | \Psi_\lambda^{\rm HF} \rangle + U[n^{\rm HF}] + 2E_x^{\rm HF}. \tag{5.3}$$

Equation 5.3 has been defined to allow for a direct comparison with the DFT $W_\lambda^{\rm DFT}[n]$ of eqs 1.59 and 1.60.
For small λ

$$W_{\lambda\to 0}^{\rm HF} = E_x^{\rm HF} + \sum_{n=2}^{\infty} n\, E_c^{{\rm MP}n}\, \lambda^{n-1}, \tag{5.4}$$

with $W_{\lambda=0}^{\rm HF} = E_x^{\rm HF}$, and where $E_c^{{\rm MP}n}$ the $n^{\rm th}$ term in the MP series. As is well-known (see, e.g., references [248, 249]), the radius of convergence of the MP series is in general smaller than 1. Here we ask the question: *what happens to* $\Psi_\lambda^{\rm HF}$ *and* $W_\lambda^{\rm HF}$ *as* $\lambda \to \infty$*?* After answering this theoretical question, we will discuss its actual relevance for constructing approximations.

5.2. Analysis of the HF $\lambda \to \infty$ limit

When λ becomes very large, the term $\lambda(\hat{V}_{ee} - \hat{J} - \hat{K})$ in eq 5.1 becomes more and more important, and we argue that the wavefunction $\Psi_\lambda^{\rm HF}$ should end up minimizing

this term alone, similarly to the DFT case (see chapter 3). The difference here is that the minimizer is not constrained to yield a fixed density, and the operator to be minimized also contains $-\hat{J}-\hat{K}$. We further argue that the expectation value of $\hat{K}$ is subleading with respect to the one of $\hat{V}_{ee}-\hat{J}$, i.e., we argue that

$$\langle \Psi_\lambda^{\mathrm{HF}} | \hat{K} | \Psi_\lambda^{\mathrm{HF}} \rangle = O(\lambda^{-1/2}) \qquad (\lambda \to \infty). \tag{5.5}$$

Before we shall support this conjecture with a variational argument, we discuss its consequences.

If eq 5.5 holds, then $\Psi_\lambda^{\mathrm{HF}}$ for $\lambda \to \infty$ ends up minimizing the even simpler operator $\lambda(\hat{V}_{ee}-\hat{J})$,

$$\lim_{\lambda\to\infty} \Psi_\lambda^{\mathrm{HF}} = \operatorname*{argmin}_{\Psi} \langle \Psi | \hat{V}_{ee} - \hat{J} | \Psi \rangle, \tag{5.6}$$

$$\lim_{\lambda\to\infty} W_\lambda^{\mathrm{HF}} = \min_{\Psi} \langle \Psi | \hat{V}_{ee} - \hat{J} | \Psi \rangle + U[n^{\mathrm{HF}}] + 2E_x^{\mathrm{HF}} + O(\lambda^{-1/2}) \tag{5.7}$$

The "asymptotic Hamiltonian"

$$\hat{H}_\infty^{\mathrm{HF}} = \hat{V}_{ee} - \hat{J}[n^{\mathrm{HF}}] = \sum_{\substack{i,j=1 \\ j>i}}^{N} \frac{1}{|\mathbf{r}_i - \mathbf{r}_j|} - \sum_{i=1}^{N} v_{\mathrm{H}}(\mathbf{r}_i; [n^{\mathrm{HF}}]), \tag{5.8}$$

is completely specified by the HF density $n^{\mathrm{HF}}(\mathbf{r})$, since $N = \int n^{\mathrm{HF}}(\mathbf{r})\,\mathrm{d}\mathbf{r}$ and $\hat{J}[n] = \sum_{i=1}^{N} v_{\mathrm{H}}(\mathbf{r}_i; [n])$.
Consequently, also the minimizer in eqs 5.6 and 5.7 is specified solely by n^{HF},

$$\lim_{\lambda\to\infty} \Psi_\lambda^{\mathrm{HF}} = \Psi_\infty^{\mathrm{HF}}[n^{\mathrm{HF}}], \tag{5.9}$$

and the minimum in eq 5.7 is a functional of the HF orbitals,

$$\lim_{\lambda\to\infty} W_\lambda^{\mathrm{HF}} = E_{\mathrm{el}}[n^{\mathrm{HF}}] + 2E_x^{\mathrm{HF}} + O(\lambda^{-1/2}). \tag{5.10}$$

The minimizer in eq 5.6 could be non unique, but this does not affect the value of the minimum, which is the object of the present investigation.
The functional $E_{\mathrm{el}}[n] = \min_{\Psi} \langle \Psi | \hat{V}_{ee} - \hat{J}[n] | \Psi \rangle + U[n]$ has a simple classical interpretation: since $\hat{H}_\infty^{\mathrm{HF}}$ is a purely multiplicative operator, the square modulus $|\Psi_\infty^{\mathrm{HF}}|^2$ of its minimizing wave function is a distribution in $\mathbb{R}^{3N}$ that is zero wherever $\hat{H}_\infty^{\mathrm{HF}}$ as a function of $\mathbf{r}_1, \ldots, \mathbf{r}_N$ does not attain its global minimum (if it were otherwise it would *not* be optimal as we could always lower the energy by increasing the weight of the wave function in the global minimum of $\hat{H}_\infty^{\mathrm{HF}}$). In other words,

$$E_{\mathrm{el}}[n] \equiv \min_{\{\mathbf{r}_1 \ldots \mathbf{r}_N\}} \left\{ \sum_{\substack{i,j=1 \\ j>i}}^{N} \frac{1}{|\mathbf{r}_i - \mathbf{r}_j|} - \sum_{i=1}^{N} v_{\mathrm{H}}(\mathbf{r}_i; [n]) + U[n] \right\} \tag{5.11}$$

is the minimum total electrostatic energy of N equal classical point charges $(-e)$ in a positive background with continuous charge density $(+e)n(\mathbf{r})$. The term $U[n]$, inherited from eq 5.3, represents the background-background repulsion.

Strictly speaking, the minimizer $\Psi_\infty^{\mathrm{HF}}$ is not in the space of allowed wavefunctions, so that the minimum is actually an infimum, similarly to the DFT case (see discussion in chapter 3).

Equations 5.9-5.10 comprise a central result of this work: they show that the strong-interaction limit of the HF adiabatic connection can be determined from a functional of the HF density, providing some theoretical justification for resumming the MP series by using a DFT-like expansion at large λ with functionals of n^{HF} [4, 127, 250], although, as we will discuss, there are still several points to be addressed.

We now analyze the functionals $\Psi_\infty^{\mathrm{HF}}[n]$ and $E_{el}[n]$, comparing them with the DFT case. We relabel, for this purpose, $\hat{H}_\lambda$ of eq 1.54 as $\hat{H}_\lambda^{\mathrm{DFT}}$ and its limiting value divided by the coupling parameter as $\hat{H}_\infty^{\mathrm{DFT}}[n]$, i.e. $\lim_{\lambda\to\infty} \frac{\hat{H}_\lambda^{\mathrm{DFT}}[n]}{\lambda} \sim \hat{H}_\infty^{\mathrm{DFT}}[n]$.

5

Comparing $\hat{H}_\infty^{\mathrm{DFT}}[n]$ with $\hat{H}_\infty^{\mathrm{HF}}[n]$ of eq 5.8, we see that both Hamiltonians consist of the electron-electron repulsion operator and of an attractive one-body potential. In the HF case the attractive potential is $-v_{\mathrm{H}}(\mathbf{r},[n])$, which, for typical Hartree-Fock densities n^{HF}, namely densities that are generated from the self-consistent restricted or unrestricted HF equations, is strong enough to create a classical bound crystal. To be more precise, $-v_{\mathrm{H}}(\mathbf{r},[n])$ is more attractive than the one-body potential $v^{\mathrm{SCE}}(\mathbf{r},[n])$. In fact, the potential $v^{\mathrm{SCE}}(\mathbf{r},[n])$, discussed in chapter 3, is generated by a charge that integrates to $N-1$ [73, 230]

$$\frac{1}{4\pi}\int \nabla^2 v^{\mathrm{SCE}}(\mathbf{r},[n])\, d\,\mathbf{r} = N-1, \tag{5.12}$$

while the attractive potential $-v_{\mathrm{H}}(\mathbf{r},[n])$ is generated by the given density $n(\mathbf{r})$, which integrates to N. For finite systems, the state $\Psi_\infty^{\mathrm{HF}}[n]$ is thus more compact than the state $\Psi_\infty^{\mathrm{DFT}}[n]$ lacking the density constraint present in the DFT adiabatic connection construction. Note, furthermore, that both $\hat{H}_\infty^{\mathrm{DFT}}[n]$ and $\hat{H}_\infty^{\mathrm{HF}}[n]$ are functionals of the density in the sense that, given a density, they can be constructed accordingly. Nevertheless, while the former is such that the same density determining the asymptotic Hamiltonian (in its external potential part) is also its resulting ground state density, this is in general not the case for the latter one. Indeed, we implicitly assumed that the domain of the functional $\hat{H}_\infty^{\mathrm{HF}}[n]$ be that of the Hartree-Fock densities n^{HF}. By virtue of the structure of the HF Hamiltonian $\hat{H}_0^{\mathrm{HF}}$, such densities are typically smooth, continuous functions, while we just argued that the ground state density output from the HF asymptotic Hamiltonian be a classical distribution, therefore a very different kind of electron density compared to that input.[1]

[1] If, for the sake of speculation, we assume that also classical distributions can be used as input to

For given occupied HF orbitals, we have the chain of inequalities

$$W_\infty^{\mathrm{HF}}[n^{\mathrm{HF}}] \leq E_{el}[n^{\mathrm{HF}}] \leq W_\infty^{\mathrm{DFT}}[n^{\mathrm{HF}}]. \tag{5.13}$$

The first one, $W_\infty^{\mathrm{HF}} \leq E_{el}[n^{\mathrm{HF}}]$, is trivial since $W_\infty^{\mathrm{HF}} = E_{el}[n^{\mathrm{HF}}] + 2E_x^{\mathrm{HF}}$ from definition 5.10 and $E_x^{\mathrm{HF}} \leq 0$. The second inequality, $E_{el}[n] \leq W_\infty^{\mathrm{DFT}}[n]$, holds for any density $n(\mathbf{r})$. To prove it, we introduce the bifunctional $\mathscr{W}[n, v]$,

$$\mathscr{W}[n, v] = \inf_\Psi \langle \Psi | \hat{V}_{ee} - \sum_{i=1}^{N} v(\mathbf{r}_i) | \Psi \rangle + \int n(\mathbf{r}) v(\mathbf{r})\, d\mathbf{r}, \tag{5.14}$$

for which we have

$$\mathscr{W}[n, v_{\mathrm{H}}[n]] = E_{el}[n] + U[n], \tag{5.15}$$

and, from the dual formulation of $W_\infty^{\mathrm{DFT}}[n]$

$$W_\infty^{\mathrm{DFT}}[n] + U[n] = \max_v \mathscr{W}[n, v], \tag{5.16}$$

which clearly completes the proof. Moreover, combining this last result with the definition of $W_\infty^{\mathrm{HF}}[n^{\mathrm{HF}}]$ (eq 5.10) we also find

$$W_\infty^{\mathrm{HF}}[n^{\mathrm{HF}}] \leq W_\infty^{\mathrm{DFT}}[n^{\mathrm{HF}}] + 2E_x^{\mathrm{HF}}[n^{\mathrm{HF}}]. \tag{5.17}$$

As an illustration of the difference between the two adiabatic connections limits, in fig 5.1, we show the two potential energy surfaces, $\hat{\mathscr{H}}_\infty^{\mathrm{DFT/HF}}(r_1, r_2, \pi)$, for the He atom.

Note that, due to the cancellation between U and $2E_x$ in a two-electron singlet system such as this one, in the case of the HF asymptotic Hamiltonian, we have

$$W_\infty^{\mathrm{HF}} \equiv \hat{\mathscr{H}}_\infty^{\mathrm{HF}}\big|_{\mathrm{min}} \tag{5.18}$$

while for the corresponding DFT functionals such relation does not hold.[2]

From the figure, we also observe, as anticipated, the contraction of the asymptotic

$\hat{H}_\infty^{\mathrm{HF}}[n]$, in the form of a quite exceptional, self-interaction-free Hartree potential, i.e. $v_{\mathrm{H}}(\boldsymbol{r}, [\check{n}(\boldsymbol{r})]) = \sum_i^N \frac{1}{|\boldsymbol{r} - \boldsymbol{r}_i|}$, with $\check{n}(\boldsymbol{r}) = \sum_i^N \delta(\boldsymbol{r} - \boldsymbol{r}_i)$, it seems indeed likely that the GS density of $\hat{H}_\infty^{\mathrm{HF}}[\check{n}]$ would exactly match that of the background, i.e. $n_\infty^{\mathrm{HF}} \equiv \check{n}$. However, for this quite pathological case, our arguments in sec 5.3 about the expectation value of the exchange operator, $\langle \lambda \hat{K} \rangle$, when $\lambda \to \infty$, would anyway no longer hold and we should be reconsidering our asymptotic Hamiltonian expression (aside from various other complications).

[2] Namely, considering definition 1.60 and rewriting V_{ee}^{SCE} as

$$V_{ee}^{\mathrm{SCE}} = \underbrace{E_{\mathrm{SCE}}}_{\equiv \hat{\mathscr{H}}_\infty^{\mathrm{DFT}}\big|_{\mathrm{min}}} - \underbrace{\int v^{\mathrm{SCE}}(\boldsymbol{r})\, n(\boldsymbol{r})\, \mathrm{d}\boldsymbol{r}}_{:= V^{\mathrm{SCE}}}, \tag{5.19}$$

we find

$$W_\infty^{\mathrm{DFT}} \equiv \hat{\mathscr{H}}_\infty^{\mathrm{DFT}}\Big|_{\mathrm{min}} - \left(V^{\mathrm{SCE}} + U\right) \tag{5.20}$$

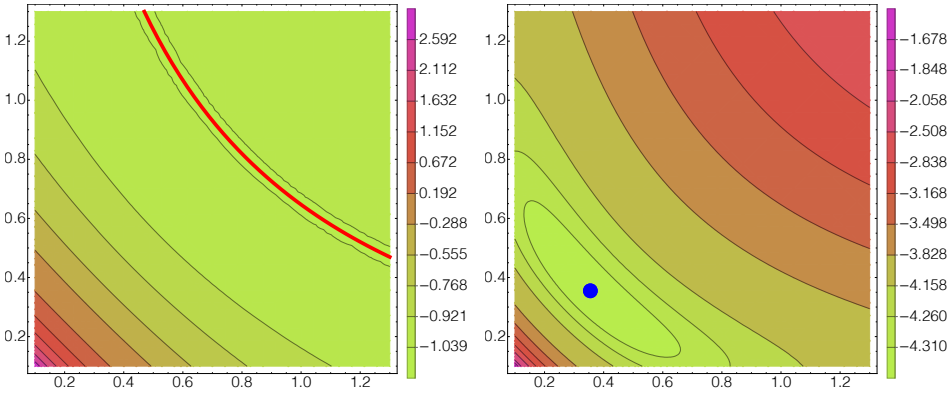

Figure 5.1: Potential energy surfaces, $\hat{\mathscr{H}}_{\infty}^{\mathrm{DFT}}(r_1, r_2, \pi)$ (left) and $\hat{\mathscr{H}}_{\infty}^{\mathrm{HF}}(r_1, r_2, \pi)$ (right), plotted along the radial distances, r_1, r_2, of the particles from the origin and with an angle π between the two vectors $\boldsymbol{r}_1$, $\boldsymbol{r}_2$. Superimposed are the corresponding minima, i.e. the degenerate minimum for the DFT asymptotic Hamiltonian in red, at about −1.039 Ha, and the unique minimum for the HF asymptotic Hamiltonian in blue, at about −4.347 Ha.

5

HF density compared to the physical one (the minimum is at $r_0^{\mathrm{HF}} \approx 0.355$ while choosing for the DFT case the minimum distance between the two particles, which corresponds to the distance, r_0^{DFT}, at which $f(r_0^{\mathrm{DFT}}) \equiv r_0^{\mathrm{DFT}}$, we find $r_0^{\mathrm{DFT}} \approx 0.809$) and the fact that, albeit unique, the HF minimum is also quite shallow.

5.3. Subleading term: variational argument

We provide, in this section, a variational argument to support the assumption of eq 5.5, sketching the main points and leaving room for a more rigourous proof. We start by considering the global minimum $\underline{R}^{\min} \equiv \{\mathbf{r}_1^{\min}, \ldots, \mathbf{r}_N^{\min}\}$ of the function $\hat{\mathscr{H}}_{\infty}^{\mathrm{HF}}$ of eq 5.8, and construct the simple trial wavefunction

$$\Psi_{\lambda}^{T}(\mathbf{r}_1, \ldots, \mathbf{r}_N) = \prod_{i=1}^{N} G_{\alpha(\lambda)}(\mathbf{r}_i - \mathbf{r}_i^{\min}), \tag{5.21}$$

where $G_{\alpha}(\mathbf{r}) = \frac{\alpha^{3/4}}{\pi^{3/4}} e^{-\frac{\alpha}{2}|\mathbf{r}|^2}$, with α a λ-dependent variational parameter that goes to infinity for large λ, $\alpha(\lambda) \sim \lambda^q$ with $q > 0$. By construction, when $\alpha \to \infty$ (i.e., when $\lambda \to \infty$) we have that

$$\lim_{\lambda \to \infty} |\Psi_{\lambda}^{T}[n^{\mathrm{HF}}]|^2 = |\Psi_{\infty}^{\mathrm{HF}}[n^{\mathrm{HF}}]|^2 \tag{5.22}$$

where $\Psi_{\infty}^{\mathrm{HF}}$ was introduced in eq 5.6 (in the case of degeneracy we can select one of the minimizers, since here we only want to obtain an upper bound to the lowest

eigenvalue of $H_\lambda^{\rm HF}$). We now analyze, for large α, the expectation value on Ψ_λ^T of each term appearing in $\hat{H}_\lambda^{\rm HF}$ of eq 5.1, obtaining

$$\langle\Psi_\lambda^T|\hat{T}|\Psi_\lambda^T\rangle = t\,\alpha \tag{5.23}$$

$$\langle\Psi_\lambda^T|\lambda(\hat{V}_{ee}-\hat{J})|\Psi_\lambda^T\rangle = \lambda(E_{el}-U)+\lambda\left(\frac{h}{\alpha}+o(\alpha^{-1})\right) \tag{5.24}$$

$$\langle\Psi_\lambda^T|-\lambda\,\hat{K}|\Psi_\lambda^T\rangle = \lambda\left(\frac{k}{\alpha}+o(\alpha^{-1})\right) \tag{5.25}$$

$$\langle\Psi_\lambda^T|\hat{V}_{\rm ext}+\hat{J}+\hat{K}|\Psi_\lambda^T\rangle \sim O(\alpha^0), \tag{5.26}$$

where t, h, and k are all *positive* numbers. This is obvious for t, but it is also true for k because the expectation of $-\hat{K}$ is positive for any wavefunction Ψ, as $\hat{K}$ has a negatively definite kernel. The fact that the expectation value of $\hat{K}$ on Ψ_λ^T vanishes as α^{-1} for large α is due to the non-locality of $\hat{K}$, which samples the Gaussians in the bra and in the ket in different points of space, and to the regularity properties of the HF orbitals (which have no delta-function singularities). The positivity of h in eq 5.24 can be proven by expanding $\hat{H}_\infty^{\rm HF}$ around $\underline{R}^{\rm min}$ up to second order, which gives an hessian matrix positive definite.

Putting together Eqs. 5.23-5.26 and replacing α with λ^q we find that, for large λ, the expectation value of $\hat{H}_\lambda^{\rm HF}$ on Ψ_λ^T behaves asymptotically as

$$\langle\Psi_\lambda^T|\hat{H}_\lambda^{\rm HF}|\Psi_\lambda^T\rangle = \lambda(E_{el}-U)+t\lambda^q+(h+k)\lambda^{1-q}+o(\lambda^{1-q}). \tag{5.27}$$

Being t, h and k positive, we see that the best variational choice to make the next leading term after $O(\lambda)$ increase with the lowest possible power of λ is $q=1/2$, as conjectured in eq 5.5. Although Ψ_λ^T of eq 5.21 is not antisymmetric, we can always properly antisymmetrize it, which only leads to corrections $O(e^{-\alpha})$ in the computation of the expectation values, similarly to the DFT case [80]. Thus, we have explicitly constructed a variational wavefunction that yields the minimum possible value for the leading term $O(\lambda)$ in the expectation of $\hat{H}_\lambda^{\rm HF}$. In fact, since $E_{el}[n^{\rm HF}]-U[n^{\rm HF}]$ is the global minimum of the multiplicative operator $\hat{V}_{ee}-\hat{J}$, there is no wavefunction that can yield a lower expectation for this operator. Moreover, since $-\hat{K}$ is positive definite, the best we can do is to make its expectation zero when $\lambda\to\infty$, which our wavefunction is able to do.

This variational argument also shows that the next leading term in $W_\lambda^{\rm HF}$ should be order $\lambda^{-1/2}$, similarly to the DFT case of eq 1.70. A quantitative estimate of this next leading term could in principle be obtained by using the normal modes around the minimum of $\hat{V}_{ee}-\hat{J}$: a unitary transformation from the $\mathbf{r}_i-\mathbf{r}_i^{\rm min}$ to the normal modes coordinates $\xi_1,\ldots,\xi_{3N}$ that diagonalize the hessian of $\hat{\mathscr{H}}_\infty^{\rm HF}$ at $\underline{R}^{\rm min}$ leads to a set of uncoupled harmonic oscillators whose spring constant scales with

λ,

$$\hat{H}_\lambda^{\mathrm{ZP}} = -\frac{1}{2}\sum_{\alpha=1}^{3N}\frac{\partial^2}{\partial\xi_\alpha^2} + \frac{\lambda}{2}\sum_{\alpha=1}^{3N}\omega_\alpha^2\xi_\alpha^2, \tag{5.28}$$

with ω_α^2 the eigenvalues of the hessian of $\mathscr{H}_\infty^{\mathrm{HF}}$ at $\underline{R}^{\mathrm{min}}$. The ground-state of $\hat{H}_\lambda^{\mathrm{ZP}}$ is obtained by occupying the lowest state of each oscillator, with the product state

$$\Psi_\lambda^{\mathrm{ZP}}(\xi_1,\dots\xi_{3N}) = \prod_{\alpha=1}^{3N}\frac{(\omega_\alpha\sqrt{\lambda})^{1/4}}{\pi^{1/4}}e^{-\sqrt{\lambda}\omega_\alpha\frac{\xi_\alpha^2}{2}}. \tag{5.29}$$

This wavefunction should provide the minimum possible expectation, to order $\lambda^{1/2}$, of $\hat{T}+\lambda(\hat{V}_{ee}-\hat{J})$. However, since $-\lambda\hat{K}$ is of the same order $\lambda^{1/2}$, we cannot exclude at this point that the minimization of the full $\hat{T}+\lambda(\hat{V}_{ee}-\hat{J}-\hat{K})$ could lead to a different set of occupied oscillator states. This investigation is the object of ongoing work (see discussion in ref [251]).
From our present treatment we have so far

$$W_{\lambda\to\infty}^{\mathrm{HF}} = W_\infty^{\mathrm{HF}} + \frac{1}{\sqrt{\lambda}}W_\infty'^{\mathrm{HF}} + \dots, \tag{5.30}$$

with

$$W_\infty^{\mathrm{HF}} = E_{el}[n^{\mathrm{HF}}] + 2E_x^{\mathrm{HF}} \tag{5.31}$$

$$W_\infty'^{\mathrm{HF}} = \frac{1}{2}\sum_{\alpha=1}^{3N}\frac{\omega_\alpha[n^{\mathrm{HF}}]}{2} + W_{K,\infty}'^{\mathrm{HF}}, \tag{5.32}$$

where $W_{K,\infty}'^{\mathrm{HF}}$ is due to the effect of $-\lambda\hat{K}$ at orders $\lambda^{1/2}$ in $\hat{H}_\lambda^{\mathrm{HF}}$ and is a functional of the occupied HF orbitals (eq 5.32 is for now a conjecture). We also see that both W_∞^{HF} and $W_\infty'^{\mathrm{HF}}$ have a part that is a functional of the HF density only, and a part that is a functional of the occupied HF orbitals, although it seems that for the latter case the dependence on the HF orbitals can be reduced to a dependence on the HF density only. In both cases, the part that is a density functional has an origin similar to the one of the DFT functionals of eq 1.70, being, respectively, a classical electrostatic energy and the potential energy of zero-point oscillations around a classical minimum. The parts that need the knowledge of the occupied HF orbitals do not appear in the DFT case. This structure should be exact, although the detailed form of $W_\infty'^{\mathrm{HF}}$ might include a different set of occupied oscillator states.

Although the $\lambda\to\infty$ limit of W_λ^{HF} has a structure similar to the one of DFT, there are many differences that need to be kept in mind. Both $W_\lambda^{\mathrm{DFT}}[\rho]$ and W_λ^{HF} are decreasing functions of λ,

$$\frac{d}{d\lambda}W_\lambda^{\mathrm{DFT}}[\rho] \le 0, \qquad \frac{d}{d\lambda}W_\lambda^{\mathrm{HF}} \le 0, \tag{5.33}$$

but $W_\lambda^{\mathrm{DFT}}[\rho]$ for $\lambda \geq 0$ is believed to be convex or at least piecewise convex (if there are crossings of states), while W_λ^{HF} is for sure not always convex. In fact, the MP2 correlation energy, already for simple atoms such as He, underestimates (in absolute value) the total correlation energy E_c^{HF}, implying that W_λ^{HF} for $0 < \lambda \ll 1$ must run below its tangent; thus, W_λ^{HF} usually starts concave for small λ and then needs to change convexity to tend to the finite asymptotic value W_∞^{HF} for large λ. Moreover, while the density constraint of the DFT adiabatic connection usually mitigates the crossing of states, the HF adiabatic connection might have jumps or kinks as λ is increased. A simple example is the $N = 1$ case, for which $W_\lambda^{\mathrm{HF}} = -U[\rho^{\mathrm{HF}}]$ for $0 \leq \lambda \leq 1$, while for $\lambda > 1$ the curve starts to decrease, tending, as $\lambda \to \infty$ to a well defined value, with the electrostatic energy determined by the configuration in which the electron is sitting in the minimum of $-v_{\mathrm{H}}(\mathbf{r}, [\rho])$ (preliminary results about the structure of the HF adiabatic connection integrand curve for the exceptional case where $N = 1$ are detailed in reference [252]).

5.4. Conclusions and perspectives

In conclusion, we have shown that by looking at the $\lambda \to \infty$ limit of the HF adiabatic connection we recover functionals of the HF density, revealing a new intriguing formal link between HF and DFT. However, we should also stress that the use of models for W_λ^{HF} taken from DFT, although somehow justified by our analysis, should at this stage still be taken with some caution. The empirical observation so far [127, 250], is that these models are not accurate for total energies, but work rather well for interaction energies, with a small variance, particularly for non-covalent complexes [127, 250]. This point requires further investigation in the future. A numerical analysis of the functionals W_∞^{HF} and $W_\infty'^{\mathrm{HF}}$, in comparison with the corresponding DFT functionals, seems also beneficial.

At the state of the art, it seems already clear that the difference between W_∞^{HF} and W_∞^{DFT} can be considerable. For example, for the He atom discussed at the end of sec 5.2, we have $W_\infty^{\mathrm{HF}} \approx -4.347$ Ha, while $W_\infty^{\mathrm{DFT}} \approx -1.50$ Ha.

Promising research lines opened by this study are to investigate whether it is possible to extract a model for the self-energy in the strong-coupling limit, to be used in the context of Green's functions approaches [253–256], and to analyze in the same spirit adiabatic connections appearing in other theories [247, 257].

6

Response potential in the strong-interaction limit of DFT: Analysis and comparison with the coupling-constant average

Using the formalism of the conditional amplitude, we study the response part of the exchange-correlation potential in the strong-coupling limit of density functional theory, analysing its peculiar features and comparing it with the response potential at physical regimes for small atoms and for the hydrogen molecule. We also use a simple one-dimensional model of a stretched heteronuclear molecule to derive exact properties of the response potential in the strong-coupling limit. The simplicity of the model allows us to unveil relevant features also of the exact Kohn-Sham potential and its different components, namely the appearance of a second peak in the correlation kinetic potential on the side of the more electronegative atom.

6.1. Introduction

In chapter 2 we have discussed the convenience of adopting the conditional probability amplitude approach to obtain an exact decomposition of the effective potential appearing in the Schrödinger equation for the square root of the density (eq 2.11) and of the XC potential of KS DFT.

The SCE limit, however, has never been analyzed from the point of view of the

conditional amplitude framework, and nothing is known about the behavior of the different components of the corresponding external potential. It is the main purpose of this work to fill this gap.

The effective equation 2.61 for $\sqrt{n(\boldsymbol{r})}$ in the SCE limit can be easily understood if we divide both sides by $\lambda\sqrt{n(\boldsymbol{r})}$,

$$-\frac{\nabla^2\sqrt{n(\boldsymbol{r})}}{2\lambda\sqrt{n(\boldsymbol{r})}}+\frac{v_{\lambda,N-1}(\boldsymbol{r})}{\lambda}+\frac{v_{\lambda,kin}(\boldsymbol{r})}{\lambda}+ v_{\lambda,cond}(\boldsymbol{r})+\frac{v^{\lambda}(\boldsymbol{r})}{\lambda}=\frac{1}{\lambda}(E^N_\lambda-E^{N-1}_{\lambda*}). \tag{6.1}$$

When $\lambda\to\infty$, we see that the first term in the left-hand-side goes to zero, as the density $n(\boldsymbol{r})$ does not change with λ and it is well behaved, with the exception of the values of $\boldsymbol{r}$ on top of the nuclear positions $\mathbf{R}_i$, where the density has a cusp and $\frac{\nabla^2\sqrt{n(\boldsymbol{r})}}{\sqrt{n(\boldsymbol{r})}}$ yields back the Coulombic divergence. Nagy and Jánosfalvi [258] have carefully analyzed the $\lambda\to\infty$ behavior at the nuclear cusps in $\frac{\hat{H}_\lambda}{\lambda}$, showing that for all λ values the kinetic divergence at a nucleus of charge Z at position $\mathbf{R}_i$ cancels exactly the external potential $-\frac{Z}{\lambda|\boldsymbol{r}-\mathbf{R}_i|}$. We can then safely disregard both the kinetic and the Coulombic divergence in the $\lambda\to\infty$ limit. The other case, which we do not consider here, where this term may diverge is when the KS highest-occupied molecular orbital (HOMO) has a nodal plane that extends to infinity [44, 45, 259].

All the remaining terms, except for $v_{\lambda,kin}(\boldsymbol{r})$, will tend to a finite, in general non-zero, limiting value, as they grow linearly with λ (for example $v^{\lambda}(\boldsymbol{r})\to\lambda v^{\mathrm{SCE}}(\boldsymbol{r})$ of eq 3.15). Notice that $v_{\lambda,cond}(\boldsymbol{r})$ appears in the equations with a factor λ in front, see eqs 2.59 and 2.62. The only delicate term is $v_{\lambda,kin}(\boldsymbol{r})$ of eq 2.58, which contains the gradient of a conditional amplitude that is collapsing into a distribution. As already discussed in chapter 3, several results in the literature suggest [34, 74, 80] that this term grows with λ only as $\sim\sqrt{\lambda}$, thus still vanishing with respect to the other terms. As shown below, the SCE limit provides a perfectly consistent treatment of the leading order of eq 2.61 when $\lambda\to\infty$, providing further evidence that the kinetic potential $v_{\lambda,kin}(\boldsymbol{r})$ should be subleading in eq 6.1.

6.2. Conditional probability amplitude and ionization potential at the SCE limit

We can now use eq 3.9 to find the conditional amplitude in the SCE limit and to partition the corresponding effective potential into its two components of eqs 2.57 and 2.59 (as said, the kinetic part disappears in this limit).

Let us now consider only one of the possible permutations in eq 3.9: in practice, as explicitly shown in appendix A, this restriction does not affect the expression

resulting from integration over $N-1$ variables. Integrating over $\boldsymbol{s}$ we get

$$|\Psi_{SCE}(\boldsymbol{r}_1,\cdots,\boldsymbol{r}_N)|^2 = \frac{n(\boldsymbol{r}_1)}{N}\,\delta(\boldsymbol{r}_2-\mathbf{f}_1(\boldsymbol{r}_1))\cdots\delta(\boldsymbol{r}_N-\mathbf{f}_{N-1}(\boldsymbol{r}_1)), \tag{6.2}$$

and applying equation 2.56 and $\boldsymbol{r}_1=\boldsymbol{r}$ we find

$$|\Phi_{SCE}(\boldsymbol{r}_2,\cdots,\boldsymbol{r}_N|\boldsymbol{r})|^2 = \delta(\boldsymbol{r}_2-\mathbf{f}_1(\boldsymbol{r}))\cdots\delta(\boldsymbol{r}_N-\mathbf{f}_{N-1}(\boldsymbol{r})). \tag{6.3}$$

Equation 6.3 shows that the conditional amplitude gets a very transparent meaning in the SCE limit, as it simply gives the position of the other $N-1$ electrons as a function of the position $\boldsymbol{r}$ of the first electron.[1]

In what follows we label with "SCE" the terms that survive when we take the limit $\lambda\to\infty$ of eq 6.1. We then use eq 6.3 to evaluate in this limit $v^{SCE}_{N-1}(\boldsymbol{r})$,

$$\begin{aligned} v^{SCE}_{N-1}(\boldsymbol{r}) &= \int\left(-\sum_{i=2}^{N} v^{SCE}_{Hxc}(\boldsymbol{r}_i)+\sum_{j>i,i=2}^{N}\frac{1}{r_{ij}}\right)\prod_{i=2}^{N}\delta(\boldsymbol{r}_i-\mathbf{f}_{i-1}(\boldsymbol{r}))\mathrm{d}\boldsymbol{r}_2\cdots\mathrm{d}\boldsymbol{r}_N - E^{N-1}_{SCE*} = \\ &= -\sum_{i=1}^{N-1} v^{SCE}_{Hxc}(\mathbf{f}_i(\boldsymbol{r}))+\sum_{j>i=1}^{N-1}\frac{1}{|\mathbf{f}_i(\boldsymbol{r})-\mathbf{f}_j(\boldsymbol{r})|}-E^{N-1}_{SCE*} \end{aligned} \tag{6.5}$$

Now we use the fact that the ground-state energy of the N-particle system with density $n(\boldsymbol{r})$ at the SCE limit is simply given by the value of the classical potential energy $\hat{V}_{ee}+\hat{V}^{SCE}$ on the manifold parametrized by the co-motion functions,

$$E^{N}_{SCE} = -\sum_{i=1}^{N} v^{SCE}_{Hxc}(\mathbf{f}_i(\boldsymbol{r}))+\sum_{i>j,\,j=1}^{N}\frac{1}{|\mathbf{f}_i(\boldsymbol{r})-\mathbf{f}_j(\boldsymbol{r})|}, \tag{6.6}$$

which allows us to rewrite the first term on the r.h.s. of equation 6.5 as

$$\begin{aligned} &-\sum_{i=1}^{N-1} v^{SCE}_{Hxc}(\mathbf{f}_i(\boldsymbol{r}))+\sum_{j>i=1}^{N-1}\frac{1}{|\mathbf{f}_i(\boldsymbol{r})-\mathbf{f}_j(\boldsymbol{r})|} = \\ &\qquad = E^{N}_{SCE}+v^{SCE}_{Hxc}(\boldsymbol{r})-\sum_{i=1}^{N-1}\frac{1}{|\boldsymbol{r}-\mathbf{f}_i(\boldsymbol{r})|} \end{aligned} \tag{6.7}$$

The last two terms in the right-hand-side of eq 6.7 vanish for $|\boldsymbol{r}|\to\infty$. On the other hand, by construction $v^{SCE}_{N-1}(\boldsymbol{r})\to 0$ when $|\boldsymbol{r}|\to\infty$, and thus necessarily

$$E^{N}_{SCE} = E^{N-1}_{SCE*}, \tag{6.8}$$

[1] To be precise, as long as we are not integrating over $\mathrm{d}\boldsymbol{r}_2\cdots\mathrm{d}\boldsymbol{r}_N$, we should still consider the wave-function of eq A.8 and, consequently, the corresponding conditional amplitude

$$|\Phi_{SCE}(\boldsymbol{r}_2,\cdots,\boldsymbol{r}_N|\boldsymbol{r}_1)|^2 = \frac{1}{(N-1)!}\sum_{\wp=1}^{(N-1)!}\prod_{i=2}^{N}\delta(\boldsymbol{r}_i-\mathbf{f}_{\wp(i)}(\boldsymbol{r}_1)) \tag{6.4}$$

which gives the position of the other $N-1$ electrons as a function of the position of electron 1, $\boldsymbol{r}_1$, in all their possible permutations.

and we obtain the final simple expression for $v_{N-1}^{SCE}(\boldsymbol{r})$,

$$v_{N-1}^{SCE}(\boldsymbol{r}) = v_{Hxc}^{SCE}(\boldsymbol{r}) - \sum_{i=1}^{N-1} \frac{1}{|\boldsymbol{r} - \mathbf{f}_i(\boldsymbol{r})|}. \tag{6.9}$$

Equation 6.8 might look puzzling, but one could also expect it from the fact that, as said, in the SCE limit we obtain the quantities that survive in eq 6.1 when we take the $\lambda \to \infty$ limit. This means that the difference $E_\lambda^N - E_{\lambda*}^{N-1}$ grows linearly with λ for large λ,

$$\lambda \to \infty \quad E_\lambda^N - E_{\lambda*}^{N-1} \sim \lambda \left(E_{SCE}^N - E_{SCE*}^{N-1}\right) + O(\sqrt{\lambda}) + ... \tag{6.10}$$

Then we see that the only way in which eq 2.63 can be satisfied when λ goes to infinity is if eq 6.8 holds. Indeed this result was already implicit in ref [73], where it was noticed that the configuration with one electron at infinity must belong to the degenerate minimum of the classical potential energy operator $\hat{V}_{ee} + \hat{V}^{SCE}$. Equation 6.10 shows that also for the next leading order $\sim \sqrt{\lambda}$ there should be no energy cost to remove one electron, a statement that is implicitly contained in ref [34].

Notice that the zero ionization energy of eq 6.8 concerns the $\lambda \to \infty$ Hamiltonian in the adiabatic connection of eq 1.54. A very different result is obtained if $v_{Hxc}^{SCE}(\boldsymbol{r})$ is used as an approximation for the Hartree-XC potential in the self-consistent KS equations, where the corresponding KS HOMO eigenvalue has been found to be very close to minus the exact ionization potential for low-density systems [83, 93], displaying the correct step structure when the number of electrons is changed in a continuous way [105] as discussed in sec 3.4.

6.3. Different types of response potentials: $v_{resp}(\boldsymbol{r})$, $\overline{v}_{resp}(\boldsymbol{r})$, $v_{resp}^{SCE}(\boldsymbol{r})$

Combination of eqs 2.34, 2.53 and 2.54 in chapter 2 already showed us that a possible decomposition of the XC potential is

$$v_{xc} = v_{c,kin} + v_{resp} + v_{xc\text{-}hole} \tag{6.11}$$

Defining the pair-density $P_2^\lambda(\boldsymbol{r}, \boldsymbol{r}')$, associated to the Hamiltonian in eq 1.54

$$P_2^\lambda(\boldsymbol{r}, \boldsymbol{r}') = N(N-1) \int |\Psi_\lambda(\boldsymbol{r}\sigma, \boldsymbol{r}'\sigma', ..., N)|^2 \mathrm{d}\sigma \mathrm{d}\sigma' \mathrm{d}\boldsymbol{x}_3 ... \mathrm{d}\boldsymbol{x}_N, \tag{6.12}$$

the corresponding exchange-correlation pair-correlation function $g_{xc}^\lambda(\boldsymbol{r}, \boldsymbol{r}')$ at a given coupling strength λ,

$$g_{xc}^\lambda(\boldsymbol{r}, \boldsymbol{r}') = \frac{P_2^\lambda(\boldsymbol{r}, \boldsymbol{r}')}{n(\boldsymbol{r}) n(\boldsymbol{r}')} - 1 \tag{6.13}$$

and the coupling-constant averaged (CCA) pair-correlation function $\overline{g}_{xc}(\boldsymbol{r},\boldsymbol{r}')$

$$\overline{g}_{xc}(\boldsymbol{r},\boldsymbol{r}') = \int_0^1 g^{\lambda}_{xc}(\boldsymbol{r},\boldsymbol{r}')\mathrm{d}\lambda. \tag{6.14}$$

we now introduce another possible decomposition of the XC potential.

6.3.1. Response potential from the coupling-constant averaged XC hole and comparison between $v_{resp}(\boldsymbol{r})$ and $\overline{v}_{resp}(\boldsymbol{r})$

The XC energy can be written in terms of the CCA $\overline{g}_{xc}(\boldsymbol{r},\boldsymbol{r}')$,

$$E_{xc}[n] = \frac{1}{2}\iint n(\boldsymbol{r})n(\boldsymbol{r}')\frac{\overline{g}_{xc}(\boldsymbol{r},\boldsymbol{r}')}{|\boldsymbol{r}-\boldsymbol{r}'|}\mathrm{d}\boldsymbol{r}\mathrm{d}\boldsymbol{r}', \tag{6.15}$$

as the integration over λ allows to recover the kinetic contribution to $E_{xc}[n]$ [28, 29, 260]. Taking the functional derivative of eq 6.15 we obtain two terms [59]

$$v_{xc}(\mathbf{r}) = \frac{\delta E_{xc}[n]}{\delta n(\boldsymbol{r})} = \overline{v}_{xc,hole}(\mathbf{r}) + \overline{v}_{resp}(\mathbf{r}), \tag{6.16}$$

where

$$\overline{v}_{xc,hole}(\mathbf{r}) = \int n(\boldsymbol{r}')\frac{\overline{g}_{xc}(\boldsymbol{r},\boldsymbol{r}')}{|\boldsymbol{r}-\boldsymbol{r}'|}\mathrm{d}\boldsymbol{r}', \tag{6.17}$$

and

$$\overline{v}_{resp}(\mathbf{r}) = \frac{1}{2}\iint \frac{n(\boldsymbol{r}')n(\boldsymbol{r}'')}{|\boldsymbol{r}'-\boldsymbol{r}''|}\frac{\delta\overline{g}_{xc}(\boldsymbol{r}',\boldsymbol{r}'')}{\delta n(\mathbf{r})}\mathrm{d}\boldsymbol{r}'\mathrm{d}\boldsymbol{r}''. \tag{6.18}$$

Equation 6.18 defines the quantity $\overline{v}_{resp}(\mathbf{r})$, but looking at eq 6.16 one can also determine it as:

$$\overline{v}_{resp}(\mathbf{r}) = v_{xc}(\mathbf{r}) - \overline{v}_{xc,hole}(\mathbf{r}), \tag{6.19}$$

which is how we have computed the response potential in sec 6.4.3. Comparing eqs. 6.11 and 6.16, we have

$$\begin{aligned}&\overline{v}_{xc,hole}(\boldsymbol{r}) + \overline{v}_{resp}(\boldsymbol{r}) = \\ &v_{c,kin}(\boldsymbol{r}) + v_{xc,hole}(\boldsymbol{r}) + v^{resp}_{c,kin}(\boldsymbol{r}) + v^{resp}_{xc,hole}(\boldsymbol{r}).\end{aligned} \tag{6.20}$$

To understand their difference, let us define the quantity $\mathfrak{f}_\lambda[n]$

$$\mathfrak{f}_\lambda[n](\boldsymbol{r}) \coloneqq \int \Phi^*_\lambda(\sigma,\boldsymbol{x}_2,\cdots,\boldsymbol{x}_N;\boldsymbol{r})\left(-\frac{\nabla^2_{\boldsymbol{r}}}{2} + \frac{\sum_{i=2}^N}{2}\frac{\lambda}{r_{1i}}\right)\Phi_\lambda(\sigma,\boldsymbol{x}_2,\cdots,\boldsymbol{x}_N;\boldsymbol{r})\,\mathrm{d}\sigma\mathrm{d}\boldsymbol{r}_2\cdots\boldsymbol{r}_N \tag{6.21}$$

such that

$$\int n(\boldsymbol{r})\mathfrak{f}_\lambda[n](\boldsymbol{r})\,\mathrm{d}\boldsymbol{r} = F_\lambda[n]. \tag{6.22}$$

Φ_λ is not a stationary state for the hamiltonian $\hat{h}_\lambda = -\frac{\nabla_r^2}{2} + \frac{\sum_{i=2}^N}{2}\frac{\lambda}{r_{1i}}$ therefore the usual Hellmann-Feynman trick is not applicable and we write

$$\frac{\partial}{\partial\lambda}\mathfrak{f}_\lambda(\boldsymbol{r}) = \left(\langle\Phi_\lambda|\frac{\partial\hat{h}_\lambda}{\partial\lambda}|\Phi_\lambda\rangle + \langle\frac{\partial\Phi_\lambda}{\partial\lambda}|\hat{h}_\lambda|\Phi_\lambda\rangle + \langle\Phi_\lambda|\hat{h}_\lambda|\frac{\partial\Phi_\lambda}{\partial\lambda}\rangle\right)(\boldsymbol{r}) \tag{6.23}$$

where the Dirac brakets stand for $\int \mathrm{d}\sigma\mathrm{d}\boldsymbol{x}_2\cdots\boldsymbol{x}_N$.
We can simplify $\langle\frac{\partial\Phi_\lambda}{\partial\lambda}|\hat{h}_\lambda|\Phi_\lambda\rangle + \langle\Phi_\lambda|\hat{h}_\lambda|\frac{\partial\Phi_\lambda}{\partial\lambda}\rangle = 2\langle\Phi_\lambda|\hat{h}_\lambda|\frac{\partial\Phi_\lambda}{\partial\lambda}\rangle$ if Φ_λ is real (or, more generally, in the form $\Phi_\lambda = R_\lambda e^{i\phi}$ where ϕ is a number that does not depend on λ). We then write

$$\mathfrak{f}_1 - \mathfrak{f}_0 = \int_0^1 \mathrm{d}\lambda\left(\frac{\partial}{\partial\lambda}\mathfrak{f}_\lambda\right). \tag{6.24}$$

Evaluating the left hand side, we immediately get, from the definition of $v_{\lambda,kin}$ and $v_{\lambda,cond}$,

$$\mathfrak{f}_1 - \mathfrak{f}_0 = v_{c,kin} + \frac{1}{2}v_{cond}. \tag{6.25}$$

Substituting back the expression of the full wavefunction, in the first term on the r.h.s. of eq 6.23, we have

$$\begin{aligned}
\langle\Phi_\lambda|\frac{\partial\hat{h}_\lambda}{\partial\lambda}|\Phi_\lambda\rangle(\boldsymbol{r}) &= \int \Phi_\lambda^*(\sigma,2,\cdots,N;\boldsymbol{r})\left(\frac{\sum_{i=2}^N}{2}\frac{1}{r_{1i}}\right)\Phi_\lambda(\sigma,2,\cdots,N;\boldsymbol{r})\,\mathrm{d}\sigma\mathrm{d}\boldsymbol{x}_2\cdots\boldsymbol{x}_N \\
&= \frac{N}{2\,n(\boldsymbol{r})}\int\sum_{i=2}^N\frac{1}{r_{1i}}|\Psi_\lambda|^2\,\mathrm{d}\sigma\mathrm{d}\boldsymbol{x}_2\cdots\boldsymbol{x}_N \\
&= \frac{N(N-1)}{2\,n(\boldsymbol{r})}\int\frac{\int|\Psi_\lambda(\boldsymbol{r}\sigma,\boldsymbol{r}\sigma,3,\cdots,N)|^2\,\mathrm{d}\sigma\mathrm{d}\sigma'\mathrm{d}\boldsymbol{x}_3\cdots\mathrm{d}\boldsymbol{x}_N}{|\boldsymbol{r}-\boldsymbol{r}'|}\mathrm{d}\boldsymbol{r}' \\
&= \frac{1}{2\,n(\boldsymbol{r})}\int\mathrm{d}\boldsymbol{r}'\,\frac{P_2^\lambda(\boldsymbol{r},\boldsymbol{r}')}{|\boldsymbol{r}-\boldsymbol{r}'|}
\end{aligned} \tag{6.26}$$

with $\boldsymbol{x}_2 = \boldsymbol{r}'\sigma$ and using, in the third line, the fact that there are $(N-1)$ pairs of indistinguishable electrons.
We recognise this quantity to be simply

$$\langle\Phi_\lambda|\frac{\partial\hat{h}_\lambda}{\partial\lambda}|\Phi_\lambda\rangle(\boldsymbol{r}) = \frac{1}{2}\int\frac{n(\boldsymbol{r}')\left(g_{xc}^\lambda(\boldsymbol{r},\boldsymbol{r}')+1\right)}{|\boldsymbol{r}-\boldsymbol{r}'|}\mathrm{d}\boldsymbol{r}' = \frac{1}{2}v_{\lambda,cond}(\boldsymbol{r}) \tag{6.27}$$

and combining eqs 6.23, 6.25 and 6.27 we find the relation

$$\overline{v}_{xc\text{-}hole} = 2\,v_{c,kin} + v_{xc\text{-}hole} - 4\int_0^1\mathrm{d}\lambda\,\langle\Phi_\lambda|\hat{h}_\lambda|\frac{\partial\Phi_\lambda}{\partial\lambda}\rangle, \tag{6.28}$$

where we have subtracted the λ-independent Hartree potential from both sides. From combination of eqs 6.28 and 6.20, it further follows

$$\overline{v}_{resp} = v_{resp} - v_{c,kin} + 4\int_0^1 \mathrm{d}\lambda \langle \Phi_\lambda | \hat{h}_\lambda | \frac{\partial \Phi_\lambda}{\partial \lambda} \rangle. \tag{6.29}$$

Both relations 6.28 and 6.29 are expressed assuming $\Phi_\lambda = R_\lambda e^{i\phi}$.

In conclusion, the coupling-constant averaged energy density (where, by "energy density" we mean some function $\tilde{w}(\boldsymbol{r})$ s.t. $\int \tilde{w}(\boldsymbol{r}) n(\boldsymbol{r}) \mathrm{d}\boldsymbol{r} = E_{xc}$) and the one with kinetic and interaction components taken separately differ because the conditional amplitude from which these energy densities are obtained has linear first order dependence on the coupling constant λ.

6.3.2. Response potential for the SCE limit

The two response potentials defined in eq 2.54 and in eq 6.18 can be both thought of as a measure that answers the question [48, 261, 262] "How sensitive is the pair-correlation function on average to local changes in the density?".
It seems quite relevant to ask what happens to it when electrons are perfectly correlated to each other: in the SCE limit.
To address this question, let us start by generalising eq 1.59 to any XC energy along the adiabatic connection as

$$E^{\lambda}_{xc}[n] = \int_0^{\lambda} W_{\lambda'}[n] \mathrm{d}\lambda'. \tag{6.30}$$

Using the expansion of the (global) AC integrand in the strongly-interacting limit (eq 1.70), to first order we obtain

$$\lambda \to \infty \quad E^{\lambda}_{xc}[n] \cong \int_0^{\lambda} W_{\infty}[n] \mathrm{d}\lambda' = \lambda W_{\infty}[n] \tag{6.31}$$

Defining the SCE XC energy as $E^{SCE}_{xc} = \lim_{\lambda\to\infty} \frac{E^{\lambda}_{xc}}{\lambda}$ in agreement with eq 3.26 we get the simple relation

$$E^{SCE}_{xc}[n] = W_{\infty}[n] = V^{SCE}_{ee}[n] - U[n]. \tag{6.32}$$

Let us then rewrite the AC integrand at $\lambda \to \infty$, in analogy to eq 6.15, as

$$W_{\infty}[n] = \frac{1}{2}\int\int n(\mathbf{r}) n(\mathbf{r}') \frac{g^{\infty}_{xc}(\mathbf{r}, \mathbf{r}')}{|\boldsymbol{r} - \boldsymbol{r}'|} \mathrm{d}\boldsymbol{r}\mathrm{d}\boldsymbol{r}'. \tag{6.33}$$

Taking the functional derivative of $W_{\infty}[n]$ w.r.t. the density we obtain

$$v^{\mathrm{SCE}}_{xc}(\mathbf{r}) = \frac{\delta W_{\infty}[n]}{\delta n(\mathbf{r})} = v^{SCE}_{xc,hole}(\mathbf{r}) + v^{SCE}_{resp}(\mathbf{r}), \tag{6.34}$$

where

$$v^{\mathrm{SCE}}_{xc\text{-}hole}(\mathbf{r}) = \int n(\mathbf{r}')\frac{g^{\infty}_{xc}(\mathbf{r},\mathbf{r}')}{|\boldsymbol{r}-\boldsymbol{r}'|}\mathrm{d}\boldsymbol{r}' \tag{6.35}$$

and

$$v^{\mathrm{SCE}}_{resp}(\mathbf{r}) = \frac{1}{2}\iint \frac{n(\mathbf{r}')n(\mathbf{r}'')}{|\boldsymbol{r}'-\boldsymbol{r}''|}\frac{\delta g^{\infty}_{xc}(\mathbf{r}',\mathbf{r}'')}{\delta n(\mathbf{r})}\mathrm{d}\boldsymbol{r}'\mathrm{d}\boldsymbol{r}''. \tag{6.36}$$

Expression 6.35 has been found explicitly to be [82]

$$v^{\mathrm{SCE}}_{xc\text{-}hole}(\mathbf{r}) = \sum_{i=1}^{N-1}\frac{1}{|\boldsymbol{r}-\mathbf{f}_i(\boldsymbol{r})|} - v_{\mathrm{H}}(\boldsymbol{r}). \tag{6.37}$$

Therefore inverting eq 6.34 we find for v^{SCE}_{resp}

$$v^{\mathrm{SCE}}_{resp}(\mathbf{r}) = v^{\mathrm{SCE}}_{Hxc}(\boldsymbol{r}) - \sum_{i=1}^{N-1}\frac{1}{|\boldsymbol{r}-\mathbf{f}_i(\boldsymbol{r})|} \tag{6.38}$$

which is exactly equal to $v^{SCE}_{N-1}(\boldsymbol{r})$ of eq 6.9 as expected.
It follows trivially from eqs 6.34 and 3.16 that both v^{SCE}_{resp} and $v^{\mathrm{SCE}}_{xc\text{-}hole}$ scales linearly with scaling of the density.

6

SCE response potential for a two-electron density

When the number of electrons equals two, we also have another expression for computing $v^{\mathrm{SCE}}_{resp}(\boldsymbol{r})$. In this case the SCE total energy $E^{N=2}_{\mathrm{SCE}}$ of sec 6.2 is equal to

$$E^{N=2}_{\mathrm{SCE}} = \frac{1}{|\boldsymbol{r}-\mathbf{f}(\boldsymbol{r})|} - v^{\mathrm{SCE}}_{Hxc}(\boldsymbol{r}) - v^{\mathrm{SCE}}_{Hxc}(\mathbf{f}(\boldsymbol{r})), \tag{6.39}$$

where the r.h.s. is the value of the SCE potential energy on the manifold parametrized by the co-motion function. This value is a degenerate minimum (see discussion in chapter 3), meaning that we can evaluate it at any point lying on the manifold, such as for $|\mathbf{r}|\to\infty$ (for a nice illustration of the degenerate minimum of the SCE potential energy, the interested reader is addressed to fig 1 of ref [80]). When $|\boldsymbol{r}|\to\infty$, the potential $v^{SCE}_{Hxc}(\boldsymbol{r})$ is gauged to go to zero. At the same time, the co-motion function $\mathbf{f}(\boldsymbol{r})$ will tend to a well defined position $\boldsymbol{r}_0$ well inside the density, i.e. $\mathbf{f}(\boldsymbol{r}\to\infty)\to\boldsymbol{r}_0$. We thus have

$$\frac{1}{|\boldsymbol{r}-\mathbf{f}(\boldsymbol{r})|} - v^{SCE}_{Hxc}(\boldsymbol{r}) - v^{SCE}_{Hxc}(\mathbf{f}(\boldsymbol{r})) = -v^{SCE}_{Hxc}(\boldsymbol{r}_0). \tag{6.40}$$

Combining eqs 6.38 and 6.40 we find

$$v^{SCE}_{resp}(\boldsymbol{r}) = -v^{SCE}_{Hxc}(\mathbf{f}(\boldsymbol{r})) + v^{SCE}_{Hxc}(\boldsymbol{r}_0). \tag{6.41}$$

6.4. Examples of CCA and SCE response potentials

We have computed the SCE response potential, $v_{resp}^{\mathrm{SCE}}(\boldsymbol{r})$, for small atoms and for the hydrogen molecule at equilibrium distance.
For the species H^-, He, Be, Ne and H_2 also accurate CCA response potentials $\overline{v}_{resp}(\boldsymbol{r})$ have been obtained.[2] Notice that, in previous works, several authors [42, 46–48, 52, 61–63, 261–263] have computed the response potential at physical coupling strength, $v_{resp}(\boldsymbol{r})$ of eq 2.54. Here we perform the computation of such response potential only for the species H^- and He using the correlated wavefunctions of reference [264].

In section 6.4.4 we also briefly discuss the extent of the error resulting from combining data coming from different methods, namely from the Lieb maximization procedure [91, 121, 227] and Hylleraas-type wavefunctions [106, 264] or Quantum Monte Carlo calculations [106, 265, 266] as explained in the next sections.

6.4.1. Computational details for the atomic densities

For the sake of clarity, we treat in separate sections the computation of $v_{resp}^{\mathrm{SCE}}(\boldsymbol{r})$ and $\overline{v}_{resp}(\boldsymbol{r})$ for atoms.

SCE response potential

The calculation of $v_{resp}^{\mathrm{SCE}}(\boldsymbol{r})$ for spherical atoms is based on the ansatz for the radial part of the co-motion functions illustrated in section 3.3. The SCE potential, $v_{Hxc}^{SCE}(r)$, is then obtained by integration of eq 3.15. Finally, we apply eq 6.38 (or, equivalently for $N=2$, eq 6.41) to get the SCE response potential.

This procedure is very 'robust' meaning that we have obtained comparable SCE response potentials using densities of different levels of accuracy. The densities we have used were obtained from

(A) CCSD calculations and aug-cc-pCVTZ basis set stored on a 0.01 bohr grid, see ref [121],

(B) Hylleraas-type wave functions, see refs [106, 264], for the two-electron systems and Quantum Monte Carlo calculations, see refs [265–267], for the others.

The cumulant function of eq 3.35 was computed either with simple interpolations between the gridpoints of a given density or in some cases (for H^-, He, and Li^+) with explicitly fitted densities, constrained to satisfy the cusp condition and the correct asymptotic behaviour.
Group (A) regards all the systems taken into account. Group (B) regards the

[2] To our knowledge, accurate CCA response potentials $\overline{v}_{resp}(\boldsymbol{r})$ (eq 6.18) are reported here for the first time.

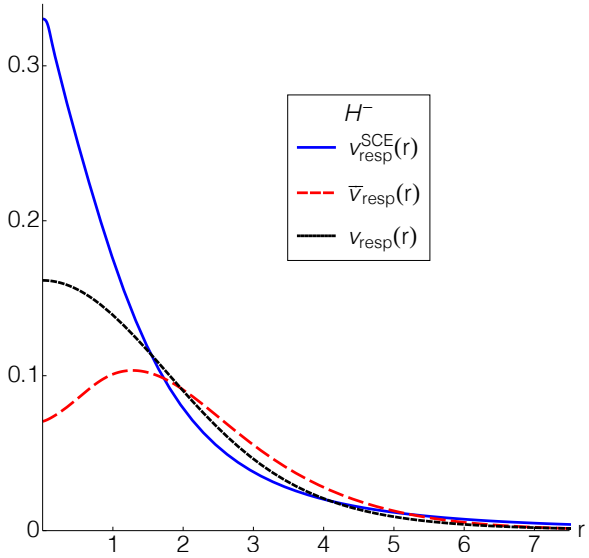

Figure 6.1: Comparison between $\overline{v}_{resp}(r)$ and $v_{resp}^{SCE}(r)$ for the H^- anion.

6

species: H^-, He, Be, and Ne. The figures in sec 6.4.3 only show the SCE response potential coming each time from the most accurate available density.

Coupling-constant averaged response potential

The equation used in practice to compute $\overline{v}_{resp}(\boldsymbol{r})$ is

$$\overline{v}_{resp}(\boldsymbol{r}) = v_{xc}(\boldsymbol{r}) - \overline{v}_{xc\text{-}hole}(\boldsymbol{r}) \tag{6.42}$$

where $\overline{v}_{xc\text{-}hole}$ has been calculated by averaging the $v_{\lambda,xc\text{-}hole}$ (eq 2.60) at each $\boldsymbol{r}$ over the interval $[0,1]$ with an increment $\Delta\lambda = 10^{-1}$. The $v_{\lambda,xc\text{-}hole}$ were obtained through the Lieb maximisation procedure and taken from refs [121, 229, 268]. The XC potentials were taken instead from Hylleraas-type calculations [106] or Quantum Monte Carlo results [106, 265, 266], as they were overall more accurate. This choice is further validated in section 6.4.4.

6.4.2. Computational details for the hydrogen molecule

For the hydrogen molecule a different approach – i.e. the dual-Kantorovich formulation (sec 3.2.2) – was used for the computation of the SCE potential and thus of the SCE response potential.

The basic idea relies on finding the SCE potential as a result of a nested optimization on a parametrized expression which has the correct asymptotic behaviour, the

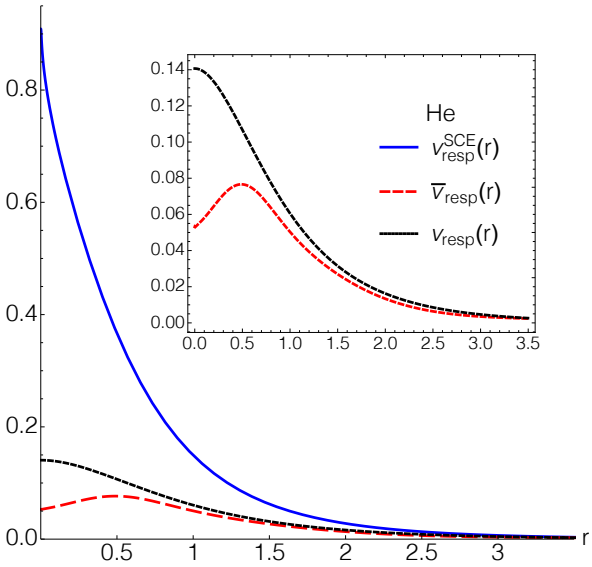

Figure 6.2: Comparison between $\overline{v}_{resp}(r)$, $v_{resp}(r)$ and $v_{resp}^{SCE}(r)$ for the He atom. In the inset we zoom in to allow for a closer comparison between the quantities $\overline{v}_{resp}$ and v_{resp}.

correct cylindrical symmetry and models the barrier region in the midbond. From the optimized potential one derives the co-motion function by inverting eq 3.15; for details see ref [95].
For the CCA exchange-correlation hole potential, $\overline{v}_{xc\text{-}hole}$, exactly the same procedure described for atoms has been used.
The XC potential for the physical system in this case was obtained within the Lieb maximisation procedure itself as in ref [121], namely as the optimized effective potential that keeps the density fixed minus the Hartree potential and the potential due to the field of the nuclei (see also section 6.4.4 for data validation).

6.4.3. Results and discussion

We start by comparing the coupling constant-averaged (CCA) and the SCE response potentials for the H^- anion, in fig 6.1: we see that on average the SCE response potential is larger than the CCA one, but there is an intermediate region, in the range $1.7 \lesssim r \lesssim 5.2$, where the CCA values are above the SCE ones. Since the SCE response potential does not contain any information on how the kinetic potential is affected by a change in the density, this could be a region where the contribution coming from the kinetic correlation response effects overcome the Coulomb correlation ones, even though we cannot exclude that already the mere Coulombic contribution to correlation is higher in the physical case. Indeed, it has

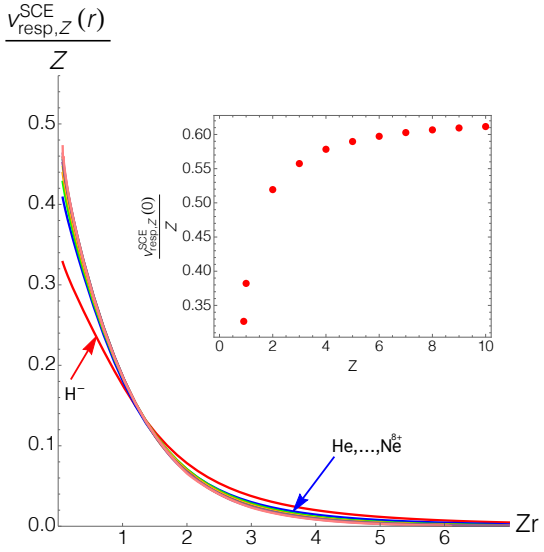

Figure 6.3: Scaled SCE response potentials, $\frac{v^{SCE}_{resp,Z}(\boldsymbol{r})}{Z}$ as a function of the scaled coordinate $Z\,r$ for the He series from H^- up to Ne^{8+}. In the inset, in which only the "slice" at $r = 0$ (i.e. the maximum values of the SCE response potentials) is plotted as a function of the nuclear charge Z, also the hypothetical system with $Z = Z_{crit}$ (see text) is considered.

been shown that the SCE pair density can be insensitive to changes in certain regions of the density [269].
Similar considerations hold when comparing the SCE response potential with the one at physical coupling strength although contrary to the CCA response potential this latter shows a maximum at the origin as well as the SCE potential does. In fig 6.2 we report the same potentials for the He atom density. Since He is less correlated than H^-, in this case the CCA potential $\overline{v}_{resp}(r)$ differs even more from the SCE one. Comparing the two species H^- and He among each other, one can further observe that the value of the distance at which the CCA response potential of the species i has a maximum, r^i_M, is also shifted leftward (closer to the nucleus) when going from $Z = 1$ to $Z = 2$, reflecting the contraction of the density. This in-

formation is also mirrored in the SCE limit by the shift in the a_1 values appearing in equation 3.36 for the computation of the co-motion functions for the two species. Indeed we find that $\frac{a_1^{H^-}}{a_1^{He}} = \frac{r_M^{H^-}}{r_M^{He}}$.

In fig 6.3, we report the SCE response potential along the He series (two-electron systems with nuclear charge $Z = 1, \cdots, 10$). In particular, we plot the scaled potential $\frac{v_{resp,Z}^{SCE}(r)}{Z}$ as a function of the scaled coordinate $Z\,r$. As expected, the response potential in the SCE limit shows an almost perfect scaling behaviour. Deviations from the linear-scaling trend (which is an exact property of the v_{resp}^{SCE} functional as discussed), are a symptom of increasing correlation effects typical of more diffuse densities, like He and H^-. Such correlation effects (curve lying below the uniformly scaled trend for small r and above for large r) are stronger closer to the nucleus. In the top-right inset of this figure, we show only the values of the maxima of the SCE response potential of each species divided by its nuclear charge, $\frac{v_{resp,Z}^{SCE}(0)}{Z}$ as a function of Z. In this inset also a hypothetical system with nuclear charge $Z_{crit} = 0.9110289$, the minimum nuclear charge that can still bind two electrons (see ref [106]), is included.

In the upper panel of fig 6.4 we show the SCE and the CCA response potentials for the Be atom together with the exchange contribution $v_{resp,x}(r)$ (corresponding to $\lambda = 0$), and the correlation contributions obtained by subtracting $v_{resp,x}(r)$ from $\overline{v}_{resp}(r)$ and $v_{resp}^{SCE}(r)$. As it was found in ref [262], the exchange-only response potential shows a clear step structure in the region of the shell boundary. The total CCA response potential also shows a step at the same position, while the SCE response potential has a kink. The kink can be understood by looking at the shape of the radial co-motion functions (see eq 3.36 and the lower panel of the same figure), which determine the structure of the SCE response potential according to eq 6.38. The SCE reference system correlates two adjacent electron positions in such a way that the density between them exactly integrates to 1, therefore the a_i appearing in equation 3.36 are simply the shells that contain always one electron each [104]. For the case of Be, the kink appears at the corresponding a_2-value, which is very close to the shell boundary. In fact, when the reference electron is at distance $r \approx a_2$ from the nucleus, a second electron is found at this same distance (but on the opposite side with respect to the nucleus), while the third electron is very close to the nucleus and the fourth is almost at infinity. This situation results in an abrupt change of the pair density for small variations of the density, as particularly the position of the fourth electron changes very rapidly with small density variations.

Another interesting feature we can observe from fig 6.4 is that the Coulomb correlation contribution to the CCA response potential, $\overline{v}_{resp,c}(r)$, appears to be negative inside the entire 1s shell region. Furthermore, while the total physical response potential is always below the SCE one, the exchange part appears to be

higher in a region quite close to the shell boundary ($0.6 \lesssim r \lesssim 1.0$). This results in the Coulomb correlation contribution for the SCE-limit case, $v^{SCE}_{resp,c}(r)$, to be also negative in that region.

In the upper panel of fig 6.5 we show the SCE response potential and its correlation part for the Ne atom. The SCE response potentials $v^{SCE}_{resp}(r)$ and $v^{SCE}_{resp,c}(r)$ are numerically less accurate, due to the higher dimensional angular minimization. Nevertheless, the relation between its structure and the corresponding co-motion functions in the lower panel of fig 6.5 is clearly visible. We also show the CCA response potentials together with the separate exchange and correlation contributions. Differently from the Be atom, neither the total response potential nor any single correlation contribution (CCA or SCE) is anywhere negative. Still the structure is very similar, showing two steps in the $v_{resp,x}(r)$ one very tiny at around 0.1 and another at around 0.4 distance from the nucleus and two wells in the $\overline{v}_{resp,c}(r)$. In fig 6.6 we show only the CCA correlation contributions to the CCA response potential of the two species for closer comparison.

In fig 6.7 the CCA response potential for the hydrogen molecule at equilibrium distance is shown, together with the SCE one. It is interesting to compare this figure with fig 3(a) of ref [48], where the response potential $v_{resp}(\boldsymbol{r})$ of eq 2.54 was reported, together with other components of the XC potential. The response potential at full coupling strength for the same system is also shown in fig 4 of ref [263], albeit a minus sign and a constant shift. The overall structure is completely different: in the case shown here there is a local minimum of $\overline{v}_{resp}(\boldsymbol{r})$ at approximately 1 bohr distance from the bond midpoint, while $v_{resp}(\boldsymbol{r})$ shown in refs [48, 263] has a maximum located at the nuclei.

In several examples we have now come to see that the details of the dependence of the conditional amplitude on the coupling-parameter can affect greatly the overall shape of the response potentials, as well as of the energy densities. It is then important to keep these different features in mind when one wants to model the response potential or the XC hole, depending on whether the target is a coupling-constant averaged quantity or the same quantity at full coupling strength.

6.4.4. Exchange response potential for N=2 and data validation

It is common use in DFT to separate potentials and energy expressions into exchange and correlation contributions. Analogously to the total XC potential, the exchange potential is defined as the functional derivative of the exchange energy, which is in turn defined as

$$E_x[n] = \langle \Psi_s(1,\ldots,N)|\hat{V}_{ee}|\Psi_s(1,\ldots,N)\rangle - U[n]. \tag{6.43}$$

For a two-electron closed-shell system we have

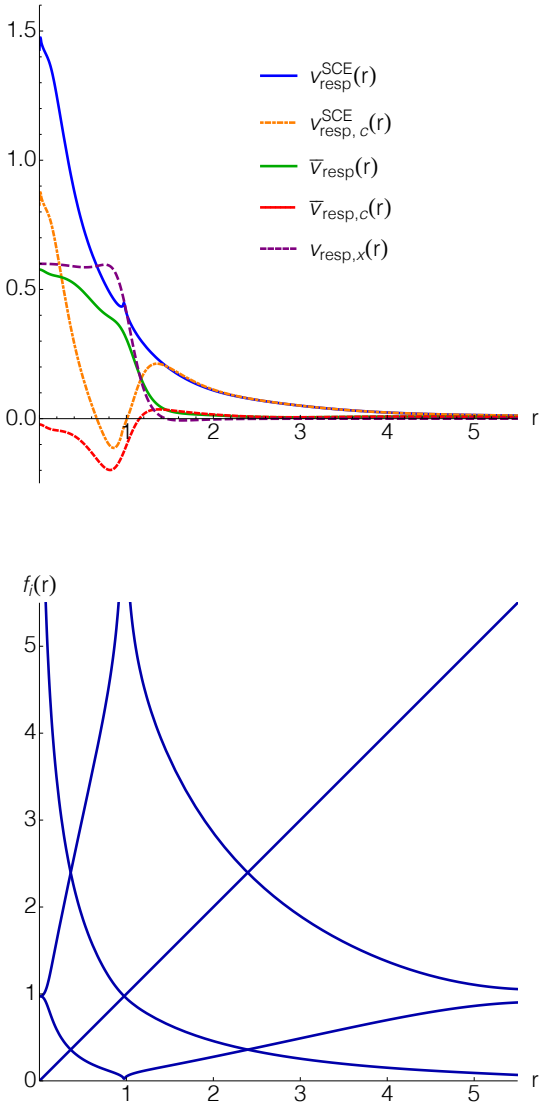

Figure 6.4: Total response potentials $\overline{v}_{resp}(r)$ and $v_{resp}^{SCE}(r)$, and their components $v_{resp,x}(r)$, $\overline{v}_{resp,c}(r)$ and $v_{resp,c}^{SCE}(r)$ (upper panel) and radial co-motion functions (lower panel) for the Be atom.

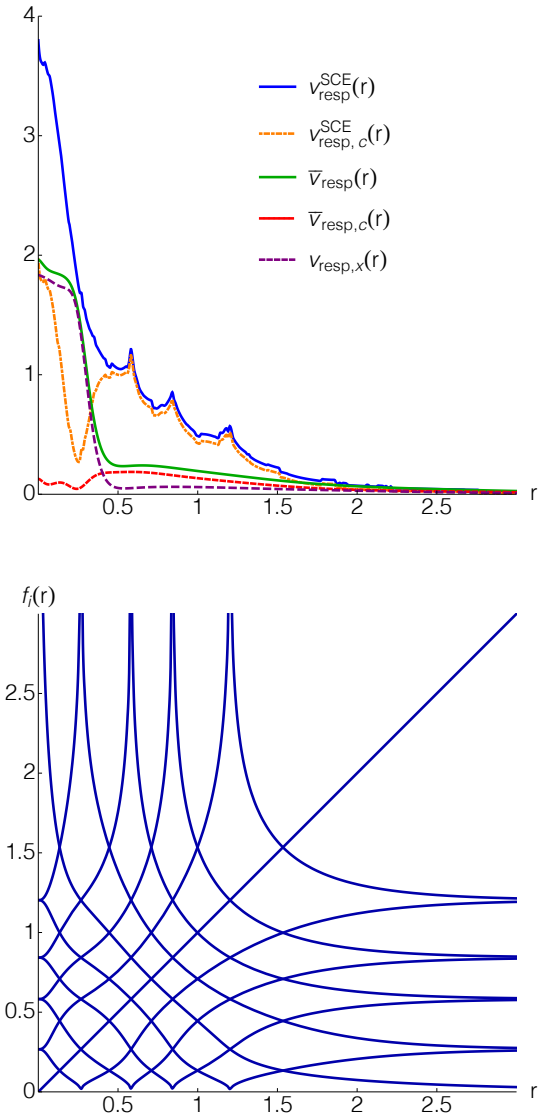

Figure 6.5: Total response potentials $\overline{v}_{resp}(r)$ and $v_{resp}^{SCE}(r)$, and their components $v_{resp,x}(r)$, $\overline{v}_{resp,c}(r)$ and $v_{resp,c}^{SCE}(r)$ (upper panel) and radial-co-motion functions (lower panel) for the Ne atom.

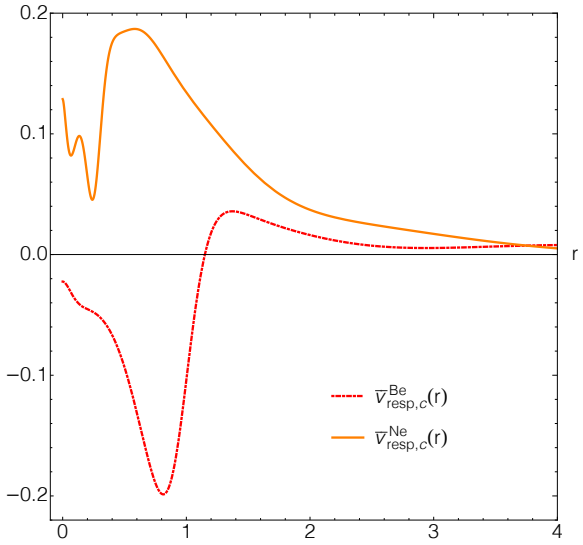

Figure 6.6: Correlation parts of the CCA response potential, $\overline{v}_{resp,c}$, for the Be and the Ne atoms.

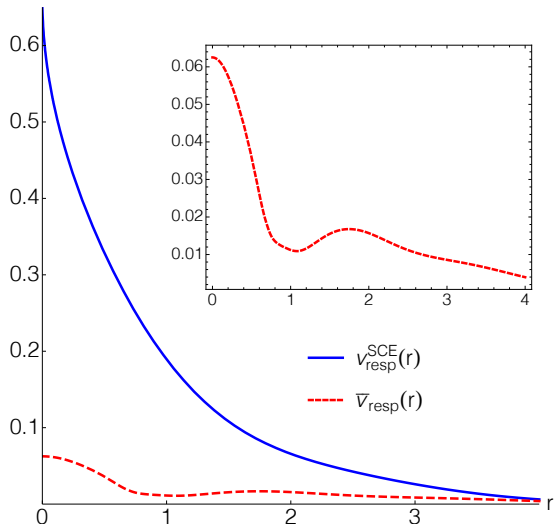

Figure 6.7: Comparison between $\overline{v}_{resp}(\boldsymbol{r})$ and $v^{SCE}_{resp}(\boldsymbol{r})$ for the H_2 molecule at the equilibrium distance, plotted along the internuclear axis, origin of the axes being at the bond midpoint. In the top-right insertion the CCA response potential of H_2 is zoomed in to allow a closer comparison with its response potential, $v_{resp}(\boldsymbol{r})$, shown in fig 3(a) of ref [48].

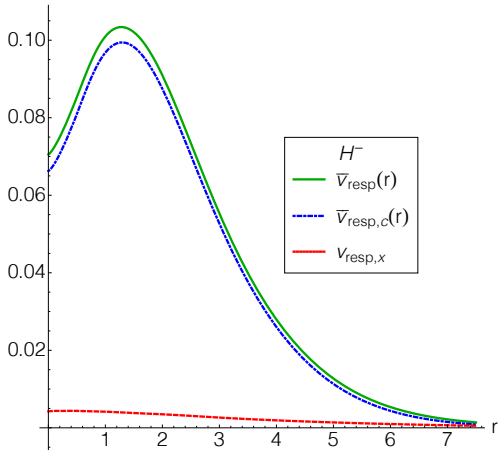

Figure 6.8: Comparison between $\overline{v}_{resp}(r)$ and $\overline{v}_{resp,c}(\boldsymbol{r})$ for the H^- atom in order to estimate the error coming from numerics and the use of different sources for $v_{xc}(\boldsymbol{r})$ and $\overline{w}(\boldsymbol{r})$.

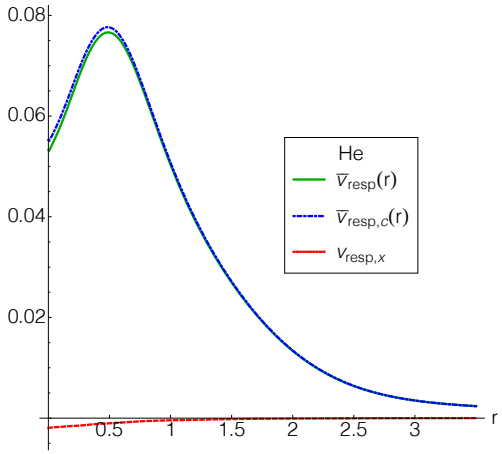

Figure 6.9: Comparison between $\overline{v}_{resp}(r)$ and $\overline{v}_{resp,c}(\boldsymbol{r})$ for the He atom in order to estimate the error coming from numerics and the use of different sources for $v_{xc}(\boldsymbol{r})$ and $\overline{w}(\boldsymbol{r})$.

$$E_x[n] = -\frac{1}{4}\int \frac{n(\boldsymbol{r})n(\boldsymbol{r}')}{|\boldsymbol{r}-\boldsymbol{r}'|}, \tag{6.44}$$

which implies $v_{resp,x}(\boldsymbol{r}) = 0$. In sec 6.4 we have shown the CCA response potential for some atoms combining quantities coming from different sources (see eq 6.42); namely refs [106, 265, 266] for the XC potentials (or their separate contributions), and refs [121, 268] for the CCA energy densities. In the case of the H_2 molecule, instead, both the total XC potential and the CCA energy density used are from the latter source.

In order to give a feeling of how our results could be affected by computational inaccuracies we show in fig 6.8 and 6.9, the difference $v_{resp,x}(\boldsymbol{r}) = v_x(\boldsymbol{r}) - 2w_0(\boldsymbol{r})$, together with the total $\overline{v}_{resp}(\boldsymbol{r})$ and $\overline{v}_{resp,c}(\boldsymbol{r}) = \overline{v}_{resp}(\boldsymbol{r}) - v_{resp,x}(\boldsymbol{r})$. The fact that the first quantity is not exactly zero and the last two are slightly different gives an idea of the numerical errors we have. As it can be noticed, the difference is between 1−10% of the quantity of interest, $\overline{v}_{resp}(\boldsymbol{r})$, and the discussion in sec 6.4.3 is not affected by this error range.

6.5. Simple model for a stretched heteronuclear dimer

The purpose of this section is to analyse the response potential in the SCE limit for the very relevant case of a dissociating heteroatomic molecule, where the exact response potential is known to develop a characteristic step structure [46, 48, 50, 51, 54, 270, 271] as discussed in sec 2.2.1.

Although numerically stable KS potentials have been presented and discussed in the literature for small molecules [61, 63, 272], an accurate calculation of the SCE potential for a stretched heterodimer is still not available. In fact, while with the dual Kantorovich procedure [95, 96] it is possible to obtain accurate values of $V_{ee}^{SCE}[n]$ for small molecules, the quality of the corresponding SCE potentials, particularly in regions of space where the density is very small, is not good enough to allow for any reliable analysis.

We then used a simplified one-dimensional (1D) model system, where only the two valence electrons involved in the stretched bond are treated explicitly. Several authors have used this kind of 1D models, which have been proven to reproduce and allow to understand the most relevant features appearing in the exact KS potential of real molecules [51, 54, 270, 271]. Here we approximate the density of the very stretched molecule as just the sum of the two "atomic" densities

$$n(x) = n_a\left(x-\frac{R}{2}\right) + n_b\left(x+\frac{R}{2}\right) = \frac{a}{2}e^{-a|x-\frac{R}{2}|} + \frac{b}{2}e^{-b|x+\frac{R}{2}|}, \tag{6.45}$$

where a and b mimic the different ionization potentials of the "atoms" (pseudopotentials or frozen cores) and the density is normalized to 2. We have chosen $a > b$,

therefore the more electronegative atom will be found to the right side of the origin (at a distance $+\frac{R}{2}$ from it) and the less electronegative to the left.

6.5.1. SCE response potential for the model stretched heterodimer

As we have only two electrons, there is only one of the "SCE shell" borders, a_i, appearing in eq 3.32. We then drop the subscript "1" and use instead "R "

$$a_R : \quad \int_{-\infty}^{a_R} n(x)\mathrm{d}x = 1 \tag{6.46}$$

to stress that the distance a_1 is a function of the separation between the centers of the exponentials in eq 6.45.
We also write down explicitly the only comotion function for the 1D two-electron case (compare eq 3.32).

$$f(x) = \begin{cases} N_e^{-1}[N_e(x)+1] & x < a_R \\ N_e^{-1}[N_e(x)-1] & x > a_R. \end{cases} \tag{6.47}$$

We have highlighted in the previous section that the border of a shell that contains one electron coincides with the reference position at which one of the comotion functions diverges. The same is true when $x \to a_R$, except that in the one-dimensional case the electron that goes to infinity has to "reappear" on the other side, $\lim_{x\to a_R^{\pm}} f(x) = \mp\infty$. Moreover, as we have only 2 electrons, we can use eq 6.41 to compute $v_{resp}^{SCE}(\boldsymbol{r})$,

$$v_{resp}^{SCE}(x) = -v^{SCE}(f(x)) + v^{SCE}(a_R), \tag{6.48}$$

which further shows that

$$v_{resp}^{SCE}(a_R) = v^{SCE}(a_R). \tag{6.49}$$

In fig 6.10 we show the SCE response potential compared to the "exact" $\overline{v}_{resp}(x)$ for the model density of eq 6.45 at internuclear separation $R = 8$, using $a = 2$ and $b = 1$. In the same figure, we also show the local-density approximation (LDA) CCA response potential $\overline{v}_{resp}^{LDA}(x)$ computed, as in ref [59], via eq 6.19,

$$\overline{v}_{resp}^{LDA}(x) = v_{xc}^{LDA}(x) - 2\epsilon_{xc}^{LDA}(x). \tag{6.50}$$

We stress that eq 6.50 is the correct definition of $\overline{v}_{resp}^{LDA}(x)$, since the energy density in LDA does not have any gauge ambiguity, being given exactly in terms of the electrostatic potential associated with the CCA exchange-correlation hole of the uniform electron gas [273]. For the one-dimensional ϵ_{xc}^{LDA}, we have used the

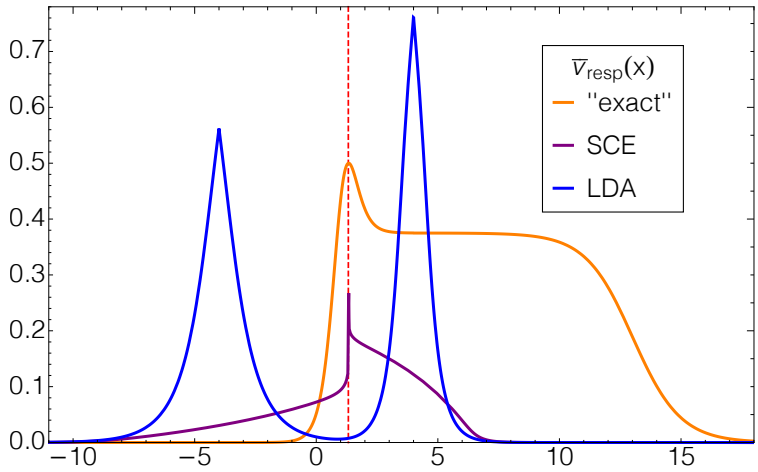

Figure 6.10: SCE response potential compared to the "exact" and the LDA $\overline{v}_{resp}(x)$ for the model density in eq 6.45 with $a = 2$, $b = 1$, and $R = 8$. The red dashed line highlights the position where $x = a_R$.

parametrization of Casula et al. [274], in which the electron-electron Coulomb interaction is renormalized at the origin [273], with thickness parameter $\mathfrak{b} = 0.1$. Notice that the SCE response potentials evaluated with the full Coulomb interaction $1/|x|$ or with the interaction renormalized at the origin [273] are indistinguishable on the scale of fig 6.10, since in the SCE limit the electron-electron distance $|x - f(x)|$ for a stretched two-electron "molecule" never explores the short-range part of the interaction.

The "exact" $\overline{v}_{resp}(x)$ has been computed by inverting the KS equation for the doubly occupied ground-state orbital $\sqrt{n(x)/2}$, disregarding the external potential given by attractive delta functions located at the "nuclei", and assuming that, for the stretched molecule, the interaction between fragments is negligible (which is asymptotically true), while the contributions coming from the Hartree potential on each fragment (the self-interaction error) are exactly canceled by the XC hole. In other words, when R is large, we have $v_{Hxc}(x) \approx \overline{v}_{resp}(x) \approx v_{c,kin}(x) + v_{resp}(x)$.

We see that, as well known, the LDA response potential completely misses the peak and the step structure of the "exact" $\overline{v}_{resp}(x)$, being, instead, way too repulsive on the atoms [59], and following essentially the density shape. The SCE response potential, instead, even though clearly not in agreement with the "exact" one, shows an interesting structure located at the peak of $\overline{v}_{resp}(x)$, and also a sort of step-like feature.

In fig 6.11 we illustrate the behavior of the SCE response potential alone as the internuclear separation R grows, for the same values of a and b of fig 6.10.

We see that the SCE response potential, contrary to the exact one, does not saturate to a step height equal to the difference of the ionization potentials of the two fragments, $\Delta I_p = |I_a - I_b|$. On the contrary, $v_{resp}^{SCE}(x)$ goes (although very slowly) to zero in the dissociation limit, similarly to what happens for the midbond peak in a homodimer, as explained in refs [55, 104]. This has to be expected, in view of the fact that, in the SCE limit, we are only taking into account the expectation of the Coulomb electron-electron interaction, which, when considering two distant one-electron fragments as in this case, is a vanishing contribution [55].
In appendix B, we use an asymptotic model for the co-motion function of eq 6.47 to derive the dependence of the peak of the SCE response potential on the internuclear distance (see eq B.4 and discussion therein).
The fact that we still observe the SCE response structure for quite large R values is related to the non-locality of the SCE potential and to the long-range nature of the Coulomb interaction. A kinetic contribution to SCE is clearly needed, something that is being currently investigated by looking at the next leading terms in the $\lambda \to \infty$ expansion [34, 80].

The peak structure of the SCE response potential is located at a_R of eq 6.46, which is given by

$$a_R = \frac{R}{2}\frac{(a-b)}{(a+b)} = \frac{R}{2}\frac{\left(1-\sqrt{\frac{I_b}{I_a}}\right)}{\left(1+\sqrt{\frac{I_b}{I_a}}\right)}. \tag{6.51}$$

If we compare this result with the one for the location of the step in the exact KS potential, given by eqs. (27) and (29) of ref [51], we see that the two expressions differ by the term $\frac{1}{\sqrt{32}}\frac{\ln\frac{I_b}{I_a}}{\sqrt{I_b}+\sqrt{I_a}}$, which becomes comparatively less important as the bond is stretched. In fig 6.10 we have reported the case $a=2$, $b=1$, and $R=8$, for which eq 6.51 gives $a_R = \frac{4}{3}$ and the correction term for the actual position of the step [51] , which is also the position at which the kinetic peak has its maximum, $x_{step} = x_{peak}$, gives $\frac{1}{\sqrt{32}}\frac{\ln\frac{I_b}{I_a}}{\sqrt{I_b}+\sqrt{I_a}} \simeq -0.23$. The reason why, in spite of this significant correction, in fig 6.10 the peak of the "exact" $\overline{v}_{resp}(x)$ visibly coincides with a_R will be clear in the following section 6.5.3.

6.5.2. Behaviour of the co-motion function for increasing internuclear distance

The features of the SCE response potential can be understood by looking at how the co-motion function changes with increasing internuclear separation R. In the 1D two-electron case considered here, eq 3.11 becomes

$$f'(x) = \frac{n(x)}{n(f(x))}. \tag{6.52}$$

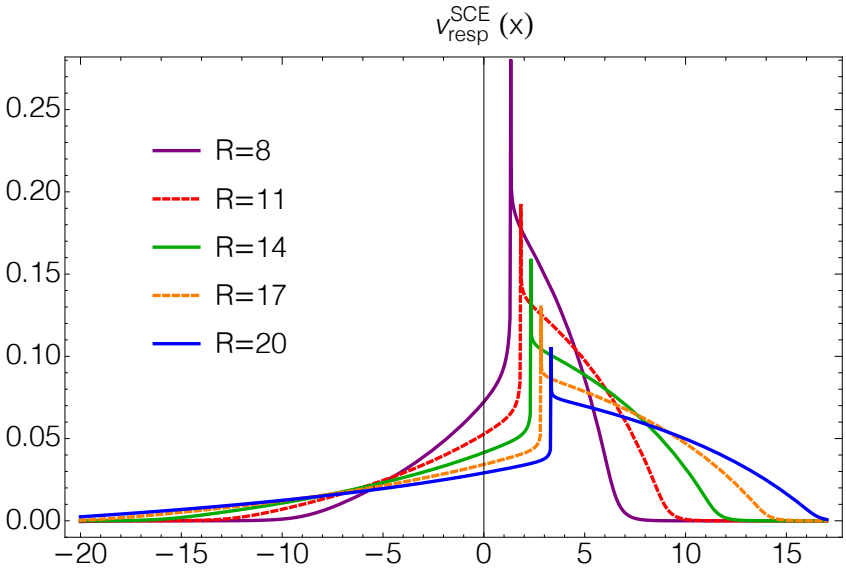

Figure 6.11: SCE response potential for the model density in eq 6.45 with $a = 2$, $b = 1$, and increasing internuclear distances, R.

For $R >> 0$, when the reference electron (e_1) is in the center of one the two "atomic" densities, e.g., at $x = -\frac{R}{2}$, the other electron (e_2) is in the center of the other "atom", $f(-\frac{R}{2}) = \frac{R}{2}$. This is a simple consequence of the fact that the overall density is normalized to two and, if the overlap in the midbond region is negligible, for symmetry reasons, the area from $-\frac{R}{2}$ to $\frac{R}{2}$ is exactly equivalent to the sum of the areas outside that range.
We see that after a critical internuclear distance, R_c, at which the overlap between the densities of the separated fragments becomes negligible, the slope of the co-motion function when e_1 is in $x = -\frac{R}{2}$ becomes equal to

$$f'(x)|_{x=-\frac{R}{2}} = \frac{n(-\frac{R}{2})}{n(\frac{R}{2})} \simeq \frac{n_b(-\frac{R}{2})}{n_a(\frac{R}{2})} = \frac{b}{a} \quad R > R_c, \tag{6.53}$$

so that there is a region where $f'(x) = \frac{b}{a}$, and, similarly, another region where $f'(x) = \frac{a}{b}$, by interchanging e_1 with e_2. Notice that the extension of these regions is different for the two branches of eq 6.47 and it is wider when the reference electron is around the less electronegative "atom" as it can be seen in fig 6.12,

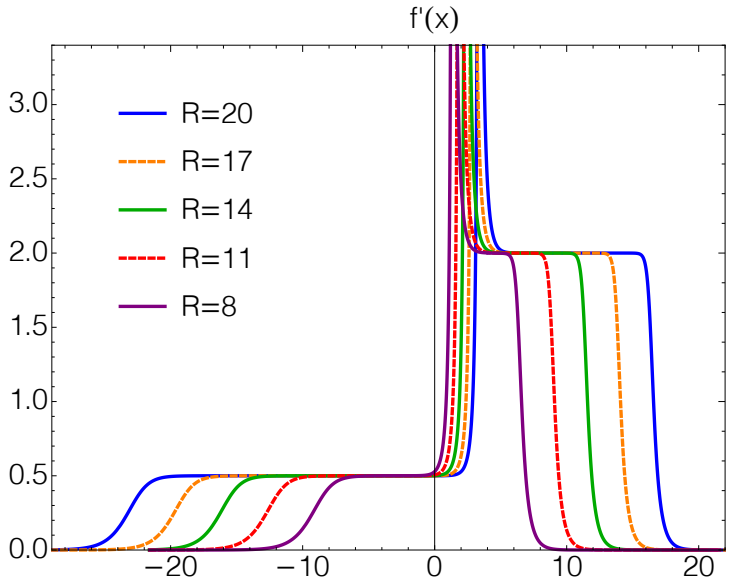

Figure 6.12: Derivative of the co-motion function for the model density in eq 6.45 with $a=2$, $b=1$, and increasing internuclear distances, R.

where we show the (numerically) exact

$$f'(x) = \frac{n_a(x-\frac{R}{2}) + n_b(x+\frac{R}{2})}{n_a(f(x)-\frac{R}{2}) + n_b(f(x)+\frac{R}{2})}. \tag{6.54}$$

There, the two regions clearly appear as left and right plateaus, with their extent increasing linearly with R.[3] These plateaus are the signature of molecular dissociation: they are absent at equilibrium distance, and start to appear as the overlap between the two densities is small. We see from eq 6.53 that they encode information on the ratio between the ionization potentials of the two fragments.

6.5.3. Careful inspection of the exact features of the KS potential for the dissociating AB molecule

The model density $n(x)$ of eq 6.45 corresponds to an asymptotic simplification of different models that appeared in the literature to study the KS potential in the dimer dissociation limit [51, 54, 270, 271]. Here we review in detail the properties of the KS potential and the two single contributions that can be extracted from this model, $v_{c,kin}(x)$ (eq 2.53) and $v_{resp}(x)$ (eq 2.54, also showing that a second peak

[3] In appendix B, we show that the sum of the left and right plateaus goes asymptotically like $2R$.

in the kinetic potential appears on the side of the more electronegative "atom", a feature that seems to have been overlooked in previous studies. In order to study the dissociation regime we use the Heitler-London wavefunction:

$$\Psi_{HL}(x_1, x_2) = \frac{1}{\sqrt{2(1+S_{AB})}}\left(\phi_a(x_1)\phi_b(x_2) + \phi_b(x_1)\phi_a(x_2)\right), \tag{6.55}$$

where $S_{AB} = \int \phi_a(x)\phi_b \mathrm{d}x$, and $\phi_{a(b)} = \sqrt{\frac{a(b)}{2}} e^{-\frac{a(b)}{2}|x-(+)\frac{R}{2}|}$. To compute the kinetic potential, in the dissociation limit, we can use eq 2.58 and the conditional amplitude coming from the Heitler-London wavefunction considering $S_{AB} = 0$, which yields the well-known expression [51, 54]

$$\begin{aligned} v_{c,kin}(x) &= \frac{1}{2}\int |\frac{d}{dx}\Phi_{HL}(x_2|x)|^2 \mathrm{d}x_2 \\ &= \frac{1}{2}\frac{\left(\phi_b(x)\phi_a'(x) - \phi_a(x)\phi_b'(x)\right)^2}{\left(\phi_a(x)^2 + \phi_b(x)^2\right)^2}, \end{aligned} \tag{6.56}$$

where we have used the fact that $v_{kin}(x) = v_{c,kin}(x)$ as the kinetic KS potential is zero for a closed-shell two-electron system. Analogously, $v_{resp}(x)$ can be obtained from v_{N-1} of eq 2.57,

$$\begin{aligned} v_{resp}(x) = &\frac{1}{2}\int |\frac{d}{dx_2}\Phi_{HL}(x_2|x)|^2 \mathrm{d}x_2 + \\ &+ \int v_{ext}^{mod}(x_2)|\Phi_{HL}(x_2|x)|^2 \mathrm{d}x_2 - E^{N-1} = \\ &= -\frac{1}{n(x)}\left(\frac{a^2}{8}\phi_b(x)^2 + \frac{b^2}{8}\phi_a(x)^2\right) + \frac{a^2}{8}, \end{aligned} \tag{6.57}$$

where $v_{ext}^{mod}(x) = -\frac{a}{2}\delta\left(x-\frac{R}{2}\right) - \frac{b}{2}\delta\left(x+\frac{R}{2}\right)$ and $E^{N-1} = -\frac{a^2}{8}$. Comparing these two contributions with the KS potential obtained from the density by inversion (subtracting the external potential due to the attractive delta peaks at the "nuclear" positions), we have in this limit, as already discussed,

$$v_{Hxc}(x) \sim \overline{v}_{resp}(x) \sim v_{c,kin}(x) + v_{resp}(x), \tag{6.58}$$

since $v_{cond}(x)$ goes to zero when the fragments are very far from each other.[4]
In fig 6.13 we show the potential obtained from the inversion of the KS equation with its two components $v_{c,kin}(x)$ and $v_{resp}(x)$.
Note that the response component itself can be split into different contributions,

[4] Recalling the discussion on sec 6.3.1, we see that since, for a two-electron model in the dissociation limit, $\hat{h}_\lambda \sim -\frac{\nabla_{r_2}^2}{2}$ then $\int_0^1 \mathrm{d}\lambda \langle\Theta_\lambda|\hat{h}_\lambda|\frac{\partial\Theta_\lambda}{\partial\lambda}\rangle \sim \frac{1}{2} v_{c,kin}$ which plugged into eqs 6.28 and 6.29 correctly gives $v_{xc\text{-}hole} \sim \overline{v}_{xc\text{-}hole}$ and $\overline{v}_{resp}(x) \sim v_{c,kin}(x) + v_{resp}(x)$, as contained in eq 6.58.

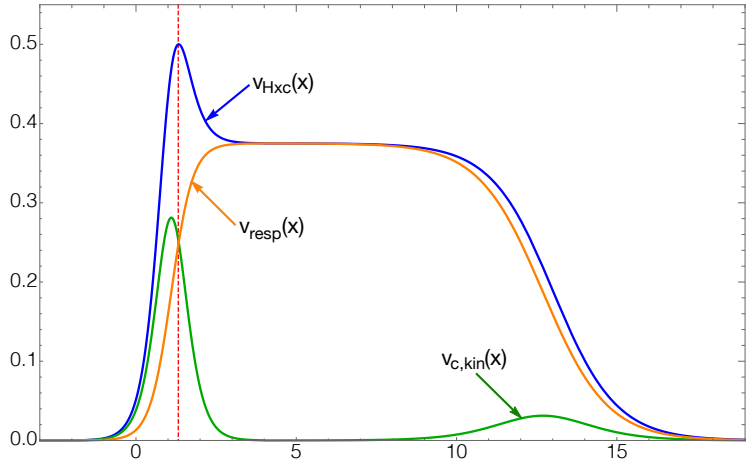

Figure 6.13: Hartree-XC potential, $v_{Hxc}(x)$, and its contributions $v_{c,kin}(x)$ and $v_{resp}(x)$ for $a=2, b=1, R=8$. The red dashed line highlights the position where $x=a_R$

namely $v_{resp} = v_{resp,x} + v_{resp,c}$. However in sec 6.4.4 we have shown that $v_{resp,x} = v^{resp}_{x\text{-}hole} = 0$ for closed shell two-electron systems as it is the case here. Moreover, $v_{resp,c} = v^{resp}_{c\text{-}hole} + v^{resp}_{c,kin}$, however in a dissociating two electron-system, since v_{cond} is going to zero, the correlation hole contribution is $v_{c\text{-}hole}$ $v_{x\text{-}hole} = -\frac{v_H}{2}$ to fully compensate the self interaction of the Hartree potential. And its response part vanishes in this limit. In conclusion, the rising of the step structure is a purely kinetic effect, i.e.

$$v_{resp}(x) \sim v^{resp}_{c,kin}(x). \tag{6.59}$$

Given the simplicity of the model, it is easy to obtain exact expressions regarding each component of the potential and their maxima, inflection points, and so forth. Some of these relevant analytic expressions are listed in tables 6.1 and 6.2.

By looking at the table, one sees, for example, that the peak of the total XC potential is not located where the peak of the kinetic correlation builds up. In particular the maximum of the Hartree-XC potential is found at

$$x_{peak,Hxc} = \frac{R}{2}\frac{(a-b)}{(a+b)}, \tag{6.62}$$

which is exactly a_R (see eq 6.51 and compare also fig 6.10). Thus, the Hartree-XC potential reaches its maximum when the density integrates to one electron (or the

Table 6.1: Some of the relevant analytic features of the analytic 1D model dimer for $x < \frac{R}{2}$. The distance $x^{(1)}_{\text{peak}}$ is the position at which the kinetic potential, $v_{c,kin}(x)$, has a maximum in between the two nuclear centers; $x^{(1)}_{\text{step}}$ is the (coinciding) position at which the response potential, $v_{resp}(x)$, has an inflection point. With the subscript "flex" we indicate the inflection point of both the total Hartree-XC potential and the kinetic potential; they are distinguished via an additional subscript, respectively "Hxc" and "k". Finally, x_{eq} is used to label the x-value at which $v_{c,kin}(x)$ and $v_{resp}(x)$ crosses.

$a \geqslant b$	$\phi_a(x) = \sqrt{\frac{a}{2}} e^{-\frac{a}{2}\lvert x-\frac{R}{2}\rvert}$	$n(x) = \lvert\phi_a(x)\rvert^2 + \lvert\phi_b(x)\rvert^2$
	$\phi_b(x) = \sqrt{\frac{b}{2}} e^{-\frac{b}{2}\lvert x+\frac{R}{2}\rvert}$	$I_\alpha = \frac{\alpha^2}{8}; \quad \alpha = a, b$
$x < \frac{R}{2}$	$\frac{\mathrm{d}v_{c,kin}(x)}{\mathrm{d}x}\lvert_{x^{(1)}_{\text{peak}}} = \frac{\mathrm{d}^2 v_{resp}(x)}{\mathrm{d}x^2}\lvert_{x^{(1)}_{\text{step}}}$	$x^{(1)}_{\text{peak}} = \frac{(a-b)R + 2\ln\frac{b}{a}}{2(a+b)}$ (6.60)
		$v_{c,kin}(x^{(1)}_{\text{peak}}) = \frac{1}{8}\left(\frac{a+b}{2}\right)^2$
		$v_{resp}(x^{(1)}_{\text{step}}) = \frac{1}{2}\frac{a^2-b^2}{8}$
		$v_{Hxc}(x^{(1)}_{\text{peak}}) = \frac{1}{32}(3a-b)(a+b)$
	$\frac{\mathrm{d}^2 v_{c,kin}(x)}{\mathrm{d}x^2}\lvert_{x^{(1)}_{\text{flex},k}} = 0$	$x_{\text{flex},k^{(1)}} = \frac{(a-b)R - 2\ln\frac{2a+\sqrt{3}a}{b}}{2(a+b)}$
	$\frac{\mathrm{d}^2 v_{c,kin}(x)}{\mathrm{d}x^2}\lvert_{x^{(2)}_{\text{flex},k}} = 0$	$x_{\text{flex},k^{(2)}} = \frac{(a-b)R - 2\ln\frac{2a-\sqrt{3}a}{b}}{2(a+b)}$
	$\frac{\mathrm{d}v_{Hxc}(x)}{\mathrm{d}x}\lvert_{x_{\text{peak},Hxc}} = 0$	$x_{\text{peak},Hxc} = \frac{(a-b)}{(a+b)}\frac{R}{2} = a_R$
	$\frac{\mathrm{d}^2 v_{Hxc}(x)}{\mathrm{d}x^2}\lvert_{x^{(1)}_{\text{flex},Hxc}} = 0$	$x^{(1)}_{\text{flex},Hxc} = \frac{(a-b)R - 2\ln\frac{(a+b+\sqrt{a^2+ab+b^2})}{b}}{2(a+b)}$
	$\frac{\mathrm{d}^2 v_{Hxc}(x)}{\mathrm{d}x^2}\lvert_{x^{(2)}_{\text{flex},Hxc}} = 0$	$x^{(2)}_{\text{flex},Hxc} = \frac{(a-b)R - 2\ln\frac{(a+b-\sqrt{a^2+ab+b^2})}{b}}{2(a+b)}$
	$v_{c,kin}(x_{eq}) = v_{resp}(x_{eq})$	$x_{eq} = \frac{(a-b)R + 2\ln 2 + 2\ln\frac{b^2}{a(b-a)}}{2(a+b)}$

Table 6.2: Some of the relevant analytic features of the analytic 1D model dime for $x > \frac{R}{2}$ in analogy with the ones listed in table 6.1, but appearing in this case somewhere far from the midbond on the side of the more electronegative fragment, are listed. For example, $x^{(2)}_{\text{peak}}$ is the second maximum of the kinetic potential, eq 6.61 (top-right entry of the second part), which also coincides with the second inflection point of the response potential as argued in the main text.

$a \geqslant b$	$\phi_a(x) = \sqrt{\frac{a}{2}}\, e^{-\frac{a}{2}\lvert x-\frac{R}{2}\rvert}$	$n(x) = \lvert\phi_a(x)\rvert^2 + \lvert\phi_b(x)\rvert^2$
	$\phi_b(x) = \sqrt{\frac{b}{2}}\, e^{-\frac{b}{2}\lvert x+\frac{R}{2}\rvert}$	$I_\alpha = \frac{\alpha^2}{8}; \quad \alpha = a, b$
$x > \frac{R}{2}$	$\frac{\mathrm{d}v_{c,kin}(x)}{\mathrm{d}x}\big\rvert_{x^{(2)}_{\text{peak}}} = \frac{\mathrm{d}^2 v_{resp}(x)}{\mathrm{d}x^2}\big\rvert_{x^{(2)}_{\text{step}}}$	$x^{(2)}_{\text{peak}} = \frac{(a+b)R - 2\ln\frac{b}{a}}{2(a-b)}$ (6.61)
		$v_{c,kin}(x^{(2)}_{\text{peak}}) = \frac{1}{8}\left(\frac{a-b}{2}\right)^2$
		$v_{resp}(x^{(2)}_{\text{step}}) = v_{resp}(x^{(1)}_{\text{step}})$
		$v_{Hxc}(x^{(2)}_{\text{peak}}) = \frac{1}{32}(3a+b)(a-b)$
	$\frac{\mathrm{d}^2 v_{c,kin}(x)}{\mathrm{d}x^2}\big\rvert_{x^{(3)}_{\text{flex},k}} = 0$	$x_{\text{flex},k^{(3)}} = \frac{(a+b)R - 2\ln\frac{(2b+\sqrt{3}b)}{a}}{2(a-b)}$
	$\frac{\mathrm{d}^2 v_{c,kin}(x)}{\mathrm{d}x^2}\big\rvert_{x^{(4)}_{\text{flex},k}} = 0$	$x_{\text{flex},k^{(4)}} = \frac{(a+b)R - 2\ln\frac{(2b-\sqrt{3}b)}{a}}{2(a-b)}$
	$\frac{\mathrm{d}^2 v_{Hxc}(x)}{\mathrm{d}x^2}\big\rvert_{x^{(3)}_{\text{flex},Hxc}} = 0$	$x^{(3)}_{\text{flex},Hxc} = \frac{(a+b)R + 2\ln\frac{(a-b+\sqrt{a^2-ab+b^2})}{b}}{2(a-b)}$

correct integer number of electrons in a general two fragments case) because this is where the two fragments must be detached from one another. From a different perspective, this is a manifestation that the response and the kinetic correlation contributions in the dissociation limit are not independent and that their sum can be sometimes more meaningful than the separate contributions. Also, by playing around with the expressions in tables 6.1 and 6.2, one realises that there can be misleading coincidental features. For example, the last entry of table 6.1 , which is the analytic expression for the distance at which the kinetic correlation potential and the response potential equate, x_{eq}, is such that the two contributions $v_{c,kin}(x)$ and $v_{resp}(x)$ crosses exactly at a_R if $a = 2$ and $b = 1$ like in fig 6.13, but this is not a general feature. Similarly if we choose $a = \frac{5}{3}b$ then the height of the kinetic peak becomes equal to the height of the step and so on.

Note here that the features listed in the table are obtained for the zero-overlap case, $S_{AB} = 0$, in eq 6.55. Nonetheless, they should become asymptotically exact in the dissociation limit.

Another feature that came to our attention and that – to the best of our knowledge – had not been discussed before, is the fact that the kinetic correlation potential has a second peak on the side of the more electronegative atom. This second maximum is located where the second inflection point of the response potential is, see fig 6.13 and eq 6.61 in tab. 6.2. To understand the appearance of the second peak, we can identify two regimes, A and B, by the leading exponential coefficient: for example, in our case, in the region starting from $-\infty$ the density of the fragment with the smallest coefficient, $n_b(x)$ is larger than the other, $n_a(x)$; approaching the A center there is a point in which $n_a(x)$ becomes larger than the other density. This transition between regimes determines both the kinetic peak and the response step. In particular the distance, $x^{(1)}$ at which the orbitals, ϕ_i (or the fragment densities, which are simply their square) equate

$$\phi_a(x^{(1)}) = \phi_b(x^{(1)}), \tag{6.63}$$

is found to coincide with that of eq 6.60 in the table, i.e. the maximum of the first kinetic peak as well as of the flex coming from the building up of the response potential step, $x^{(1)} = x^{(1)}_{\text{peak}} = x^{(1)}_{\text{step}}$. Note also that this distance is always somewhere in between the two centers of the fragments, $-\frac{R}{2} < x^{(1)}_{\text{peak}} < \frac{R}{2}$.
Nonetheless, since $n_b(x)$ is asymptotically dominating, by going further in the direction of $+\infty$, the 'B regime' is to be encountered again and the two fragment densities, though both very small in magnitude, will be equal again, at some point, $x^{(2)}$

$$\phi_a(x^{(2)}) = \phi_b(x^{(2)}). \tag{6.64}$$

At this distance also another kinetic peak is appearing as well as another flex coming from the exhaustion of the response potential step or, in short, $x^{(2)} = x^{(2)}_{\text{peak}} =$

$x^{(2)}_{\text{step}}$. This is in agreement with the observation in the work of Baerends and coworkers that steps in the response potential and peaks in the kinetic correlation potential are always related [42, 261]. Note that this secondary peak is not visible when looking instead at the CCA response potential, again showing the importance of keeping in mind which contribution of the XC potential one is targeting when designing approximations.

6.6. Conclusions

In the present work we have derived the modulus squared of the conditional amplitude in the $\lambda \to \infty$ (SCE) limit as well as a consistent definition of its corresponding response potential. In the simple 1D model of a dissociating molecule (eq 6.45), it is found that interesting similarities between dissociation features of the exchange-correlation potential and SCE features, such as the behaviour of the co-motion function for increasing internuclear distance or the structure of the SCE response potential itself, can be established. For example, in the dissociation regime, the slope of the co-motion function is determined by the ratio between the ionization potentials of the fragments (compare fig 6.12), whereby the step height of the exchange-correlation potential is determined by their difference. In addition, the co-motion function confers to the SCE response potential an asymmetric structure which indicates on which side of the system the more electronegative fragment is located.

Further analyzing the different components of the exchange-correlation potential that are relevant in the dissociation limit, namely v_{resp} and $v_{c,kin}$, or $\overline{v}_{resp}$, we have identified the presence of a second peak of lower intensity in the kinetic correlation potential on the side of the more electronegative atom and, by comparison, we have observed that the peak of the coupling-constant averaged response potential asymptotically coincides with that of the SCE response potential itself. Our work shows that the SCE framework encodes more than few pieces of information on the physical system and that useful guidelines in the design of highly non-local density functional approximations (based on integrals of the density) can be drawn from it. A step further in this direction will be to study exact properties of the kinetic potential that appears as the next leading term ($\sim \lambda^{-1/2}$) in the expansion of the adiabatic connection integrand in the $\lambda \to \infty$ limit [34], as well as spin effects that have been shown [80] to enter at orders $\sim e^{-\sqrt{\lambda}}$.

We have also reported, for some small systems (He series, Be, Ne, and H_2), the response potential coupling-constant averaged along the adiabatic connection; the study of this different response potential complements that of the response potential at full coupling strength and could provide other hints for the construction of approximate XC functionals, especially of a new generation of DFAs based on local quantities along the adiabatic connection [6, 121, 229, 232].

7

Sum-rules of the response potential in the strong-interaction limit of DFT

The response part of the exchange-correlation potential of Kohn–Sham density functional theory plays a very important role, for example for the calculation of accurate band gaps and excitation energies. Here we analyze this part of the potential in the limit of infinite interaction in density functional theory, showing that in the one-dimensional case it satisfies a very simple sum rule.

7.1. Introduction

The investigation of the exact properties and features of $v_{xc}(\boldsymbol{r})$ has always played an important role in understanding and building approximations [42, 46–48, 51, 52, 54, 55, 61–63, 261, 265, 266, 270–272]. In this work we focus on the XC potential in the SCE limit, $v_{xc}^{\mathrm{SCE}}(\boldsymbol{r})$, and particularly on its response part, which has revealed several interesting features as discussed in the previous chapter.

The response part of the XC potential has been shown to be critical for the correct description of virtual KS orbitals' levels, needed for the calculation of molecular excitation energies in TDDFT [58, 59], as well as for the proper description of electron localization in a dissociating heteronuclear molecule [46–48, 51, 54, 262, 272] and for the construction of the Levy-Zahariev potential [230].

Here we show that, in cases in which the SCE limit can be solved exactly (one-

dimensional and spherically symmetric systems), its response potential satisfies a simple sum rule, see Eqs. 7.6, 7.16 and 7.20.

7.2. Sum-rule of the SCE response potential

We can use 3.15 and 6.38 to derive the following expression for the gradient of the SCE response potential with $w(\boldsymbol{r}) \equiv 1/|\boldsymbol{x}|$

$$\begin{aligned} \nabla v_{resp}^{\mathrm{SCE}} &= \sum_{i=1}^{N-1} \Big((\nabla w)(\boldsymbol{r} - \mathbf{f}_i(\boldsymbol{r}) - (\nabla w)(\boldsymbol{r} - \mathbf{f}_i(\boldsymbol{r}))\,(1 - \nabla \mathbf{f}_i) \Big) \\ &= \sum_{i=2}^{N} (\nabla w)(\boldsymbol{r} - \mathbf{f}_i(\boldsymbol{r})) \cdot \nabla \mathbf{f}_i(\boldsymbol{r}) \end{aligned} \tag{7.1}$$

where $(\nabla w)(\boldsymbol{r} - \mathbf{f}_i(\boldsymbol{r})) = (\nabla_{\boldsymbol{x}} w(\boldsymbol{x}))\big|_{\boldsymbol{x}=(\boldsymbol{r}-\mathbf{f}_i(\boldsymbol{r}))} = -\frac{(\boldsymbol{r}-\mathbf{f}_i(\boldsymbol{r}))}{|(\boldsymbol{r}-\mathbf{f}_i(\boldsymbol{r}))|^3}$. To clarify, let us work out the expression of the SCE response potential per component in Cartesian coordinates

$$\partial_\mu v_{\mathrm{resp}}^{\mathrm{SCE}}(\boldsymbol{r}) = -\sum_{\nu=1}^{D} \sum_{i=2}^{N} \frac{\boldsymbol{r}_\nu - \mathbf{f}_{i,\nu}(\boldsymbol{r})}{|\boldsymbol{r} - \mathbf{f}_i(\boldsymbol{r})|^3} \partial_\mu \mathbf{f}_{i,\nu}(\boldsymbol{r}). \tag{7.2}$$

For the case $D = 1$, the response potential can now directly be calculated as an integral. In the following sections we are going to prove the exact behaviour of the integral of the SCE response potential corresponding to an N-electron 1D density and the one corresponding to a spherical two-electron density. As discussed in chapter 3, these are the two cases in which the co-motion functions are the optimal maps.

7.2.1. Sum-rule of the SCE response potential for a 1D density

The sum-rule of the SCE response function in 1D (for Coulomb interaction) relates the integral over the response function to the number of electrons. To illustrate the idea, we will first consider the simplest situation: a symmetric 2-electron density. Next we release the symmetry constraint and then generalise to an arbitrary amount of particles.

Symmetric two-electron density in 1D

In the case of a symmetric 1D density with only two electrons, we see that $a_1 = 0$ and the SCE response potential can be expressed as

$$v_{\mathrm{resp}}^{\mathrm{SCE}}(x) = \begin{cases} \displaystyle\int_{-\infty}^{x} \mathrm{d}y \, \frac{f'(y)}{\big(y - f(y)\big)^2} & (x \le 0) \\ \displaystyle\int_{x}^{\infty} \mathrm{d}y \, \frac{f'(y)}{\big(y - f(y)\big)^2} & (x \ge 0), \end{cases} \tag{7.3}$$

where we used that the potential can be obtained by integrating from either side, as the response potential is symmetric.

Let us only consider the negative side of the SCE response potential. By interchanging the order of integration, we find for the integral over the response function

$$\int_{-\infty}^{0} \mathrm{d}x\, v_{\mathrm{resp}}^{\mathrm{SCE}}(x) = -\int_{-\infty}^{0} \mathrm{d}y\, \frac{y f'(y)}{\big(y - f(y)\big)^2}. \tag{7.4a}$$

We can also make a change of variables $u = -f(y)$, keeping in mind that, due to the property in 3.12, $f^{-1}(x) = f(x)$

$$\int_{-\infty}^{0} \mathrm{d}x\, v_{\mathrm{resp}}^{\mathrm{SCE}}(x) = \int_{-\infty}^{0} \mathrm{d}u\, \frac{f(u)}{\big(f(u) - u\big)^2}. \tag{7.4b}$$

We can combine these two expressions to write the integral over the SCE response function as

$$\int_{-\infty}^{0} \mathrm{d}x\, v_{\mathrm{resp}}^{\mathrm{SCE}}(x) = -\frac{1}{2}\int_{-\infty}^{0} \mathrm{d}u\, \frac{y f'(y) - f(y)}{\big(y - f(y)\big)^2} = -\frac{1}{2}\frac{y}{y - f(y)}\Big|_{-\infty}^{0} = \frac{1}{2}. \tag{7.5}$$

As the SCE response potential is a symmetric function, we find that the integral over the real line gives

$$\int_{-\infty}^{\infty} \mathrm{d}x\, v_{\mathrm{resp}}^{\mathrm{SCE}}(x) = 1. \tag{7.6}$$

General two-electron density in 1D

In the case of a non-symmetric density we now have almost the same expression for the SCE response potential as in 7.3, except that we need to cut it at $a_1 = N_e^{-1}(1)$ instead of zero

$$v_{\mathrm{resp}}^{\mathrm{SCE}}(x) = \begin{cases} \displaystyle\int_{-\infty}^{x} \mathrm{d}y\, \frac{f'(y)}{\big(y - f(y)\big)^2} & (x \le a_1) \\ \displaystyle\int_{x}^{\infty} \mathrm{d}y\, \frac{f'(y)}{\big(y - f(y)\big)^2} & (x \ge a_1), \end{cases} \tag{7.7}$$

where we used again that it does not matter from which side we do the integration. Though physically reasonable, we need to show explicitly that $v_{\mathrm{resp}}^{\mathrm{SCE}}(-\infty) = v_{\mathrm{resp}}^{\mathrm{SCE}}(+\infty)$. To this purpose, let us work out the following identities

$$\mathrm{d}N_e(x) = n(x)\,\mathrm{d}x, \tag{7.8a}$$

$$\frac{\mathrm{d}N_e^{-1}(v)}{\mathrm{d}v} = \frac{1}{n\big(N_e^{-1}(v)\big)}. \tag{7.8b}$$

Now we work out the response function at $x = +\infty$ by performing the full integral

$$\begin{aligned} v_{\text{resp}}^{\text{SCE}}(\infty) &= \int_{-\infty}^{a_1} \mathrm{d}y \, \frac{f'(y)}{\big(y - f(y)\big)^2} - \int_{a_1}^{\infty} \mathrm{d}y \, \frac{f'(y)}{\big(y - f(y)\big)^2} \\ &= \int_0^1 \mathrm{d}v \, \frac{1/n\big(N_e^{-1}(v+1)\big)}{\big(N_e^{-1}(v) - N_e^{-1}(v+1)\big)^2} + \\ &\quad - \int_1^2 \mathrm{d}v \, \frac{1/n\big(N_e^{-1}(v-1)\big)}{\big(N_e^{-1}(v) - N_e^{-1}(v-1)\big)^2} \\ &= \int_0^1 \mathrm{d}v \, \frac{1}{\big(N_e^{-1}(v) - N_e^{-1}(v+1)\big)^2} \\ &\quad \times \left(\frac{1}{n\big(N_e^{-1}(v+1)\big)} - \frac{1}{n\big(N_e^{-1}(v)\big)} \right) \\ &= \left[\frac{1}{N_e^{-1}(v) - N_e^{-1}(v+1)} \right]_0^1 = 0. \end{aligned} \tag{7.9}$$

This explicit demonstration trivially generalises to general N by including a summation over the contributions from each particle.

Now let us first consider the integral over $(-\infty, a_1)$. Again by changing the order of integration, we find

$$\int_{-\infty}^{a_1} \mathrm{d}x \, v_{\text{resp}}^{\text{SCE}}(x) = a_1 \, v(a_1) - \int_{-\infty}^{a_1} \mathrm{d}y \, \frac{y f'(y)}{\big(y - f(y)\big)^2}. \tag{7.10a}$$

The integral over (a_1, ∞) yields

$$\int_{a_1}^{\infty} \mathrm{d}x \, v_{\text{resp}}^{\text{SCE}}(x) = \int_{a_1}^{\infty} \mathrm{d}y \, \frac{y f'(y)}{\big(y - f(y)\big)^2} - a_1 \, v(a_1), \tag{7.10b}$$

so the full integral over the response function becomes

$$\int_{-\infty}^{\infty} \mathrm{d}x \, v_{\text{resp}}^{\text{SCE}}(x) = \left(\int_{a_1}^{\infty} \mathrm{d}y - \int_{-\infty}^{a_1} \mathrm{d}y \right) \frac{y f'(y)}{\big(y - f(y)\big)^2}. \tag{7.11a}$$

Now making the transformation $u = f(y)$, we obtain the following alternative expression

$$\int_{-\infty}^{\infty} \mathrm{d}x \, v_{\text{resp}}^{\text{SCE}}(x) = \left(\int_{-\infty}^{a_1} \mathrm{d}u - \int_{a_1}^{\infty} \mathrm{d}u \right) \frac{f(u)}{\big(f(u) - u\big)^2}. \tag{7.11b}$$

If we now take the average over 7.11a and 7.11b, we find again that the full integral

yields

$$\begin{aligned}\int_{-\infty}^{\infty}\mathrm{d}x\, v_{\mathrm{resp}}^{\mathrm{SCE}}(x) &= \frac{1}{2}\left(\int_{a_1}^{\infty}\mathrm{d}y - \int_{-\infty}^{a_1}\mathrm{d}y\right)\frac{yf'(y)-f(y)}{\big(y-f(y)\big)^2} = \\ &= \frac{1}{2}\left(\frac{y}{y-f(y)}\Big|_{a_1}^{\infty} - \frac{y}{y-f(y)}\Big|_{-\infty}^{a_1}\right) = 1. \end{aligned} \tag{7.12}$$

Arbitrary amount of electrons in 1D

As the number of electrons exceeds two, we deal with a set of co-motion functions. As we do not have $f = f^{-1}$ anymore, we need to find the inverses of each co-motion functions in 3.32. These are

$$f_i^{-1}(x) = \begin{cases} N_e^{-1}\big(N_e(x)-i\big) & \text{for } x < a_i \\ N_e^{-1}\big(N_e(x)-i+N\big) & \text{for } x > a_i \ , \end{cases} \tag{7.13}$$

where we see that, as expected, they are also co-motion functions, $f_i^{-1} = f_{N-i}$.

Now let us consider the general SCE response potential in 1D

$$v_{\mathrm{resp}}^{\mathrm{SCE}}(x) = \sum_{i=1}^{N-1}\Big(\theta(\bar{a}_i - x)\int_{-\infty}^{x}\mathrm{d}y + \theta(x-\bar{a}_i)\int_{x}^{\infty}\mathrm{d}y\Big)\frac{f_i'(y)}{\big(y-f_i(y)\big)^2}, \tag{7.14}$$

where the expression for $x > \bar{a}_i$ is again justified by 7.9 for each f_i.

By interchanging the integration again, the integral over the SCE response potential can be expressed as

$$\int_{-\infty}^{\infty}\mathrm{d}x\, v_{\mathrm{resp}}^{\mathrm{SCE}}(x) = \sum_{i=1}^{N-1}\left(\int_{\bar{a}_i}^{\infty}\mathrm{d}y - \int_{-\infty}^{\bar{a}_i}\mathrm{d}y\right)\frac{yf_i'(y)}{\big(y-f_i(y)\big)^2}. \tag{7.15a}$$

Making the variable transformation $u = f_i(y)$, we find

$$\begin{aligned}\int_{-\infty}^{\infty}\mathrm{d}x\, v_{\mathrm{resp}}^{\mathrm{SCE}}(x) &= \sum_{i=1}^{N-1}\left(\int_{-\infty}^{a_i}\mathrm{d}u - \int_{a_i}^{\infty}\mathrm{d}u\right)\frac{f_i^{-1}(u)}{\big(f_i^{-1}(u)-u\big)^2} \\ &= \sum_{i=1}^{N-1}\left(\int_{-\infty}^{\bar{a}_{N-i}}\mathrm{d}u - \int_{\bar{a}_{N-i}}^{\infty}\mathrm{d}u\right)\frac{f_{N-i}(u)}{\big(f_{N-i}(u)-u\big)^2}. \end{aligned} \tag{7.15b}$$

As the summation can be done in any order, we can combine it with the previous expression to find

$$\int_{-\infty}^{\infty}\mathrm{d}x\, v_{\mathrm{resp}}^{\mathrm{SCE}}(x) = \frac{1}{2}\sum_{i=1}^{N-1}\left(\int_{\bar{a}_i}^{\infty}\mathrm{d}y - \int_{-\infty}^{\bar{a}_i}\mathrm{d}y\right)\frac{yf_i'(y)-f_i(y)}{\big(y-f_i(y)\big)^2} = N-1, \tag{7.16}$$

which proves the interesting property that the integral over the SCE response potential for an N-electron 1D density (and Coulomb interaction) gives $N-1$.

7.2.2. Sum-rule of the SCE response potential for spherical two-electron densities

The differential equation for the response potential 7.1 in the spherical two-electron case is readily worked out as

$$\frac{\mathrm{d}}{\mathrm{d}r} v_{\mathrm{resp}}^{\mathrm{SCE}}(r) = \frac{f'(r)}{(r+f(r))^2}, \tag{7.17}$$

where $|\boldsymbol{r} - \mathbf{f}(\boldsymbol{r})| = r + f(r)$, since the electrons need to be situated opposite to each other with respect to the origin to minimise their repulsion. Using the standard gauge again, we have

$$v_{\mathrm{resp}}^{\mathrm{SCE}}(s) = -\int_s^\infty \mathrm{d}r \, \frac{\mathrm{d}}{\mathrm{d}r} v_{\mathrm{resp}}^{\mathrm{SCE}}(r). \tag{7.18}$$

We now evaluate the following integral over the response potential

$$\int_0^\infty \mathrm{d}s \, v_{\mathrm{resp}}^{\mathrm{SCE}}(s) = -\int_0^\infty \mathrm{d}r \, \frac{r f'(r)}{(r+f(r))^2}. \tag{7.19a}$$

Finally, as seen in the 1D case, via the usual transformation $u = f(r)$, we write equivalently the last expression in the above equations as

$$\int_0^\infty \mathrm{d}s \, v_{\mathrm{resp}}^{\mathrm{SCE}}(s) = \int_0^\infty \mathrm{d}u \, \frac{f(u)}{(u+f(u))^2}. \tag{7.19b}$$

By averaging between the two, one obtains that the integral over the positive real line of the SCE response potential for a spherical two-electron density gives

$$\int_0^\infty \mathrm{d}r \, v_{\mathrm{resp}}^{\mathrm{SCE}}(r) = \frac{1}{2}\int_0^\infty \mathrm{d}u \, \frac{f(u) - u f'(u)}{(u+f(u))^2} = \frac{1}{2}. \tag{7.20}$$

7.3. Concluding remarks

We have analyzed the SCE response potential and shown that it satisfies a simple sum rule in the one-dimensional and in the $N = 2$ spherically symmetric case. This latter case might be a special one, as it is mathematically equivalent to a 1D case, thus requiring further investigation for a generalisation to 3D systems. Additional investigations are also required whether the sum-rules could also be established for the physical interacting system, either with or without the kinetic part of the response potential.

8

Kinetic energy density–density functional theory

The contents presented in this chapter are a collection of preliminary results and thoughts that represent a follow-up study – in collaboration with I. Theophilou, M. Ruggenthaler, N.Lathiotakis, A. Rubio – on a first investigation in the discrete case [275]. Many of the ideas shared here are still quite unsettled and we do not exclude that some fundamental aspects might have been overlooked. Nonetheless, we decided to include such contents in this thesis work as we believe that they still raise some interesting points and provide some hints for future directions.

The motivation for this work stems from the consideration that the design of approximate density functionals that can correctly account for the kinetic contribution missed by the KS kinetic energy functional is somehow missing from the Density Functional Theory literature.[1]
In practice, the way in which the kinetic correlation contribution is typically tackled is via integration over the adiabatic connection.
It is little debatable that the availability of an *explicit* functional of the kinetic energy in one-body reduced density matrix (1RDM) functional theory [276] represents one of the most striking (theoretical) advantages of such theory over DFT.
In chapters 2 and 6, we have touched upon certain features of the XC potential emerging in the case of a dissociating molecule that have a kinetic origin.
In particular, we remind here that these contributions can be energetically negligeable, for example: in a dissociating Hydrogen molecule the correlation kinetic

[1] Or at least, we are not aware of any work where this contribution has been modelled *per se*.

energy contribution is vanishing or in a heteronuclear molecule, the rising of the step structure comes from the response component which does not enter directly in the computation of the XC energy. Nevertheless, their occurrence inside the KS potential is crucial to have the density converge to correctly separated fragments upon dissociation, preventing unphysical fractional distribution of electron charge between the fragments.

Here, we ask ourselves whether it is possible to facilitate the modelling of the kinetic correlation contribution in approximate functionals, by introducing a position-dependent mass to which the kinetic energy density, τ, is associated. In such a way, the functionals of interest become not only density functionals but bifunctionals of the density and of the kinetic energy density, $F[n,\tau]$.
The invocation of a position-dependent mass of the particles in quantum mechanics is not at all new and there is a vast related literature in several different fields (see e.g. reference [277] and references therein). Recently, a position-dependent mass has been argued to appear naturally in the context of thermal DFT [278].
In the present context, schematically, we explore the possibility of the mapping

$$\underbrace{\Big\{v(\boldsymbol{r}),\ m(\boldsymbol{r})\Big\}}_{\text{external quantities}} \longleftrightarrow \underbrace{\Big\{n(\boldsymbol{r}),\ \tau(\boldsymbol{r})\Big\}}_{\text{internal quantities}} \tag{8.1}$$

between the pair *density-kinetic energy density* as "internal" quantities and that of *external potential-position dependent mass* as "external" quantities. In other words we would like to build a kinetic energy density-density functional theory (keDFT). However, whether a theorem analogous to the Hohenberg-Kohn one for such a mapping can be established is not clear at the state of the art.
Moreover, aiming for connecting the interacting system to a fictitious non-interacting system in the Kohn-Sham spirit (keKS), in addition to a proof of 8.1 ("$\{v,m\}$-representability of the pair $\{n,\tau\}$"), we also need to have a non-interacting system delivering the same pair of internal quantities as the interacting one, by means of a different pair of external quantities, namely an effective potential v^{ke} and an effective mass m^{ke}. In summary, we require the two bijective mappings between pairs

$$\Big\{v(\boldsymbol{r}),\ m(\boldsymbol{r})\Big\} \longleftrightarrow \Big\{n(\boldsymbol{r}),\ \tau(\boldsymbol{r})\Big\} \longleftrightarrow \Big\{v^{ke}(\boldsymbol{r}), m^{ke}(\boldsymbol{r})\Big\}. \tag{8.2}$$

We signal at this point that the use of meta-GGA functionals [123, 279, 280], within the generalised Kohn-Sham approach (GKS) [281], is closely interlaced with the feasibility of the mapping 8.2.
For example, it has been argued [282] that the GKS method for solving SCF equations containing a meta-GGA functional can be physically interpreted as introducing a position-dependent mass in the kinetic energy operator and that, to first order in the *density*, there is no difference in going from the local KS Hamiltonian (OEP method [33]) to the GKS one. However, the discussion on the subject is far

from settled, and many implicit assumptions (see e.g. reference [283]) – onto which the increasingly popular use of meta-GGA density functionals relies – still need to be addressed and, hopefully, understood.

8.1. Fundamental challenges

Like any energy density, also the kinetic energy density is not a uniquely defined quantity. Therefore the first step in the direction of constructing a kinetic energy density-density functional theory is to decide which gauge we want to consider.

The most common definition of kinetic energy density is the positive definite expression

$$\tau^P(\boldsymbol{r}) \coloneqq \frac{N}{2\,m(\boldsymbol{r})} \sum_\sigma \int |\nabla_{\boldsymbol{r}} \Psi(\boldsymbol{r}\sigma, \cdots, \boldsymbol{x}_N)|^2 \,\mathrm{d}\boldsymbol{r}_2 \cdots \mathrm{d}\boldsymbol{r}_N \tag{8.3}$$

where $m(\boldsymbol{r})$ is just the unit constant if we are dealing with the interacting system. Equation 8.3, within the assumption that the ground state wavefunction be real (aside from a trivial phase factor), can be rewritten as

$$\begin{aligned} \tau^P(\boldsymbol{r}) &= \frac{N}{8\,m(\boldsymbol{r})} \sum_\sigma \int \frac{\left(\nabla_{\boldsymbol{r}} |\Psi(\boldsymbol{r}\sigma, \cdots, \boldsymbol{x}_N)|^2\right)^2}{|\Psi(\boldsymbol{r}\sigma, \cdots, \boldsymbol{x}_N)|^2} \,\mathrm{d}\boldsymbol{r}_2 \cdots \mathrm{d}\boldsymbol{r}_N \\ &= \frac{N}{8\,m(\boldsymbol{r})} \sum_\sigma \int \nabla_{\boldsymbol{r}} \mathrm{D}(\boldsymbol{r}\sigma, \cdots, \boldsymbol{x}_N) \cdot \nabla_{\boldsymbol{r}} \log \mathrm{D}(\boldsymbol{r}\sigma, \cdots, \boldsymbol{x}_N) \,\mathrm{d}\boldsymbol{r}_2 \cdots \mathrm{d}\boldsymbol{r}_N \end{aligned} \tag{8.4}$$

with $\mathrm{D}(\boldsymbol{r}\sigma, \cdots, \boldsymbol{x}_N) \coloneqq |\Psi(\boldsymbol{r}\sigma, \cdots, \boldsymbol{x}_N)|^2$ and can be interpreted as a measure of information in the context of information theory (see for example refs [284, 285]).

The other common expression is the one with the Laplacian operator. However, while in the usual case the placement of the mass w.r.t. the nabla operator is irrelevant, here we have two possible definitions, namely

$$\tau^{L1}(\boldsymbol{r}) = -\frac{N}{2\,m(\boldsymbol{r})} \sum_\sigma \int \Psi^*(\boldsymbol{r}\sigma, \cdots, \boldsymbol{x}_N) \nabla^2_{\boldsymbol{r}} \Psi(\boldsymbol{r}\sigma, \cdots, \boldsymbol{x}_N) \,\mathrm{d}\boldsymbol{r}_2 \cdots \mathrm{d}\boldsymbol{r}_N \tag{8.5}$$

and

$$\tau^{L2}(\boldsymbol{r}) = -\frac{N}{2} \sum_\sigma \int \Psi^*(\boldsymbol{r}\sigma, \cdots, \boldsymbol{x}_N) \nabla_{\boldsymbol{r}} \cdot \frac{1}{m(\boldsymbol{r})} \nabla_{\boldsymbol{r}} \Psi(\boldsymbol{r}\sigma, \cdots, \boldsymbol{x}_N) \,\mathrm{d}\boldsymbol{r}_2 \cdots \mathrm{d}\boldsymbol{r}_N. \tag{8.6}$$

In the present work, we will only consider mostly the kinetic energy density τ^P, for its aforementioned properties, and sometimes the definitions τ^{L1} and τ^{L2}(mainly for comparison purposes). Of course, infinitely many other kinetic energy density definitions are possible. Furthermore, it must be noted that the inclusion of a position-dependent mass increases the amount of possible expressions of the kinetic

energy operator itself.[2] Here, we will only consider the generalized Sturm-Liouville operator

$$\hat{t}_m(\boldsymbol{r}) = -\frac{1}{2}\nabla\frac{1}{m(\boldsymbol{r})}\nabla. \tag{8.9}$$

and $\hat{T}_m = \sum_i^N \hat{t}_m(\boldsymbol{r}_i)$.

In order to construct a kinetic energy density-density functional theory resorting to a fictitious non-interacting system, we need to circumvent the obstacle that the interacting and the non-interacting one-body reduced density matrices cannot be trivially made equal. We have explored three ways of doing so, namely

1. abandon the usual linear setting and impose *a priori* that the non-interacting system satisfy KS-like equations (8.10) including the position-dependent mass in the expressions which we want to equalize (eq 8.12). In other words, the position-dependent mass is *not* a local Lagrange multiplier enforcing the constraint that the kinetic energy density of the target and that of the auxiliary system match;

2. adhere to the usual linear setting in which the position-dependent mass is introduced as a local Lagrange multiplier. Namely, instead of requiring eq 8.12, we require eq 8.34. With this latter condition, we are forced to introduce another degree of freedom such that the two kinetic energy densities of the interacting and of the non-interacting systems can still be made equal. We do so by adopting a non-trivial position-dependent phase factor in the orbitals of the non-interacting system (the same for all orbitals).

3. borrowing the strategy from Generalised-Kohn-Sham theory [281], freely minimise a modified kinetic energy functional $T_{\mathfrak{v}}$ coming from a non-local energy operator $\hat{T}_{\mathfrak{v}}$ formally identical to expression 8.9 but where the scalar potential $\mathfrak{v}$ is fixed not by imposing a constraint on the resulting non-interacting kinetic energy density as in the former two settings (eqs 8.12 and 8.34) but by imposing a condition on the remainder functional $R^{T_{\mathfrak{v}}}$ (eq 8.57).

8

[2] For instance, an entire family of kinetic energy operators has been suggested by O. von Roos [286] which are still Hermitian under quite general assumptions, namely

$$\hat{\mathfrak{t}}[m] := -\frac{1}{4}\left(m^\alpha\nabla m^\beta\nabla m^\gamma + m^\gamma\nabla m^\beta\nabla m^\alpha\right) \tag{8.7}$$

where $m = m(\boldsymbol{r})$ and the constants α, β, γ are constrained to satisfy

$$\alpha + \beta + \gamma = -1 \tag{8.8}$$

but are otherwise arbitrary. As discussed in the main text, we limit ourselves to the choice $\alpha = \gamma = 0$ and $\beta = -1$.

8.2. Discussion of different settings

For each of the different settings listed above, we present numerical results obtained for the first few terms of the Hooke's atom series [287] briefly reviewed in appendix C, as well as for the species H^- and He using the correlated wavefunctions of reference [264]. In the next subsections, to distinguish among the different settings, we will relabel the quantities $\{v^{ke}, m^{ke}\}$ as $\{v^{nl}, m^{nl}\}$, $\{v^{l}, m^{l}\}$ and $\{v^{mGKS}, m^{mGKS}\}$ respectively. Accordingly, the orbitals of the different kinds of non-interacting systems, generally identified with ψ_i^{ke} to distinguish them from the usual KS ones, will be relabeled as ψ_i^{nl}, ψ_i^{l} and ψ_i^{mGKS}.

8.2.1. Non-linear setting

By construction, our master equations in this setting are

$$\left(-\frac{1}{2}\nabla\cdot\left(\frac{1}{m^{nl}}\nabla\right)+v^{nl}\right)(\mathbf{r})\psi_i^{nl}(\mathbf{x})=\epsilon_i^{nl}\psi_i^{nl}(\mathbf{x}) \tag{8.10}$$

with the constraints

$$n_{\text{int}}(\mathbf{r})=\sum_{i,\sigma}|\psi_i^{nl}|^2(\boldsymbol{r}) \tag{8.11}$$

and

$$\tau^P_{\text{int}}(\boldsymbol{r})=\left(\frac{1}{2\,m^{nl}}\sum_{i,\sigma}\left|\nabla\psi_i^{nl}\right|^2\right)(\boldsymbol{r}) \tag{8.12}$$

where n_{int} is the electron density and τ^P_{int} the kinetic energy density (in the gauge 8.3) of the interacting system, which we want to target.

Bounds on m^{nl}

We see that, from our use of positive definite quantities, we immediately have $m^{nl}\geq 0$. For the upper bound, given eq 8.12, it would then be sufficient to prove that the interacting kinetic energy density is everywhere greater or equal than the non interacting kinetic energy density *without* the inclusion of the mass, i.e. that

$$\tau^P_{\text{int}}(\boldsymbol{r})\geq\left(\frac{1}{2}\sum_{i,\sigma}\left|\nabla\psi_i^{nl}\right|^2\right)(\boldsymbol{r}) \tag{8.13}$$

to conclude that $0\leq m^{nl}\leq 1$.

Currently, we are able to show that $0\leq m^{nl}\leq 1$ only for two-electron singlet systems. In these systems, from requiring the interacting and the non-interacting densities to be the same, namely

$$\psi^{nl}(\boldsymbol{r})=\sqrt{\frac{n(\boldsymbol{r})}{2}}, \tag{8.14}$$

with $\psi^{nl}(\boldsymbol{r}) = \sum_\sigma \psi^{nl}(\boldsymbol{x})$, we have that the non-interacting kinetic energy density corresponds to the Von Weizsäcker kinetic energy density, τ^P_{VW}, in the same gauge

$$\tau^P_{VW}(\boldsymbol{r}) = \frac{|\nabla n|^2}{8\,n}(\boldsymbol{r}). \tag{8.15}$$

The Von Weizsäcker kinetic energy density τ^P_{VW} is however proven to be a lower bound to any kinetic energy density coming from a wavefunction associated to the same density, i.e.

$$\tau^P_{VW}[n](\boldsymbol{r}) \leq \frac{N}{2}\sum_\sigma \int |\nabla \Psi_n(\boldsymbol{x}, \boldsymbol{x}_2, \cdots, \boldsymbol{x}_N)|^2 \mathrm{d}\boldsymbol{r}_2 \cdots \mathrm{d}\boldsymbol{r}_N \tag{8.16}$$

by means of the Cauchy-Schwarz inequality [288]. Nonetheless, it is quite easy to show that asymptotically the position-dependent mass in this setting goes like the unit constant,[3] by means of the Dyson orbitals, d_i.
These are defined as

$$d_i(\mathbf{x}) = \sqrt{N}\int \Psi^{N-1}_i(2,\ldots,N)^* \Psi^N_0(\mathbf{x}, \boldsymbol{x}_2, \cdots, \boldsymbol{x}_N)\mathrm{d}\boldsymbol{x}_2 \cdots \mathrm{d}\boldsymbol{x}_N, \tag{8.17}$$

and allow the following exact expansion of the GS wavefunction

$$\Psi^N_0(\mathbf{x}, \boldsymbol{x}_2, \cdots, \boldsymbol{x}_N) = N^{-1/2}\sum_{i=0}^{\infty} d_i(\mathbf{x})\Psi^{N-1}_i(\boldsymbol{x}_2, \cdots, \boldsymbol{x}_N). \tag{8.18}$$

Given 8.18, we can rewrite τ^P_{int} as

$$\tau^P_{\text{int}}[n](\boldsymbol{r}) = \sum_i^\infty \left(\sum_\sigma |\nabla d_i|^2\right)(\boldsymbol{r}) \tag{8.19}$$

and, consequently

$$m^{nl}(\boldsymbol{r}) = \left(\sum_\sigma \frac{\sum_i^N \left|\nabla \psi^{nl}_i\right|^2}{\sum_i^\infty |\nabla d_i|^2}\right)(\boldsymbol{r}). \tag{8.20}$$

On the other hand, it is true that both the N-electron sum over the modulus squared of the orbitals ψ^{nl}_i and the infinite sum over the modulus squared of the Dyson orbitals deliver the interacting density

$$n(\boldsymbol{r}) \equiv \left(\sum_i^N \sum_\sigma \left|\psi^{nl}_i\right|^2\right)(\boldsymbol{r}) \equiv \left(\sum_i^\infty \sum_\sigma |d_i|^2\right)(\boldsymbol{r}). \tag{8.21}$$

As extensively discussed in chapter 2, in regular KS theory the decay of each KS orbital is governed by its respective eigenvalue which dictates that the most diffuse

[3] In principle, there is no reason why the asymptotic value of m^{nl} should also be its maximum value.

orbital is the one with the smallest eigenvalue (the HOMO). Although the keKS equations are endowed with different structure (eq 8.10), yet necessarily the most diffuse of the keKS orbitals, "ψ_H^{nl}", will bear by construction the correct asymptotic behaviour, i.e. $\psi_H^{nl}(|\boldsymbol{r}| \to \infty) \sim n^{1/2}(|\boldsymbol{r}| \to \infty)$. A similar reasoning holds for the set of Dyson orbitals: in this case it is the first Dyson orbital that inherits the asymptotic behaviour of the square root of density, i.e. $d_0(|\mathbf{r}| \longrightarrow \infty) \sim n^{1/2}(|\mathbf{r}| \longrightarrow \infty)$ [289] and we conclude that

$$m^{nl}(|\boldsymbol{r}| \to \infty) \sim \frac{|\nabla \psi_H^{nl}|^2}{|\nabla d_0|^2} \sim 1. \tag{8.22}$$

Examples of v^{nl} and m^{nl} for two-electron singlet systems

We are again focusing on two-electron singlet systems, which allow for an explicit construction of the quantities of interest, v^{nl} and m^{nl}, without the need of a numerical inversion algorithm.

In practice, from the constraint of the density (eq 8.14), we have that

$$m^{nl} = \frac{|\nabla n|^2}{8\, n\, \tau_{\text{int}}^P} \tag{8.23}$$

and

$$v^{nl} = \frac{1}{2\sqrt{n}} \left(\nabla \left(\frac{1}{m^{nl}} \right) \cdot \nabla \sqrt{n} + \frac{1}{m^{nl}} \nabla^2 \sqrt{n} \right) - I_p. \tag{8.24}$$

We start by applying eqs 8.23 and 8.24 on the Hooke's atom series [287], an exactly solvable model briefly reviewed in appendix C. In fig 8.1 we show the analytical mass potentials, m^{nl}, corresponding to n = 2,…, N, where n is roughly speaking a measure of increasing correlation and is related to the degree of the polynomial involved in the exact solution expression (see appendix).

From eq 8.23 and given that τ_{int}^P and n at the denominator are well-behaved functions vanishing only asymptotically, it is clear that the mass will become zero whenever the density shows a minimum or a maximum. Thus we see that up to n = 3, m^{nl} is zero only at the origin, while for the more correlated ones, n = 4,5,6, there is also some positive distance, r_c, at which again these potentials become zero. This is related to the "cusp catastrophe" (discussed in appendix C), i.e. the fact that for n > 4 the density is minimum at the origin and maximum in r_c (see fig C.1 for the density profiles). In fig 8.2, we plot the corresponding Hartree-XC potential (we subtract the external potential as it diverges like r^2). It is found that for the n ⩽ 3 cases there is a divergence to $-\infty$ at the origin; while for the cases n ⩾ 4 there are two divergences, at the origin and at r_c, both to $+\infty$. We expect that the keKS mass and potential of a Hydrogen molecule will face a problem very similar to what we observe in the Hooke's atom for the cases $n \geqslant 4$, as the density will be minimum at the midbond, leading to a zero kinetic-energy density at this position

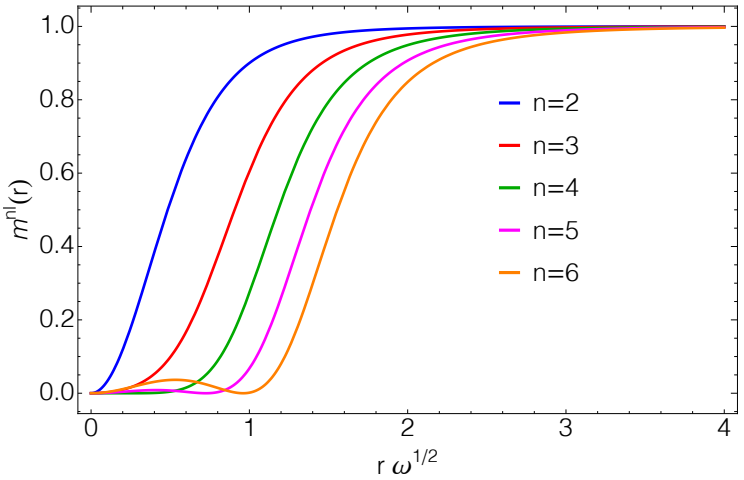

Figure 8.1: Scaled mass potentials, $m^{nl}(r)$, for the Hooke's atom series with n = 2,...,N.

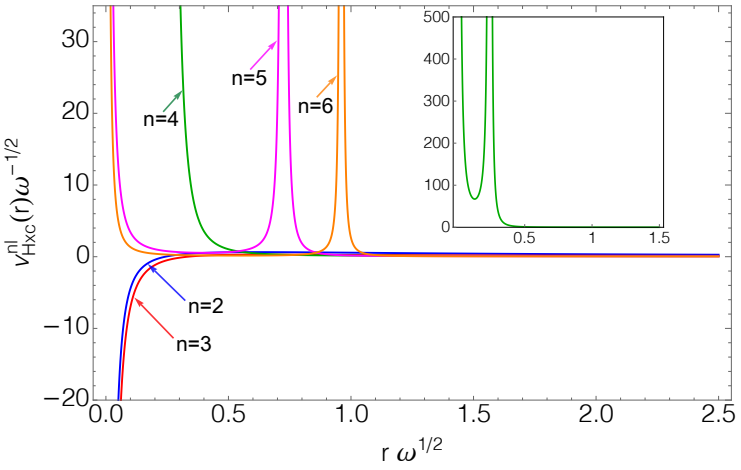

Figure 8.2: Scaled Hartree-XC keKS potential, v^{nl}_{Hxc}, for the Hooke's atom series with n = 2,...,N.

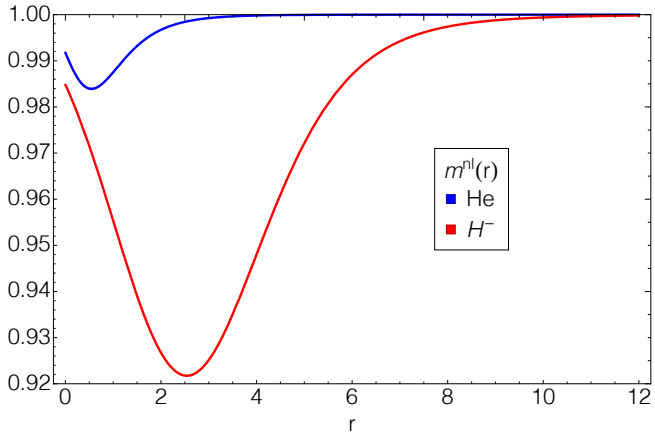

Figure 8.3: Mass potentials, $m^{nl}(r)$, for the species H^- and He.

and resulting in a divergence in the potential. As discussed in sec 2.2.1, the profile of the kinetic potential shows that the circumstance in which the reference electron crosses the midbond region corresponds to the maximum "speed" of rearrangement of the conditional amplitude (location of the peak). In this sense, finding the effective position-dependent mass to be smaller in this region is sensible, however we would like it to be not exactly zero. Note that an increasing number of occupied orbitals is expected to make the occurrence of zeros in the kinetic-energy density less likely.

In fig 8.3, we plot the keKS mass potential for the species H^- and He, where the interacting kinetic energy density has been calculated numerically using the very accurate wavefunction of reference [264]. We observe that the mass is not going to one at the nucleus. This is in agreement with the results shown in reference [290] where an expansion for the interacting and the non-interacting kinetic energy density at the nucleus is derived. Using such expansion, to first-order, the position-dependent mass introduced in eq 8.12, for a two-electron singlet system, can be written as

$$m^{nl}(|\mathbf{r}| \to 0) \sim \frac{Z^2 n(0)}{Z^2 n(0) + E_{ii}} \tag{8.25}$$

where Z is the nuclear charge and E_{ii} is a positive value defined as

$$E_{ii} = 3N \int \frac{|a_{1m}|^2}{4\pi} \mathrm{d}\mathbf{X}. \tag{8.26}$$

In eq 8.26, "$\mathbf{X}$" are the spatial-spin coordinates of the remaining $N-1$ electrons and the spin coordinate of the reference electron: $\mathbf{X} = (\sigma, \boldsymbol{x}_2, \cdots, \boldsymbol{x}_N)$, the reference

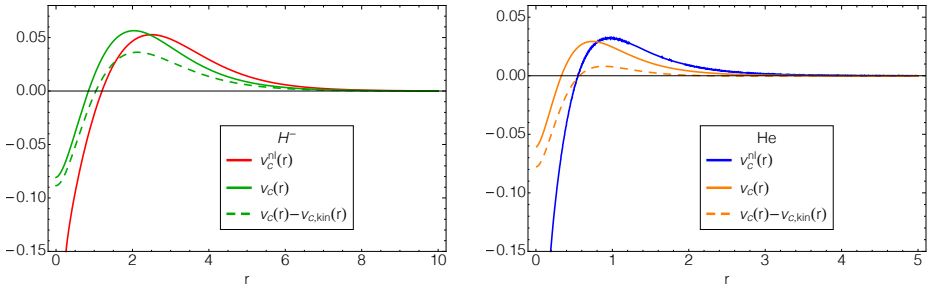

Figure 8.4: Comparison between the quantities v_c^{nl}, v_c and $v_c - v_{c,kin}$ for the Hydrogen anion (left) and the Helium atom (right).

electron is located very close to the nucleus and a_{1m} is a coefficient coming from the expansion of the interacting wavefunction into spherical harmonics

$$\begin{aligned}\Psi(\mathbf{r},\mathbf{X}) &= \Psi(0,\mathbf{X}) + a(\mathbf{X})r + b(\mathbf{X})r^2 + \cdots \\ &\quad + \sum_{m=-1}^{1}\left(a_{1m}(\mathbf{X})r + b_{1m}(\mathbf{X})r^2\right)Y_{1m}(\hat{r}) + \cdots \end{aligned} \tag{8.27}$$

The fact that the mass be not zero at the nucleus, placed at the origin, affects the value of the effective potential v_{Hxc}^{nl} in the following way. At zero the usual kinetic term $-\frac{\nabla^2\sqrt{n}}{2\sqrt{n}}$ exactly cancels the external potential $-\frac{Z}{r}$. Decreasing the usual kinetic term by a factor $\frac{1}{m^{nl}(0)}$ leaves a fraction of the external potential unbalanced, leading to the divergent behaviour around the origin

$$v_{Hxc}^{nl}(|\mathbf{r}|\to 0) \sim \left(1 - \frac{1}{m^{nl}(0)}\right)\frac{Z}{r}. \tag{8.28}$$

This is observed in fig 8.4 where we show the correlation contribution of the keKS potential in this setting, v_c^{nl},[4] for the Hydrogen anion and the Helium atom, in comparison with the correlation contribution of the usual KS potential, v_c, as well as this latter depleted of the kinetic potential term, $v_c - v_{c,kin} = v_{c\text{-}hole} + v^{resp}$.

Discussion on v^{nl} and m^{nl} in the Laplacian gauge

Finally, let us remark that using definition 8.5 in this setting, we obtain

$$m^{nl,L1} = \frac{\sum_{i,\sigma}\psi_i^*\nabla^2\psi_i}{N\int\Psi^*(\boldsymbol{r}\sigma,\cdots,\boldsymbol{x}_N)\nabla^2\Psi(\boldsymbol{r}\sigma,\cdots,\boldsymbol{x}_N)}. \tag{8.29}$$

[4] Assuming that the role of the exchange contribution in this framework is also that of simply canceling the self interaction error for a two-electron singlet state, i.e. $v_x^{nl} = v_x = -\frac{v_H}{2}$.

where here $\psi_i = \psi_i^{nl,L1}$. The denominator of the r.h.s. of equation 8.29 is expected to go to zero at least once for quite general wavefunctions and therefore to produce divergences in the corresponding mass. As an example, for two electron systems with real ground state wavefunctions (such as those studied)

$$\tau_{\text{int}}^{L1} = -\frac{1}{2}\sqrt{n}\nabla^2\sqrt{n} + v_{kin}n \tag{8.30}$$

then

$$m^{nl,L1} = \frac{\sqrt{n}\nabla^2\sqrt{n}}{\sqrt{n}\nabla^2\sqrt{n} - 2\,v_{kin}n} = \frac{\nabla^2 n - \frac{(\nabla n)^2}{2n}}{\nabla^2 n - \frac{(\nabla n)^2}{2n} - 4\,v_{kin}n} \tag{8.31}$$

Therefore, for any value of $\boldsymbol{r}$ for which $v_{kin} \equiv \frac{\nabla^2 n}{4n} - \frac{(\nabla n)^2}{8n}$, the mass will show a divergence. Such divergence(s) is (are) reflected on the potential in the form of infinite negative well(s).

Moreover, because in the singlet case eq 8.29 also translates to

$$m^{nl,L1} = \frac{\left(v_s - I_p\right)}{\left(v_s - I_p\right) - v_{kin}}, \tag{8.32}$$

the potential, $v^{nl,L1}$, becomes

$$\begin{aligned} v^{nl,L1} &= \frac{\nabla^2\sqrt{n}}{2\,m^{nl,L1}\sqrt{n}} + \frac{\nabla\sqrt{n}\cdot\nabla(m^{nl,L1})^{-1}}{2\sqrt{n}} + I_p \\ &= (v_s - v_{kin}) + \frac{\nabla\sqrt{n}\cdot\nabla(m^{nl,L1})^{-1}}{2\sqrt{n}} \end{aligned} \tag{8.33}$$

and the effective potential differs from the usual KS potential depleted of the (correlation) kinetic contribution, $v_s - v_{kin}$, by the term $\frac{\nabla\sqrt{n}\cdot\nabla(m^{nl,L1})^{-1}}{2\sqrt{n}}$. In fig 8.5 we show the masses, $m^{nl,L1}$, and the corresponding correlation potentials, $v^{nl,L1}$ in comparison with the usual correlation potential v_c and the term $v_c - v_{kin}$ (right) for three illustrative species: Hooke's atom with n = 2 and n = 6 and the Hydrogen anion. In the first two cases, it is apparent that the term $\frac{\nabla\sqrt{n}\cdot\nabla(m^{nl,L1})^{-1}}{2\sqrt{n}}$ is generally very small, excluding where it diverges.

Concerning the use of definition 8.6, we postpone its discussion to section 8.2.3 for reasons that will be clear later.

8.2.2. Linear setting

In the linear setting, we modify the requirement of the non-interacting system kinetic energy density to

$$\tau_{\text{int}}^{P}(\boldsymbol{r}) = \left(\frac{1}{2}\sum_{i,\sigma}\left|\nabla\psi_i^l\right|^2\right)(\boldsymbol{r}). \tag{8.34}$$

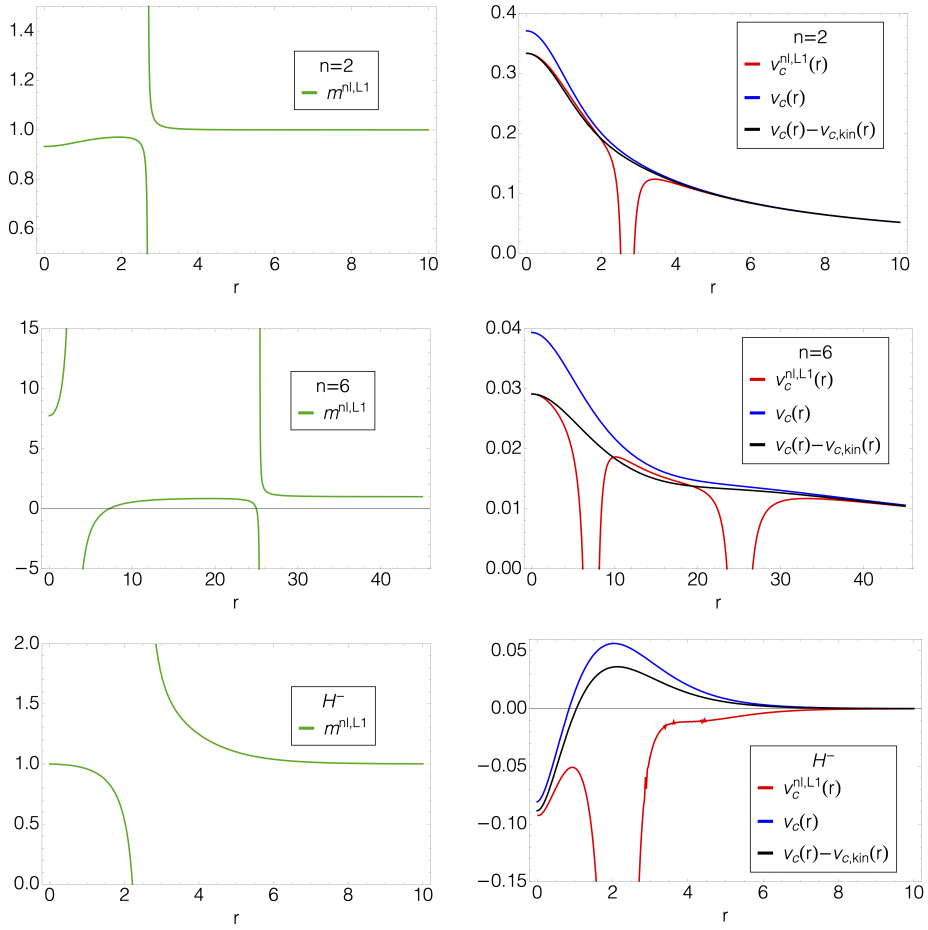

Figure 8.5: Position dependent masses in the gauge of eq 8.5, $m^{nl,L1}$ (left), and corresponding correlation potentials, $v^{nl,L1}$ in comparison with the usual correlation potential v_c and this latter term depleted of the kinetic contribution, $v_c - v_{kin}$ (right) for three species: Hooke's atom with n = 2 and n = 6 and the Hydrogen anion.

Equipped with 8.34, we construct a Lagrangian expression similar to that of sec 1.3.1 but where the constraints on the density and on the kinetic energy density are simultaneously imposed. Aiming for a non-interacting description, we are left with no energy expression to minimise. Therefore we look for the stationarity equations of a zero-Hamiltonian and consider the Lagrangian made of the constraints only

$$\begin{aligned} L_{n,\tau^P} &= -\sum_{i,j}^{N} \tilde{\epsilon}_{ij}\left(\langle\tilde{\psi}_i^l|\tilde{\psi}_j^l\rangle - \delta_{ij}\right) + \int \mathrm{d}\mathbf{r}\, \tilde{v}^l(\mathbf{r})\left(\sum_{i,\sigma}|\tilde{\psi}_i^l|^2 - n\right)(\mathbf{r}) \\ &\quad + \int \mathrm{d}\mathbf{r}\, \tilde{v}_m^l(\mathbf{r})\left(\frac{\sum_{i,\sigma}|\nabla\tilde{\psi}_i^l|^2}{2} - \tau_{\text{int}}^P\right)(\mathbf{r}). \end{aligned} \tag{8.35}$$

whose minimisation gives

$$\left(-\frac{1}{2}\nabla\cdot\left(v_m^l\nabla\right) + v^l\right)(\mathbf{r})\,\psi_i^l(\boldsymbol{x}) = \epsilon_i^l\psi_i^l(\boldsymbol{x}), \tag{8.36}$$

where, upon substituting $v_m^l = \left(m^l\right)^{-1}$, we are left with self-consistent equations that are structurally identical to those considered in the non-linear setting (eq 8.10). The fundamental difference is that now the orbitals have a non-trivial imaginary phase and can be decomposed as

$$\psi_i^l(\boldsymbol{x}) = R_i(\boldsymbol{x})e^{i\theta(\boldsymbol{r})}. \tag{8.37}$$

Therefore eq 8.36 can be separated into its real and imaginary parts[5]

$$\left(-\frac{1}{2}\nabla\cdot\left(v_m^l\nabla\right) + v^l + \frac{|\nabla\theta|^2}{2\,m^l}\right)(\boldsymbol{r})\,R_i(\boldsymbol{x}) = \epsilon_i^l R_i(\boldsymbol{x}) \tag{8.40}$$

$$\left(-\frac{1}{2}\nabla\cdot\left(v_m^l\nabla\right) - \frac{\nabla\ln\left(\sum_\sigma R_i\right)}{m^l}\cdot\nabla\right)(\boldsymbol{r})\,\theta(\boldsymbol{r}) = 0. \tag{8.41}$$

8

Examples of v^l and m^l for two-electron singlet systems

For two-electron singlet systems, the constraint on the density here gives

$$\psi^l(\boldsymbol{r}) = \sum_\sigma \psi^l(\boldsymbol{x}) = \sqrt{\frac{n(\boldsymbol{r})}{2}}\, e^{i\theta(\boldsymbol{r})} \tag{8.42}$$

[5] by working out

$$\nabla\psi_i^l(\boldsymbol{r}) = e^{i\theta(\boldsymbol{r})}\left(\nabla R_i + i\,R_i\nabla\theta\right)(\boldsymbol{r}) \tag{8.38}$$

$$\nabla^2\psi_i^l(\boldsymbol{r}) = e^{i\theta(\boldsymbol{r})}\left(\nabla^2 R_i - R_i|\nabla\theta|^2 + 2\,i\,\nabla R_i\cdot\nabla\theta + i R_i\nabla^2\theta\right)(\boldsymbol{r}) \tag{8.39}$$

with $\psi_i^l(\boldsymbol{r}) = \sum_\sigma \psi_i^l(\boldsymbol{x})$ and $R_i^l(\boldsymbol{r}) = \sum_\sigma R_i^l(\boldsymbol{x})$.

and we can rewrite eqs 8.34, 8.40 and 8.41 as

$$\begin{cases} \tau^P_{\text{int}} = \frac{|\nabla n|^2}{8n} + \frac{n}{2}|\nabla\theta|^2 \\ \left(-\frac{1}{2}\nabla\cdot\left(\frac{1}{m^l}\nabla\right) + \frac{|\nabla\theta|^2}{2m^l} + (v^l - \epsilon)\right)\sqrt{n} = 0 \\ \left(-\frac{1}{2}\nabla\cdot\left(\frac{1}{m^l}\nabla\right) - \frac{\nabla\ln(\sqrt{n})}{m^l}\cdot\nabla\right)\theta = 0 \end{cases} \tag{8.43}$$

For spherical systems, the set of eqs 8.43, has the following analytical solutions

$$\begin{cases} \theta(r) = \int_0^\infty \sqrt{2\,v_{kin}(r)}\,\mathrm{d}r + c \qquad \text{with} \quad v_{kin} = \frac{1}{n}\left(\tau^P_{\text{int}} - \frac{n'^2}{8n}\right) \\ m^l(r) = \tilde{c}\,r^2\theta'(r)n(r) \\ v^l(r) = \frac{1}{4\,m^l(r)n(r)}\left(n''(r) + \frac{2}{r}n'(r) - \frac{n'^2(r)}{2\,n(r)} - \frac{m^{l\prime}(r)\,n'(r)}{m^l(r)} - 2\theta'(r)^2 n(r)\right) + \epsilon \end{cases} \tag{8.44}$$

where we have picked $c = 0$ and $\tilde{c} = 1$. We show the resulting quantities $\theta(r)$, $m^l(r)$ and $v^l(r)$ for the Hooke's atom series in figures 8.6, 8.7 and 8.8 and for the Hydrogen anion and Helium atom in figures 8.9, 8.10 and 8.11.

It is remarkable that by means of a position-dependent phase, $\theta(r)$, which looks simple and well-behaved in all cases studied, we can straightforwardly equalize the interacting and the non-interacting kinetic energy densities while still preserving the density constraint. Nonetheless, it is uncertain how to interpret the profile of the position-dependent mass, $m^l(r)$, and that of the effective potential, $v^l(r)$: what we observe is that both Lagrange multipliers v^l_m and v^l diverge at the boundaries of the domain.

As a final remark, we observe that the two position-dependent masses, m^{nl} and m^l (in the non-linear and in the linear settings) for spherical systems are simply related to one another

$$m^{nl}(r) = \frac{r^4\,n'^2(r)}{4\,(m^l(r))^2 + r^4\,n'^2(r)} \tag{8.45}$$

since both their expressions involve the kinetic potential v_{kin} which might then be expressed as

$$v_{kin}(r) = \frac{(m^l(r))^2}{2\,r^4 n^2(r)} = \frac{n'^2}{8\,n^2}(r)\left(\frac{1}{m^{nl}(r)} - 1\right). \tag{8.46}$$

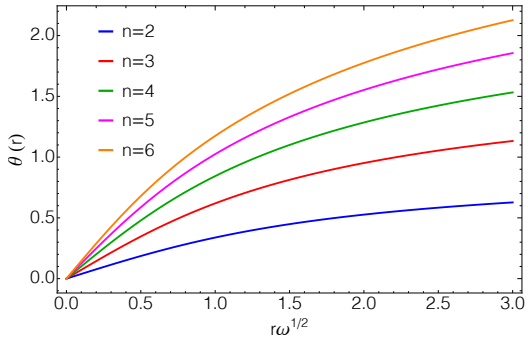

Figure 8.6: Non-trivial phase factor, $\theta(r)$, for the Hooke's atom series with $n = 2,\ldots,N$

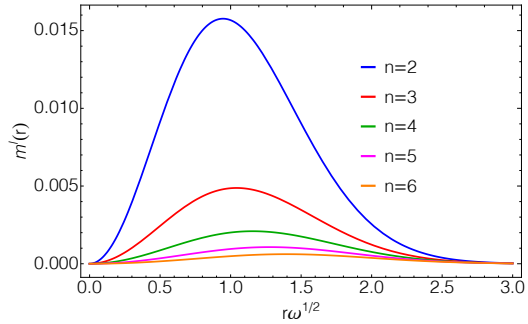

Figure 8.7: Mass potentials, $m^l(r)$, for the Hooke's atom series with $n = 2,\ldots,N$.

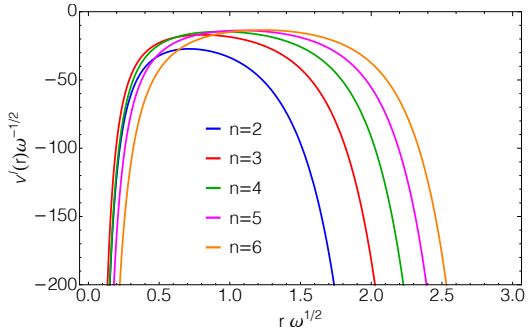

Figure 8.8: Effective potentials, $v^l(r)$, for the Hooke's atom series with $n = 2,\ldots,N$.

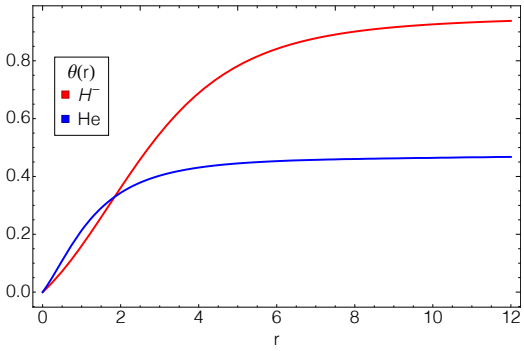

Figure 8.9: Non-trivial phase factor, $\theta(r)$, for the species H^- and He.

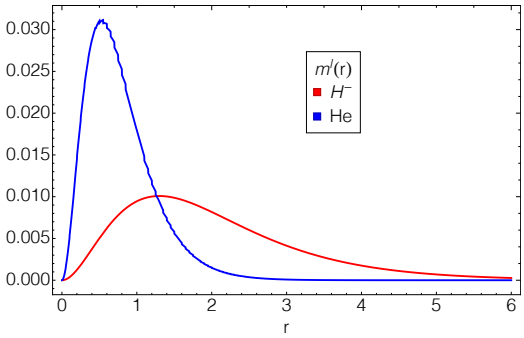

Figure 8.10: Mass potentials, $m^l(r)$, for the species H^- and He.

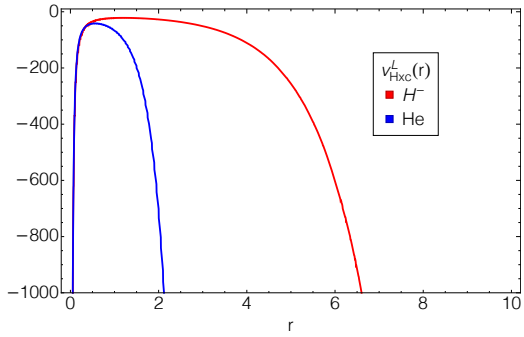

Figure 8.11: Effective potentials depleted of the nuclear fields, $v^l_{Hxc}(r)$, for the species H^- and He.

Discussion on v^l and m^l in the Laplacian gauge

Let us remark that, in the linear setting, neither of the Laplacian gauged kinetic energy densities, τ^{L1}(eq 8.5) or τ^{L2}(eq 8.6), is admissible. This latter is simply not admissible because the position-dependent mass cannot be treated as an external Lagrange multiplier. To see why the former is not admissible we need to work out the requirement

$$\begin{aligned}\tau^{L1}_{\text{int}}(\boldsymbol{r}) &= \sum_{j,\sigma} \psi^l_j(\boldsymbol{x})\nabla^2\psi^l_j(\boldsymbol{x}) \\ &= \frac{1}{2}\sum_j R_j\left(\nabla^2 R_j - R_j|\nabla\theta|^2 + 2\,i\nabla R_j\cdot\nabla\theta + i\,R_j\nabla^2\theta\right)(\boldsymbol{r}) \end{aligned} \tag{8.47}$$

We now want the imaginary part on the l.h.s. to go to zero (the kinetic energy density of an interacting system can always be transformed into a real valued quantity), i.e.

$$\left(2\nabla R_j\cdot\nabla\theta + R_j\nabla^2\theta\right) = 0 \tag{8.48}$$

However, eq 8.48 for the two-electron singlet case, gives

$$\begin{aligned} &2\nabla\sqrt{n}\cdot\nabla\theta + \sqrt{n}\nabla^2\theta = 0 \\ &2\,\frac{\nabla\sqrt{n}}{\sqrt{n}} = -\frac{\nabla^2\theta}{\nabla\theta} \end{aligned} \tag{8.49}$$

and, restricting to spherical systems,

$$\begin{aligned} &-\frac{\mathrm{d}}{\mathrm{d}r}\ln(n(r)) = \frac{2}{r} + \frac{\mathrm{d}}{\mathrm{d}r}\ln(\theta'(r)) \\ &\ln(n(r)) + \ln\left(r^2\theta'(r)\right) = c' \Rightarrow \boxed{\theta'(r) = \frac{c''}{n(r)\,r^2}} \end{aligned} \tag{8.50}$$

which fixes the derivative of the phase factor, θ', times an arbitrary constant.

On the other hand, combination of eqs 8.47 and 8.48, for this case (spherical two-electron singlet) gives

$$\tau^{L1}_{\text{int}}(r) = \frac{1}{2\sqrt{2}}\left(\left(\frac{\mathrm{d}^2}{\mathrm{d}r^2} + \frac{2}{r}\frac{\mathrm{d}}{\mathrm{d}r}\right)\sqrt{n(r)} - \sqrt{n(r)}\theta'^2(r)\right) \tag{8.51}$$

Since equation 8.50 is an extremely simple density functional, we see no reason why its insertion into eq 8.51 should satisfy it for any spherical density. In other words, in the linear setting it seems clear that the choice of possible gauges for kinetic energy densities is greatly reduced.

Intermezzo

In the keKS constructions we have discussed up to now, there is no clear relationship between the total energy of the interacting system and the effective mass and local potential $\{m^{ke}, v^{ke}\}$. This happens because, when taking the functional derivative of the auxiliary system energy w.r.t. the density, we do not know how to express that piece of functional derivative which contains the kinetic energy density (and the position-dependent mass). In fact, by the Hohenberg-Kohn theorem the variables τ and n are dependent, but their dependence is still not understood or studied at all.

In practice, we can still combine the expression for the interacting kinetic energy obtained from either keKS construction with any preferred density functional approximation, $E_{xc}^{\mathrm{DFA}} = U + W_1^{\mathrm{DFA}} + T_c^{\mathrm{DFA}}$, by recalling that

$$W_1^{\mathrm{DFA}}[n] \quad = \quad E_x^{\mathrm{DFA}}[n] + 2\,E_c^{\mathrm{DFA}}[n] - \frac{\partial\, E_c^{\mathrm{DFA}}\left[n_\gamma\right]}{\partial\,\gamma}\Big|_{\gamma=1}. \tag{8.52}$$

Nevertheless, the theoretical question of how to connect the keKS construction to the total energy of the interacting system stays open.

In the next subsection, we present another keKS setting, where such connection is set from the beginning. We basically apply the generalised-Kohn-Sham formalism [281] to a particular case of non-local operator.

8.2.3. Generalised Kohn-Sham setting

Let us introduce an energy functional $T_{\mathfrak{v}}[\Psi_s]$ of N-electron Slater determinants Ψ_s.

$$T_{\mathfrak{v}}[\Psi_s] \coloneqq \langle \Psi_s | \hat{T}_{\mathfrak{v}} | \Psi_s \rangle \tag{8.53}$$

where $\hat{T}_{\mathfrak{v}}$ can be defined as

$$\hat{T}_{\mathfrak{v}} \quad = \quad -\frac{1}{2}\sum_{i=1}^{N} \nabla_{\boldsymbol{r}_i} \cdot \left(\mathfrak{v}(\mathbf{r}_i)\nabla_{\boldsymbol{r}_i}\right) \tag{8.54}$$

and $\mathfrak{v}$ is, for the moment, undefined. Then we define the energy of our auxiliary system Ψ_s as

$$E^S[\{\psi_i\}; v] = T_{\mathfrak{v}}[\Psi_s] + \int \tilde{v}(\mathbf{r})\, n(\mathbf{r})\, \mathrm{d}\mathbf{r} \tag{8.55}$$

where $n(\mathbf{r}) = \sum_{i,\sigma} |\psi_i(\mathbf{x})|^2$.
If we minimise eq 8.55 by the usual Lagrange procedure we obtain

$$\hat{O}^{T_{\mathfrak{v}}}[\{\psi_i\}]\psi_j + \tilde{v}\,\psi_j = \epsilon_j \psi_j \tag{8.56}$$

with $\hat{O}^{T_{\mathfrak{v}}}[\{\psi_i\}]\psi_j = \frac{\delta\, T_{\mathfrak{v}}[\{\psi_i\}]}{\delta\, \psi_j^*} = -\frac{1}{2}\nabla \cdot \left(\mathfrak{v} \sum_\sigma \nabla \psi_j\right)(\mathbf{r})$. Eqs 8.56 are also structurally identical to eqs 8.10.

At the stationary point, eq 8.56 is satisfied and we label $\psi_i \to \psi_i^{mGKS}$, $\tilde{v} \to v^{mGKS}$, $\epsilon_i \to \epsilon_i^{mGKS}$, where "mGKS" stands for "mass-dependent Generalised Kohn-Sham".

We could now determine the energy of an interacting system exactly in terms of $T_{\mathfrak{v}}[\{\psi_i\}]$ by introducing an *ad hoc* functional $R^{T_{\mathfrak{v}}}[n[\{\psi_i\}]]$ determined by $T_{\mathfrak{v}}[\{\psi_i\}]$ such that

$$E_0[v] = \min_{\{\psi_i\}\to N}\{T_{\mathfrak{v}}[\{\psi_i\}] + R^{T_{\mathfrak{v}}}[n[\{\psi_i\}]] + \int v(\mathbf{r})\, n(\mathbf{r})\, \mathrm{d}\mathbf{r}\} \tag{8.57}$$

with v the external potential of the interacting system. So long as the functional $R^{T_{\mathfrak{v}}}[n]$ is an *explicit* functional of the density, the minimization in 8.57 leads to the same kind of equations as eqs 8.56 with $v^{mGKS} = v_R + v$ and $v_R = \frac{\delta R^{T_{\mathfrak{v}}}}{\delta n}$.
Since $\mathfrak{v}$ is still completely undetermined we have derived a general scheme where we can devise in reverse which piece of the Kohn-Sham potential we want to use as a Lagrange multiplier v^{mGKS} (ideally a term which we know how to approximate well) and which other part we want to feed to the operator $\hat{T}_{\mathfrak{v}}$.

We may label "mGKS complement" potential, v_c^{mGKS}, the component that we want to "drop out" from the usual KS potential the and we may decompose the KS potential in any preferred fashion as long as both v^{mGKS} and v_c^{mGKS} are well-defined functional derivatives

$$v_s = v^{mGKS} + v_c^{mGKS}. \tag{8.58}$$

For the sake of interpreting $\mathfrak{v}^{-1}$ as an effective mass, we would like that

$$\mathfrak{v}(\boldsymbol{r}) \geq 0. \tag{8.59}$$

However, as the scalar potential $\mathfrak{v}$ depends on v^{mGKS} and needs to satisfy eq 8.57, we might not have enough freedom to impose eq 8.59. We shall see later on that this is going to be the case for values of $n > 3$ in the Hooke's atom series.
Because eq 8.59 cannot be satisfied for all systems, we are no longer guaranteed that minimisation of eq 8.55 will, just as for the KS system, always penalise the phase factor. In other words, contrary to the KS ones we are not guaranteed that the mGKS orbitals are real. For simplicity, we are going to assume that the orbitals are real (just as we do in the non-linear setting).

Let us now focus on the choice

$$v_c^{mGKS} = v_{c,kin}. \tag{8.60}$$

Quite interestingly, under the assumption that the mGKS orbitals equate the KS orbitals, i.e. $\psi_i^{mGKS} = \psi_i^s$, (which is by construction satisfied in two-electron singlet systems), we obtain

$$-\frac{1}{2}\psi_i^{mGKS}\nabla\cdot\mathfrak{v}^{v_{c,kin}}\nabla\psi_i^{mGKS} = \tau_{\text{int}}^{L2} \tag{8.61}$$

where by $\mathfrak{v}^{v_{c,kin}}$ we indicate the dependence of the non-local operator on eq 8.60. In other words, assuming that eq 8.57 can be satisfied for the choice 8.60, the simple minimisation of eq 8.55 delivers a non-interacting kinetic energy density in the Laplacian gauge 8.6 that *locally* matches the interacting kinetic energy density in the same gauge.[6] Equation 8.61 is a remarkable result, as we have managed to write an explicit expression for an effective position-dependent mass, $m^{v_s-v_{c,kin}} = (\mathfrak{v}^{v_{c,kin}})^{-1}$, as a functional of the interacting kinetic energy density τ^{L2}_{int}, while still minimising a non interacting kinetic energy functional ($T_{\mathfrak{v}}$) under the sole density constraint.

More in general, within the assumption $\psi_i^{mGKS} = \psi_i^s$, one will obtain a non-interacting kinetic energy corresponding to

$$-\frac{1}{2}\psi_i^{mGKS}\nabla\cdot\mathfrak{v}^{v_c^{mGKS}}\nabla\psi_i^{mGKS} = \tau_s^{L2} + v_c^{mGKS}\, n. \tag{8.62}$$

where $\tau_s^{L2} = -\frac{1}{2}\psi_i^s\nabla^2\psi_i^s$. For simplicity, we will now focus on the case 8.60, and we will always refer to $m^{v_s-v_{c,kin}}$ as "m^{mGKS}" although as already discussed, v^{mGKS} – on which the properties of m^{mGKS} depend – can be anything as long as it is a functional derivative.[7]

Examples of m^{mGKS} for two-electron singlet systems

For spherical two-electron singlet systems, $\mathfrak{v}$ is our only unknown and the set of equations 8.56 reduces to an equation of the kind

$$a(r)\,\mathfrak{v}'(r) + b(r)\,\mathfrak{v}(r) + c(r) = 0 \tag{8.63}$$

whose solution reads

$$\mathfrak{v}(r) = \left(k - \int_0^r \frac{c(s)}{a(s)} e^{\int_0^r \frac{b(t)}{a(t)}\mathrm{d}t}\right) e^{-\int_0^r \frac{b(t)}{a(t)}\mathrm{d}t}. \tag{8.64}$$

However, there is a catch in the choice of the equation we decide to solve. Namely, labeling the only spatial orbital $\psi^{mGKS} = \sqrt{\frac{n}{2}} = \phi$ for notational convenience, we have

$$\phi'\,\mathfrak{v}' + \left(\phi'' + \frac{2}{r}\phi'\right)\mathfrak{v} - 2\left(v^{mGKS} - \epsilon\right) = 0 \tag{8.65a}$$

with $a = \phi'$, $b = \left(\phi'' + \frac{2}{r}\phi'\right)$ and $c = -2\left(v^{mGKS} - \epsilon\right)$ or

$$\phi'\,\mathfrak{v}' + \left(\phi'' + \frac{2}{r}\phi'\right)\mathfrak{v} + 2\,v_c^{mGKS}\phi - \left(\phi'' + \frac{2}{r}\phi'\right) = 0 \tag{8.65b}$$

[6] As already noticed, for the interacting system there is no distinction between the two gauges 8.5 and 8.6, i.e. $\tau^{L1}_{\text{int}} = \tau^{L2}_{\text{int}}$.

[7] For example, one could wonder what m^{mGKS} would be by choosing $v^{mGKS} = v$ or $v^{mGKS} = v + v_H$, etc. In particular, we shall briefly consider the case $v^{mGKS} = v_s$ to fix the degree of freedom intrinsic in the fact that the nabla operator is acting on $(m^{mGKS})^{-1}$.

where a and b are as before and $c = 2\,v_c^{mGKS}\phi - \left(\phi'' + \frac{2}{r}\phi'\right)$.
Equation 8.65b is a consequence of the fact that

$$\left(v^{mGKS} - \epsilon_i^s\right)\psi_i^{mGKS} = \frac{\nabla^2}{2}\psi_i^s - v_c^{mGKS}\psi_i^s \tag{8.66}$$

which holds only as long as $\psi_i^{mGKS} = \psi_i^s$ (true for two-electron singlets).

The catch is in the fact that while in eq 8.65b we only need to fix the constant k, in the first equation (eq 8.65a) the solution is written in terms of two unknown constants: $\{k, \epsilon\}$. Suppose, we have fixed k, we can find a different solution, $\mathfrak{v}$, for any arbitrary value of ϵ which still satisfies eq 8.63.

In the examples that are going to be presented we do not perform any self-consistent iteration but we plug in either equation (eq 8.65a or eq 8.65b) the exact ingredients.[8] Precisely because eq 8.66 is satisfied with such exact ingredients, both equations lead to the same solution (for each given k). However, we reiterate that, for a given k, we can solve eq 8.65a for any arbitrary value of ϵ. Choosing $\epsilon \neq -I_p$ would no longer satisfy eq 8.66 and the $\mathfrak{v}$ resulting from the two equations would be different.

Due to its dependence on ϵ we then decide to discard eq 8.65a and focus on eq 8.65b. To fix k, we simply decide to pick $v^{mGKS} = v_s$ (i.e. $v_c^{mGKS} = 0$) and choose among the set of solutions 8.64 that one for which $\mathfrak{v}^0 = 1$. This fixes $k = 0$.

Left-multiplying eq 8.65b by the orbital ϕ allow us to write an explicit solution to $\mathfrak{v}^{v_{c,kin}}$ in terms of the interacting kinetic energy in the gauge 8.6 as pledged in eq 8.61. Considering that, for the spherical case, we can manipulate the exponential function in eq 8.64 in a very convenient form

$$\frac{b(t)}{a(t)} = \left(\frac{\phi''(t)}{\phi'(t)} + \frac{2}{t}\right) = \frac{\mathrm{d}}{\mathrm{d}t}\ln\left(\phi'(t)\,t^2\right), \tag{8.67}$$

we obtain

$$\mathfrak{v}^{v_{c,kin}}(r) = \frac{2\int_0^r \frac{\tau_{\mathrm{int}}^{L2}(s)\,s^2}{\phi(s)}\mathrm{d}s}{\phi'(r)\,r^2}. \tag{8.68}$$

In figs 8.12 and 8.13, we show the position-dependent masses, $m^{mGKS}(r)$, obtained as the inverse of eq 8.68, for the Hooke's atom series and the Hydrogen anion and He atom.

As anticipated, we observe that for the Hooke's atom series there is not enough freedom to force the effective mass to be always positive, even allowing for different values of k. Another feature we observe is that the effective mass is non-negligeable

[8] These exact ingredients are $v^{mGKS} = v_{cond} + v_{N-1} + v$ and the exact ionisation potential $\epsilon = -I_p$ to get $\mathfrak{v}$ from eq 8.65a or the exact $v_c^{mGKS} = v_{kin}$ to get it from eq 8.65b in addition to the interacting ground state density which is required in both equations.

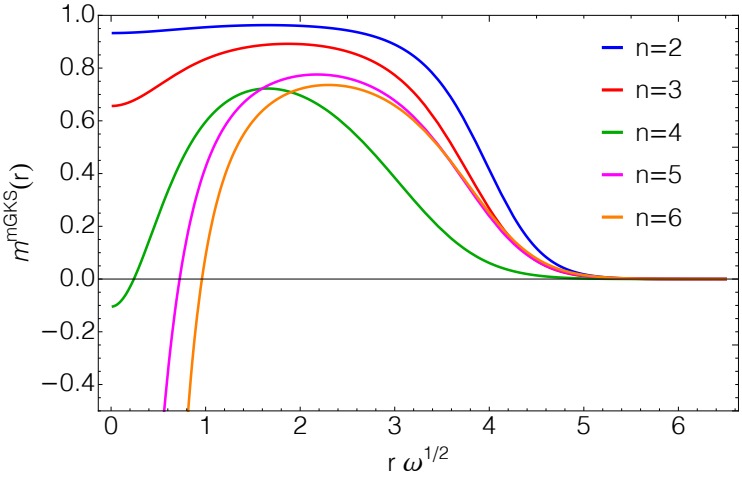

Figure 8.12: Scaled mass potentials, $m^{mGKS}(r)$, for the Hooke's atom series with n = 2,...,N.

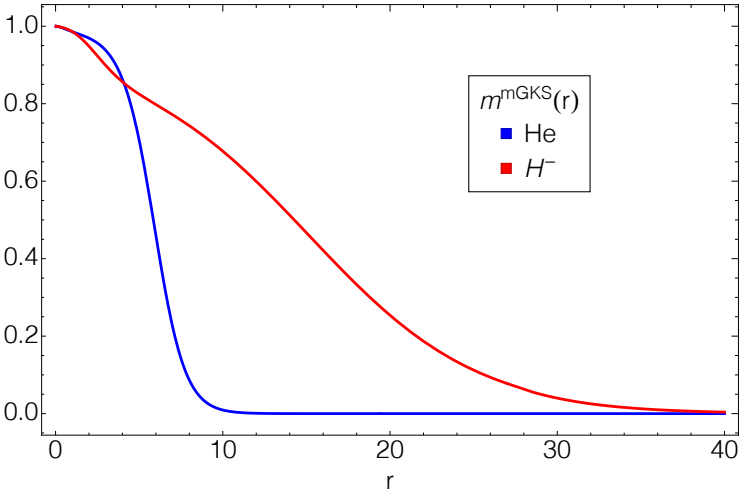

Figure 8.13: Mass potentials, $m^{mGKS}(r)$, for the Hydrogen anion and the He atom.

even at values of the distance from the origin at which the density itself seems negligeable. Finally, we stress that only the effective mass needs to be found in this setting and not the effective potential, because this latter is exactly what we have constrained ($v^{mGKS} = v_{resp} + v_{cond} + v$) and we know it to be a well-behaved function, asymptotically going to zero. In this sense, compared to the former settings where either the effective mass or the effective potential or both were diverging this latter seems promising.

Local behaviour of m^{mGKS} around the origin

Rewriting $\mathfrak{v} = 1 + \delta\mathfrak{v}$, eq8.65b is turned into

$$\nabla \cdot (\delta\mathfrak{v}\nabla)\phi_i + 2\, v_c^{mGKS}\phi_i = 0 \tag{8.69}$$

and the mass is then obtained in terms of $\delta\mathfrak{v}$ as

$$m^{mGKS}(r) = \frac{1}{1 + \delta\mathfrak{v}(r)}. \tag{8.70}$$

Equation 8.69, for two electron spherical system and with $v_c^{mGKS} = v_{kin}$, can be rewritten as

$$\delta\mathfrak{v}'\left(\frac{\phi'}{\phi}\right) + \delta\mathfrak{v}\left(\frac{\phi''}{\phi} + \frac{2}{r}\frac{\phi'}{\phi}\right) + 2\, v_{kin} = 0 \tag{8.71}$$

and we can substitute

$$\begin{aligned} \frac{\phi'}{\phi} &= \frac{n'}{2n} \\ \frac{\phi''}{\phi} &= -\frac{n'^2}{4n^2} + \frac{n''}{2n} \end{aligned} \tag{8.72}$$

We want to analyse the local behaviour of $\delta\mathfrak{v}$ at the boundary of its domain and we will start by the origin. However we need to distinguish here among the situation where the density is an analytical function at the origin as in the case of the Hooke's atom series or when it is non-analytical and determined by the cusp condition (eq 1.4).

In the first case we have

$$\delta\mathfrak{v}'\left(\frac{n'}{2n}\right) + \delta\mathfrak{v}\left(-\frac{n'2}{4n^2} + \frac{n''}{2n} + \frac{n'}{rn}\right) = 2\, v_{kin} \tag{8.73}$$

the first term goes clearly to zero as $n'(r)|_{r\to 0} = 0$, while we need to further analyse the third tem in parenthesis using L'Hôpital's rule as $\lim_{r\to 0} \frac{n'}{rn} \sim \frac{0}{0}$. Therefore we look at the derivatives of numerator and denominator

$$\frac{\mathrm{d}}{\mathrm{d}r}\left(\frac{n'(r)}{r\, n(r)}\right) = \frac{n''}{n} - \frac{n'}{n^2} \tag{8.74}$$

and when $r \to 0$ only the term $\frac{n''}{n}$ survives. In conclusion, we are left with

$$\begin{aligned} \delta\mathfrak{v}\left(\frac{3\,n''}{2\,n}\right) &\sim -2\,v_{kin} \\ \delta\mathfrak{v} &\sim -\frac{4\,v_{kin}\,n}{3\,n''} \end{aligned} \tag{8.75}$$

or

$$m^{mGKS}_{\text{midB}}(r \to 0) \sim \frac{1}{1 - \frac{4\,v_{kin}(0)\,n(0)}{3\,n''(0)}} \tag{8.76}$$

where we have used the subscript "midB" for midbond, as we have already stressed that one could consider the density at the origin of the Hooke's atom series with n>3 as a model for the density at the midbond of two equal fragments in a molecular species and where the sign of m^{mGKS}_{midB} depends on whether $\frac{4\,v_{kin}(0)\,n(0)}{3\,n''(0)}$ is greater or smaller than one.

For atomic densities, we know that, at the nucleus position which we set at the origin, the density behaves like $n'(r)|_{r\to 0} \sim -2\,Z\,n(0)$. For this case, it is easier to look at what happens to $\delta\mathfrak{v}$ starting from its solution, i.e.

$$\delta\mathfrak{v}(r) = -\frac{2\int_0^r v_{kin}(s)\phi(s)s^2\mathrm{d}s}{\phi'(r)r^2} \tag{8.77}$$

The $r \to 0$ limit of the above equation is again of the kind $\frac{0}{0}$ therefore we look at the corresponding derivatives finding

$$\lim_{r\to 0}\delta\mathfrak{v}(r) \sim -\lim_{r\to 0}\left(\frac{2\,v_{kin}(r)}{\frac{\phi''(r)}{\phi(r)} + \frac{2}{r}\frac{\phi'(r)}{\phi(r)}}\right) \sim 0 \tag{8.78}$$

where we have used that all the functions (ϕ, ϕ', ϕ'', v_{kin}) excluding $1/r$ have finite values in $r = 0$.[9]

Consequently

$$m^{mGKS}(r \to 0) \sim 1 \tag{8.79}$$

as visible in fig 8.13.

Incidentally, we observe that, by plugging into eq 8.77 either one among the expressions for v_{kin} reported in eq 8.46 then using eq 8.70, one finds the relation between m^{mGKS} and the previously discussed position-dependent masses (m^{nl} and m^{l}) in the spherically symmetric two-electron singlet cases.

[9] In particular from eq 8.25, $v_{kin}(0) \sim \frac{E_{ii}}{2\,n(0)}$ follows.

Asymptotic behaviour of m^{mGKS}

Using the asymptotic expansion of atomic and molecular wavefunctions [289]

$$\phi(r\to\infty)\sim r^{\beta}e^{-\alpha r} \tag{8.80}$$

with $\alpha=\sqrt{-2\epsilon_H}$ and $\beta=\frac{2(Z-N+1)}{\alpha}-1$ (Z being the nuclear charge and N the number of electrons) then

$$\phi'(r\to\infty) \sim e^{-\alpha r}r^{\beta-1}\left(\beta-\alpha r\right) \tag{8.81}$$
$$\phi''(r\to\infty) \sim e^{-\alpha r}r^{\beta-2}\left((\beta-\alpha r)^2-\beta\right) \tag{8.82}$$

Plugging eqs 8.80, 8.81 and 8.82 into eq 8.69 with $v_c^{mGKS}=v_{kin}=v_{c,kin}$, remembering that $v_{c,kin}$ is short-ranged [41, 49], and multiplying both sides by $\left(e^{\alpha r}r^{2-\beta}\right)$, we find

$$\left(\alpha^2r^2+\beta+\beta^2-2\alpha r(1+\beta)\right)\delta\mathfrak{v}(r)+r(\beta-\alpha r)\delta\mathfrak{v}'(r)=0 \tag{8.83}$$

Leaving only the higher order terms, $\sim r^2$,

$$\alpha^2\delta\mathfrak{v}(r)-\alpha\delta\mathfrak{v}'(r)=0 \tag{8.84}$$

which is satisfied for

$$\delta\mathfrak{v}(r\to\infty)\sim c\,e^{\alpha r} \tag{8.85}$$

therefore

$$m^{mGKS}(r\to\infty)\sim\frac{1}{1+c\,e^{\alpha r}}. \tag{8.86}$$

A similar analysis on the Hooke's atom density $\phi_{\text{harm}}(r\to\infty)\sim r^q e^{-\frac{\omega}{2}r^2}$ [45], with $q=\left(\frac{I_p}{\omega}-\frac{3}{2}\right)\in\mathbb{R}^+$ and $I_p=-(E^N-E^{N-1})$, shows that

$$m^{mGKS}_{\text{harm}}(r\to\infty)\sim\frac{1}{1+c\,e^{\frac{\omega}{2}r^2}}. \tag{8.87}$$

8.3. DFAs for keKS and final notes

At the end of sec 1.3.2 we have sketched the algorithm for regular KS equations (eqs 1.50 and 1.51). In the keKS formalism we would have an algorithm of the kind

$$v^{ke(i)}=v_{\text{H}}\left[n^{(i)}\right]+v^{ke}\left[n^{(i)},\tau^{(i)}\right]+v \tag{8.88}$$
$$m^{ke(i)}=1+m^{ke}_{Hxc}\left[\{\psi_j\}^{(i)},\tau^{(i)}\right] \tag{8.89}$$
$$\{\psi_j\}^{(i+1)}=\underset{\{\psi_j\}}{\text{argmin}}\left(T_{m^{ke(i)}}\left[\{\psi_j\}^{(i)}\right]+\int v^{ke(i)}(\boldsymbol{r})n(\boldsymbol{r})\mathrm{d}\boldsymbol{r}\right) \tag{8.90}$$

where m^{ke}_{Hxc} is defined as the difference $m^{ke}_{Hxc} := \left(m^{ke(i)} - 1\right)$ and it basically measures the distortion of the fictitious electron mass due to kinetic correlation effects. In practice, we compute from a guess density (a set of guess orbitals) and a guess kinetic energy density the initial effective potential v^{ke} and mass m^{ke}. Next, we solve eqs 8.10 to obtain updated orbitals delivering an updated density via eq 8.11 and an updated kinetic energy density via eq 8.12, eq 8.34 or eq 8.61 according to which setting we are in. Note that, in the linear setting, we construct at the same time also an approximate phase factor, $\theta^{(i)}\left[\{\psi_j\}^{(i)}, \tau^{(i)}\right]$. Finally, we plug the updated density and kinetic energy density (internal quantities) into the functionals v^{ke} and m^{ke} for the external quantities and loop until convergence is reached.

Among the next steps for developing a kinetic energy density-density functional theory, the need for novel density functional approximations which depend on both n and τ for the unknown effective potentials v^{ke} and m^{ke} stands out. A good candidate model seems to be the series of finite uniform electron gases [291, 292] which depend on two parameters for a given dimension. These two parameters are related to the number of electrons and the radius of the sphere on which the uniform gas is spread. They can be coupled to any quantity of interest as recently shown in reference [293], where a model for the exchange energy is constructed as a functional of the density and the curvature of the Fermi hole.

At the state of the art however, a parametrization of the correlation quantities is available only for the finite uniform electron gas with two particles. Future work will be focused in the direction of building such explicit bifunctionals which will hopefully introduce more flexibility than that brought by the most common density functional approximations for KS-DFT. As a first hint, we looked at the approximate m^{nl}, m^{l} and m^{mGKS} that were obtained using the LDA kinetic energy density t_c^{LDA} as an approximation to v_{kin}. We show them in figure 8.14 for the Hydrogen anion in comparison with the ones already shown coming from the accurate wavefunction of ref [264]. The LDA models used are PW92 [294] and the above-mentioned two-electron glomium. In the bottom panel representing the mGKS setting, we show the results coming from both eq 8.65a and eq 8.65b, within the same approximation. It seems clear that by approximating v^{mGKS} as $v^{mGKS} \approx \epsilon_c - t_c + \frac{v_{\mathrm{H}}}{2} + v$ and inputting the exact ionization potential [295], we obtain much less accurate masses than considering $v_c^{mGKS} \approx t_c$. The much smaller accuracy ought probably to be attributed to the self-interaction error present in the approximate v_{mGKS} and absent in the approximate v_c^{mGKS}.

Concerning the Hermiticity of the operator $\hat{t}_m$ (eq 8.9), we should probably remark that it is quite a subtle issue: $\hat{t}_m$ is clearly Hermitian in the space of square-integrable functions as long as the boundary terms are zero. This is the case if the position-dependent mass is constant, otherwise one needs to study the analytical behaviour of the mass at the boundaries. This aspect deserves a proper investigation.

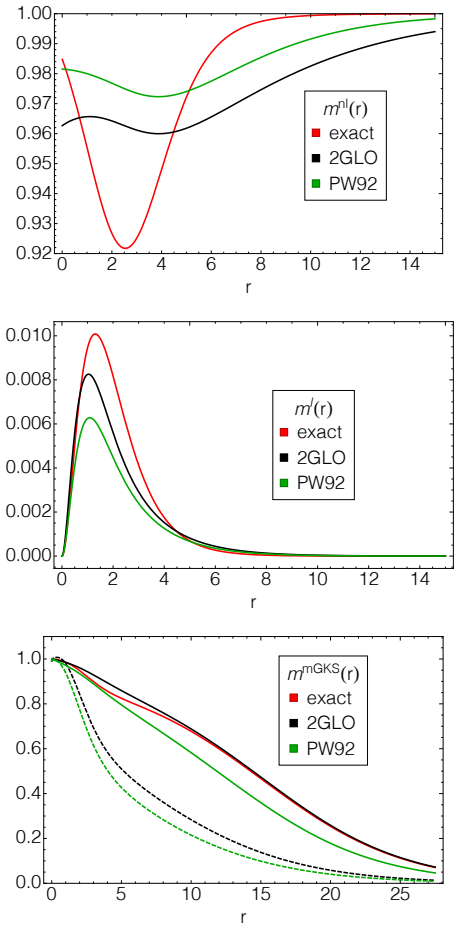

Figure 8.14: Position dependent masses m^{nl}(top), m^{l}(middle) and m^{mGKS}(bottom) for the Hydrogen anion coming from the accurate wavefunction of ref [264] (in red) or using the LDA kinetic energy density t_c^{LDA} as an approximation to v_{kin}. The LDA models used are PW92 [294] (in green) and the two-electron glomium [291–293] (in black). In the bottom panel, we show the results coming from eq 8.65a (dashed) and eq 8.65b (solid curve), within the same approximation, as discussed in the main text.

As a final note, we want to pinpoint that although one of the motivations for a kinetic energy density functional theory was that of separating the Coulomb from the kinetic correlation contributions, where the formers would be included via the usual effective potential while the latters would be handled via a non local operator, it might be that this goal is far from our reach due to the presence of a kinetic response part in the KS potential, $v_{c,kin}^{resp}$ (eq 2.52). This is blatant in the last presented setting (sec 8.2.3) where we have unwittingly obtained a matching between the kinetic energy densities of the interacting and of the non-interacting system by splitting up the KS potential as $v_s = \underbrace{v_{c,kin}}_{v_c^{mGKS}} + \underbrace{v_{resp} + v_{cond} + v}_{v^{mGKS}}$. Namely, we have kept the full response potential, kinetic piece included, in the role of Lagrange multiplier together with the electrostatic potential of the conditional density and the external potential. Nevertheless, in light of the fact that this piece is nowadays absent from any approximation, even though failing to properly disentangle all of the kinetic correlation components from the effective external potential, a kinetic energy density-density functional theory could in practice still bring about considerable improvements in treating systems where the balance between inter-particle repulsion and particles kinetic energy is especially delicate.

Appendices

A

Redundancy of the permutations

In order to account for the indistinguishability among electrons the modulus squared of the SCE wavefunction has been usually expressed as in eq 3.9. If we now perform the integration over d**s** we can rewrite it as

$$|\Psi_{SCE}(\mathbf{r}_1,\cdots,\mathbf{r}_N)|^2 = \frac{1}{N!}\sum_{\wp=1}^{N!}\left(\frac{\rho(\boldsymbol{r}_1)}{N}\prod_{i=2}^{N}\delta(\boldsymbol{r}_i-\mathbf{f}_{\wp(i)}(\boldsymbol{r}_1))+\right.$$
$$\left.+\frac{\rho(\boldsymbol{r}_2)}{N}\prod_{i=1,i\neq 2}^{N}\delta(\boldsymbol{r}_i-\mathbf{f}_{\wp(i)}(\boldsymbol{r}_2))+\cdots+\frac{\rho(\boldsymbol{r}_N)}{N}\prod_{i=1}^{N-1}\delta(\boldsymbol{r}_i-\mathbf{f}_{\wp(i)}(\boldsymbol{r}_N))\right) \qquad \text{(A.1)}$$

Now we want to show that each of the N terms inside brackets in eq. A.1 are equal to one another. To show such thing we will abstract from the three-electron case.
For the three-electron case $\wp = 1\cdots 6$, in details:

$$\wp = 1 \begin{cases} \boldsymbol{r}_1 = \mathbf{f}_{1(1)}(\boldsymbol{s}) = \boldsymbol{s} \\ \boldsymbol{r}_2 = \mathbf{f}_{1(2)}(\boldsymbol{s}) = \mathbf{f}_1(\boldsymbol{s}) \\ \boldsymbol{r}_3 = \mathbf{f}_{1(3)}(\boldsymbol{s}) = \mathbf{f}_2(\boldsymbol{s}) \end{cases}$$

$$\wp = 2 \begin{cases} \boldsymbol{r}_1 = \mathbf{f}_{6(1)}(\boldsymbol{s}) = \boldsymbol{s} \\ \boldsymbol{r}_2 = \mathbf{f}_{6(2)}(\boldsymbol{s}) = \mathbf{f}_2(\boldsymbol{s}) \\ \boldsymbol{r}_3 = \mathbf{f}_{6(3)}(\boldsymbol{s}) = \mathbf{f}_1(\boldsymbol{s}) \end{cases}$$

$$\wp = 3 \begin{cases} \boldsymbol{r}_1 = \mathbf{f}_{4(1)}(\boldsymbol{s}) = \mathbf{f}_1(\boldsymbol{s}) \\ \boldsymbol{r}_2 = \mathbf{f}_{4(2)}(\boldsymbol{s}) = \boldsymbol{s} \\ \boldsymbol{r}_3 = \mathbf{f}_{4(3)}(\boldsymbol{s}) = \mathbf{f}_2(\boldsymbol{s}) \end{cases}$$

$$\wp = 4 \begin{cases} \boldsymbol{r}_1 = \mathbf{f}_{3(1)}(\boldsymbol{s}) = \mathbf{f}_2(\boldsymbol{s}) \\ \boldsymbol{r}_2 = \mathbf{f}_{3(2)}(\boldsymbol{s}) = \boldsymbol{s} \\ \boldsymbol{r}_3 = \mathbf{f}_{3(3)}(\boldsymbol{s}) = \mathbf{f}_1(\boldsymbol{s}) \end{cases}$$

$$\wp = 5 \begin{cases} \boldsymbol{r}_1 = \mathbf{f}_{2(1)}(\boldsymbol{s}) = \mathbf{f}_1(\boldsymbol{s}) \\ \boldsymbol{r}_2 = \mathbf{f}_{2(2)}(\boldsymbol{s}) = \mathbf{f}_2(\boldsymbol{s}) \\ \boldsymbol{r}_3 = \mathbf{f}_{2(3)}(\boldsymbol{s}) = \boldsymbol{s} \end{cases}$$

$$\wp = 6 \begin{cases} \boldsymbol{r}_1 = \mathbf{f}_{5(1)}(\boldsymbol{s}) = \mathbf{f}_2(\boldsymbol{s}) \\ \boldsymbol{r}_2 = \mathbf{f}_{5(2)}(\boldsymbol{s}) = \mathbf{f}_1(\boldsymbol{s}) \\ \boldsymbol{r}_3 = \mathbf{f}_{5(3)}(\boldsymbol{s}) = \boldsymbol{s} \end{cases}$$

so that the wavefunction is expanded into:

$$\begin{aligned} |\Psi_{\mathrm{SCE}}(\boldsymbol{r}_1,\boldsymbol{r}_2,\boldsymbol{r}_3)|^2 = \\ = \frac{1}{6}\Bigg(& \frac{n(\boldsymbol{r}_1)}{3}\delta(\boldsymbol{r}_2-\mathbf{f}_1(\boldsymbol{r}_1))\delta(\boldsymbol{r}_3-\mathbf{f}_2(\boldsymbol{r}_1)) + \underbrace{\frac{n(\boldsymbol{r}_1)}{3}\delta(\boldsymbol{r}_2-\mathbf{f}_2(\boldsymbol{r}_1))\delta(\boldsymbol{r}_3-\mathbf{f}_1(\boldsymbol{r}_1))}_{\wp=2} + \\ & + \frac{n(\boldsymbol{r}_2)}{3}\delta(\boldsymbol{r}_1-\mathbf{f}_2(\boldsymbol{r}_2))\delta(\boldsymbol{r}_3-\mathbf{f}_1(\boldsymbol{r}_2)) + \underbrace{\frac{n(\boldsymbol{r}_2)}{3}\delta(\boldsymbol{r}_1-\mathbf{f}_1(\boldsymbol{r}_2))\delta(\boldsymbol{r}_3-\mathbf{f}_2(\boldsymbol{r}_2))}_{\wp=4} + \\ & + \frac{n(\boldsymbol{r}_3)}{3}\big(\delta(\boldsymbol{r}_1-\mathbf{f}_1(\boldsymbol{r}_3))\delta(\boldsymbol{r}_2-\mathbf{f}_2(\boldsymbol{r}_3)) + \delta(\boldsymbol{r}_1-\mathbf{f}_2(\boldsymbol{r}_3))\delta(\boldsymbol{r}_2-\mathbf{f}_1(\boldsymbol{r}_3))\big)\Bigg) \end{aligned} \tag{A.2}$$

We now consider one permutation, e.g. $\wp = 4$ (underlined), and we are going to show that this term is equivalent to the $\wp = 2$ term (also highlighted for the purpose) in the three steps listed below.

1. Using the properties $\delta(f(x)) = \frac{1}{f'(x_0)}\delta(x-x_0)$ and $g(x)\delta(x-y) \equiv g(y)\delta(x-y)$ of the Delta functions on $\delta(\boldsymbol{r}_1 - \mathbf{f}_2(\boldsymbol{r}_2))$, we can rewrite this permutation as

$$\frac{n(\mathbf{f}_1^{-1}(\boldsymbol{r}_1))}{3\det\left(\partial_{f_{2,\alpha}^{-1}} f_{2,\beta}(\mathbf{f}_1^{-1}(\boldsymbol{r}_1))\right)}\delta\left(\boldsymbol{r}_2 - \mathbf{f}_1^{-1}(\boldsymbol{r}_1)\right)\delta\left(\boldsymbol{r}_3 - \mathbf{f}_2(\mathbf{f}_1^{-1}(\boldsymbol{r}_1))\right), \tag{A.3}$$

where the indices $\alpha, \beta = x, y, z$, and $\det\left(\partial_\alpha g_\beta(\boldsymbol{r})\right)$ denotes the determinant of the Jacobian matrix for $\mathbf{g}(\boldsymbol{r})$.

2. Using the property of the inverse function $\mathbf{g}^{-1}(\mathbf{g}(\boldsymbol{r})) = \boldsymbol{r}$ whose Jacobian of both sides gives

$$\begin{bmatrix} \frac{\partial}{\partial g_x} g_x^{-1}(\mathbf{g}(\boldsymbol{r})) & \frac{\partial}{\partial g_y} g_x^{-1}(\mathbf{g}(\boldsymbol{r})) & \frac{\partial}{\partial g_z} g_x^{-1}(\mathbf{g}(\boldsymbol{r})) \\ \frac{\partial}{\partial g_x} g_y^{-1}(\mathbf{g}(\boldsymbol{r})) & \frac{\partial}{\partial g_y} g_y^{-1}(\mathbf{g}(\boldsymbol{r})) & \frac{\partial}{\partial g_z} g_y^{-1}(\mathbf{g}(\boldsymbol{r})) \\ \frac{\partial}{\partial g_x} g_z^{-1}(\mathbf{g}(\boldsymbol{r})) & \frac{\partial}{\partial g_y} g_z^{-1}(\mathbf{g}(\boldsymbol{r})) & \frac{\partial}{\partial g_z} g_z^{-1}(\mathbf{g}(\boldsymbol{r})) \end{bmatrix} \times \begin{bmatrix} \frac{\partial}{\partial x} g_i(\boldsymbol{r}) & \frac{\partial}{\partial x} g_j(\boldsymbol{r}) & \frac{\partial}{\partial x} g_k(\boldsymbol{r}) \\ \frac{\partial}{\partial y} g_i(\boldsymbol{r}) & \frac{\partial}{\partial y} g_j(\boldsymbol{r}) & \frac{\partial}{\partial y} g_k(\boldsymbol{r}) \\ \frac{\partial}{\partial z} g_i(\boldsymbol{r}) & \frac{\partial}{\partial z} g_j(\boldsymbol{r}) & \frac{\partial}{\partial z} g_k(\boldsymbol{r}) \end{bmatrix} = \mathbb{I} \tag{A.4}$$

we have

$$\det\left(\partial_{g_\alpha} g_\beta^{-1}(\mathbf{g}(\boldsymbol{r}))\right) = \left(\det\left(\partial_\alpha g_\beta(\boldsymbol{r})\right)\right)^{-1}, \tag{A.5}$$

where again $\alpha, \beta = x, y, z$.
By setting $\mathbf{g}(\boldsymbol{x}) = \mathbf{f}_1^{-1}(\boldsymbol{x})$ and $\mathbf{g}^{-1}(\boldsymbol{x}) = \mathbf{f}_1(\boldsymbol{x})$, term (A.3) is further rewritten as:

$$\frac{n(\mathbf{f}_1^{-1}(\boldsymbol{r}_1))}{3}\det\left(\partial_\alpha f_{1,\beta}^{-1}(\boldsymbol{r}_1)\right)\delta\left(\boldsymbol{r}_2 - \mathbf{f}_1^{-1}(\boldsymbol{r}_1)\right)\delta\left(\boldsymbol{r}_3 - \mathbf{f}_2(\mathbf{f}_1^{-1}(\boldsymbol{r}_1))\right). \tag{A.6}$$

3. Finally, using the fundamental properties of the co-motion functions, eqs. 3.11, and 3.12, where the fact that they form a cyclic group implies that the inverse of a co-motion function is another co-motion function in the group, the term (A.6) transforms into:

$$\frac{n(\boldsymbol{r}_1)}{3}\delta(\boldsymbol{r}_2 - \mathbf{f}_2(\boldsymbol{r}_1))\delta(\boldsymbol{r}_3 - \mathbf{f}_1(\boldsymbol{r}_1)), \tag{A.7}$$

which can be recognised as permutation $\wp = 2$.

The same reasoning in three steps is applicable to all the terms of a general N-electron case.

To summarise, we believe we have shown that $N! - (N-1)!$ terms are redundant in expression 3.9 as all of these can be tranformed into one of the $(N-1)!$ terms having the same density prefactor. Therefore, choosing for example to express the density as a function of the coordinates of electron 1, the SCE wavefunction can be written as

$$|\Psi_{\mathrm{SCE}}(\boldsymbol{r}_1, \cdots, \boldsymbol{r}_N)|^2 = \frac{1}{(N-1)!}\frac{n(\boldsymbol{r}_1)}{N}\sum_{\wp=1}^{(N-1)!}\prod_{i=2}^{N}\delta(\boldsymbol{r}_i - \mathbf{f}_{\wp(i)}(\boldsymbol{r}_1)) \tag{A.8}$$

This also means that, upon integration over $N-1$ variables, we obtain $\mathfrak{n}$ identical terms with $\mathfrak{n} = \Gamma(N)$. Consequently, we can consider only one of such non redundant permutations – properly rescaled by the factor $\mathfrak{n}$ – if we are interested in calculating functions of one particle coordinates as are the one-body potentials defined in chapter 2 and as it was done in practice in the derivation of v_{N-1}^{SCE}, section 6.2

B

Analytical 1D model for v_{Hxc}^{SCE} and v_{resp}^{SCE} in the dissociation limit

In chapter 6, we have seen that the shape of the co-motion function for the density of eq 6.45 becomes asymtotically the same at any internuclear distance ("saturation" phenomenon), behaving, in particular, as a constant in the asymptotic regions $x \ll 1$ and $x \gg 1$ and as a linear curve with coefficients, $m^{<} = \frac{b}{a}$ and $m^{>} = \frac{a}{b}$ close to a_R (eq 6.51).
If we now approximates the small regions where the co-motion function switches from the constant to the linear behaviour and those where it diverges (it is sufficient to know each one of such regions, only for one branch as the co-motion is symmetric w.r.t. the axis $y = x$) with sharp angles, we can determine the asymptotic co-motion function

$$f_{\text{mod}}(y) = \begin{cases} a_R & y \leq x_T^{<} \\ m^{<} y + c^{<} & x_T^{<} < y < a_R \\ \infty & y = a_R{}^{1} \\ m^{>} y + c^{>} & a_R < y \leq x_T^{>} \\ a_R & y > x_T^{>} \end{cases} \tag{B.1}$$

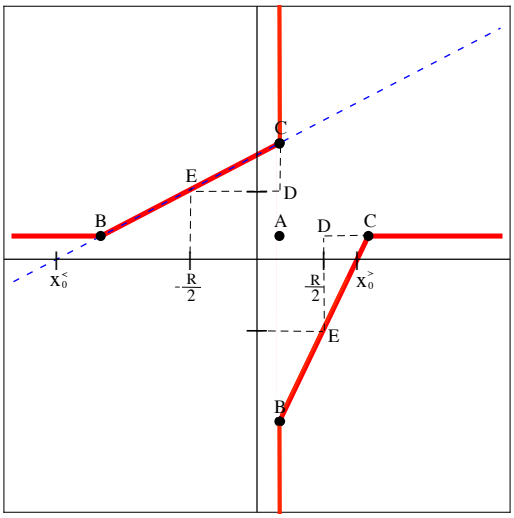

Figure B.1: Asymptotic co-motion function of eq B.1.

where $x_T^<$ ($x_T^>$) is the distance at which the co-motion function switches from constant (linear) to linear (constant), while $c^<$ ($c^>$) is the constant shifting the zero of the linear region to the negative (positive) x- axis.

Assuming that eq B.1 is a good model for the co-motion, we need very few considerations to determine all the quantities needed to calculate the SCE potential and its response part from it.
In particular, considering the two identical right triangles ABC plotted in fig B.1, where the point A is $A = \{a_R, a_R\}$, we can determine their catheti $\overline{AB}$ and $\overline{AC}$ from

$$\begin{cases} \overline{AB}\left(\overline{AC}\right)^{-1} &= \frac{a}{b} \\ \overline{AB} + \overline{AC} &= 2R \end{cases} \tag{B.2}$$

where the first equation follows directly from eq 6.53, while the second is an extension of the discussion contained in section 6.5.2, but it takes a bit more of details to support it.
When the reference electron is situated slightly off $-\frac{R}{2}$, say $-\frac{R}{2}+\epsilon$ the second electron will be displaced by an amount $\frac{b}{a}\epsilon$ by the property of the right triangles.[2]

[1] We can arbitrarily pick a side, namely if $f_{\text{mod}}(a_R) = \infty$ or $f_{\text{mod}}(a_R) = -\infty$. The same is true for the inequalities, where we can arbitrarily decide whether $f_{\text{mod}}(x_T^<) = a_R$ or $f_{\text{mod}}(x_T^<) = m^< y + c^<$. Such single points choices do not affect the SCE Hartree XC potential as it is obtained from an integral expression containing f_{mod} nor they affect the SCE response potential, as long as $f_{\text{mod}}(a_R)$ diverges.
[2] And using physical arguments: because the density is less diffuse in the right fragment, the displace-

Let us now consider the displacement from $-\frac{R}{2}$ to a_R, corresponding to the $\overline{\mathrm{DE}}$ segment in fig B.1.
The co-motion then increases by an amount $\frac{b}{a}\left(\frac{R}{2}+a_R\right)$ (the $\overline{\mathrm{DC}}$ segment in the figure).
On the other hand, because of its symmetry, the displacement of the co-motion on one branch corresponds to the displacement of the variable of the reference electron on the other branch. Furthermore, what happens from $-\frac{R}{2}$ "*onward*" must be mirrored by what happens from $-\frac{R}{2}$ "*backward*" bringing us to the conclusion that the segment $\overline{\mathrm{AB}}+\overline{\mathrm{AC}}=2\left(\left(1+\frac{b}{a}\right)\frac{R}{2}+\left(1+\frac{b}{a}\right)a_R\right)=2R$.
Once $\overline{\mathrm{AB}}$ and $\overline{\mathrm{AC}}$ are known, evaluating all the quantities specifying the asymptotic co-motion in eq B.1 is just a matter of basic trigonometry, providing

$$\begin{aligned} x_T^< &= -(\overline{\mathrm{AB}}-a_R) \\ x_T^> &= a_R+\overline{\mathrm{AC}} \\ x_0^< &= x_T^<-\frac{a}{b}a_R \\ x_0^> &= x_T^>-\frac{b}{a}a_R \\ c^< &= -m^< x_0^< \\ c^> &= -m^> x_0^> \end{aligned} \tag{B.3}$$

where $x_0^<$ ($x_0^>$) is the zero of the function $m^< x+c^<$ ($m^> x+c^>$), see fig B.1.

Table B.1: Values of the maximum of v_{Hxc}^{SCE} for the density in eq 6.45 and the parameters $a=2$, $b=1$ at different internuclear distance, R.

R	$v_{Hxc}^{\mathrm{SCE}}(a_R)$ numerical	modelled
3	0.684	0.75
8	0.278	0.281
11	0.203	0.205
14	0.160	0.161
17	0.132	0.132
20	0.113	0.113

The modelled Hartree XC SCE potential, $v_{Hxc,\mathrm{mod}}^{\mathrm{SCE}}$, obtained from $v_{Hxc,\mathrm{mod}}^{\mathrm{SCE}}(x)=-\int_{-\infty}^{x}\left(f_{\mathrm{mod}}(y)-y\right)^{-2}\mathrm{d}y$ (see eq 3.15), compares nicely with the numerically exact

ment has to be rescaled such that the chunk of density between the two electron positions integrate always to one (eq 3.33).

one as shown in the right colum of fig B.2. In addition to the profile of the modelled potential, we report in table B.1, the values obtained for the maximum, which is the most delicate point.

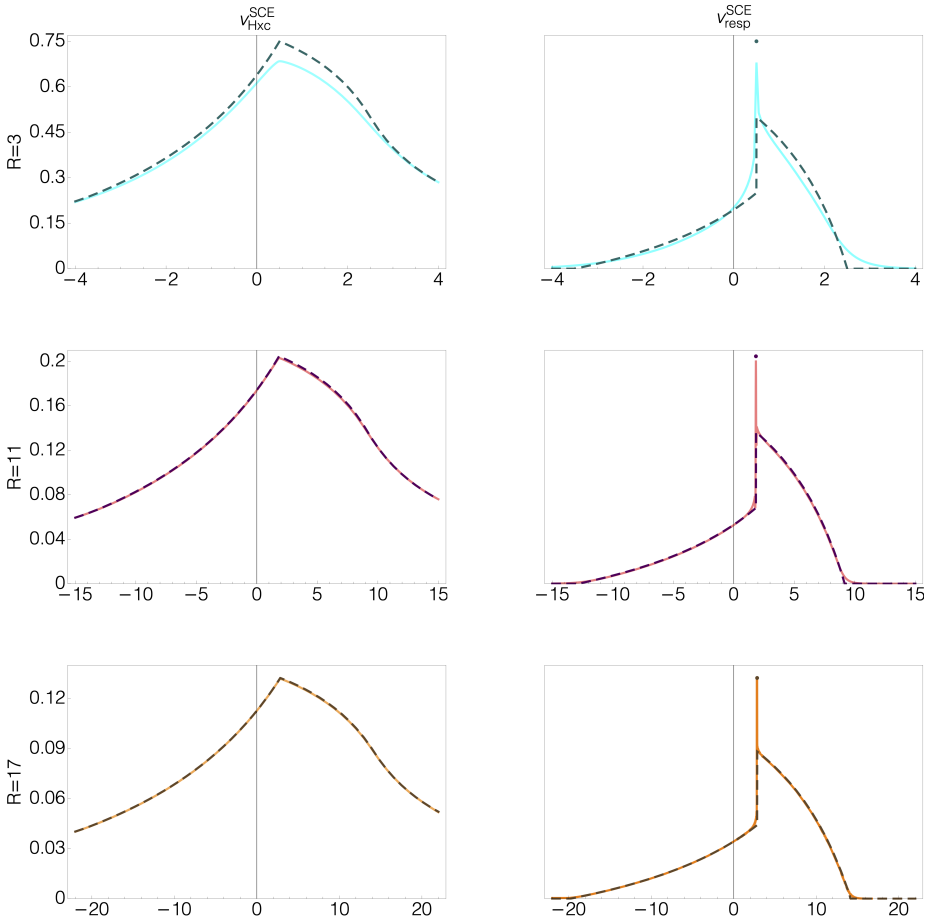

Figure B.2: Comparison of between the numerical (thick) and the modelled (dashed) v_{Hxc}^{SCE} (right) and the numerical (thick) and the modelled (dashed) v_{resp}^{SCE} at different internuclear distances. Notice that, because within the model the local behaviour of the co-motion around the divergence is not treated, the response potential $v_{resp}^{SCE}(x)$ shows a pointwise jump in $x = a_R$.

The analytical expression for the dependence of the maximum of the Hartree

XC SCE we obtain is

$$v_{Hxc}^{\mathrm{SCE}}(a_R) = \frac{(a+b)^2}{2\,a\,b\,R} \tag{B.4}$$

Equation B.4 shows that when the two fragment densities are equal, the maximum value decreases like $\frac{2}{R}$. In the right column of fig B.2, we report the comparison between the modelled and the numerical SCE response potentials, obtained from eq 6.48. It is quite interesting to notice that the SCE response potential resulting from our model co-motion (eq B.1) shows a pointwise jump in $x = a_R$. It is evident that, in order to correctly describe how this potential behaves around its maximum, we need to include also the knowledge of how the co-motion function diverges, while this information is not needed in the case of the maximum of the SCE Hartree XC potential. Nonetheless, our modelled SCE response potential correctly integrates to exactly one as it should (see discussion in chapter 7).
Moreover, excluding for a moment the point $f_{\mathrm{mod}}(a_r) = \infty$ from our model co-motion, we can evaluate the analytical behaviour of the step structure of the modelled SCE response potential, $v_{resp,\mathrm{mod}}^{\mathrm{SCE}}$, i.e. the difference from its left and right limits towards a_R, getting

$$\left| \lim_{x \to a_R^+} v_{resp,\mathrm{mod}}^{\mathrm{SCE}}(x) - \lim_{x \to a_R^-} v_{resp,\mathrm{mod}}^{\mathrm{SCE}}(x) \right| = \frac{a^2 - b^2}{2\,a\,b\,R}. \tag{B.5}$$

C

The Hooke's atom series

The Hooke's atom series consists of two electrons bound by an harmonic external potential, with hamiltonian

$$\hat{H} = -\frac{1}{2}\left(\nabla_1^2 + \nabla_2^2\right) + \frac{\omega^2}{2}\left(r_1^2 + r_2^2\right) + \frac{1}{r_{12}}, \tag{C.1}$$

with $r_i = |\mathbf{r}_i|$ and $r_{12} = |\mathbf{r}_1 - \mathbf{r}_2|$. At large ω the system has high-density and is in the weakly correlated regime, which can be fully described by using the scaled coordinates $\mathbf{s}_i \equiv \sqrt{\omega}\,\mathbf{r}_i$, while as $\omega \to 0$ the system becomes more and more correlated [296], and the relevant scaled variables are $\tilde{\mathbf{s}}_i \equiv \omega^{2/3}\,\mathbf{r}_i$.

As well known, there is an infinite set of special values of ω for which the hamiltonian (C.1) is analytically solvable [287] once rewritten in terms of center of mass and relative coordinates. These analytic solutions have the center of mass in the ground-state of an harmonic oscillator with mass $m = 2$ and frequency $\sqrt{2}\omega$, and the relative coordinate in an s-wave with the radial part described by a gaussian times a polynomial [287]. We denote here the various analytic solutions with the degree $n-1$ of the polynomial in r_{12}. At $n = 1$ we have the non-interacting system, and as n increases the system becomes more and more correlated, with ω smaller and smaller [287]. The values of ω corresponding to $l = 0$ and the different values of n considered in chapter 8 are reported in Table C.1.

In fig C.1 we plot the scaled densities for the different Hooke's atom up to $n = 6$. Notice that , while for $n = 2,3$ along the series, the maximum of the density is situated at the origin, for $n > 3$ it is found at some positive distance and at the origin the density shows its minimum (a situation sometimes referred to as "cusp catastrophe" [296]).

Table C.1: Values of ω for the various analytic solutions of the hamiltonian of Eq. (C.1) considered here, corresponding to $l = 0$ and different degrees $n-1$ of the polynomial in the solution for the relative coordinate r_{12} [287].

n	ω
2	$1/2$
3	$1/10$
4	$\frac{1}{24}\left(5-\sqrt{17}\right)$
5	$\frac{1}{712}\left(35-3\sqrt{57}\right)$
6	$\frac{191-\sqrt{25141}\left(\sqrt{3}\sin\left(\frac{1}{3}\tan^{-1}\left(\frac{1458\sqrt{262235}}{3915791}\right)\right)+\cos\left(\frac{1}{3}\tan^{-1}\left(\frac{1458\sqrt{262235}}{3915791}\right)\right)\right)}{1620}$

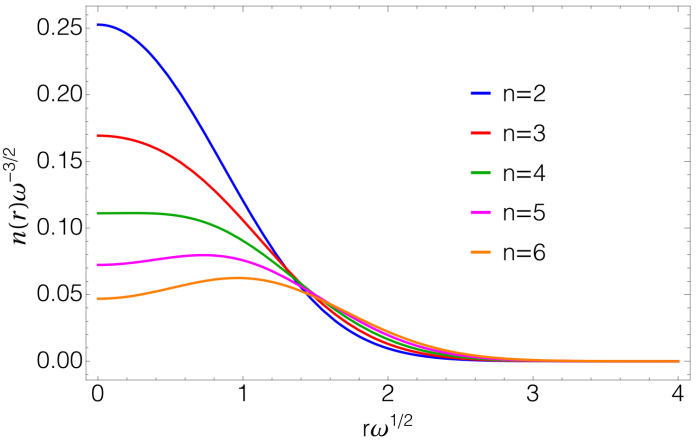

Figure C.1: Scaled densities for the Hooke's atom series with $n = 2,\ldots,6$

Summary

The results comprised in this thesis move along a diverse path exploring both approximations and exact properties of density functionals and support the significance of the strong-interaction limit of DFT (and possibly also of HF theory) in the development of approximate density functionals. Few considerations on such results, together with future directions that can be envisaged from them, are in order in this summary.

The assessment of model density functionals, based on interpolations along the adiabatic connection and containing the strong-interaction limit ingredient, on cases which are typically challenging for standard density functionals, such as gold and silver metal clusters, has shown that this class of functionals deserves further studies. A self-consistent (SC) implementation seems due to definitely assess their quality. However, we remind that they are complicated nonlinear functionals of the Kohn–Sham orbitals and eigenvalues making their efficient SC implementation a hard task. This is the object of ongoing work. A further complication towards their application in a SC procedure is that they typically contain a piece in the XC potential which is diverging asymptotically [6]. Such behaviour comes from the fact that the $\lambda \to \infty$ limit energy functional is usually approximated by the much cheaper semilocal expression derived within the pointcharge-plus-continuum (PC) model, which is a gradient expansion and should therefore be somehow "renormalized" to avoid asymptotic divergence. More in general, efforts should be made in the direction of making them applicable for routinely calculations, while preserving their non-empirical character.

At the same time, the outcome that such interpolations, approximating the XC energy in a post-SC scheme, are optimal when used as corrections to the HF uncorrelated energy, triggered a study on the strong-interaction limit in this theory. Several aspects need now to be understood about the different properties of the HF adiabatic connection curve as compared to the DFT one in order to be able to properly transfer DFT strategies into this context. In some sense, the strong-interaction limit in the HF adiabatic connection seems simpler, thanks to the lack of the density constraint. Nevertheless, it could be useful to devise an approximate model similar to the PC one also for this reference system, especially in view of approximating the zero-point oscillations energy term, entering at order $\sqrt{\lambda}$ as in the DFT case but looking quite more complex, due to the presence of the exchange energy operator, absent in DFT.

On a parallel track, we focused on digging out exact properties of the XC potential. In particular, we have connected two decompositions of the exact XC potential,

i.e. the one coming from the conditional amplitude formalism and the one coming from integrating λ-dependent local potentials along the adiabatic connection, showing their different redistribution among terms having physically transparent meanings (see eq 6.58 and fig 6.13). Furthermore, we have derived the SCE response potential and compared it to the exact one, finding that, although the SCE description lacks the fundamental kinetic correlation component, the structure of its response potential mimics certain features of the exact one closer than approximations where the kinetic correlation component is accounted for (see fig 6.10 and eq B.5). We attribute this capability to a distinctive feature of all SCE functionals, that is their dependence on *integrals* of the density, typically absent from the Jacob's ladder narrative. Future directions inspired by such findings include modeling the missing kinetic correlation component in terms of functionals that depend on the distances at which the (spherically averaged) density integrates to an integer, within the quite recently proposed multiple-radii approach [109, 110].

Germane to the need for a more accurate description of the kinetic correlation component, the project presented in the last chapter and motivated by recent results on a lattice [275] explores the idea of introducing a position-dependent mass that could tune the kinetic energy density of a non-interacting system with that of the interacting one. However, the ulterior scalar potential embodied in the mass introduces a variety of possibilities on how to set up the theory, which we have partially explored and tested on model and simple chemical systems. At the state of the art, several questions are still open, both at the fundamental and at the computational level, and further investigations are needed before assessing if and how the introduction of a position-dependent mass can improve the description of the kinetic correlation within KS-DFT.

Acknowledgements

In the past four years, I have had the chance to be inspired by several outstanding scientists working in the Department of Theoretical Chemistry of this university: by Paola, my promotor, in the first place.

She gave me the opportunity to be immersed in the rare mixture of extraordinary expertises that characterises herself, as well as the group as a whole at a higher scale – and I am grateful for it.

I also would like to thank some more people that gave me a hand walking through this experience in one way or another.

Klaas, my copromotor, especially for getting intrigued by my conjecture and making it grow into a paper. Frieda, who has always been extremely kind and offered me her help with some bureaucracy when I really needed it. Eduardo and Fabio, who hosted me in Lecce and made me feel welcomed. Augusto who arrived 'late' in the group but has been a greatly comforting element. Ziad who trusted me immediately for no apparent reason. Lenka who helped me choosing the dress for my sister's wedding when I was starting panicking. My sister, Silvia, for her help with the cover.

I should also thank two gems of Amsterdam: Henk, who is probably the most pedagogical (Tai chi) teacher on Earth, and Jeffrey, whose strenuous cultural activism is simply moving [297]. I thank my psychotherapist Vittorio. He gave me his friendship and also his most needed technical help. I want to thank Juri and Derk, who were my companions along the path since the start.

I want to thank Juri for staying close to me for all this time, for all his support.

You kept reminding me things about myself I kept overlooking.

Flavio, Megghi, Silvia, Eugenia, Anita, Niki, Albi, Mario, Vincenzo, Luca, Iga, Francesco, Daniele, Ayush, Souloke, Tim, Cami, Marta, Maria, Rosa, Denise, Stephanie, Laureen, Stefan, Jelena, Maggie, Martina, Marco, Angela, Roberta, Ciccio, Giovanna, Andrea, Mario, Bianca Maria... Thank you.

Finally, I would like to go a little bit off the conventional track and 'acknowledge' some bad things that were present too.

My Ph.D. experience started with a twisted ankle and ended with a broken arm. Metaphorically speaking, these events represent pretty well the dose of pain that came along with it.

There were, I think, two kinds of causes: on one side, the general state of academic environment, whose 'toxicity' is being gradually recognised (see e.g. ref-

erences [298, 299], where the focus is on the conditions of the Ph.D. students population).

On the other side, a set of specific circumstances concerning my individual experience: the VU administration, my condition of immigrant/expat in Amsterdam, my own character finding relatively few matches, etc.

I am not entering into details, but I would like to make a cross-cutting point I truly care about: most of it was *unnecessary* pain.

I emphasise the word *unnecessary* in contrast with the tendency, very common also in Academia, to idolise 'resilience' and turn the story around by saying that you need pain to strengthen up. In fairness, I find such argument dishonest, coward and perverse. Notwithstanding the importance of being resilient, I find that the (ab)use of its concept is disruptive and reactionary as it lessens the seriousness of the problems at stake and somehow denies there being a need (and room) for improvement.

List of Publications

[1] S. Giarrusso, P. Gori-Giorgi, F. Della Sala, and E. Fabiano, *Assessment of interaction-strength interpolation formulas for gold and silver clusters,* J. Chem. Phys. **148**, 134106 (2018).

[2] S. Giarrusso, S. Vuckovic, and P. Gori-Giorgi, *Response potential in the strong-interaction limit of DFT: Analysis and comparison with the coupling-constant average,* J. Chem. Theory Comput. **14**, 4151 (2018).

[3] S. Giarrusso, P. Gori-Giorgi, and K. J. Giesbertz, *Sum-rules of the response potential in the strongly-interacting limit of DFT,* Eur. Phys. J. B **91**, 186 (2018).

[4] M. Seidl, S. Giarrusso, S. Vuckovic, E. Fabiano, and P. Gori-Giorgi, *Communication: Strong-interaction limit of an adiabatic connection in Hartree-Fock theory,* J. Chem. Phys. **149**, 241101 (2018).

[5] E. Fabiano, S. Smiga, S. Giarrusso, T. J. Daas, F. Della Sala, I. Grabowski, and P. Gori-Giorgi, *Investigation of the exchange-correlation potentials of functionals based on the adiabatic connection interpolation,* J. Chem. Theory Comput. **15**, 1006 (2019).

[6] S. Giarrusso and P. Gori-Giorgi, *Exchange-correlation energy densities and response potentials: Connection between two definitions and analytical model for the strong-coupling limit of a stretched bond,* submitted to J. Phys. Chem. A (2019), 10.26434/chemrxiv.10283678.v1.

Bibliography

[1] K. Sharkas, J. Toulouse, and A. Savin, *Double-hybrid density-functional theory made rigorous,* J. Chem. Phys. **134**, 064113 (2011).

[2] S. Ghosh, P. Verma, C. J. Cramer, L. Gagliardi, and D. G. Truhlar, *Combining wave function methods with density functional theory for excited states,* Chem. Rev. **118**, 7249 (2018).

[3] S. Vuckovic, S. Song, J. Kozlowski, E. Sim, and K. Burke, *Density functional analysis: The theory of density-corrected DFT,* J. Chem. Theory. Comput. (2019).

[4] E. Fabiano, P. Gori-Giorgi, M. Seidl, and F. Della Sala, *Interaction-strength interpolation method for main-group chemistry: Benchmarking, limitations, and perspectives,* J. Chem. Theory. Comput. **12**, 4885 (2016).

[5] L. A. Constantin, *Correlation energy functionals from adiabatic connection formalism,* Phys. Rev. B **99**, 085117 (2019).

[6] E. Fabiano, S. Smiga, S. Giarrusso, T. J. Daas, F. Della Sala, I. Grabowski, and P. Gori-Giorgi, *Investigation of the exchange-correlation potentials of functionals based on the adiabatic connection interpolation,* J. Chem. Theory Comput. **15**, 1006 (2019).

[7] S. Vuckovic, P. Gori-Giorgi, F. Della Sala, and E. Fabiano, *Restoring size consistency of approximate functionals constructed from the adiabatic connection,* J. Phys. Chem. Lett. **9**, 3137 (2018).

[8] P. Hohenberg and W. Kohn, *Inhomogeneous electron gas,* Phys. Rev. **136**, B 864 (1964).

[9] G. Stefanucci and R. Van Leeuwen, *Nonequilibrium many-body theory of quantum systems: a modern introduction* (Cambridge University Press, 2013).

[10] L. H. Thomas, *The calculation of atomic fields,* Mathematical Proceedings of the Cambridge Philosophical Society **23**, 542 (1927).

[11] E. Fermi, *Statistical method to determine some properties of atoms,* Rend. Accad. Naz. Lincei **6**, 5 (1927).

[12] J. C. Slater, *A simplification of the hartree-fock method,* Phys. Rev. **81**, 385 (1951).

[13] D. J. Tozer, V. E. Ingamells, and N. C. Handy, *Exchange-correlation potentials,* J. Chem. Phys. **105**, 9200 (1996).

[14] N. C. Handy, *The importance of colle–salvetti for computational density functional theory,* Theor. Chim. Acc. **123**, 165 (2009).

[15] E. Engel and R. M. Dreizler, *Density Functional Theory: An Advanced Course* (Springer, 2011).

[16] W. Kohn, *Highlights of condensed-matter theory,* in *Proceedings of the international school of physics "Enrico Fermi", Course LXXXIX*, edited by F. Bassani, F. Fumi, and M. P. Tosi (North Holland, Amsterdam, 1983) p. 1.

[17] R. van Leeuwen, *Density functional approach to the many-body problem: key concepts and exact functionals,* Adv. Quantum Chem. **43**, 24 (2003).

[18] A. Pribram-Jones, S. Pittalis, E. Gross, and K. Burke, *Thermal density functional theory in context,* in *Frontiers and Challenges in Warm Dense Matter*, edited by F. Graziani, M. P. Desjarlais, R. Redmer, and S. B. Trickey (Springer, 2014) pp. 25–60.

[19] M. Levy, *Universal variational functionals of electron densities, first-order density matrices, and natural spin-orbitals and solution of the v-representability problem,* Proc. Natl. Acad. Sci. **76**, 6062 (1979).

[20] M. Levy, *Electron densities in search of hamiltonians,* Phys. Rev. A **26**, 1200 (1982).

[21] E. H. Lieb, *Density functionals for Coulomb systems,* Int. J. Quantum. Chem. **24**, 243 (1983).

[22] J. E. Harriman, *Orthonormal orbitals for the representation of an arbitrary density,* Phys. Rev. A **24**, 680 (1981).

[23] W. Kohn and L. J. Sham, *Self-consistent equations including exchange and correlation effects,* Phys. Rev. **140**, A 1133 (1965).

[24] S. Kvaal, U. Ekström, A. M. Teale, and T. Helgaker, *Differentiable but exact formulation of density-functional theory,* J. Chem. Phys. **140**, 18A518 (2014).

[25] P. R. T. Schipper, O. V. Gritsenko, and E. J.Baerends, *One-determinantal pure state versus ensemble Kohn-Sham solutions in the case of strong electron correlation: CH2 and C2,* Theor. Chim. Acc. **99**, 329 (1998).

[26] K. Giesbertz and E. Baerends, *Aufbau derived from a unified treatment of occupation numbers in Hartree–Fock, Kohn–Sham , and natural orbital theories with the Karush–Kuhn–Tucker conditions for the inequality constraints ni≤ 1 and ni≥ 0,* J. Chem. Phys. **132**, 194108 (2010).

[27] J. Harris and R. Jones, *The surface energy of a bounded electron gas,* J. Phys. F: Met. Phys. **4**, 1170 (1974).

[28] O. Gunnarsson and B. I. Lundqvist, *Exchange and correlation in atoms, molecules, and solids by the spin-density-functional formalism,* Phys. Rev. B **13**, 4274 (1976).

[29] D. C. Langreth and J. P. Perdew, *The exchange-correlation energy of a metallic surface,* Solid. State Commun. **17**, 1425 (1975).

[30] D. C. Langreth, *New theoretical support for density-functional theory as commonly applied,* Phys. Rev. Lett. **52**, 2317 (1984).

[31] M. Levy and J. P. Perdew, *Hellmann–Feynman, virial, and scaling requisites for the exact universal density functionals. shape of the correlation potential and diamagnetic susceptibility for atoms,* Phys. Rev. A **32**, 2010 (1985).

[32] A. Görling and M. Levy, *Correlation-energy functional and its high-density limit obtained from a coupling-constant perturbation expansion,* Phys. Rev. B **47**, 13105 (1993).

[33] J. D. Talman and W. F. Shadwick, *Optimized effective atomic central potential,* Phys. Rev. A **14**, 36 (1976).

[34] P. Gori-Giorgi, G. Vignale, and M. Seidl, *Electronic zero-point oscillations in the strong-interaction limit of density functional theory,* J. Chem. Theory Comput. **5**, 743 (2009).

[35] E. H. Lieb and S. Oxford, *Improved lower bound on the indirect coulomb energy,* Int. J. Quantum. Chem. **19**, 427 (1981).

[36] M. Lewin, E. H. Lieb, and R. Seiringer, *A floating wigner crystal with no boundary charge fluctuations,* arXiv preprint arXiv:1905.09138 (2019).

[37] G. K.-L. Chan and N. C. Handy, *Optimized lieb-oxford bound for the exchange-correlation energy,* Phys. Rev. A **59**, 3075 (1999).

[38] M. Levy and J. P. Perdew, *Tight bound and convexity constraint on the exchange-correlation-energy functional in the low-density limit, and other formal tests of generalized-gradient approximations,* Phys. Rev. B **48**, 11638 (1993).

[39] G. Hunter, *Conditional probability amplitudes in wave mechanics,* Int. J. Quantum Chem. **9**, 237 (1975).

[40] G. Hunter, *Ionization potentials and conditional amplitudes,* Int. J. Quantum Chem. Symp. **9**, 311 (1975).

[41] M. Levy, J. P. Perdew, and V. Sahni, *Exact differential equation for the density and ionization energy of a many-particle system,* Phys. Rev. A **30**, 2745 (1984).

[42] M. A. Buijse, E. J. Baerends, and J. G. Snijders, *Analysis of correlation in terms of exact local potentials: Applications to two-electron systems,* Phys. Rev. A **40**, 4190 (1989).

[43] J. Katriel and E. R. Davidson, *Asymptotic behavior of atomic and molecular wave functions,* Proc. Natl. Acad. Sci. USA **77**, 4403 (1980).

[44] P. Gori-Giorgi, T. Gál, and E. J. Baerends, *Asymptotic behaviour of the electron density and the Kohn–Sham potential in case of a Kohn-Sham HOMO nodal plane,* Mol. Phys. **114**, 1086 (2016).

[45] P. Gori-Giorgi and E. J. Baerends, *Asymptotic nodal planes in the electron density and the potential in the effective equation for the square root of the density,* Eur. Phys. J. B **91**, 160 (2018).

[46] O. V. Gritsenko and E. J. Baerends, *Effect of molecular dissociation on the exchange-correlation Kohn-Sham potential,* Phys. Rev. A **54**, 1957 (1996).

[47] O. V. Gritsenko, R. van Leeuwen, and E. J. Baerends, *Molecular exchange-correlation Kohn-Sham potential and energy density from ab initio first- and second-order density matrices: Examples for XH (X= Li, B, F),* J. Chem. Phys. **104**, 8535 (1996).

[48] E. J. Baerends and O. V. Gritsenko, *A quantum chemical view of density functional theory,* J. Phys. Chem. A **101**, 5383 (1997).

[49] C.-O. Almbladh and U. von Barth, *Exact results for the charge and spin densities, exchange-correlation and density-functional eigenvalues,* Phys. Rev. B **31**, 3232 (1985).

[50] C. O. Almbladh and U. von Barth, *Density-functional theory and excitation energies,* in *Density functional methods in physics*, edited by R. M. Dreizler and J. da Providência (Springer, 1985) pp. 209–231.

[51] D. G. Tempel, T. J. Martínez, and N. T. Maitra, *Revisiting molecular dissociation in density functional theory: A simple model,* J. Chem. Theory. Comput. **5**, 770 (2009).

[52] S. V. Kohut, A. M. Polgar, and V. N. Staroverov, *Origin of the step structure of molecular exchange–correlation potentials,* Phys. Chem. Chem. Phys. **18**, 20938 (2016).

[53] R. van Leeuwen and E. J. Baerends, *An analysis of nonlocal density functionals in chemical bonding,* Int. J. Quantum Chem. **52**, 711 (1994).

[54] N. Helbig, I. V. Tokatly, and A. Rubio, *Exact Kohn–Sham potential of strongly correlated finite systems,* J. Chem. Phys. **131**, 224105 (2009).

[55] Z.-J. Ying, V. Brosco, G. M. Lopez, D. Varsano, P. Gori-Giorgi, and J. Lorenzana, *Anomalous scaling and breakdown of conventional density functional theory methods for the description of mott phenomena and stretched bonds,* Phys. Rev. B **94**, 075154 (2016).

[56] N. T. Maitra, *Undoing static correlation: Long-range charge transfer in time-dependent density-functional theory,* J. Chem. Phys. **122**, 234104 (2005).

[57] P. Elliott, J. I. Fuks, A. Rubio, and N. T. Maitra, *Universal dynamical steps in the exact time-dependent exchange-correlation potential,* Phys. Rev. Lett. **109**, 266404 (2012).

[58] R. Van Meer, O. Gritsenko, and E. Baerends, *Physical meaning of virtual Kohn–Sham orbitals and orbital energies: an ideal basis for the description of molecular excitations,* J. Chem. Theory Comput. **10**, 4432 (2014).

[59] O. Gritsenko, Ł. Mentel, and E. Baerends, *On the errors of local density (lda) and generalized gradient (gga) approximations to the Kohn-Sham potential and orbital energies,* J. Chem. Phys. **144**, 204114 (2016).

[60] R. van Leeuwen, *Kohn-Sham potentials in density functional theory*, Academisch proefschrift, Vrije Universiteit van Amsterdam (1994).

[61] R. Cuevas-Saavedra, P. W. Ayers, and V. N. Staroverov, *Kohn–Sham exchange-correlation potentials from second-order reduced density matrices,* J. Chem. Phys. **143**, 244116 (2015).

[62] R. Cuevas-Saavedra and V. N. Staroverov, *Exact expressions for the Kohn–Sham exchange-correlation potential in terms of wave-function-based quantities,* Mol. Phys. **114**, 1050 (2016).

[63] I. G. Ryabinkin, E. Ospadov, and V. N. Staroverov, *Exact exchange-correlation potentials of singlet two-electron systems,* J. Chem. Phys. **147**, 164117 (2017).

[64] O. V. Gritsenko, R. van Leeuwen, E. van Lenthe, and E. J. Baerends, *Self-consistent approximation to the Kohn-Sham exchange potential,* Phys. Rev. A **51**, 1944 (1995).

[65] M. Kuisma, J. Ojanen, J. Enkovaara, and T. T. Rantala, *Kohn-Sham potential with discontinuity for band gap materials,* Phys. Rev. B **82**, 115106 (2010).

[66] S. Giarrusso, S. Vuckovic, and P. Gori-Giorgi, *Response potential in the strong-interaction limit of DFT: Analysis and comparison with the coupling-constant average,* J. Chem. Theory Comput. **14**, 4151 (2018).

[67] N. March, *Differential equation for the ground-state density in finite and extended inhomogeneous electron gases,* Physics Letters A **113**, 66 (1985).

[68] N. March, *The density amplitude $\rho 1/2$ and the potential which generates it,* Journal of Computational Chemistry **8**, 375 (1987).

[69] M. Levy, *Density-functional exchange correlation through coordinate scaling in adiabatic connection and correlation hole,* Phys. Rev. A **43**, 4637 (1991).

[70] L. Sham, *Local exchange approximations and the virial theorem,* Phys. Rev. A **1**, 969 (1970).

[71] M. Seidl, J. P. Perdew, and M. Levy, *Strictly correlated electrons in density-functional theory,* Phys. Rev. A **59**, 51 (1999).

[72] M. Seidl, *Strong-interaction limit of density-functional theory,* Phys. Rev. A **60**, 4387 (1999).

[73] M. Seidl, P. Gori-Giorgi, and A. Savin, *Strictly correlated electrons in density-functional theory: A general formulation with applications to spherical densities,* Phys. Rev. A **75**, 042511/12 (2007).

[74] M. Lewin, *Semi-classical limit of the Levy–Lieb functional in density functional theory,* C. R. Math. **356**, 449 (2018).

[75] C. Cotar, G. Friesecke, and C. Klüppelberg, *Smoothing of transport plans with fixed marginals and rigorous semiclassical limit of the hohenberg–kohn functional,* Arch. Ration. Mech. An. **228**, 891 (2018).

[76] M. Colombo and S. Di Marino, *Equality between monge and kantorovich multimarginal problems with coulomb cost,* Annali di Matematica Pura ed Applicata (1923-) **194**, 307 (2015).

[77] M. Seidl, S. Di Marino, A. Gerolin, L. Nenna, K. J. Giesbertz, and P. Gori-Giorgi, *The strictly-correlated electron functional for spherically symmetric systems revisited,* arXiv preprint arXiv:1702.05022 (2017).

[78] M. Seidl, S. Giarrusso, S. Vuckovic, E. Fabiano, and P. Gori-Giorgi, *Communication: Strong-interaction limit of an adiabatic connection in hartree-fock theory,* J. Chem. Phys. **149**, 241101 (2018).

[79] F. Malet, A. Mirtschink, J. C. Cremon, S. M. Reimann, and P. Gori-Giorgi, *Kohn-Sham density functional theory for quantum wires in arbitrary correlation regimes,* Phys. Rev. B **87**, 115146 (2013).

[80] J. Grossi, D. P. Kooi, K. J. H. Giesbertz, M. Seidl, A. J. Cohen, P. Mori-Sánchez, and P. Gori-Giorgi, *Fermionic statistics in the strongly correlated limit of density functional theory,* J. Chem. Theory Comput. **13**, 6089 (2017).

[81] S. Giarrusso, P. Gori-Giorgi, and K. J. Giesbertz, *Sum-rules of the response potential in the strongly-interacting limit of DFT,* Eur. Phys. J. B **91**, 186 (2018).

[82] A. Mirtschink, M. Seidl, and P. Gori-Giorgi, *Energy densities in the strong-interaction limit of density functional theory,* J. Chem. Theory Comput. **8**, 3097 (2012).

[83] F. Malet and P. Gori-Giorgi, *Strong correlation in Kohn-Sham density functional theory, volume = 109, year = 2012, bdsk-url-1 = https://doi.org/10.1103/PhysRevLett.109.246402,* Phys. Rev. Lett. , 246402.

[84] G. Buttazzo, L. De Pascale, and P. Gori-Giorgi, *Optimal-transport formulation of electronic density-functional theory,* Phys. Rev. A **85**, 062502 (2012).

[85] C. Cotar, G. Friesecke, and C. Klüppelberg, *Density functional theory and optimal transportation with coulomb cost,* Comm. Pure Appl. Math. **66**, 548 (2013).

[86] G. Monge, *Mémoire sur la théorie des déblais et des remblais* (Histoire Acad. Sciences, Paris, 1781).

[87] L. V. Kantorovich, *On the transfer of masses,* Dokl. Akad. Nauk. SSSR. **37**, 227 (1942).

[88] C. Villani, *Topics in Optimal Transportation* (Grad. Stud. Math. **58**, Amer. Math. Soc., Providence, 2003).

[89] M. Colombo, L. De Pascale, and S. Di Marino, *Multimarginal optimal transport maps for one-dimensional repulsive costs,* Canad. J. Math **67**, 350 (2015).

[90] M. Lewin, P. Gori-Giorgi, and B. Pass, *Optimal transport methods in density functional theory,* (1994).

[91] A. M. Teale, S. Coriani, and T. Helgaker, *Accurate calculation and modeling of the adiabatic connection in density functional theory,* J. Chem. Phys. **132**, 164115 (2010).

[92] M. Colombo, S. Di Marino, and F. Stra, *Continuity of multimarginal optimal transport with repulsive cost,* SIAM Journal on Mathematical Analysis **51**, 2903 (2019).

[93] C. B. Mendl, F. Malet, and P. Gori-Giorgi, *Wigner localization in quantum dots from Kohn-Sham density functional theory without symmetry breaking,* Phys. Rev. B **89**, 125106 (2014).

[94] S. Vuckovic, *Fully Nonlocal Exchange-Correlation Functionals from the Strong-coupling limit of Density Functional Theory*, Academisch proefschrift, Vrije Universiteit van Amsterdam (2017).

[95] S. Vuckovic, L. O. Wagner, A. Mirtschink, and P. Gori-Giorgi, *Hydrogen molecule dissociation curve with functionals based on the strictly correlated regime,* J. Chem. Theory Comput. **11**, 3153 (2015).

[96] C. B. Mendl and L. Lin, *Kantorovich dual solution for strictly correlated electrons in atoms and molecules,* Phys. Rev. B **87**, 125106 (2013).

[97] G. Friesecke and D. Vögler, *Breaking the curse of dimension in multi-marginal kantorovich optimal transport on finite state spaces,* SIAM Journal on Mathematical Analysis **50**, 3996 (2018).

[98] Y. Khoo and L. Ying, *Convex relaxation approaches for strictly correlated density functional theory,* SIAM Journal on Scientific Computing **41**, B773 (2019).

[99] J.-D. Benamou, G. Carlier, M. Cuturi, L. Nenna, and G. Peyré, *Iterative bregman projections for regularized transportation problems,* SIAM J. on Sci. Comput. **37**, A1111 (2015).

[100] J.-D. Benamou, G. Carlier, and L. Nenna, *A numerical method to solve multi-marginal optimal transport problems with coulomb cost,* in *Splitting Methods in Communication, Imaging, Science, and Engineering* (Springer, 2016) pp. 577–601.

[101] M. Cuturi, *Sinkhorn distances: Lightspeed computation of optimal transport,* in *Advances in neural information processing systems* (2013) pp. 2292–2300.

[102] P. Gori-Giorgi and M. Seidl, *Density functional theory for strongly-interacting electrons: perspectives for physics and chemistry,* Phys. Chem. Chem. Phys **12**, 14405 (2010).

[103] F. Malet, A. Mirtschink, C. B. Mendl, J. Bjerlin, E. O. Karabulut, S. M. Reimann, and P. Gori-Giorgi, *Density-functional theory for strongly correlated bosonic and fermionic ultracold dipolar and ionic gases,* Phys. Rev. Lett. **115**, 033006 (2015).

[104] F. Malet, A. Mirtschink, K. J. H. Giesbertz, L. O. Wagner, and P. Gori-Giorgi, *Exchange-correlation functionals from the strong interaction limit of DFT: applications to model chemical systems,* Phys. Chem. Chem. Phys. **16**, 14551 (2014).

[105] A. Mirtschink, M. Seidl, and P. Gori-Giorgi, *The derivative discontinuity in the strong-interaction limit of density functional theory,* Phys. Rev. Lett. **111**, 126402 (2013).

[106] A. Mirtschink, C. J. Umrigar, J. D. Morgan III, and P. Gori-Giorgi, *Energy density functionals from the strong-coupling limit applied to the anions of the he isoelectronic series,* J. Chem. Phys. **140**, 18A532 (2014).

[107] P. Gori-Giorgi, J. G. Angyan, and A. Savin, *Charge density reconstitution from approximate exchange-correlation holes,* Canad. J. of Chem. **87**, 1444 (2009).

[108] M. Seidl, S. Vuckovic, and P. Gori-Giorgi, *Challenging the lieb–oxford bound in a systematic way,* Mol. Phys. **114**, 1076 (2016).

[109] S. Vuckovic and P. Gori-Giorgi, *Simple fully nonlocal density functionals for electronic repulsion energy,* J. Phys. Chem. Lett. **8**, 2799 (2017), pMID: 28581751.

[110] S. Vuckovic, *Density functionals from the multiple-radii approach: analysis and recovery of the kinetic correlation energy,* J. Chem. Theory Comput. (2019).

[111] S. Vuckovic and T. Gould, *Range-separation and the multiple radii functional approximation inspired by the strongly interacting limit of density functional theory,* (2019).

[112] A. D. Becke, *A new mixing of Hartree–Fock and local density-functional theories,* J. Chem. Phys. **98**, 1372 (1993).

[113] A. D. Becke, *Density-functional thermochemistry. III. the role of exact exchange,* J. Chem. Phys. **98**, 5648 (1993).

[114] M. Ernzerhof, *Construction of the adiabatic connection,* Chem. Phys. Lett. **263**, 499 (1996).

[115] G. A. Baker, *Essentials of Padé approximants* (academic press, 1975).

[116] M. Seidl, J. P. Perdew, and S. Kurth, *Simulation of all-order density-functional perturbation theory, using the second order and the strong-correlation limit,* Phys. Rev. Lett. **84**, 5070 (2000).

[117] M. Seidl, J. P. Perdew, and S. Kurth, *Density functionals for the strong-interaction limit,* Phys. Rev. A **62**, 012502 (2000).

[118] Z.-F. Liu and K. Burke, *Adiabatic connection in the low-density limit,* Phys. Rev. A **79**, 064503 (2009).

[119] E. Fabiano, P. Gori-Giorgi, M. Seidl, and F. Della Sala, *Interaction-strength interpolation method for main-group chemistry: Benchmarking, limitations, and perspectives,* J. Chem. Theory Comput. **12**, 4885 (2016).

[120] S. Giarrusso, P. Gori-Giorgi, F. Della Sala, and E. Fabiano, *Assessment of interaction-strength interpolation formulas for gold and silver clusters,* J. Chem. Phys. **148**, 134106 (2018).

[121] S. Vuckovic, T. J. P. Irons, A. Savin, A. M. Teale, and P. Gori-Giorgi, *Exchange–correlation functionals via local interpolation along the adiabatic connection,* J. Chem. Theory Comput. **12**, 2598 (2016).

[122] D. P. Kooi and P. Gori-Giorgi, *Local and global interpolations along the adiabatic connection of DFT: a study at different correlation regimes,* Theor. Chim. Acc. **137**, 166 (2018).

[123] J. P. Perdew, S. Kurth, A. Zupan, and P. Blaha, Phys. Rev. Lett. **82**, 2544 (1999).

[124] M. Seidl, J. P. Perdew, and S. Kurth, *Erratum: Density functionals for the strong-interaction limit [Phys. Rev. A 62, 012502 (2000)],* Phys. Rev. A **72**, 029904(E) (2005).

[125] P. Gori-Giorgi and A. Savin, *Degeneracy and size consistency in electronic density functional theory,* in *Journal of Physics: Conference Series*, Vol. 117 (IOP Publishing, 2008) p. 012017.

[126] A. Savin, *Is size-consistency possible with density functional approximations?* Chemical Physics **356**, 91 (2009).

[127] S. Vuckovic, P. Gori-Giorgi, F. Della Sala, and E. Fabiano, *Restoring size consistency of approximate functionals constructed from the adiabatic connection,* J. Phys. Chem. Lett. **9**, 3137 (2018).

[128] H. Schmidbaur, *The fascinating implications of new results in gold chemistry,* Gold Bulletin **23**, 11 (1990).

[129] M.-C. Daniel and D. Astruc, *Gold nanoparticles: assembly, supramolecular chemistry, quantum-size-related properties, and applications toward biology, catalysis, and nanotechnology,* Chemical Reviews **104**, 293 (2004).

[130] P. Pyykkö, *Theoretical chemistry of gold,* Angew. Chem. Int. Ed. **43**, 4412 (2004).

[131] P. Pyykkö, *Theoretical chemistry of gold. II,* Inorganica Chimica Acta **358**, 4113 (2005), protagonists in chemistry - Hubert Schmidbaur.

[132] P. Pyykkö, *Theoretical chemistry of gold. III,* Chem. Soc. Rev. **37**, 1967 (2008).

[133] V. W.-W. Yam and E. C.-C. Cheng, *Highlights on the recent advances in gold chemistry-a photophysical perspective,* Chem. Soc. Rev. **37**, 1806 (2008).

[134] G. J. Hutchings, M. Brust, and H. Schmidbaur, *Gold-an introductory perspective,* Chem. Soc. Rev. **37**, 1759 (2008).

[135] S. Yamazoe, K. Koyasu, and T. Tsukuda, *Nonscalable oxidation catalysis of gold clusters,* Accounts of Chemical Research **47**, 816 (2014).

[136] T. Ayako and H. Masatake, *Size- and structure-specificity in catalysis by gold clusters,* Chemistry Letters **43**, 380 (2014).

[137] C. Louis and O. Pluchery, eds., *Gold Nanoparticles for Physics, Chemistry and Biology* (World Scientific, Singapore, 2017).

[138] M. Haruta, *Gold as a novel catalyst in the 21st century: Preparation, working mechanism and applications,* Gold Bulletin **37**, 27 (2004).

[139] T. Takei, T. Akita, I. Nakamura, T. Fujitani, M. Okumura, K. Okazaki, J. Huang, T. Ishida, and M. Haruta, *Chapter one - heterogeneous catalysis by gold,* (Academic Press, 2012) pp. 1 – 126.

[140] T. Ishida, H. Koga, M. Okumura, and M. Haruta, *Advances in gold catalysis and understanding the catalytic mechanism,* The Chemical Record **16**, 2278 (2016).

[141] A. Mathew and T. Pradeep, *Noble metal clusters: Applications in energy, environment, and biology,* Particle & Particle Systems Characterization **31**, 1017 (2014).

[142] M. Pereiro, D. Baldomir, J. Botana, J. E. Arias, K. Warda, and L. Wojtczak, *Biomedical applications of small silver clusters,* Journal of Applied Physics **103**, 07A315 (2008).

[143] S. M. Novikov, V. N. Popok, A. B. Evlyukhin, M. Hanif, P. Morgen, J. Fiutowski, J. Beermann, H.-G. Rubahn, and S. I. Bozhevolnyi, *Highly stable monocrystalline silver clusters for plasmonic applications,* Langmuir **33**, 6062 (2017).

[144] I. Díez and R. H. A. Ras, *Few-atom silver clusters as fluorescent reporters,* in *Advanced Fluorescence Reporters in Chemistry and Biology II: Molecular Constructions, Polymers and Nanoparticles*, edited by A. P. Demchenko (Springer Berlin Heidelberg, Berlin, Heidelberg, 2010) pp. 307–332.

[145] M. Ganguly, J. Jana, A. Pal, and T. Pal, *Synergism of gold and silver invites enhanced fluorescence for practical applications,* RSC Adv. **6**, 17683 (2016).

[146] T. M. Bernhardt, *Gas-phase kinetics and catalytic reactions of small silver and gold clusters,* International Journal of Mass Spectrometry **243**, 1 (2005).

[147] L. D. Socaciu, J. Hagen, J. L. Roux, D. Popolan, T. M. Bernhardt, L. Wöste, and Štefan Vajda, *Strongly cluster size dependent reaction behavior of co with o2 on free silver cluster anions,* J. Chem. Phys. **120**, 2078 (2004).

[148] T. Vosch, Y. Antoku, J.-C. Hsiang, C. I. Richards, J. I. Gonzalez, and R. M. Dickson, *Strongly emissive individual dna-encapsulated ag nanoclusters as single-molecule fluorophores,* **104**, 12616 (2007).

[149] S. A. Khan, D. Senapati, T. Senapati, P. Bonifassi, Z. Fan, A. K. Singh, A. Neeley, G. Hill, and P. C. Ray, *Size dependent nonlinear optical properties of silver quantum clusters,* Chem. Phys. Lett. **512**, 92 (2011).

[150] E. C. Tyo and S. Vajda, *Catalysis by clusters with precise numbers of atoms,* Nature Nanotechnology **10**, 577–588 (2015).

[151] M. Yang, K. A. Jackson, and J. Jellinek, *First-principles study of intermediate size silver clusters: Shape evolution and its impact on cluster properties,* J. Chem. Phys. **125**, 144308–1 (2006).

[152] B. Yoon, P. Koskinen, B. Huber, O. Kostko, B. von Issendorff, H. Häkkinen, M. Moseler, and U. Landman, *Size-dependent structural evolution and chemical reactivity of gold clusters,* ChemPhysChem **8**, 157 (2007).

[153] N. Shao, W. Huang, Y. Gao, L.-M. Wang, X. Li, L.-S. Wang, and X. C. Zeng, *Probing the structural evolution of medium-sized gold clusters: Aun− (n = 27–35),* Journal of the American Chemical Society **132**, 6596 (2010).

[154] X. Xing, B. Yoon, U. Landman, and J. H. Parks, *Structural evolution of au nanoclusters: From planar to cage to tubular motifs,* Phys. Rev. B **74**, 165423 (2006).

[155] H. Hakkinen, *Atomic and electronic structure of gold clusters: understanding flakes, cages and superatoms from simple concepts,* Chem. Soc. Rev. **37**, 1847 (2008).

[156] L.-M. Wang and L.-S. Wang, *Probing the electronic properties and structural evolution of anionic gold clusters in the gas phase,* Nanoscale **4**, 4038 (2012).

[157] Y. Dong and M. Springborg, *Unbiased determination of structural and electronic properties of gold clusters with up to 58 atoms,* J. Phys. Chem.C **111**, 12528 (2007).

[158] A. Tanwar, E. Fabiano, P. E. Trevisanutto, L. Chiodo, and F. Della Sala, *Accurate ionization potential of gold anionic clusters from density functional theory and many-body perturbation theory,* The European Physical Journal B **86**, 161 (2013).

[159] E. Fabiano, L. A. Constantin, and F. D. Sala, *Exchange-correlation generalized gradient approximation for gold nanostructures,* J. Chem. Phys. **134**, 194112 (2011).

[160] E. Fabiano, M. Piacenza, and F. Della Sala, *Structural and electronic properties of gold microclusters: assessment of the localized Hartree-Fock method,* Phys. Chem. Chem. Phys. **11**, 9160 (2009).

[161] M. V. Popa, *The electronic properties of the silver clusters in gas phase and water,* Int. J. Comp. Theor. Chem. **3**, 36 (2015).

[162] R. K. Hailstone and J. Tan, *Electronic properties of chemically produced silver clusters: Photobleaching studies,* Journal of Imaging Science and Technology **46**, 81 (2002).

[163] M. L. McKee and A. Samokhvalov, *Density functional study of neutral and charged silver clusters ag_n with n = 2–22. evolution of properties and structure,* J. Phys. Chem.A **121**, 5018 (2017).

[164] K. Duanmu and D. G. Truhlar, *Validation of methods for computational catalyst design: Geometries, structures, and energies of neutral and charged silver clusters,* J. Phys. Chem.C **119**, 9617 (2015).

[165] P. Weis, T. Bierweiler, S. Gilb, and M. M. Kappes, *Structures of small silver cluster cations (ag_n^+, $n < 12$): Ion mobility measurements versus density functional and mp2 calculations,* Chem. Phys. Lett. **355**, 355 (2002).

[166] D. Schooss, P. Weis, O. Hampe, and M. M. Kappes, *Determining the size-dependent structure of ligand-free gold-cluster ions,* Philosophical Transactions of the Royal Society of London A: Mathematical, Physical and Engineering Sciences **368**, 1211 (2010), http://rsta.royalsocietypublishing.org/content/368/1915/1211.full.pdf .

[167] K. J. Taylor, C. L. PettietteHall, O. Cheshnovsky, and R. E. Smalley, *Ultraviolet photoelectron spectra of coinage metal clusters,* J. Chem. Phys. **96**, 3319 (1992).

[168] B. F. J. J and S. McIndoe, *Spectroscopic and mass spectrometric methods for the characterisation of metal clusters,* Coordination Chemistry Reviews **200**, 901 (2000).

[169] D. P. Wooddruff, ed., *Atomic Clusters: From Gas Phase to Deposited* (Elsevier, Amsterdam, 2007).

[170] A. Fielicke, A. Kirilyuk, C. Ratsch, J. Behler, M. Scheffler, G. von Helden, and G. Meijer, *Structure determination of isolated metal clusters via far-infrared spectroscopy,* Phys. Rev. Lett. **93**, 023401 (2004).

[171] M. Haertelt, V. J. F. Lapoutre, J. M. Bakker, B. Redlich, D. J. Harding, A. Fielicke, and G. Meijer, *Structure determination of anionic metal clusters via infrared resonance enhanced multiple photon electron detachment spectroscopy,* J. Phys. Chem. Lett. **2**, 1720 (2011).

[172] C. S. Creaser, J. R. Griffiths, C. J. Bramwell, S. Noreen, C. A. Hill, and C. L. P. Thomas, *Ion mobility spectrometry: a review. part 1. structural analysis by mobility measurement,* Analyst **129**, 984 (2004).

[173] F. Lanucara, S. W. Holman, C. J. Gray, and E. C. E., *The power of ion mobility-mass spectrometry for structural characterization and the study of conformational dynamics,* Nature Chem. **6**, 281 (2014).

[174] H. Häkkinen, B. Yoon, U. Landman, X. Li, H.-J. Zhai, and L.-S. Wang, *On the electronic and atomic structures of small AuN- (N = 4–14) clusters: a photoelectron spectroscopy and density-functional study,* J. Phys. Chem.A **107**, 6168 (2003).

[175] F. Furche, R. Ahlrichs, P. Weis, C. Jacob, S. Gilb, T. Bierweiler, and M. M. Kappes, *The structures of small gold cluster anions as determined by a combination of ion mobility measurements and density functional calculations,* J. Chem. Phys. **117**, 6982 (2002).

[176] M. P. Johansson, A. Lechtken, D. Schooss, M. M. Kappes, and F. Furche, *2d-3d transition of gold cluster anions resolved,* Phys. Rev. A **77**, 053202 (2008).

[177] A. Lechtken, C. Neiss, M. M. Kappes, and D. Schooss, *Structure determination of gold clusters by trapped ion electron diffraction: Au14–au19-,* Phys. Chem. Chem. Phys. **11**, 4344 (2009).

[178] M. N. Blom, D. Schooss, J. Stairs, and M. M. Kappes, *Experimental structure determination of silver cluster ions (agn+,19n79),* J. Chem. Phys. **124**, 244308 (2006).

[179] *A theoretical challenge: Transition-metal compounds,* CHIMIA International Journal for Chemistry **63** (2009).

[180] K. Hirao, ed., *Recent Advances in Multireference Methods* (World Scientific, Singapore, 1999).

[181] B. O. Roos, *Multiconfigurational quantum chemistry,* in *Theory and Applications of Computational Chemistry: The First Forty Years*, edited by C. E. Dykstra, G. Frenking, K. S. Kim, and S. G. E. (Elsevier, Amsterdam, 2005).

[182] C. Møller and M. S. Plesset, *Note on an approximation treatment for many-electron systems,* Phys. Rev. **46**, 618 (1934).

[183] D. Cremer, *Møller–plesset perturbation theory: from small molecule methods to methods for thousands of atoms,* Wiley Interdisciplinary Reviews: Computational Molecular Science **1**, 509 (2011).

[184] C. D. Sherrill and H. F. S. III, *The configuration interaction method: Advances in highly correlated approaches,* (Academic Press, 1999) pp. 143 – 269.

[185] I. Shavitt, *The history and evolution of configuration interaction,* Molecular Physics **94**, 3 (1998).

[186] T. D. Crawford and H. F. Schaefer III, *An introduction to coupled cluster theory for computational chemists,* in *Reviews in Computational Chemistry*, edited by K. B. Lipkowitz and D. B. Boyd (Wiley-VCH, New York, 2000).

[187] J. Čížek, *Origins of coupled cluster technique for atoms and molecules,* Theoretica chimica acta **80**, 91 (1991).

[188] W. Kohn and L. J. Sham, *Self-consistent equations including exchange and correlation effects,* Phys. Rev. **140**, A1133 (1965).

[189] E. K. U. Gross and R. M. Dreizler, *Density Functional Theory* (Springer Science+Business Media, New York, 1995).

[190] F. M. Bickelhaupt and E. J. Baerends, *Kohn-sham density functional theory: Predicting and understanding chemistry,* in *Reviews in Computational Chemistry* (John Wiley & Sons, Inc., 2007) pp. 1–86.

[191] S. V. N. Scuseria G. E., *Progress in the development of exchange-correlation functionals,* in *Theory and Applications of Computational Chemistry: The First Forty Years*, edited by C. E. Dykstra, G. Frenking, K. S. Kim, and S. G. E. (Elsevier, Amsterdam, 2005).

[192] F. Della Sala, E. Fabiano, and L. A. Constantin, *Kinetic-energy-density dependent semilocal exchange-correlation functionals,* International Journal of Quantum Chemistry **116**, 1641 (2016).

[193] M. Chen, J. E. Dyer, K. Li, and D. A. Dixon, *Prediction of structures and atomization energies of small silver clusters, (Ag)n, n < 100,* J. Phys. Chem.A **117**, 8298 (2013).

[194] G. Zanti and D. Peeters, *Electronic structure analysis of small gold clusters Au_m (m ≤ 16) by density functional theory,* Theor. Chim. Acc. **132**, 1300 (2012).

[195] H. Baek, J. Moon, and J. Kim, *Benchmark study of density functional theory for neutral gold clusters, aun (n = 2–8),* J. Phys. Chem.A **121**, 2410 (2017).

[196] A. D. Becke, *A new mixing of hartree–fock and local densityfunctional theories,* J. Chem. Phys. **98**, 1372 (1993).

[197] J. P. Perdew, M. Ernzerhof, and K. Burke, *Rationale for mixing exact exchange with density functional approximations,* J. Chem. Phys. **105**, 9982 (1996).

[198] E. Fabiano, L. A. Constantin, P. Cortona, and F. Della Sala, *Global hybrids from the semiclassical atom theory satisfying the local density linear response,* J. Chem. Theory Comput. **11**, 122 (2015).

[199] E. Fabiano, P. Gori-Giorgi, M. Seidl, and F. Della Sala, *Interaction-strength interpolation method for main-group chemistry: Benchmarking, limitations, and perspectives,* J. Chem. Theory Comput. **12**, 4885 (2016).

[200] J. P. Perdew, K. Burke, and M. Ernzerhof, *Generalized gradient approximation made simple,* Phys. Rev. Lett. **77**, 3865 (1996).

[201] C. Adamo and V. Barone, *Toward reliable density functional methods without adjustable parameters: The pbe0 model,* J. Chem. Phys. **110**, 6158 (1999).

[202] S. Grimme, *Semiempirical hybrid density functional with perturbative second-order correlation,* J. Chem. Phys. **124**, 034108 (2006).

[203] G. D. P. III and R. J. Bartlett, *A full coupled-cluster singles and doubles model: The inclusion of disconnected triples,* J. Chem. Phys. **76**, 1910 (1982).

[204] J. A. Pople, M. Head-Gordon, and K. Raghavachari, *Quadratic configuration interaction. a general technique for determining electron correlation energies,* J. Chem. Phys. **87**, 5968 (1987).

[205] G. E. Scuseria, C. L. Janssen, and H. F. S. III, *An efficient reformulation of the closedshell coupled cluster single and double excitation (ccsd) equations,* J. Chem. Phys. **89**, 7382 (1988).

[206] K. Raghavachari, G. W. Trucks, J. A. Pople, and M. Head-Gordon, *A fifth-order perturbation comparison of electron correlation theories,* Chem. Phys. Lett. **157**, 479 (1989).

[207] J. P. Perdew, A. Ruzsinszky, G. I. Csonka, L. A. Constantin, and J. Sun, *Workhorse semilocal density functional for condensed matter physics and quantum chemistry,* Phys. Rev. Lett. **103**, 026403 (2009).

[208] F. Weigend and R. Ahlrichs, *Balanced basis sets of split valence, triple zeta valence and quadruple zeta valence quality for h to rn: Design and assessment of accuracy,* Phys. Chem. Chem. Phys. **7**, 3297 (2005).

[209] TURBOMOLE, TURBOMOLE, V7.0; TURBOMOLE GmbH: Karlsruhe, Germany, 2011. http://www.turbomole.com (accessed March 2017).

[210] F. Furche, R. Ahlrichs, C. Hättig, W. Klopper, M. Sierka, and F. Weigend, *Turbomole,* Wiley Interdisciplinary Reviews: Computational Molecular Science **4**, 91 (2014).

[211] J. G. Hill and K. A. Peterson, *Explicitly correlated coupled cluster calculations for molecules containing group 11 (Cu, Ag, Au) and 12 (Zn, Cd, Hg) elements: Optimized complementary auxiliary basis sets for valence and core–valence basis sets,* J. Chem. Theory Comput. **8**, 518 (2012).

[212] D. Figgen, G. Rauhut, M. Dolg, and H. Stoll, *Energy-consistent pseudopotentials for group 11 and 12 atoms: adjustment to multi-configuration Dirac–Hartree–Fock data,* Chemical Physics **311**, 227 (2005), relativistic Effects in Heavy-Element Chemistry and Physics. In Memoriam Bernd A. Hess (1954–2004).

[213] J. van der Tol, D. Jia, Y. Li, V. Chernyy, J. M. Bakker, M. T. Nguyen, P. Lievens, and E. Janssens, *Structural assignment of small cationic silver clusters by far-infrared spectroscopy and dft calculations,* Phys. Chem. Chem. Phys. **19**, 19360 (2017).

[214] S. Krückeberg, G. Dietrich, K. Lützenkirchen, L. Schweikhard, C. Walther, and J. Ziegler, *The dissociation channels of silver clusters agn+, 3 ≤ n ≤ 20,* International Journal of Mass Spectrometry and Ion Processes **155**, 141 (1996).

[215] M. Mantina, R. Valero, and D. G. Truhlar, *Validation study of the ability of density functionals to predict the planar-to-three-dimensional structural transition in anionic gold clusters,* J. Chem. Phys. **131**, 064706 (2009).

[216] L. A. Constantin, E. Fabiano, and F. Della Sala, *Meta-GGA exchange-correlation functional with a balanced treatment of nonlocality,* J. Chem. Theory Comput. **9**, 2256 (2013).

[217] L. A. Constantin, E. Fabiano, and F. D. Sala, *Semilocal dynamical correlation with increased localization,* Phys. Rev. B **86**, 035130 (2012).

[218] L. A. Constantin, E. Fabiano, and F. Della Sala, *Construction of a general semilocal exchange-correlation hole model: Application to nonempirical meta-GGA functionals,* Phys. Rev. B **88**, 125112 (2013).

[219] H.-P. Loock, L. M. Beaty, and B. Simard, *Reassessment of the first ionization potentials of copper, silver, and gold,* Phys. Rev. A **59**, 873 (2009).

[220] H. Häkkinen, B. Yoon, U. Landman, X. Li, H. J. Zhai, and L. Wang, J. Phys. Chem. A **107**, 6168 (2003).

[221] K. Balasubramanian and P. Y. Feng, Chem. Phys. Lett **159**, 452 (1989).

[222] K. P. Huber and G. Herzberg, *Molecular Spectra and Molecular Structure* (Springer, 1979).

[223] V. Beutel, H.-G. Kramer, G. Bhale, M. Kuhn, K. Weyers, and W. Demtroder, *High-resolution isotope selective laser spectroscopy of ag_2 molecules,* J. Chem. Phys. **98**, 2699 (1993).

[224] V. A. Spasov, T. H. Lee, J. P. Maberry, and K. Ervin, J. Chem. Phys. **110**, 5208 (1999).

[225] H. M. Lee, M. Ge, B. R. Sahu, P. Tarakeshwar, and K. S. Kim, J. Phys. Chem. B **107**, 9994 (2003).

[226] F. Colonna and A. Savin, *Correlation energies for some two- and four-electron systems along the adiabatic connection in density functional theory,* J. Chem. Phys. **110**, 2828 (1999).

[227] A. M. Teale, S. Coriani, and T. Helgaker, *The calculation of adiabatic-connection curves from full configuration-interaction densities: Two-electron systems,* J. Chem. Phys. **130**, 104111 (2009).

[228] Y. Zhou, H. Bahmann, and M. Ernzerhof, *Construction of exchange-correlation functionals through interpolation between the non-interacting and the strong-correlation limit,* J. Chem. Phys. **143**, 124103 (2015).

[229] S. Vuckovic, T. J. P. Irons, L. O. Wagner, A. M. Teale, and P. Gori-Giorgi, *Interpolated energy densities, correlation indicators and lower bounds from approximations to the strong coupling limit of DFT,* Phys. Chem. Chem. Phys. **19**, 6169 (2017).

[230] S. Vuckovic, M. Levy, and P. Gori-Giorgi, *Augmented potential, energy densities, and virial relations in the weak-and strong-interaction limits of DFT,* J. Chem. Phys. **147**, 214107 (2017).

[231] L. O. Wagner and P. Gori-Giorgi, *Electron avoidance: A nonlocal radius for strong correlation,* Phys. Rev. A **90**, 052512 (2014).

[232] H. Bahmann, Y. Zhou, and M. Ernzerhof, *The shell model for the exchange-correlation hole in the strong-correlation limit,* J. Chem. Phys. **145**, 124104 (2016).

[233] J. P. Perdew, M. Ernzerhof, and K. Burke, *Rationale for mixing exact exchange with density functional approximations,* J. Chem. Phys. **105**, 9982 (1996).

[234] J. Heyd, G. E. Scuseria, and M. Ernzerhof, J. Chem. Phys. **118**, 8207 (2003).

[235] Y. Zhao and D. G. Truhlar, *Density functionals with broad applicability in chemistry,* Accounts of chemical research **41**, 157 (2008).

[236] J. Jaramillo, G. E. Scuseria, and M. Ernzerhof, *Local hybrid functionals,* J. Chem. Phys. **118**, 1068 (2003).

[237] A. V. Arbuznikov and M. Kaupp, *Local hybrid exchange-correlation functionals based on the dimensionless density gradient,* Chem. Phys. Lett. **440**, 160 (2007).

[238] S. Grimme, *Semiempirical hybrid density functional with perturbative second-order correlation,* J. Chem. Phys. **124**, 034108 (2006).

[239] L. Goerigk and S. Grimme, *Efficient and accurate double-hybrid-meta-GGA density functionals evaluation with the extended gmtkn30 database for general main group thermochemistry, kinetics, and noncovalent interactions,* J. Chem. Theory Comput. **7**, 291 (2010).

[240] N. Q. Su and X. Xu, *Construction of a parameter-free doubly hybrid density functional from adiabatic connection,* J. Chem. Phys. **140**, 18A512 (2014).

[241] P. M. Gill, B. G. Johnson, J. A. Pople, and M. J. Frisch, *An investigation of the performance of a hybrid of hartree-fock and density functional theory,* Int. J. Quantum Chem. **44**, 319 (1992).

[242] N. Oliphant and R. J. Bartlett, *A systematic comparison of molecular properties obtained using Hartree–Fock, a hybrid Hartree–Fock density-functional-theory, and coupled-cluster methods,* J. Chem. Phys. **100**, 6550 (1994).

[243] M.-C. Kim, E. Sim, and K. Burke, *Communication: Avoiding unbound anions in density functional calculations,* J. Chem. Phys. **134**, 171103 (2011).

[244] M.-C. Kim, E. Sim, and K. Burke, *Ions in solution: Density corrected density functional theory (DC-DFT),* J. Chem. Phys. **140**, 18A528 (2014).

[245] M.-C. Kim, E. Sim, and K. Burke, *Understanding and reducing errors in density functional calculations,* Phys. Rev. Lett. **111**, 073003 (2013).

[246] E. Sim, S. Song, and K. Burke, *Quantifying density errors in DFT,* J. Phys. Chem. Lett. **9**, 6385 (2018).

[247] K. Pernal, *Correlation energy from random phase approximations: A reduced density matrices perspective,* Int. J. Quantum Chem. **118**, e25462 (2018).

[248] J. Olsen, O. Christiansen, H. Koch, and P. Jo/rgensen, *Surprising cases of divergent behavior in mo/ller–plesset perturbation theory,* J. Chem. Phys. **105**, 5082 (1996).

[249] B. Forsberg, Z. He, Y. He, and D. Cremer, *Convergence behavior of the møller–plesset perturbation series: use of feenberg scaling for the exclusion of backdoor intruder states,* Int. J. Quantum Chem. **76**, 306 (2000).

[250] S. Giarrusso, P. Gori-Giorgi, F. Della Sala, and E. Fabiano, *Assessment of interaction-strength interpolation formulas for gold and silver clusters,* J. Chem. Phys. **148**, 134106 (2018).

[251] J. Grossi, *Quantum fluctuations and kinetic correlation in the strongly interacting limit of density functional theory*, Academisch proefschrift, Vrije Universiteit van Amsterdam (2019).

[252] T. J. Daas, *Investigation of the strong-interaction limit of an adiabatic connection in Hartree-Fock theory*, Master thesis, Vrije Universiteit van Amsterdam (2019).

[253] L. Hedin, *New method for calculating the one-particle green's function with application to the electron-gas problem,* Phys. Rev. **139**, A796 (1965).

[254] J. Schirmer and G. Angonoa, *On green's function calculations of the static self-energy part, the ground state energy and expectation values,* J. Chem. Phys. **91**, 1754 (1989).

[255] W. Tarantino, P. Romaniello, J. Berger, and L. Reining, *Self-consistent dyson equation and self-energy functionals: An analysis and illustration on the example of the hubbard atom,* Phys. Rev. B **96**, 045124 (2017).

[256] P.-F. Loos, P. Romaniello, and J. Berger, *Green functions and self-consistency: insights from the spherium model,* J. Chem. Theory Comput. **14**, 3071 (2018).

[257] K. Pernal, *Electron correlation from the adiabatic connection for multireference wave functions,* Phys. Rev. Lett. **120**, 013001 (2018).

[258] Á. Nagy and Z. Jánosfalvi, *Exact energy expression in the strong-interaction limit of the density functional theory,* Philosophical Magazine **86**, 2101 (2006).

[259] T. Aschebrock, R. Armiento, and S. Kümmel, *Orbital nodal surfaces: Topological challenges for density functionals,* Phys. Rev. B **95**, 245118 (2017).

[260] J. P. Perdew and D. C. Langreth, *Exchange-correlation energy of a metallic surface: Wave-vector analysis,* Phys. Rev. B **15**, 2884 (1977).

[261] O. Gritsenko, R. van Leeuwen, and E. J. Baerends, *Analysis of electron interaction and atomic shell structure in terms of local potentials,* J. Chem. Phys. **101**, 8955 (1994).

[262] R. van Leeuwen, O. Gritsenko, and E. J. Baerends, *Step structure in the atomic Kohn-Sham potential,* Z. Phys. D **33**, 229 (1995).

[263] I. G. Ryabinkin and V. N. Staroverov, *Average local ionization energy generalized to correlated wavefunctions,* J. Chem. Phys. **141**, 084107 (2014).

[264] D. E. Freund, B. D. Huxtable, and J. D. Morgan, *Variational calculations on the helium isoelectronic sequence,* Phys. Rev. A **29**, 980 (1984).

[265] C. J. Umrigar and X. Gonze, *Accurate exchange-correlation potentials and total-energy components for the helium isoelectronic series,* Phys. Rev. A **50**, 3827 (1994).

[266] C. Filippi, X. Gonze, and C. J. Umrigar, *Generalized gradient approximations to density functional theory: comparison with exact results,* in *Recent developments and applications in modern DFT*, edited by J. M. Seminario (Elsevier, Amsterdam, 1996) pp. 295–321.

[267] A. I. Al-Sharif, R. Resta, and C. J. Umrigar, *Evidence of physical reality in the Kohn-Sham potential: The case of atomic ne,* Phys. Rev. A **57**, 2466 (1998).

[268] T. J. Irons and A. M. Teale, *The coupling constant averaged exchange–correlation energy density,* Mol. Phys. **114**, 484 (2015).

[269] G. Lani, S. Di Marino, A. Gerolin, R. van Leeuwen, and P. Gori-Giorgi, *The adiabatic strictly-correlated-electrons functional: kernel and exact properties,* Phys. Chem. Chem. Phys. **18**, 21092 (2016).

[270] A. Benítex and C. R. Proetto, *Kohn-Sham potential for a strongly correlated finite system with fractional occupancy,* Phys. Rev. A **94**, 052506 (2016).

[271] M. J. P. Hodgson, J. D. Ramsden, and R. W. Godby, *Origin of static and dynamic steps in exact Kohn-Sham potentials,* Phys. Rev. B **93**, 155146 (2016).

[272] M. J. P. Hodgson, E. Kraisler, A. Schild, and E. K. U. Gross, *How interatomic steps in the exact kohn–sham potential relate to derivative discontinuities of the energy,* J. Phys. Chem. Lett. **8**, 5974 (2017).

[273] G. F. Giuliani and G. Vignale, *Quantum Theory of the Electron Liquid* (Cambridge University Press, New York, 2005).

[274] M. Casula, S. Sorella, and G. Senatore, *Ground state properties of the one-dimensional coulomb gas using the lattice regularized diffusion monte carlo method,* Phys. Rev. B **74**, 245427 (2006).

[275] I. Theophilou, F. Buchholz, F. G. Eich, M. Ruggenthaler, and A. Rubio, *Kinetic-energy density-functional theory on a lattice,* J. Chem. Theory Comput. **14**, 4072 (2018).

[276] K. Pernal and K. J. Giesbertz, *Reduced density matrix functional theory (rdmft) and linear response time-dependent rdmft (td-rdmft),* in *Density-Functional Methods for Excited States*, edited by M. F. M. Ferré and M. Huix-Rotllant (Springer, 2015) pp. 125–183.

[277] M. Rego-Monteiro, L. M. Rodrigues, and E. Curado, *Position-dependent mass quantum hamiltonians: general approach and duality,* Journal of Physics A: Mathematical and Theoretical **49**, 125203 (2016).

[278] F. G. Eich, M. Di Ventra, and G. Vignale, *Density-functional theory of thermoelectric phenomena,* Phys. Rev. Lett. **112**, 196401 (2014).

[279] C. Adamo, M. Ernzerhof, and G. E. Scuseria, *The meta-GGA functional: Thermochemistry with a kinetic energy density dependent exchange-correlation functional,* J. Chem. Phys. **112**, 2643 (2000).

[280] J. Tao, J. P. Perdew, V. N. Staroverov, and G. E. Scuseria, Phys. Rev. Lett. **91**, 146401 (2003).

[281] A. Seidl, A. Görling, P. Vogl, J. Majewski, and M. Levy, *Generalized Kohn-Sham schemes and the band-gap problem,* Phys. Rev. B **53**, 3764 (1996).

[282] F. Eich and M. Hellgren, *Derivative discontinuity and exchange-correlation potential of meta-GGAs in density-functional theory,* J. Chem. Phys. **141**, 224107 (2014).

[283] F. Zahariev, S. S. Leang, and M. S. Gordon, *Functional derivatives of meta-generalized gradient approximation (meta-GGA) type exchange-correlation density functionals,* J. Chem. Phys. **138**, 244108 (2013).

[284] S. B. Sears, R. G. Parr, and U. Dinur, *On the quantum-mechanical kinetic energy as a measure of the information in a distribution,* Israel Journal of Chemistry **19**, 165 (1980).

[285] P. W. Ayers, R. G. Parr, and A. Nagy, *Local kinetic energy and local temperature in the density-functional theory of electronic structure,* Int. J. Quantum Chem. **90**, 309 (2002).

[286] O. von Roos, *Position-dependent effective masses in semiconductor theory,* Phys. Rev. B **27**, 7547 (1983).

[287] M. Taut, *Two electrons in an external oscillator potential: Particular analytic solutions of a coulomb correlation problem,* Phys. Rev. A **48**, 3561 (1993).

[288] T. Helgaker, P. Jørgensen, and J. Olsen, *Density-functional Theory: A Convex Treatment* (Wiley Blackwell, (to be published)).

[289] J. Katriel and E. R. Davidson, *Asymptotic behavior of atomic and molecular wave functions,* Proc. Natl. Acad. Sci. USA **77**, 4403 (1980).

[290] Z. Qian and V. Sahni, *Asymptotic near-nucleus structure of the electron-interaction potential in local effective potential theories,* Phys. Rev. A **75**, 032517 (2007).

[291] P.-F. Loos and P. M. Gill, *Thinking outside the box: The uniform electron gas on a hypersphere,* J. Chem. Phys. **135**, 214111 (2011).

[292] P. M. Gill and P.-F. Loos, *Uniform electron gases,* Theor. Chim. Acc. **131**, 1069 (2012).

[293] P.-F. Loos, *Exchange functionals based on finite uniform electron gases,* J. Chem. Phys. **146**, 114108 (2017), https://doi.org/10.1063/1.4978409 .

[294] J. P. Perdew and Y. Wang, *Accurate and simple analytic representation of the electron-gas correlation energy,* Phys. Rev. B **45**, 13244 (1992).

[295] J. Bartmess, *NIST chemistry webbook, NIST standard reference database number 69,* WG Mallard, PJ Linstrom (Eds.) **20899** (2001).

[296] J. Cioslowski and K. Pernal, *The ground state of harmonium,* J. Chem. Phys. **113**, 8434 (2000).

[297] `https://radar.squat.net/en/amsterdam/jeffreys-cinemas/events`.

[298] K. Levecque, F. Anseel, A. De Beuckelaer, J. Van der Heyden, and L. Gisle, *Work organization and mental health problems in PhD students,* Research Policy **46**, 868 (2017).

[299] T. M. Evans, L. Bira, J. B. Gastelum, L. T. Weiss, and N. L. Vanderford, *Evidence for a mental health crisis in graduate education,* Nature biotechnology **36**, 282 (2018).